Coupled nitrogen and oxygen isotope effects of anaerobic ammonium oxidation (anammox)

Kanae KOBAYASHI

This dissertation is submitted for the degree of Doctor of Philosophy
Division of Environmental Engineering
Graduate School of Engineering, Hokkaido University

Examination Committee: Professor Satoshi Okabe
Professor Hisashi Satoh
Professor Katsuki Kimura
Associate Professor Mamoru Oshiki

Abstract

Natural abundance of stable nitrogen (N) and oxygen (O) isotopes ($\delta^{15}N$ and $\delta^{18}O$) are invaluable biogeochemical tracers for assessing the N transformations in the environment. To fully exploit these tracers, the N and O isotope effects ($^{15}\varepsilon$ and $^{18}\varepsilon$) associated with the respective N transformation processes must be known. Anaerobic ammonium oxidation (anammox) and denitrification are the two major sinks of fixed N. In addition, anammox bacteria contribute to re-oxidation of nitrite (NO_2^-) to nitrate (NO_3^-), because they fix CO_2 into biomass with reducing equivalents generated from oxidation of NO_2^- to NO_3^-. NO_3^- production by anammox bacteria influences the NO_2^- and NO_3^- N and O isotope effects in freshwater and marine systems. Despite the significant importance of anammox bacteria in the global N cycle, $^{15}\varepsilon$ and $^{18}\varepsilon$ of anammox are not well known. Therefore, the never yet determined $^{15}\varepsilon$ and $^{18}\varepsilon$ associated with anammox were investigated in this study.

Firstly, the $^{15}\varepsilon$ were determined for '*Ca.* Scalindua sp.', '*Ca.* Jettenia caeni', and '*Ca.* Brocadia sinica' growing in continuous enrichment cultures. All three anammox species yielded similar $^{15}\varepsilon$ values of NH_4^+ oxidation to N_2 ($^{15}\varepsilon_{NH4\rightarrow N2}$ = 30.9 ~ 32.7‰) and inverse kinetic isotope effects of NO_2^- oxidation to NO_3^- ($^{15}\varepsilon_{NO2\rightarrow NO3}$ = - 45.3‰ ~ - 30.1‰). In contrast, the values of NO_2^- reduction to N_2 was significantly different among three species ($^{15}\varepsilon_{NO2\rightarrow N2}$ = 5.9 ~ 29.5‰), which is probably because individual anammox bacteria species might possess different types of nitrite reductase.

Secondly, the $^{18}\varepsilon$ were determined for '*Ca.* Scalindua sp.', which is a putative marine species. Determination of $^{18}\varepsilon$ of anammox is more challenging because the $\delta^{18}O_{NO2}$ value is affected by abiotic O isotope exchange between NO_2^- and H_2O (k_{eq}, $^{18}\varepsilon_{eq}$) and incorporation of a water-derived O atom into NO_3^- during NO_2^- oxidation to NO_3^- ($^{18}\varepsilon_{H2O}$). In order to determine abiotic $k_{eq,}$ $^{18}\varepsilon_{eq}$, and $^{18}\varepsilon_{H2O}$, batch experiments with different $\delta^{18}O_{H2O}$ values of medium were conducted. Oxygen isotope ratio measurements of NO_2^- and NO_3^- by the azide method and denitrifier method are sensitive to the $\delta^{18}O$ of sample water. However, the influence of $\delta^{18}O_{H2O}$ on those measurements has not been quantitatively evaluated and documented so far. Therefore, the influence of $\delta^{18}O_{H2O}$ of sample on $\delta^{18}O$ analysis of NO_2^- and NO_3^- were quantitatively evaluated. Then, the rate of abiotic O isotope exchange between NO_2^- and H_2O: k_{eq} = 1.13 × 10^{-2} (h^{-1}), as well as equilibrium isotope effects: $^{18}\varepsilon_{eq}$ = 11.9‰ were experimentally determined. To determine $^{18}\varepsilon$ of each reaction, batch culture experiments with different $\delta^{18}O_{H2O}$ values of medium ($\delta^{18}O_{H2O}$ = -12.6 ~ 110.1‰) were conducted for '*Ca.* Scalindua sp.'. A numerical model was developed for estimation of respective $^{18}\varepsilon$ of anammox reaction, resulting in $^{18}\varepsilon_{NO2\rightarrow N2}$ = 9.8 ~10.5‰, $^{18}\varepsilon_{NO2\rightarrow NO3}$ = -3.3 ~ -1.9‰, and $^{18}\varepsilon_{H2O}$= 24.1 ~ 25.6‰, respectively. These $^{18}\varepsilon$ values were determined for the first time in the world.

These obtained dual N and O isotopic effects could provide significant insights into the contribution of anammox bacteria to the fixed N loss and NO_2^- reoxidation in (recycling N) in various natural environments.

Acknowledgments

First and foremost, I would like to thank my supervisor, Prof. Satoshi Okabe. I worked under his supervision for almost six years. Every time when I wanted to challenge, he supported and gave valuable comments and took time for discussion. I'm very appreciate that he trusted me and gave me a chance to try new field of research works and collaborate with researchers in another research institute. Through my Ph.D. life, I have learned so much from him not only scientific aspects but also personal aspects. Owing to his warm and kind supervision, I always felt fun to progress my research works and kept a passion for study. I never forget this grateful feeling. Thank you for all the time with you.

Then, I thank Prof. Keisuke Koba from Center for Ecological Research in Kyoto University for telling me how stable isotope helps understanding of ecology. I always consulted about the research plan and learned many things from him about stable isotopes from basic to advance. Without his kind help and advice, I could not progress my research works at all.

I'm grateful to Associate Prof. Mamoru Oshiki. Many thanks for telling me the way to purify enzyme and giving me advice. From this year, I was very happy to work with him in the same laboratory. I enjoyed the discussion. I also appreciate that he gave me advices for my career after graduation.

I want to say thanks word to Assistant Prof. Masaaki Kitajima. Thanks for valuable comments and discussion in laboratory seminar. When I consulted about how to write research proposal, he kindly supported me and gave comments. It brought chance to conduct my research work where I wanted.

Then, I thank Dr. Keitaro Fukushima and Dr. Yuji Onishi from Center for Ecological Research in Kyoto University. When I visited CER to analyze my samples, they very kindly supported my works and gave me many advices for my manuscript. Even though, a lot of works existed, I really enjoyed the time with them. I never forget their kindness.

I feel appreciating for Dr. Kazuya Nishina from National Institute for Environmental Studies. I'm not good at constructing a numerical model. However, he kindly told me how to do it. Without his help, I must have given up calculating the complex isotope effect of anammox.

I thank Dr. Akiko Makabe from JAMSTEC and Dr. Midori Yano from NARO. Since I was undergraduate, they have told me how to treat isotope sample very well. Owing to their kind instruction, I could perform experiments.

I would like also to thank to all laboratory members. I really enjoyed laboratory life with them. I especially would like to thank Dr. Muhammad Ali, Dr. Zhang Lei, Yuko Yamashita, Minori Ushiyama, Amrini Amalia Shafdar, Atsushi Kamigaito, Akimichi Kamizono, Emi Morimoto, Xi Lan, Baku Tsukada and Erika Matsumoto for progressing research work with me. I'll never forget the precious and fun research life with them.

Finally, I want to express my appreciation to my parents, who support and understand my decision any time.

Table of Contents

Chapter 1
INTRODUCTION

1.1. Human-induced nitrogen imbalances

Late in the 19th century, the development of the Harber-Bosch processes which produce nitrogenous fertilizers initiated an unexpected increase in anthropogenic loading of reactive nitrogen (N) to the biosphere (**Fig. 1.1.1**) (Peñuelas *et al.*, 2013). Anthropogenic N inputs led to environmental problems such as eutrophication of terrestrial and aquatic systems, global acidification and loss of biodiversity (Gruber and Galloway, 2008). The N cycle is one of the Earth-system processes which beyond planetary boundaries as well as biodiversity loss and climate change. The 'planetary boundaries' is defined as the safe operating space for humanity with respect to the Earth system and are associated with the planet's biophysical subsystems or processes (Rockström *et al.*, 2009). The inexorable increase in the reactive N to ecosystems has no equivalent in the Earth's history.

Anthropogenic N load to especially coastal sediments significantly impacts the ecosystems worldwide (Seitzinger *et al.*, 2002). Thus, understanding marine N cycle with emphasis on both N removal and N_2O production is important for improving predictions of long-term impacts of human activity on the environment. Estimation and visualization of N cycle is indispensable information to formulate environmental protection policies.

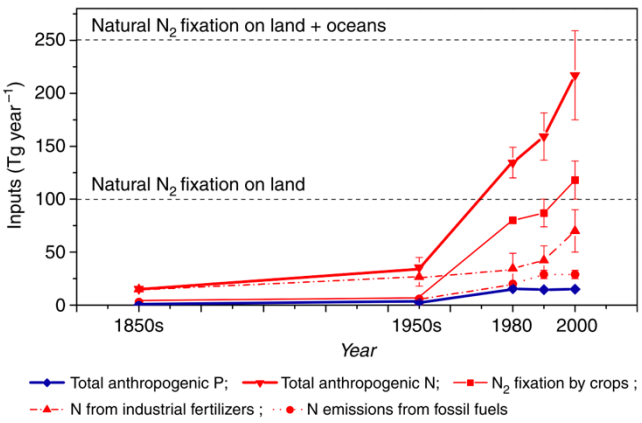

Figure 1.1.1 Anthropogenic N and P inputs to the biosphere after 1850s (Peñuelas *et al.*, 2013)**.**

1.2. Nitrogen cycle

Nitrogen is a fundamental component of living organisms, and its availability can limit primary production. The primary form of bioavailable N in the environment is nitrate (NO_3^-), nitrite (NO_2^-) and ammonium (NH_4^+). The N cycle is a complex web of microbially mediated reactions (**Fig.1.2.1**). Nitrogen fixation introduces new forms of bioavailable N ($N_2 + 8H^+ \rightarrow 2NH_3 + H_2$). Nitrification occurs as a two-step process whereby ammonia-oxidizing bacteria (AOB) and ammonia-oxidizing archaea (AOA) convert ammonia (NH_3) to NO_2^- ($NH_3 \rightarrow NO_2^-$) and nitrite-oxidizing bacteria (NOB) convert NO_2^- to NO_3^- ($NO_2^- \rightarrow NO_3^-$). The novel *Nitrospira* species that can oxidize NH_3 completely to NO_3^- were recently discovered and named "Comammox" (Daims *et al.*, 2015; Kessel *et al.*, 2015). Denitrification in the water column and marine sediments was only known pathway to remove bioavailable N from the deep-ocean inventory. Denitrification is the stepwise reduction of NO_3^- to NO_2^- ($NO_3^- \rightarrow NO_2^-$), and then to nitric oxide (NO), nitrous oxide (N_2O), and dinitrogen (N_2). After the discovery of anaerobic ammonium oxidation (anammox) (Mulder *et al.*, 1995), anammox is considered as an alternative N loss pathway to heterotrophic denitrification in both marine sediments and water columns (Thamdrup and Dalsgaard, 2002; Kuypers *et al.*, 2003). Therefore, anammox and heterotrophic denitrification are major nitrogen loss in anoxic marine ecosystems, whereas NO_3^- reduction to NO_2^- along with dissimilatory nitrate reduction to ammonium (DNRA) are major remineralization pathways.

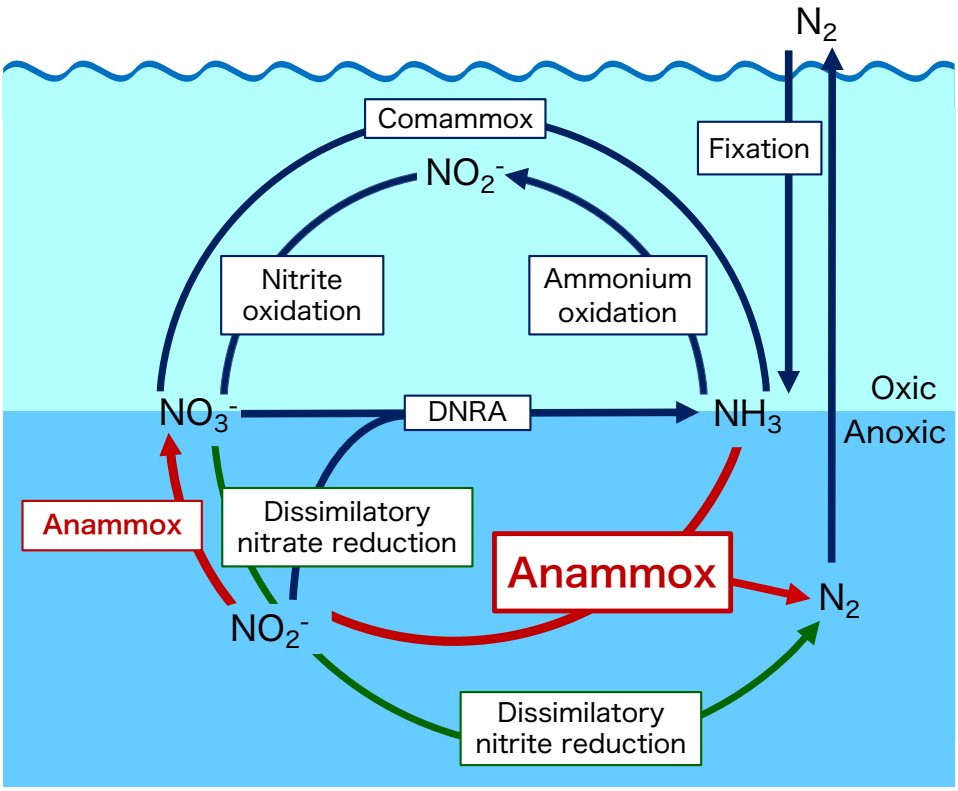

Figure 1.2.1 An outline of biological N cycle

1.3. Current understanding of anammox physiology, ecology, and biochemistry

Anammox bacteria oxidize NH_4^+ directly to N_2 gas with NO_2^- as the terminal electron acceptor in the absence of oxygen, and NO_2^- is concomitantly oxidized to NO_3^- as shown in the following stoichiometric equation (Lotti *et al.*, 2014):

$$1NH_4^+ + 1.146NO_2^- + 0.071HCO_3^- + 0.057H^+ \rightarrow 0.986N_2 + 0.161NO_3^- + 0.071CH_{1.74}O_{0.31}N_{0.20} + 2.002H_2O$$

The following biochemical pathway has been proposed for anammox reaction: first, NO_2^- is reduced to nitric oxide (NO) by either cytochrome *cd*$_1$-type or copper-containing nitrite reductase (Fe-NIR or Cu-NIR, respectively) (Strous *et al.*, 2006; Hira *et al.*, 2012); second, the produced NO is first reduced to NH_2OH, which is consequently coupled with NH_3 to form hydrazine (N_2H_4) by hydrazine synthase (Hzs) (Kartal *et al.*, 2011; Dietl *et al.*, 2015); and finally, the N_2H_4 is oxidised to N_2 gas by hydrazine dehydrogenase (Hdh) (Shimamura *et al.*, 2007; Kartal *et al.*, 2011). Anammox bacteria are phylogenetically diverse and possess different enzymes and metabolic pathways (Oshiki *et al.*, 2016). For example, recent genomic studies revealed that '*Ca*. K. stuttgartiensis' and '*Ca*. S. profunda' possess a cytochrome *cd*$_1$ (iron, Fe)-type NO-forming nitrite reductase (Fe-NIR), whereas '*Ca*. J. caeni' has a copper (Cu)-containing NO-forming nitrite reductase (Cu-NIR). Interestingly, '*Ca*. B. fulgida' (Gori *et al.*, 2011), '*Ca*. B. sinica' (Oshiki *et al.*, 2015), and '*Ca*. B. sapporoensis' (Narita *et al.*, 2017) possess neither Fe-NIR nor Cu-NIR, and thus might carry as yet unidentified nitrite reductase(s).

1.4. Contribution of anaerobic ammonium oxidation (anammox) to fixed N loss

Anaerobic ammonium oxidation (anammox) and denitrification are the two major sinks of fixed nitrogen (N) in the ocean. It has been estimated that these microbial processes together remove 230 - 450 Tg N yr^{-1} from the global ocean (Codispoti, 2007; Gruber and Galloway, 2008), which is thought to occur mainly in oxygen deficient water columns and sediments. Despite great efforts to quantify the magnitude of the sources (N_2 fixation) and sinks of fixed N, the oceanic N budget is still poorly constrained. The estimated N losses (denitrification and anammox) exceeds inputs (N_2 fixation) by a factor of two (Codispoti *et al.*, 2001; Brandes and Devol, 2002). This discrepancy is partly because the rates and mechanisms of N loss processes including anammox are not fully understood even though an increasing number of studies have highlighted the significant contributions of anammox bacteria for the regional N fluxes (Kuypers *et al.*, 2003, 2005; Thamdrup *et al.*, 2006; Kalvelage *et al.*, 2013; Babbin *et al.*, 2017).

The rates of anammox and related N transformations in the natural environment were usually determined in short-term batch incubation experiments with various combinations of ^{15}N-labeled and unlabeled N compounds (Dalsgaard *et al.*, 2003; Kuypers *et al.*, 2005; Kalvelage *et al.*, 2011; Babbin

et al., 2017). The ^{15}N tracer experiment is an incubation-based batch experiment, in which collected water samples are incubated with a heavy isotope enriched substrate (usually 99% ^{15}N) and the heavy isotope enrichment in the products is measured over time. The occurrence of anammox was also supported by the identification of anammox bacteria by their signature 16S rRNA genes and ladderane biomarkers (Kuypers *et al.*, 2003; Lam and Kuypers, 2011). However, measuring the reaction rate with incubation experiments are labor intensive and had proven to be challenge, due to O_2 sensitivity of those processes and difficulty of maintaining an anoxic incubation condition (Dalsgaard *et al.*, 2003, 2014; Kalvelage *et al.*, 2011; Peters *et al.*, 2016). In addition, these ^{15}N tracer experiments have the potential defects and limitations such as potential stimulation or inhibition of transformation rates and change in microbial community during incubation (Peters *et al.*, 2016). Organic matter stoichiometry also affects the ratio of anammox and denitrification (Babbin *et al.*, 2014). This is because while anammox, an autotrophic metabolism, removes CO_2 from the water column, denitrification, typically a heterotrophic process, is a source of CO_2. Furthermore, short-term batch incubations provide only a "snapshot" view of the time-varying complex oceanic N cycling processes (Santoro and Casciotti, 2011). On the other hand, measurement of natural abundance of N and O isotopes is integrative measurements that reflect the accumulated effects of N cycle processes over larger scales of time and space (Peters *et al.*, 2016).

1.5. Natural abundance stable isotope measurements

The natural abundance stable isotope measurements have long provided insights into ecological studies. Isotope measurements are chemical measurements that allow detailed nuanced views of element cycling in all systems (Fry, 2006). Isotopes are forms of the same element that differ in the number of neutrons in the nucleus. For instance, ^{15}N nitrogen has one more neutron than ^{14}N nitrogen in its nucleus. An extra neutron in the ^{15}N isotope makes the nucleus more heavier than the ^{14}N isotope, but does not affect most chemistry that is related to reaction in the electron shell (Fry, 2006). However, in the kinetic reactions, the light isotopes usually react faster than heavier ones. The extra neutron makes a slight difference in the kinetic reaction (**Fig. 1.5.1**). Isotopes do not react exactly the same even though they are nearly identical in chemical structure. This differential isotope behavior is known as isotope fractionation.

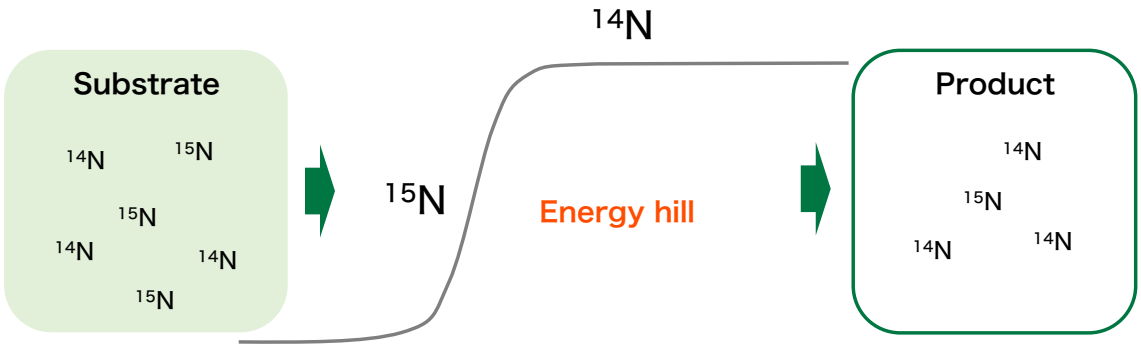

Figure 1.5.1 The differential isotope behavior during the kinetic reaction (Modified by Fry, 2006). ^{15}N has an extra neutron. It is harder to push the heavier molecules up an energy hill. Thus, heavier isotopes react slower.

1.6. Notation of isotopes

Isotope values are presented as delta (δ) notation. The delta values denote a difference measurement made relative to the standards. The N and O isotope composition of international standards are summarized in **Table 1. 6**. δ values are presented as follows.

$$\delta^{H} X = [(R_{SMAPLE}/ R_{STANDARD} - 1)] \times 1000 ‰$$

The superscript H means the heavy isotope mass of the element X (e. g. ^{15}N, ^{18}O). R is the ratio of the heavy isotope to the light isotope for the element (e. g. $^{15}R = {}^{15}N/{}^{14}N$). According to this definition, samples with higher delta values are relatively enriched in the heavy isotope and are heavier than the international standards. Samples with lower delta values are relatively enriched in the light isotope and are lighter than the international standards. If delta value is 0‰, it means there is no difference from the international standards.

Table 1. 6 The N and O isotope composition of international standards. Atmospheric air (AIR) and standard seawater; Vienna Standard Mean Ocean Water (VSMOW) are the international standards of N and O isotope composition.

Element	International standard	Stable isotope	Abundance ratio
N	AIR	^{14}N	0.996337
		^{15}N	0.003663
O	VSMOW	^{16}O	0.9976206
		^{17}O	0.000379
		^{18}O	0.0020004

1.7. Notation of isotope effects

The isotope fractionation arises from a difference in the reaction rate constant for light isotopes (^{14}N, ^{16}O) and heavy isotopes (^{15}N, ^{18}O). The isotope fractionation factor α is given by the ratio of the reaction rate constant for light (^{L}k) and heavy (^{H}k) isotopes.

Isotope fractionation factor $\alpha = {}^{L}k / {}^{H}k$

According to the definition of isotope fractionation factor, if there is no effect of the isotope substitution of light for heavy isotopes, the reaction rate constants would be equal and α would be 1. If the light isotope reacts 2% faster than heavy isotope, α would be 1.02. To make this fractionation difference easier to see, the value of isotope effect (ε) are derived from α values.

Isotope effect :$\varepsilon = (\alpha - 1) \times 1000‰$

For normal kinetic isotope fractionation, ^{L}k will be larger than ^{H}k, and thus $\alpha > 1$ and $\varepsilon > 0$. For inverse isotope fractionation, ^{L}k is lower than ^{H}k, thus $\alpha < 1$ and $\varepsilon < 0$.

1.8. Natural abundance stable isotope measurements to assess N cycle

Natural abundance N and O stable isotope ratios in dissolved inorganic N compounds (NH_4^+, NO_2^- and NO_3^-) have provided many insights into the biogeochemical processes comprising the N cycle over long space and time scales, compared to instantaneous rate measurements (Casciotti, Buchwald, *et al.*, 2010; Peters *et al.*, 2016). Biogeochemical and microbial processes change the distribution of isotopes, and the variations in the stable isotope composition could be used to constrain rates and pathways of N transformations. In order to correctly interpret the distributions of N and O isotope ratios in the natural environment, knowledge about the isotopic effects associated with key microbial processes is essential. The kinetic N and O isotope effects associated with microbial ammonium oxidation (Casciotti *et al.*, 2003; Casciotti, McIlvin, *et al.*, 2010; Santoro and Casciotti, 2011; Buchwald *et al.*, 2012; Nishizawa *et al.*, 2016; Mooshammer *et al.*, 2020), nitrite oxidation (Casciotti, 2009; Buchwald and Casciotti, 2010), dissimilatory nitrite reduction to nitric oxide (Martin and Casciotti, 2016), dissimilatory nitrate reduction (denitrification) (Granger et al., 2008; Kritee *et al.*, 2012) and assimilatory nitrate reduction (Granger *et al.*, 2010; Karsh *et al.*, 2012) have been determined for laboratory cultures of corresponding bacteria. Despite the importance of anammox bacteria in the global N cycle, the N isotope effect ($^{15}\varepsilon$) associated with anammox metabolism has been determined for only one freshwater anammox strain, "*Ca.* Kuenenia stuttgartiensis" (Brunner *et al.*, 2013). The kinetic O isotope effect ($^{18}\varepsilon$) of each anammox metabolism has not yet been determined. Consequently, their impacts on the distributions of N and O isotopes in the natural environments could not be addressed. Therefore, $^{15}\varepsilon$ and as yet unknown $^{18}\varepsilon$ associated with anammox were investigated in this study.

1.9. References

Babbin, A.R., Keil, R.G., Devol, A.H., and Ward, B.B. (2014) Organic Matter Stoichiometry, Flux, and Oxygen Control Nitrogen Loss in the Ocean. *Science* 344: 406–408.

Babbin, A.R., Peters, B.D., Mordy, C.W., Widner, B., Casciotti, K.L., and Ward, B.B. (2017) Multiple metabolisms constrain the anaerobic nitrite budget in the Eastern Tropical South Pacific. *Global Biogeochem Cycles* 31: 258–271.

Brandes, J.A. and Devol, A.H. (2002) A global marine-fixed nitrogen isotopic budget: Implications for Holocene nitrogen cycling. *Global Biogeochem Cycles* 16: 1120.

Brunner, B., Contreras, S., Lehmann, M.F., Matantseva, O., Rollog, M., Kalvelage, T., et al. (2013) Nitrogen isotope effects induced by anammox bacteria. *Proc Natl Acad Sci U S A* 110: 18994–18999.

Buchwald, C. and Casciotti, K.L. (2010) Oxygen isotopic fractionation and exchange during bacterial nitrite oxidation. *Limnol Oceanogr* 55: 1064–1074.

Buchwald, C., Santoro, A.E., McIlvin, M.R., and Casciotti, K.L. (2012) Oxygen isotopic composition of nitrate and nitrite produced by nitrifying cocultures and natural marine assemblages. *Limnol Oceanogr* 57: 1361–1375.

Casciotti, K.L. (2009) Inverse kinetic isotope fractionation during bacterial nitrite oxidation. *Geochim Cosmochim Acta* 73: 2061–2076.

Casciotti, K.L., Buchwald, C., Santoro, A.E., and Frame, C. (2010) Assessment of nitrogen and oxygen isotopic fractionation during nitrification and its expression in the marine environment. Methods in Enzymology 486: 253-280.

Casciotti, K.L., McIlvin, M., and Buchwald, C. (2010) Oxygen isotopic exchange and fractionation during bacterial ammonia oxidation. *Limnol Oceanogr* 55: 753–762.

Casciotti, K.L., Sigman, D.M., and Ward, B.B. (2003) Linking Diversity and Stable Isotope Fractionation in Ammonia-Oxidizing Bacteria. *Geomicrobiol J* 20: 335–353.

Codispoti, L. A. (2007) An oceanic fixed nitrogen sink exceeding 400 Tg N a? vs the concept of homeostasis in the fixed-nitrogen inventory. *Biogeosciences, European Geosciences Union*: 233-253.

Codispoti, L.A., Brandes, J.A., Christensen, J.P., Devol, A.H., Naqvi, S.W.A., Paerl, H.W., and Yoshinari, T. (2001) The oceanic fixed nitrogen and nitrous oxide budgets: Moving targets as we enter the anthropocene? *Sci Mar* 65: 85–105.

Daims, H., Elena, V., Palatinszky, M., Vierheilig, J., Bulaev, A., Kirkegaard, R.H., et al. (2015) Complete nitrification by *Nitrospira* bacteria.

Dalsgaard, T., Canfield, D.E., Petersen, J., Thamdrup, B., and Acuña-González, J. (2003) N_2 production by the anammox reaction in the anoxic water column of Golfo Dulce, Costa Rica. *Nature* 422: 606–608.

Dalsgaard, T., Stewart, F.J., Thamdrup, B., De Brabandere, L., Revsbech, N.P., Ulloa, O., et al. (2014) Oxygen at nanomolar levels reversibly suppresses process rates and gene expression in anammox and denitrification in the oxygen minimum zone off Northern Chile. *MBio* 5: 1–14.

Dietl, A., Ferousi, C., Maalcke, W.J., Menzel, A., de Vries, S., Keltjens, J.T., et al. (2015) The inner workings of the hydrazine synthase multiprotein complex. *Nature* 527: 394–397.

Fry, B. (2006) Stable Isotope Ecology, Spribger Science + Business Media, LLC.

Gori, F., Tringe, S.G., Kartal, B., Machiori, E., and Jetten, M.S.M. (2011) The metagenomic basis of anammox metabolism in *Candidatus* 'Brocadia fulgida.' *Biochem Soc Trans* 39: 1799–1804.

Granger, J. and Sigman, D.M. (2008) Nitrogen and oxygen isotope fractionation during dissimilatory nitrate reduction by denitrifying bacteria. *Limnol Oceanogr* 53: 2533–2545.

Granger, J., Sigman, D.M., Rohde, M.M., Maldonado, M.T., and Tortell, P.D. (2010) N and O isotope effects during nitrate assimilation by unicellular prokaryotic and eukaryotic plankton cultures. *Geochim Cosmochim Acta* 74: 1030–1040.

Gruber, N. and Galloway, J.N. (2008) An Earth-system perspective of the global nitrogen cycle. *Nature* 451: 293–6.

Hira, D., Toh, H., Migita, C.T., Okubo, H., Nishiyama, T., Hattori, M., et al. (2012) Anammox organism KSU-1 expresses a NirK-type copper-containing nitrite reductase instead of a NirS-type with cytochrome cd 1. *FEBS Lett* 586: 1658–1663.

Kalvelage, T., Jensen, M.M., Contreras, S., Revsbech, N.P., Lam, P., Günter, M., et al. (2011) Oxygen sensitivity of anammox and coupled N-cycle processes in oxygen minimum zones. *PLoS One* 6 (12):e29299.

Kalvelage, T., Lavik, G., Lam, P., Contreras, S., Arteaga, L., Löscher, C.R., et al. (2013) Nitrogen cycling driven by organic matter export in the South Pacific oxygen minimum zone. *Nat Geosci* 6: 228–234.

Karsh, K.L., Granger, J., Kritee, K., and Sigman, D.M. (2012) Eukaryotic assimilatory nitrate reductase fractionates N and O isotopes with a ratio near unity. *Environ Sci Technol* 46: 5727–5735.

Kartal, B., Maalcke, W.J., de Almeida, N.M., Cirpus, I., Gloerich, J., Geerts, W., et al. (2011) Molecular mechanism of anaerobic ammonium oxidation. *Nature* 479: 127-U159.

Van Kessel, M.A.H.J., Speth, D.R., Albertsen, M., Nielsen, P.H., Op Den Camp, H.J.M., Kartal, B., et al. (2015) Complete nitrification by a single microorganism. *Nature* 528: 555–559.

Kritee, K., Sigman, D.M., Granger, J., Ward, B.B., Jayakumar, A., and Deutsch, C. (2012) Reduced isotope fractionation by denitrification under conditions relevant to the ocean. *Geochim Cosmochim Acta* 92: 243–259.

Kuypers, M.M.M., Lavik, G., Woebken, D., Schmid, M., Fuchs, B.M., Amann, R., et al. (2005) Massive nitrogen loss from the Benguela upwelling system through anaerobic ammonium oxidation. *Proc Natl Acad Sci* 102: 6478–6483.

Kuypers, M.M.M., Sliekers, A.O., Lavik, G., Schmid, M., Jorgensen, B.B., Kuenen, J.G., et al. (2003) Anaerobic Ammonium Oxidation by Anammox Bacteria in the Black Sea. *Nature* 422: 608–611.

Lam, P. and Kuypers, M.M.M. (2011) Microbial Nitrogen Cycling Processes in Oxygen Minimum Zones. *Ann Rev Mar Sci* 3: 317–345.

Lotti, T., Kleerebezem, R., Lubello, C., and van Loosdrecht, M.C.M. (2014) Physiological and kinetic characterization of a suspended cell anammox culture. *Water Res* 60: 1–14.

Martin, T.S. and Casciotti, K.L. (2016) Nitrogen and oxygen isotopic fractionation during microbial nitrite reduction. *Limnol Oceanogr* 61: 1134–1143.

Mooshammer, M., Alves, R.J.E., Bayer, B., Melcher, M., Stieglmeier, M., Jochum, L., et al. (2020)

Nitrogen Isotope Fractionation During Archaeal Ammonia Oxidation: Coupled Estimates From Measurements of Residual Ammonium and Accumulated Nitrite. *Front Microbiol* 11: 1–9.

Mulder, A., van de Graaf, A.A., Robertson, L.A., and Kuenen, J.G. (1995) Anaerobic ammonium oxidation discovered in a denitrifying fluidized bed reactor. *FEMS Microbiol Ecol* 16: 177–183.

Narita, Y., Zhang, L., Kimura, Z. ichiro, Ali, M., Fujii, T., and Okabe, S. (2017) Enrichment and physiological characterization of an anaerobic ammonium-oxidizing bacterium '*Candidatus* Brocadia sapporoensis.' *Syst Appl Microbiol* 40: 448–457.

Nishizawa, M., Sakai, S., Konno, U., Nakahara, N., Takaki, Y., Saito, Y., et al. (2016) Nitrogen and oxygen isotope effects of ammonia oxidation by thermophilic *Thaumarchaeota* from a geothermal water stream. *Appl Environ Microbiol* 82: AEM.00250-16.

Oshiki, M., Satoh, H., and Okabe, S. (2016) Ecology and physiology of anaerobic ammonium oxidizing bacteria. *Environ Microbiol* 18: 2784–2796.

Oshiki, M., Shinyako-Hata, K., Satoh, H., and Okabe, S. (2015) Draft Genome Sequence of an Anaerobic Ammonium-Oxidizing Bacterium,"*Candidatus* Brocadia sinica." *Genome Announc* 3 (2): e00267-15.

Peñuelas, J., Poulter, B., Sardans, J., Ciais, P., Van Der Velde, M., Bopp, L., et al. (2013) Human-induced nitrogen-phosphorus imbalances alter natural and managed ecosystems across the globe. *Nat Commun* 4:2934.

Peters, B.D., Babbin, A.R., Lettmann, K.A., Mordy, C.W., Ulloa, O., Ward, B.B., and Casciotti, K.L. (2016) Vertical modeling of the nitrogen cycle in the eastern tropical South Pacific oxygen deficient zone using high-resolution concentration and isotope measurements. *Global Biogeochem Cycles* 30: 1661–1681.

Rockström, J., W. Steffen, K. Noone, Å. Persson, F. S. Chapin, E. F. Lambin, et al. (2009) A safe operation space for humanity. *Nature* 461: 472–475.

Santoro, A.E. and Casciotti, K.L. (2011) Enrichment and characterization of ammonia-oxidizing archaea from the open ocean: phylogeny, physiology and stable isotope fractionation. *Isme J* 5: 1796–1808.

Seitzinger, S.P., Kroeze, C., Bouwman, A.F., Caraco, N., Dentener, F., and Styles, R. V. (2002) Global Patterns of Dissolved Inorganic and Particulate Nitrogen Inputs to Coastal Systems : Recent Conditions and Future Projections. *Estuaries* 25: 640–655.

Shimamura, M., Nishiyama, T., Shigetomo, H., Toyomoto, T., Kawahara, Y., Furukawa, K., and Fujii, T. (2007) Isolation of a multiheme protein with features of a hydrazine-oxidizing enzyme from an anaerobic ammonium-oxidizing enrichment culture. *Appl Environ Microbiol* 73: 1065–1072.

Strous, M., Pelletier, E., Mangenot, S., Rattei, T., Lehner, A., Taylor, M.W., et al. (2006) Deciphering the evolution and metabolism of an anammox bacterium from a community genome. *Nature* 440: 790–794.

Thamdrup, B. and Dalsgaard, T. (2002) Production of N_2 through anaerobic ammonium oxidation coupled to nitrate reduction in marine sediments. *Appl Environ Microbiol* 68: 1312–1318.

Thamdrup, B., Jensen, M.M., Ulloa, O., Farı, L., and Escribano, R. (2006) Anaerobic ammonium oxidation in the oxygen-deficient waters off northern Chile. *Limnol Ocean* 51: 2145–2156.

Chapter 2

LITERATURE REVIEW: Nitrogen and oxygen isotope effects of N related microorganisms; What are the control factors for isotope effects?

2.1. Introduction

The natural abundance stable nitrogen isotope ratios of nitrate (NO_3^-) and nitrite (NO_2^-) ($\delta^{15}N_{NO3-}$ and $\delta^{15}N_{NO2-}$, respectively) record the history of processes that have contributed to production and consumption of NO_3^- and NO_2^-. Thus, nitrogen stable isotope models have been constructed to estimate the marine fixed nitrogen budget (Brandes and Devol, 2002; Deutsch *et al.*, 2004). However, it has a limitation that N inputs and losses partially erase $\delta^{15}N$ signals with each other in case of mixed water column (Sigman *et al.*, 2005). For instance, nitrogen fixation and denitrification have counteracting effects on $\delta^{15}N_{NO3-}$. Nitrogen fixation adds new NO_3^- and decreases $\delta^{15}N_{NO3-}$, while denitrification increases $\delta^{15}N_{NO3-}$ by removing NO_3^-. If the two processes occur in the same region or if waters from these regions were mixed vigorously, the tracer signals of both processes are reduced (Deutsch *et al.*, 2001).

Difficulty in constraining the marine fixed N budget has prompted the use of NO_2^- and NO_3^- $\delta^{18}O$ values ($\delta^{18}O_{NO2}$[% vs. VSMOW] = $\{(^{18}R_{NO2}/^{18}R_{VSMOW}) - 1\} \times 1000$, and $\delta^{18}O_{NO3}$[% vs. VSMOW] = $\{(^{18}R_{NO3}/^{18}R_{VSMOW}) - 1\} \times 1000$, where $^{18}R = {}^{18}O : {}^{16}O$ and VSMOW refers to the standard Vienna Standard Mean Ocean Water). After measurement methods of the $\delta^{18}O$ of NO_3^-(Sigman *et al.*, 2001; Casciotti *et al.*, 2002) and NO_2^- (McIlvin and Altabet, 2005; Casciotti *et al.*, 2007) have been developed, investigations using coupled fractionation of the N and O isotopes of NO_3^- in the ocean were started (Lehmann *et al.*, 2004; Sigman *et al.*, 2005; Wankel *et al.*, 2007). Those investigations were reviewed by Kendall *et al.*, 2007 and Casciotti, 2016. The $\delta^{18}O$ value of NO_3^- and NO_2^- are controlled by a different set of process than the $\delta^{15}N$ values **(Fig. 2.1).** For example, during NO_3^- uptake and regeneration, N atoms are recycled between fixed N pools, while O atoms are removed, then replaced by the nitrification. In short, while the N isotope budget is sensitive to input (nitrogen fixation) and output (denitrification and anammox) processes, the O isotopes in NO_2^- and NO_3^- are sensitive to internal cycling (DNRA, regeneration, nitrification, anammox) (Buchwald *et al.*, 2012). In this way, the coupled N and O isotope analyses provide complementary signatures of co-occurring N transformation processes that could not be revealed by

N isotope measurement alone (Casciotti, 2016). To interpret the value of $\delta^{15}N$ and $\delta^{18}O$ of NO_2^- and NO_3^- in the environment, the N and O isotope effects associated with each source and sink process must be known. The kinetic isotope effect is a result of small differences in the rate of enzymatic reaction with molecules containing heavy and light isotopes of constant atoms which denoted as $\varepsilon = ([^{light}k / {}^{heavy}k] - 1) \times 1000$, when expressed in per mil (‰). $^{light}k$ and $^{heavy}k$ are the rate constants for enzymatic reaction with light and heavy isotopically substituted substrates (Mariotti *et al.*, 1981). In addition to enzyme level isotope effect, physiological factors may play a role in expressed isotope effects for a multi-step process that involves transport of substrate between extra-cellular and intra-cellular pools (Casciotti *et al.*, 2003). Thus, it is important to understand both of enzyme level isotope effects and physiological factors affecting on expressed isotope effects to interpret natural abundance N and O isotopic distributions in the environment and make experimental strategy to analyze isotope effects. Here I reviewed the recent progress in our understanding of N and O isotope effects of N related microorganisms and factors affecting the expressed isotope effects.

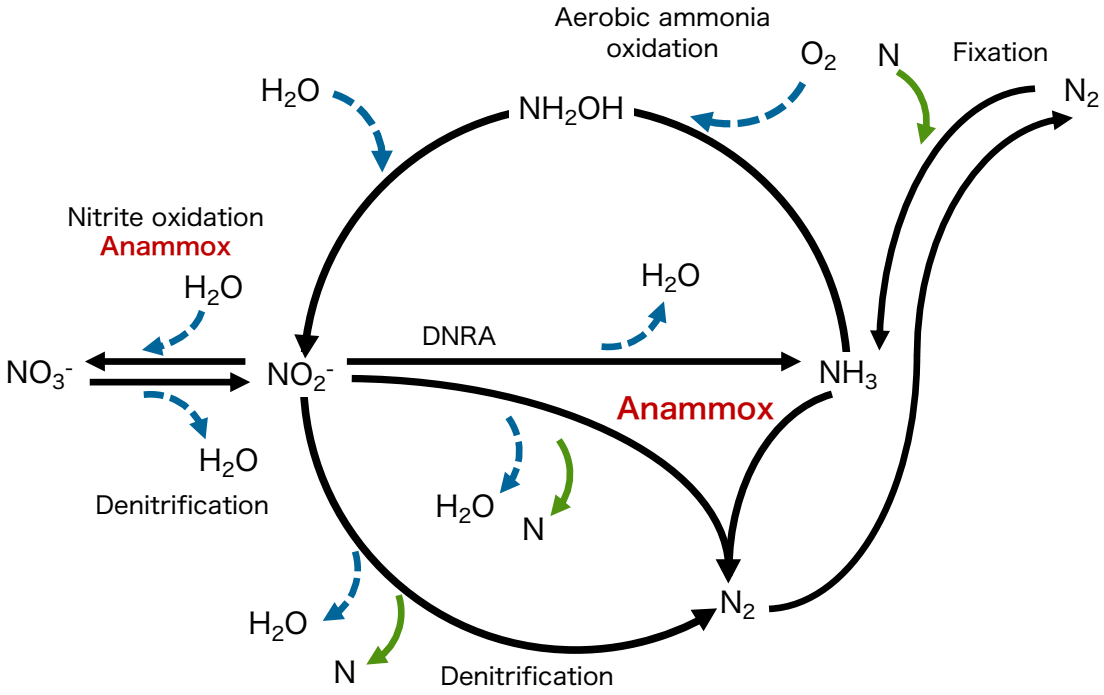

Figure 2. 1 Nitrogen and oxygen isotope systematics of N cycle-related microbial processes. Black solid arrows are reaction pathways. Green solid arrows indicate reaction in which nitrogen is added and/or removed. Blue dashed arrows indicate reactions in which oxygen is added and/or removed.

2.2. Overview of nitrogen and oxygen isotope effects

2.2.1 Nitrogen fixation

Nitrogen fixation introduces new forms of bioavailable nitrogen ($N_2 + 8H^+ \rightarrow 2NH_3 + H_2$). Nitrogen isotope effects of bacterial nitrogen fixation were mainly determined by using pure cultures of *Azotobacter* species (Hoering and Ford, 1960; Delwiche and Steyn, 1970; Yamazaki *et al.*, 1987) and cyanobacterial species (Bauersachs *et al.*, 2009). They showed weak isotope effects ($^{15}\varepsilon$ = -3.7 ~ 3.9 ‰).

2.2.2 Nitrification

Nitrification occurs as a two-step process whereby ammonia-oxidizing bacteria (AOB) and ammonia-oxidizing archaea (AOA) convert ammonia to nitrite ($NH_3 \rightarrow NO_2^-$) and nitrite-oxidizing bacteria (NOB) convert nitrite to nitrate ($NO_2^- \rightarrow NO_3^-$). There is a potential difference in ammonia oxidation pathway between AOB and AOA (Walker *et al.*, 2010; Stahl and de la Torre, 2012), however, the similar range of nitrogen isotope effect has been reported for AOA and AOB. The nitrogen isotope effect of AOB was 14.2 ‰ to 38.2 ‰ (Delwiche and Steyn, 1970; Mariotti *et al.*, 1981; Yoshida, 1988; Casciotti *et al.*, 2003), and that of AOA was 22 ‰ to 40.1 ‰ (Santoro and Casciotti, 2011; Nishizawa *et al.*, 2016; Mooshammer *et al.*, 2020). During ammonia oxidation, dioxygen (O_2) is incorporated during the oxidation of ammonia to hydroxylamine (NH_2OH), while H_2O is incorporated during the oxidation of NH_2OH to NO_2^- (**Fig. 2.2**). During ammonia oxidation, three kinetic isotope effects are involved: (1) selection of hydroxylamine ($^{18}\varepsilon_{k,\ NH2OH}$), (2) incorporation of oxygen from O_2 ($^{18}\varepsilon_{k,\ O2}$) and (3) incorporation of oxygen from H_2O ($^{18}\varepsilon_{k,\ H2O,\ 1}$). In addition to those oxygen isotope effects, the fractional isotope exchange of NO_2^- oxygen atoms that has been catalyzed by ammonia-oxidizing microorganisms (x_{AOM}) were determined (Casciotti *et al.*, 2010). Until now, the combined oxygen isotope effect of incorporation of O_2 and H_2O ($^{18}\varepsilon_{k,\ O2} + {}^{18}\varepsilon_{k,\ H2O,1}$) and isotope exchange ($x_{AOM}$) were reported for AOB ($^{18}\varepsilon_{k,\ O2} + {}^{18}\varepsilon_{k,\ H2O,1}$ = 17.9 ~ 37.6 ‰, x_{AOM} = 0.01 ~ 0.25 %)(Casciotti *et al.*, 2010) and AOA ($^{18}\varepsilon_{k,\ O2} + {}^{18}\varepsilon_{k,\ H2O,1}$ = 26 ‰, x_{AOM} = 0.46 %)(Nishizawa *et al.*, 2016). The (1) selection of hydroxylamine ($^{18}\varepsilon_{k,\ NH2OH}$) has not been determined so far.

NO_2^- oxidation ($NO_2^- \rightarrow NO_3^-$) is the second step in the nitrification, and it plays role in the regeneration of NO_3^- in the environment. The nitrogen isotope effects of NOB were inverse

kinetic isotope effect (- 20.6 ‰ ~ - 9.1 ‰), by which NO_2^- pool is depleted in ^{15}N (Casciotti, 2009; Buchwald and Casciotti, 2010; Jacob *et al.*, 2017). During NO_2^- oxidation, H_2O is incorporated (**Fig. 2.2**). Therefore, two oxygen isotope effects should be determined: (1) selection of NO_2^- ($^{18}\varepsilon_{k,\ NO2\text{-}}$) and (2) incorporation of oxygen from H_2O ($^{18}\varepsilon_{k,\ H2O,2}$). The oxygen isotope effect of NO_2^- oxidation ($^{18}\varepsilon_{k,\ NO2\text{-}}$) was also inverse kinetic isotope effect ranging from - 8.3 ‰ to - 0.7 ‰ (Buchwald and Casciotti, 2010). This unique N and O kinetic isotope effects of NO_2^- oxidation might help to better identify its role in the environment. The oxygen isotope effect of H_2O incorporation ($^{18}\varepsilon_{k,\ H2O,2}$) was determined to be 12.8‰ to 18.2‰ (Buchwald and Casciotti, 2010). In addition to those oxygen isotope effects, the fractional exchange of NO_2^- oxygen atoms that has been catalyzed by NOB (x_{NOB}) were determined to be 0.002 % ~ 0.015% (Buchwald and Casciotti, 2010).

The novel *Nitrospira* species were recently discovered, which can oxidize ammonia completely to NO_3^- (comammox; COMplete AMMonium OXidation)(Daims *et al.*, 2015; Van Kessel *et al.*, 2015). To date, both of nitrogen and oxygen isotope effects of commamox have not been reported.

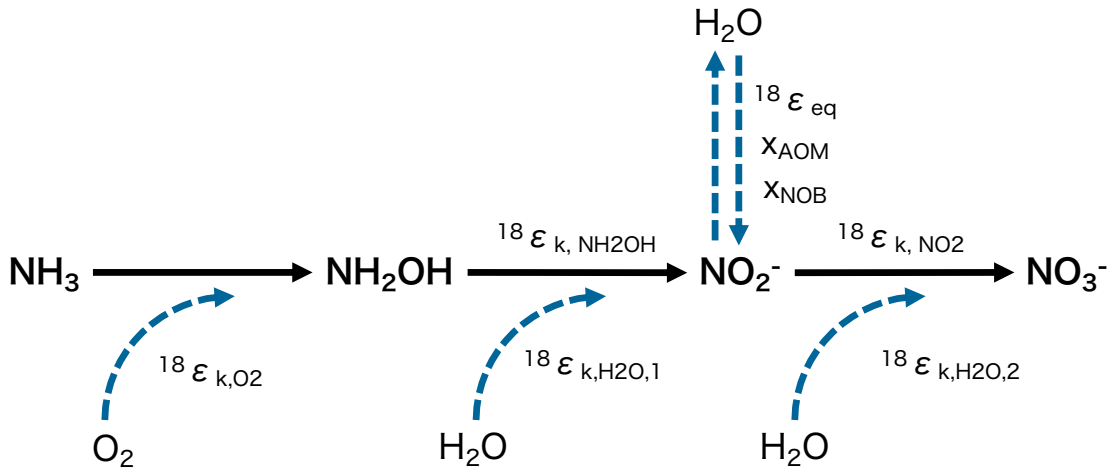

Figure. 2.2 Oxygen isotope systematics during nitrification

2.2.3 Denitrification

Denitrification is the stepwise reduction of nitrate to nitrite ($NO_3^- \rightarrow NO_2^-$), and then to nitric oxide (NO), nitrous oxide (N_2O), and dinitrogen (N_2). It removes bioavailable nitrogen from the environment. Nitrogen isotope effects of dissimilatory NO_3^- reduction to NO_2^- have been studied

with pure cultures of bacterial denitrifiers. The values of nitrogen isotope effect ranged from 5.4 to 29.5 ‰ (Delwiche and Steyn, 1970; Barford *et al.*, 1999; Granger *et al.*, 2006; Granger and Sigman, 2008; Kritee *et al.*, 2012). The variety of experiments were performed to determine nitrogen isotope effect of NO_3^- reduction. However, the information on oxygen isotope effects of dissimilatory nitrate reduction is still limited. The coupled N and O isotope effects were reported for two seawater strains and three freshwater strains ($^{18}\varepsilon$ = 4.8 ~ 22.8 ‰) (Granger and Sigman, 2008). The second step of denitrification is NO_2^- reduction. Compared to the information about NO_3^- reduction, there are a few reports about N and O isotope effect of NO_2^- reduction. NO_2^- reduction isotope effects are especially important when considering the nitrogen cycling in oceanic oxygen minimum zones (ODZs) where NO_2^- accumulated (Martin and Casciotti, 2016). NO_2^- reduction showed nitrogen isotope effect from 8.0 to 22.0 ‰ (Bryan *et al.*, 1983; Martin and Casciotti, 2016) and oxygen isotope effect from 2.0 to 6.0 ‰ (Martin and Casciotti, 2016). The nitrogen and oxygen isotope effect of N_2O reduction to N_2 was only reported with pure cultures of bacterial denitrifier and soil incubation. N_2O reduction showed nitrogen isotope effect from 1.8 to 12.9 ‰ (Barford *et al.*, 1999; Ostrom *et al.*, 2007) and oxygen isotope effect from 5.1 to 25.1‰ (Ostrom *et al.*, 2007).

2.2.4 Anammox

Anaerobic ammonium oxidation (anammox) and denitrification are the two major sinks of fixed nitrogen in the ocean. Anammox bacteria oxidize NH_4^+ directly to N_2 gas with NO_2^- as the terminal electron acceptor in the absence of oxygen, and NO_2^- is concomitantly oxidized to NO_3^-. The N isotope effect associated with anammox metabolism was determined only for one of freshwater anammox strains, "*Ca.* Kunenia stuttgartiensis", to date (Brunner *et al.*, 2013). The O isotope effect ($^{18}\varepsilon$) of anammox metabolism has never been determined so far. The nitrogen isotope effect of ammonium oxidation was from 23.5 to 29.1 ‰. The nitrogen isotope effect of NO_2^- reduction was 16.0 ‰. Interestingly, the NO_2^- oxidation of anammox expressed inverse kinetic isotope effect ($^{15}\varepsilon$= -31.1 ‰) as same as nitrite-oxidizing bacteria (Brunner *et al.*, 2013).

Table 1 Nitrogen isotope effects for microbial processes

Process	Reaction process	$^{15}\varepsilon$	References
N fixation	$N_2 + 8H \rightarrow NH_3 + H_2$	−3.7 ～ 3.9	(1)-(4)
Aerobic Ammonia oxidation (AOB)	$NH_3 \rightarrow NO_2^-$	14.2 ~ 38.2	(2), (5)-(7)
Aerobic Ammonia oxidation (AOA)	$NH_3 \rightarrow NO_2^-$	22 ~ 40.1	(8)-(10)
Nitrite oxidation	$NO_2^- \rightarrow NO_3^-$	−20.6 ~ −9.1	(11)-(13)
Dissimilatory nitrate reduction	$NO_3^- \rightarrow NO_2^-$	5.9 ~29.5	(2), (14)-(17)
Dissimilatory nitrate reduction	$NO_2^- \rightarrow NO$	8.0 ~ 22.0	(18), (19)
Nitrous oxide reduction	$N_2O \rightarrow N_2$	1.8 ~12.9	(14), (20)
	$NH_4^+ \rightarrow N_2$	23.5 ~ 29.1	
Anammox	$NO_2^- \rightarrow N_2$	16.0	(21)
	$NO_2^- \rightarrow NO_3^-$	-31.1	

References

(1) Hoering and Ford, 1960
(2) Delwiche and Steyn, 1970
(3) Yamazaki et al., 1987
(4) Bauersachs et al., 2009
(5) Mariotti et al., 1981
(6) Yoshida 1988
(7) Casciotti et al., 2003
(8) Santro and Casciotti, 2011
(9) Nishizawa et al., 2016
(10) Mooshammer et al., 2020
(11) Casciotti, 2009
(12) Buchwald and Casciotti 2010
(13) Jacob et al., 2017
(14) Barford et al., 1999
(15) Granger et al., 2006
(16) Granger and Sigman, 2008
(17) Kritee et al., 2012
(18) Bryan et al., 1983
(19) Martin and Casciotti, 2016
(20) Ostrom et al., 2007
(21) Brunner et al., 2013

Table 2 Oxygen isotope effects for microbial processes

Process	Reaction process	Description	$^{18}\varepsilon$	References
Aerobic Ammonia oxidation (AOB)	$NH_3 \rightarrow NO_2^-$	$^{18}\varepsilon_{k,\,O2} + {}^{18}\varepsilon_{k,\,H2O,1}$	17.9 ~ 37.6	(1)
Aerobic Ammonia oxidation (AOA)	$NH_3 \rightarrow NO_2^-$	$^{18}\varepsilon_{k,\,O2} + {}^{18}\varepsilon_{k,\,H2O,1}$	26	(2)
Nitrite oxidation	$NO_2^- \rightarrow NO_3^-$	$^{18}\varepsilon_{k,\,NO2-}$	−8.3 ~ − 0.7	(3)
		$^{18}\varepsilon_{k,\,O2} + {}^{18}\varepsilon_{k,\,H2O,1}$	12.8 ~ 18.2	
Dissimilatory nitrate reduction	$NO_3^- \rightarrow NO_2^-$	$^{18}\varepsilon_{(NO3- \rightarrow NO2-)}$	4.8 ~ 22.8	(4)
Dissimilatory nitrate reduction	$NO_2^- \rightarrow NO$	$^{18}\varepsilon_{(NO2- \rightarrow NO)}$	2.0 ~ 6.0	(5)
Nitrous oxide reduction	$N_2O \rightarrow N_2$	$^{18}\varepsilon_{(N2O \rightarrow N2)}$	5.1 ~ 25.1	(6)

References

(1) Casciotti et al., 2010
(2) Nishizawa et al., 2016
(3) Buchwald and Casciotti, 2010
(4) Granger and Sigman, 2008
(5) Martin and Casciotti, 2016
(6) Ostrom et al., 2007

2.3. Physiological factors affecting on expressed isotope effect

In order to interpret natural abundance N and O isotopic distributions in the environment and make experimental strategy to analyze isotope effect, physiological factors affecting on expressed isotope effects should be known. The influence of the following five physiological factors: pH, substrate concentration, temperature, species difference, and oxygen partial pressure were discussed (**Table 3**).

Table 3 Summary of relationship between physiological factors and isotope effects of N cycle-related microbial processes

Processes / Factors	N_2 fixation	Nitrification			Denitrification		Anammox
		AOB	AOA	NOB	$NO_3^- \rightarrow NO_2^-$	$NO_2^- \rightarrow N_2$	
pH			○ (1)				
Substrate concentration & reaction rate		▲ (2), (3)	▲(4)	○ (5)	○ (6)	○ (7)	
Temperature	▲ (8)	○ (9)	○ (1), (4)			○ (10)	
Species difference	▲(11)	○ (3), (9)	○ (1), (4)	○ (5)	○ (12), (13)	○ (14)	
Partial pressure of oxygen	−	△ (15)			−	−	−

○ Cause isotope effect difference, ▲ No clear relationship, − Not applicable

References

(1) Nishizawa et al., 2016
(2) Mariotti et al., 1981
(3) Casciotti et al., 2003
(4) Santro and Casciotti 2011
(5) Buchwald and Casciotti, 2010
(6) Kritee et al., 2012
(7) Bryan et al., 1983
(8) Bauersachs et al., 2009
(9) Casciotti et al., 2010
(10) Mariotti et al., 1982
(11) Bauersachs et al., 2009
(12) Granger and Sigman, 2008
(13) Treibergs and Granger, 2017
(14) Martin and Casciotti, 2016
(15) Buchwald et al., 2012

2.3.1 Initial substrate concentration and reaction rate

The effects of initial substrate concentration and reaction rate were widely examined for nitrification and denitrification. During ammonia oxidation, initial ammonium concentrations which ranged from 500 μM and 25 mM did not cause variation of nitrogen isotope effects of *N. europaea* (Mariotti *et al.*, 1981). Changes of initial concentration from 5 μM to 1000 μM also showed no change of nitrogen isotope effect of *N. europaea.* There was no clear relationship between rates of ammonia oxidation and nitrogen isotope effect (Casciotti *et al.*, 2003). The range of nitrogen isotope effect of AOA was large (22 to 40.1‰) and the physiological reason was unknown (Santoro and Casciotti, 2011; Nishizawa *et al.*, 2016). However, unbalanced growth could lead to accumulation of intermediate products in multi-step oxidation pathway and lead to larger errors of nitrogen isotope

effects. At high initial ammonium concentration (25-77 μM), the value of $^{15}\varepsilon_{NH3}$ was constant. On the other hand, at low initial ammonium concentration the $^{15}\varepsilon_{NH3}$ values were more variable. The direct relationship between initial substrate concentration and $^{15}\varepsilon_{NH3}$ could not be observed (Santoro and Casciotti, 2011). The nitrogen and oxygen isotope effects for NO_2^- oxidation by *N. mobilis* were smaller at lower initial concentrations, when the initial NO_2^- concentration was varied from 5 to 500 μM (Buchwald and Casciotti, 2010).

The relationships between N isotope effect and cell specific NO_3^- reduction rate was examined by changing initial NO_3^- concentration from 15 to 800 μM by three strains : *Paracoccus denitrificans, Pseudomonas chlororaphis* and *Marinobacter sp.* (Kritee *et al.*, 2012). For all three species, $^{15}\varepsilon$ of NO_3^- reduction were smaller when the cell specific NO_3^- reduction rates were low (Kritee et al. 2012). As for NO_2^- reduction, the observed N isotope effect was increased linearly with velocity (as a fraction of maximum velocity) when the NO_2^- concentration was varied (between 140 μM and 860 μM) (Bryan *et al.*, 1983).

2.3.2 pH

Nitrogen isotope effects were analyzed in both continuous culture and batch culture of Thermophilic *Thaumarchaeota*, "*Ca.* Nitrosocaldus."(Nishizawa *et al.*, 2016). The nitrogen isotope effects for ammonia oxidation ($^{15}\varepsilon_{k,\ \Sigma NH3/NO2-}$) were 24.7 ‰ ± 2.1 ‰ in the batch culture experiments (pH = 8.2 ~ 8.6) and 32.0 ‰ ± 1.4 ‰ in the continuous-culture experiments (pH = 8.0). The ambient pH affects the NH_3/NH_4^+ ratio. This 7 ‰ difference might be attributed to the effect of ambient pH on the kinetics of a rate-limiting step in ammonia oxidation (Nishizawa *et al.*, 2016).

2.3.3 Temperature

The higher temperature would promote greater NO_2^- oxygen isotope exchange with intracellular water. Therefore, The value of x_{AOM} of thermophilic "*Ca.* Nitrosocaldus" (x_{AOM} = 0.46 ± 0.14 at 70°C) (Nishizawa *et al.*, 2016) was higher than those of marine AOA (x_{AOM}= 0.08 at 22-23°C) (Santoro and Casciotti, 2011) and several mesophilic AOB strains (0.01 ~ 0.25 at 23°C) (Casciotti *et al.*, 2010). The temperature dependence of the isotope effect of NO_2^- reduction to N_2O by denitrifier was investigated, and weaker isotope effects were observed by increasing reaction rate at higher temperature (Mariotti *et al.*, 1982). The nitrogen isotope effect of biological N_2 fixation by *Cyanobacterium Anabaena* was not significantly changed by increasing temperature (Bauersachs *et*

al., 2009).

2.3.4 Species level difference

Several pure culture species were used to analyze the N and O isotope effect. The species level differences are discussed in terms of phylogeny, types of enzyme and structure of enzyme.

Nitrogen fixation

The nitrogen isotope effects of bacterial nitrogen fixation were not significantly different among cultures (Bauersachs *et al.*, 2009).

Ammonia oxidation

The range of N isotope effects for ammonia oxidation of five AOB strains : *Nitrosomonas europaea*, *Nitrosomonas eutropha, Nitrosospira tenuis*, *Nitrosomonas* sp. C-113a and *Nitrosomonas marina* were measured (14.2 ~ 38.2 ‰)(Casciotti et al., 2003). Similarities of observed $^{15}\varepsilon$ might relate to the similarities in amino acid sequence for the α-subunit of ammonia monooxygenase (*amoA*)(Casciotti *et al.*, 2003).

The oxygen isotope effects for four AOB strains : *Nitrosomonas* sp. C-113a, *Nitrosococcus oceani*, *Nitrosospira briensis* and *Nitrosomonas europaea* were determined (Casciotti *et al.*, 2010). Combined oxygen isotope effect ($^{18}\varepsilon_{k,\,O2} + {}^{18}\varepsilon_{k,\,H2O,1}$) for oxygen atom incorporation from O_2 and H_2O were estimated. Among four AOB strains, the *Nitrosomonas* species had similarly low combined oxygen isotope effects (+17.9% and +19.3%), while *N. briensis* and *N. oceani* had larger combined oxygen isotope effects (+30.3% and +37.6%, respectively). However, the reason for the differences among species was not known (Casciotti *et al.*, 2010).

Nitrite oxidation

The N and O isotope effects of NO_2^- oxidation were measured for four NOB strains : *Nitrococcus mobilis*, *Nitrobacter* sp. Nb 297, *Nitrobacter* sp. Nb 355 and *Nitrospira marina* (Buchwald and Casciotti, 2010). The nitrogen and oxygen isotope effects for NO_2^- oxidation were similar in *N. mobilis* and *Nitrobacter* species ($^{15}\varepsilon_{k,NO2}$ = -20.2 ~ -20.6 ‰, $^{18}\varepsilon_{k,\,NO2}$ = -8.2 ~ -6.5 ‰). However, N and O isotope effects were smaller in *N. marina*($^{15}\varepsilon_{k,NO2}$ = -9.1‰, $^{18}\varepsilon_{k,\,NO2}$ = -1.3‰). These differences could be related to the location of NO_2^- oxidation or differences in active sites of

the nitrite oxidoreductase (Nxr) (Buchwald and Casciotti, 2010).

Denitrification ($NO_3^- \rightarrow NO_2^-$)

Nitrogen and oxygen isotope effects of four denitrifiers including two seawater strains: *Pseudomonas stutzeri, Ochrobactrum* sp., and two freshwater strains: *Paracoccus denitrificans, Pseudomonas chlororaphis*) were determined (Granger and Sigman, 2008). The nitrogen isotope effects were determined to be in the range between 5‰ and 25‰. Similarly, the oxygen isotope effects were ranged between 5‰ and 23‰. The N and O isotope effects were not dependent on species differences. Between marine species and freshwater species, distinct differences could not be observed. The linear regressions of $\delta^{18}O$ and $\delta^{15}N$ ($\Delta\delta^{18}O$:$\Delta\delta^{15}N$) yielded the slopes that were consistently close to 1. On the other hand, an aerobic denitrification by *Rhodobacter sphaeroides* showed a narrower range of nitrogen and oxygen isotope effects than the four denitrifiers. The value of $^{15}\varepsilon$ ranged between 13‰ to 20‰, and the value of $^{18}\varepsilon$ ranged between 8‰ and 13‰. *R. sphaeroides* showed $\Delta\delta^{18}O$:$\Delta\delta^{15}N = 0.62 \pm 0.02$, which was clearly distinct from the value of the four denitrifiers ($\Delta\delta^{18}O$:$\Delta\delta^{15}N = 1$).

Denitrification ($NO_2^- \rightarrow NO$)

The nitrogen and oxygen isotope effect for NO_2^- reduction was analyzed for three strains of denitrifier carrying the copper-containing nitrite reductase (Cu-NIR): *Pseudomonas aeruginosa* (PA01), *Pseudomonas chlororaphis* (ATCC 43928), and *Pseudomonas stutzeri* (ATCC 14405), and three strains of denitrifier carrying the cytochrome cd_1-containing nitrite reductase (Fe-NIR): *Pseudomonas aureofaciens* (ATCC 13985), *Achromobacter xylosoxidans* (ATCC 15173), and *Ochrobactrum* sp. strain 3CB4 (Martin and Casciotti, 2016). The growth conditions were similar for all cultures (initial NO_2^- concentrations, pH and cell densities). The $^{15}\varepsilon$ and $^{18}\varepsilon$ of the three strains carrying the Cu-NIR were 22 ± 2 ‰ and 2 ± 2 ‰, respectively. In contrast, $^{15}\varepsilon$ and $^{18}\varepsilon$ of the three strains carrying the Fe-NIR were 8 ± 2 ‰ and 6 ± 2 ‰, respectively. This difference in isotope effects could arise from the distinct mechanisms for binding NO_2^- at the active site of the respective enzymes (Martin and Casciotti, 2016).

2.3.5 Partial pressure of oxygen

During nitrification, the biochemical sources of oxygen atoms are dioxygen and water.

Dioxygen is incorporated during the oxidation of ammonia to hydroxylamine (NH_2OH), while water is incorporated during the oxidation of hydroxylamine to NO_2^-. Thus, partial pressure of oxygen (pO_2) could be valuable factor affecting oxygen isotope effect of ammonia oxidation, and two levels of partial pressure of oxygen (pO_2) were tested: 20.265 kPa (air) and 0.811 kPa (Casciotti *et al.*, 2010). Lower pO_2 (0.811 kPa) slowed ammonia oxidation rate for all AOB strains: *Nitrosomonas* sp. C-113a, *Nitrosomonas* europaea, *Nitrosococcus* oceani and *Nitrosospira* briensis. However, decreased oxygen isotope effects were observed only in *Nitrosomonas* species and there were no significant changes in the isotope effects for other species. (Casciotti *et al.*, 2010)

2.4 References

Barford, C.C., Montoya, J.P., and Altabet, M.A. (1999) Steady-State nitrogen isotope effects of N_2 and N_2O production in *Paracoccus denitrificans*. *Appl Environ Microbiol* 65: 989–994.

Bauersachs, T., Schouten, S., Compaore, J., Wollenzien, U., Stal, L.J., and Sinninghe Damste, J.S. (2009) Nitrogen isotopic fractionation associated with growth on dinitrogen gas and nitrate by cyanobacteria. *Limnol Oceanogr* 54: 1403–1411.

Brandes, J.A. and Devol, A.H. (2002) A global marine-fixed nitrogen isotopic budget: Implications for Holocene nitrogen cycling. *Global Biogeochem Cycles* 16: 1120.

Brunner, B., Contreras, S., Lehmann, M.F., Matantseva, O., Rollog, M., Kalvelage, T., et al. (2013) Nitrogen isotope effects induced by anammox bacteria. *Proc Natl Acad Sci* 110: 18994–18999.

Bryan, B.A., Shearer, G., Skeeters, J.L., and Kohl, D.H. (1983) Variable expression of the nitrogen isotope effect associated with denitrification of nitrite. *J Biol Chem* 258: 8613–8617.

Buchwald, C. and Casciotti, K.L. (2010) Oxygen isotopic fractionation and exchange during bacterial nitrite oxidation. *Limnol Oceanogr* 55: 1064–1074.

Buchwald, C., Santoro, A.E., McIlvin, M.R., and Casciotti, K.L. (2012) Oxygen isotopic composition of nitrate and nitrite produced by nitrifying cocultures and natural marine assemblages. *Limnol Oceanogr* 57: 1361–1375.

Casciotti, K.L. (2009) Inverse kinetic isotope fractionation during bacterial nitrite oxidation. *Geochim Cosmochim Acta* 73: 2061–2076.

Casciotti, Karen L (2016) Nitrite isotopes as tracers of marine N cycle processes. *Phil Trans R Soc A* 374: 20150295.

Casciotti, Karen L. (2016) Nitrogen and oxygen isotopic studies of the marine nitrogen cycle. *Ann Rev Mar Sci* 8: 379–407.

Casciotti, K.L., Bohlke, J.K., McIlvin, M.R., Mroczkowski, S.J., and Hannon, J.E. (2007) Oxygen isotopes in nitrite: Analysis, calibration, and equilibration. *Anal Chem* 79: 2427–2436.

Casciotti, K.L., McIlvin, M., and Buchwald, C. (2010) Oxygen isotopic exchange and fractionation

during bacterial ammonia oxidation. *Limnol Oceanogr* 55: 753–762.

Casciotti, K.L., Sigman, D.M., Hastings, M.G., Bohlke, J.K., and Hilkert, A. (2002) Measurement of the oxygen isotopic composition of nitrate seawater and freshwater using the dentirifier method. *Anal Chem* 74: 4905-4912.

Casciotti, K.L., Sigman, D.M., and Ward, B.B. (2003) Linking diversity and stable isotope fractionation in ammonia-oxidizing bacteria. *Geomicrobiol J* 20: 335–353.

Daims, H., Elena, V., Palatinszky, M., Vierheilig, J., Bulaev, A., Kirkegaard, R.H., et al. (2015) Complete nitrification by *Nitrospira* bacteria. *Nature* 528: 504–509.

Delwiche, C.C. and Steyn, P.L. (1970) Nitrogen Isotope Fractionation in Soils and Microbial Reactions. *Environ Sci Technol* 4: 929–935.

Deutsch, C., Key, R.M., Sarmiento, J.L., and Ganachaud, A. (2001) Denitrification and N_2 fixation in the Pacific Ocean. *Global biogeochemical cycles* 15: 483–506.

Deutsch, C., Sigman, D.M., Thunell, R.C., Meckler, A.N., and Haug, G.H. (2004) Isotopic constraints on glacial/interglacial changes in the oceanic nitrogen budget. *Global Biogeochem Cycles* 18: GB4012.

Granger, J. and Sigman, D.M. (2008) Nitrogen and oxygen isotope fractionation during dissimilatory nitrate reduction by denitrifying bacteria. *Limnol Oceanogr* 53: 2533–2545.

Granger, J., Sigman, D.M., Prokopenko, M.G., Lehmann, M.F., and Tortell, P.D. (2006) A method for nitrite removal in nitrate N and O isotope analyses. *Limnol Oceanogr Methods* 4: 205–212.

Hoering, T.C. and Ford, H.T. (1960) The isotope effect in the fixation of nitrogen by *Azotobacter*. *J Am Chem Soc* 82: 376–378.

Jacob, J., Nowka, B., Merten, V., Sanders, T., Spieck, E., and Dähnke, K. (2017) Oxidation kinetics and inverse isotope effect of marine nitrite-oxidizing isolates. *Aquat Microb Ecol* 80: 289–300.

Kendall, C., Elliott, E.M., and Wankel, S.D. (2007) Tracing anthropogenic inputs of nitrogen to ecosystems. In *Stable Isotopes in Ecology and Environmental Science*. 375–449.

Van Kessel, M.A.H.J., Speth, D.R., Albertsen, M., Nielsen, P.H., Op Den Camp, H.J.M., Kartal, B., et al. (2015) Complete nitrification by a single microorganism. *Nature* 528: 555–559.

Kritee, K., Sigman, D.M., Granger, J., Ward, B.B., Jayakumar, A., and Deutsch, C. (2012) Reduced isotope fractionation by denitrification under conditions relevant to the ocean. *Geochim Cosmochim Acta* 92: 243–259.

Lehmann, M.F., Sigman, D.M., and Berelson, W.M. (2004) Coupling the $^{15}N/^{14}N$ and $^{18}O/^{16}O$ of nitrate as a constraint on benthic nitrogen cycling. *Mar Chem* 88: 1–20.

Mariotti, A., Germon, J.C., and Leclerc, A. (1982) Nitrogen isotope fractionation associated with the $NO_2^- \rightarrow N_2O$ step of denitrification in soils. *Can J Soil Sci* 62: 227–239.

Mariotti, A., J. C. Germon, P. Hubert, Kaiser, P., Letolle, R., Tardieux, A., and Tardieux, P. (1981) Experimental determination of nitrogen kinetic isotope fractionation: Some principles;

illustration for the denitrification and nitrification processes. *Plant Soil* 430: 413–430.

Martin, T.S. and Casciotti, K.L. (2016) Nitrogen and oxygen isotopic fractionation during microbial nitrite reduction. *Limnol Oceanogr* 61: 1134–1143.

McIlvin, M.R. and Altabet, M.A. (2005) Chemical conversion of nitrate and nitrite to nitrous oxide for nitrogen and oxygen isotopic analysis in freshwater and seawater. *Anal Chem* 77: 5589–5595.

Mooshammer, M., Alves, R.J.E., Bayer, B., Melcher, M., Stieglmeier, M., Jochum, L., et al. (2020) Nitrogen isotope fractionation during Archaeal ammonia oxidation: Coupled estimates from measurements of residual ammonium and accumulated nitrite. *Front Microbiol* 11: 1–9.

Nishizawa, M., Sakai, S., Konno, U., Nakahara, N., Takaki, Y., Saito, Y., et al. (2016) Nitrogen and oxygen isotope effects of ammonia oxidation by thermophilic *Thaumarchaeota* from a geothermal water stream. *Appl Environ Microbiol* 82: AEM.00250-16.

Ostrom, N.E., Piit, A., Sutka, R., Ostrom, P.H., Grandy, A.S., Huizinga, K.M., and Robertson, G.P. (2007) Isotopologue effects during N_2O reduction in soils and in pure cultures of denitrifiers. *J Geophys Res Biogeosciences* 112: 1–12.

Santoro, A.E. and Casciotti, K.L. (2011) Enrichment and characterization of ammonia-oxidizing archaea from the open ocean: phylogeny, physiology and stable isotope fractionation. *ISME J* 5: 1796–1808.

Sigman, D.M., Casciotti, K.L., Andreani, M., Barford, C., Galanter, M., and Bhlke, J.K. (2001) A bacterial method for the nitrogen isotopic analysis of nitrate in seawater and freshwater. *Anal Chem* 73: 4145–4153.

Sigman, D.M., Granger, J., DiFiore, P.J., Lehmann, M.M., Ho, R., Cane, G., and van Geen, A. (2005) Coupled nitrogen and oxygen isotope measurements of nitrate along the eastern North Pacific margin. *Global Biogeochem Cycles* 19: 1–14.

Stahl, D.A. and de la Torre, J.R. (2012) Physiology and diversity of ammonia-oxidizing Archaea. *Annu Rev Microbiol* 66: 83–101.

Walker, C.B., De La Torre, J.R., Klotz, M.G., Urakawa, H., Pinel, N., Arp, D.J., et al. (2010) Nitrosopumilus maritimus genome reveals unique mechanisms for nitrification and autotrophy in globally distributed marine crenarchaea. *Proc Natl Acad Sci U S A* 107: 8818–8823.

Wankel, S.D., Kendall, C., Pennington, J.T., Chavez, F.P., and Paytan, A. (2007) Nitrification in the euphotic zone as evidenced by nitrate dual isotopic composition: Observations from Monterey Bay, California. *Global Biogeochem Cycles* 21: 1–13.

Yamazaki, T., Yoshida, N., Wada, E., and Matsuo, S. (1987) N_2O reduction by *Azotobacter vinelandii* with emphasis on kinetic nitrogen isotope effects. *Plant Cell Physiol* 28: 263–271.

Yoshida, N. (1988) ^{15}N-depleted N_2O as a product of nitrification. *Nature* 335: 528–529.

Chapter 3

Dual nitrogen and oxygen isotope effect during anaerobic ammonium oxidation by anammox bacteria in continuous enrichment culture experiments

Abstract

Natural abundance of stable nitrogen (N) and oxygen (O) isotopes are invaluable biogeochemical tracers for assessing the N transformations in the environment. To fully exploit these tracers, the N and O isotope effects ($^{15}\varepsilon$ and $^{18}\varepsilon$) associated with the respective nitrogen transformation processes must be known. However, the N and O isotope effects of anaerobic ammonium oxidation (anammox), one of the major fixed N sinks and NO_3^- producers, are not well known. Here, we report the dual N and O isotope effects associated with anammox by three different anammox bacteria including "*Ca.* Scalindua japonica", a putative marine species, which were measured in continuous enrichment culture experiments. All three anammox species yielded similar N isotope effects of NH_4^+ oxidation to N_2 ($^{15}\varepsilon_{NH4\rightarrow N2}$) ranging from 30.9‰ to 32.7‰ and inverse kinetic isotope effects of NO_2^- oxidation to NO_3^- ($^{15}\varepsilon_{NO2\rightarrow NO3}$ = -45.3‰ to -30.1‰). In contrast, $^{15}\varepsilon_{NO2\rightarrow N2}$ (NO_2^- reduction to N_2) were significantly different among three species, which is probably because individual anammox bacteria species possess different types of nitrite reductase. We also report the combined O isotope effects for NO_2^- oxidation ($^{18}E_{NO2\rightarrow NO3}$) by anammox bacteria. These obtained dual N and O isotopic effects could provide significant insights into the contribution of anammox bacteria to the fixed N loss and NO_2^- reoxidation (N recycling) in various natural environments.

3.1. Introduction

Both nitrogen (N) and oxygen (O) isotopes of fixed nitrogen compounds (i.e., ammonia, nitrite, and nitrate) are fractionated during their microbial production and consumption processes comprising the global marine N cycle. Thus, measurements of nitrogen ($^{15}N/^{14}N$) and oxygen ($^{18}O/^{16}O$) isotope ratios of fixed nitrogen compounds have long been used as invaluable biogeochemical stable isotopic tracers to estimate the global marine N budget (Brandes and Devol, 2002; Sigman *et al.*, 2009). The dual N and O isotope analyses provide complementary signatures of co-occurring N transformation processes that could not be revealed by N isotope measurement alone (Casciotti, 2016). By convention, these stable isotope ratios are expressed in delta notation ($\delta^{15}N$ and $\delta^{18}O$) in per mille (‰) versus atmospheric N_2 (air) and Vienna Standard Mean Ocean Water (VSMOW): $\delta^{15}N = ([^{15}N/^{14}N]_{sample} / [^{15}N/^{14}N]_{air} - 1) \times 1{,}000$ and $\delta^{18}O = ([^{18}O/^{16}O]_{sample} / [^{18}O/^{16}O]_{VSMOW} - 1) \times 1{,}000$, respectively. To quantitatively assess the impacts of these processes on dissolved nitrogen species, the degree of isotope fractionation is quantified by the kinetic isotope effect, ε (‰) = $[(k_L / k_H) - 1] \times 1000$, where k_L / k_H is the ratio of the reaction rate constants between the light (k_L) and heavy (k_H) isotopically substituted substrates. The kinetic N and O isotope effects ($^{15}\varepsilon$ and $^{18}\varepsilon$, respectively) for key microbial processes provide the basis for interpretation of natural abundance N isotopic distributions in the ocean, freshwater, terrestrial and groundwater ecosystems.

The kinetic N and O isotope effects associated with microbial ammonium oxidation (Casciotti *et al.*, 2003, 2010; Santoro and Casciotti, 2011; Buchwald *et al.*, 2012; Nishizawa *et al.*, 2016), nitrite oxidation (Casciotti, 2009; Buchwald and Casciotti, 2010), dissimilatory nitrite reduction to nitric oxide (Martin and Casciotti, 2016), dissimilatory nitrate reduction (denitrification) (Granger et al., 2008; Kritee *et al.*, 2012) and assimilatory nitrate reduction (Granger *et al.*, 2010; Karsh *et al.*, 2012) have been determined for laboratory cultures of corresponding bacteria (**Fig. 3. 1**). These isotope effects vary depending on the microbial species (Granger and Sigman, 2008), enzymes (Martin and Casciotti, 2016), growth conditions and/or rates of reaction (Casciotti *et al.*, 2003). Furthermore, the coupled N and O isotope measurements of NO_x (nitrate and/or nitrite) have been performed in the North Pacific margin (e.g., Sigman *et al.*, 2005; Casciotti and McIlvin, 2007; Buchwald *et al.*, 2015), Hadal oceans (Nunoura *et al.*, 2015), and the Peru oxygen deficient zone (ODZ) (Casciotti *et al.*, 2013; Bourbonnais *et al.*, 2015; Hu *et al.*, 2016) to assess the regional N cycles. However, there is still

much uncertainty with regard to the N cycling processes, especially in ODZs because the isotope effects are not well known for all of the relevant processes.

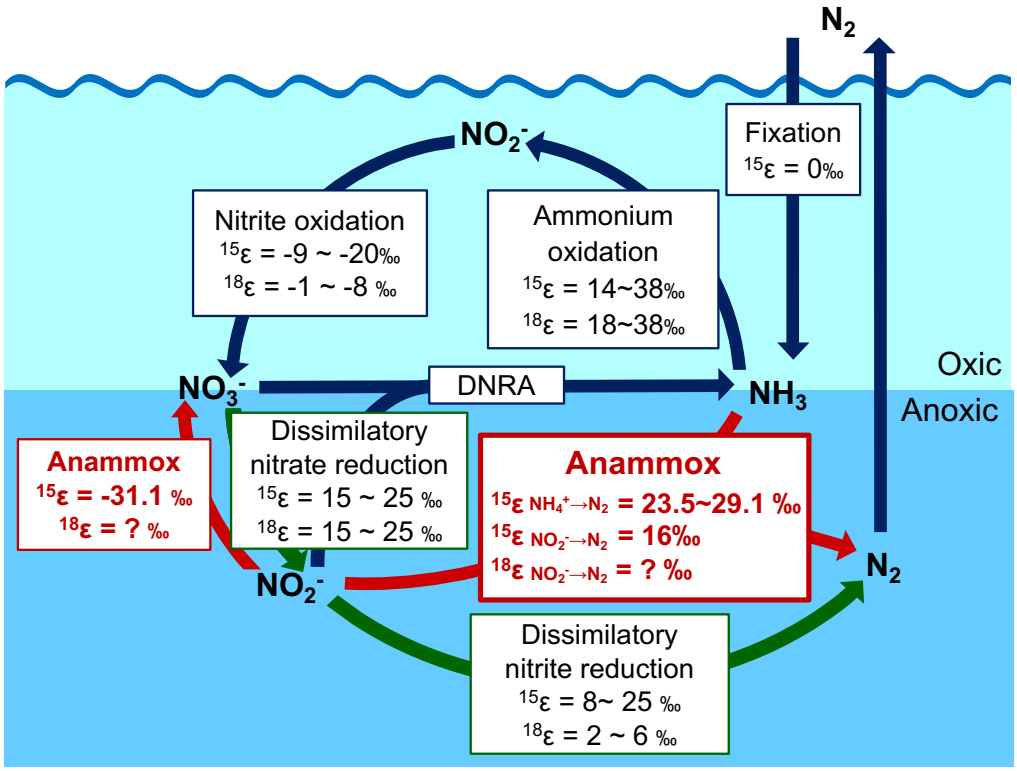

Figure 3.1 Marine microbial nitrogen cycle with the reported N and O isotope effects ($^{15}\varepsilon$ and $^{18}\varepsilon$, respectively) of key transformation processes. The O isotope effects of anammox have not been determined yet.

Anaerobic ammonium oxidation (anammox) and denitrification are the two major sinks of fixed nitrogen (N) in the ocean. It has been estimated that these microbial processes together remove 230-450 Tg N yr^{-1} from the global ocean (Codispoti, 2007; Gruber and Galloway, 2008), which is thought to occur mainly in oxygen deficient water columns and sediments. Furthermore, anammox bacteria also contribute to re-oxidation of nitrite to nitrate (i.e., recycling N), because they fix CO_2 into biomass with reducing equivalents generated from oxidation of nitrite to nitrate (Kartal *et al.*, 2013). Nitrate production by anammox bacteria significantly influences the nitrite and nitrate N and O isotope effects in freshwater and marine systems, which, however, has been overlooked so far (Granger and Wankel, 2016). Despite the

importance of anammox bacteria in the global N cycle (Kuypers *et al.*, 2003, 2005; Thamdrup *et al.*, 2006; Kalvelage *et al.*, 2013; Babbin *et al.*, 2017), the N isotope effect ($^{15}\varepsilon$) associated with anammox metabolism has been determined for only one freshwater anammox strain, "*Ca.* Kuenenia stuttgartiensis" (Brunner *et al.*, 2013). The kinetic O isotope effect ($^{18}\varepsilon$) of anammox metabolism has not yet been determined. Consequently, their impacts on the distributions of N and O isotopes in the natural environmets could not be addressed.

Five candidatus genera, '*Ca.* Brocadia' (Strous *et al.*, 1999), '*Ca.* Kuenenia' (Schmid *et al.*, 2000), '*Ca.* Scalindua' (Schmid *et al.*, 2003), '*Ca.* Anammoxoglobus' (Kartal, Rattray, *et al.*, 2007) and *'Ca.* Jettenia' (Quan *et al.*, 2008) and about 20 candidatus species have been tentatively identified to date. The genus '*Ca.* Scalindua' is halotolerant and the most abundant anammox bacteria found in marine environments (Awata et al., 2013). We therefore hypothesized that the nitrite and nitrate N and O isotope effects induced by different genera of anammox bacteria might be different since they are phylogenetically diverse and might possess different enzymes (e.g., nitrite reductase) and consequently different metabolic pathways (Oshiki *et al.*, 2016). Especially, the determination of isotope effects of marine anammox species, '*Ca.* Scalindua', is essential to better understand the natural abundance of stable isotope ratios (δ^{18}O and δ^{15}N) in the ocean.

Here we analyzed the N and O isotope effects ($^{15}\varepsilon$ and $^{18}\varepsilon$) of nitrite and nitrate associated with anammox metabolism by three anammox species: '*Ca.* S. japonica', '*Ca.* J. caeni', and '*Ca.* B. sinica' in continuous enrichment cultures. We found that species-dependent N and O isotope effects ($^{15}\varepsilon$ and $^{18}\varepsilon$), which could provide significant insights into the relative contribution of anammox bacteria to the fixed N loss and nitrite re-oxidation (recycling N) in various natural environments.

3. 2. Material and method

3.2.1 Continuous culture experiment

Free-living planktonic cultures of three anammox bacteria species were enriched and cultivated in 3 L membrane bioreactors (MBRs) equipped with a hollow fiber membrane module (pore size 0.1 µm, polyethylene) as previously described (Awata *et al.*, 2013; Oshiki *et al.*, 2013; Ali *et al.*, 2015)(**Fig. 3.2.1**). The pH was not controlled but was always between 7.9 - 8.0 for "*Ca*. S. japonica", 8.6 - 8.9 for "*Ca.* J. caeni", and 7.3 - 7.4 for "*Ca.* B. sinica", respectively. The temperature was controlled at 25°C for "*Ca*. S. japonica", 30°C for "*Ca.* J. caeni", and 37°C for "*Ca*. B. sinica", respectively. The details of reactor operation and culture preparation are given in **Figure 3.2.1**. Once the MBRs have reached a steady state (the concentrations of nitrogen compounds (NH_4^+, NO_2^-, and NO_3^-) in the effluents stabilized after about 2-month operation), three or four sub-samples of MBR influent and effluent (permeate) were taken. After sampling, pH was measured and immediately filtered using 0.2-µm cellulose acetate filter (Advantec) for concentration and isotopic measurements of NH_4^+, NO_2^- and NO_3^-.

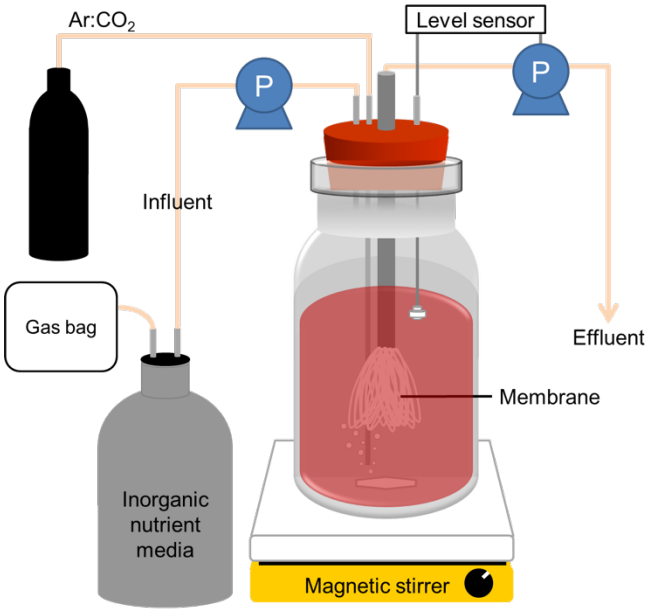

Fig. 3.2.1 Schematic drawing of membrane bioreactors (MBRs). The MBRs were equipped with a hollow-fiber membrane unit composed of 300 polyethylene tubes (0.1 μm-pore, 1-mm diam., 70-mm long tubes). A peristaltic pump MP-1000 (EYELA, Tokyo, Japan) was directly connected to the membrane unit. Water level in the MBR was controlled using a water level sensor (HL-S1A, ASONE, Japan). The MBR culture medium was continuously mixed using a magnetic stirrer working at 200 rpm. To maintain anoxic condition, a mixed gas (Ar: CO_2 = 95:5) was purged into the culture medium at a flowrate of 10 ml min^{-1}.

3.2.2 Sample preparation for isotopic analysis

After filtration, immediately samples were adjusted to pH 2 by adding 2M H_2SO_4 solution and then stored at -20°C until analysis for N isotope of NH_4^+ to prevent NH_4^+ from volatilizing. To analyze N and O isotope of NO_2^-, after filtration, immediately sample solution was adjusted to pH 12 by adding 2M NaOH solution and stored at -20°C until analysis to prevent O isotope exchange between NO_2^- and H_2O during sample storage. To analyze N and O isotope of NO_3^-, after filtration, if the concentration ratio of NO_2^- / NO_3^- was over 5%, NO_2^- in the sample solution was immediately removed by adding sulfamic acid (H_3NSO_3), because NO_2^- interferes with NO_3^- isotope analysis. The concentration of NO_2^- was measured with naphthylethylenediamine method (APHA *et al.*, 2012) to confirm NO_2^- was completely removed. We confirmed that NO_2^- was completely removed in all samples. Then, sample solution was adjusted to pH 8.5-9 by adding 2M NaOH solution and stored at -20°C until analysis.

3.2.3 Chemical analyses

The concentration of NH_4^+ was measured by the indophenol blue method (APHA *et al.*, 2012) with a multi-label plate reader (ARVO MX 1420-01J; PerkinElmer; Waltham, MA, USA). The NO_2^- concentration was measured by the naphthylethylenediamine method (APHA *et al.*, 2012). The concentration of NO_3^- was measured using ion chromatographs (IC-2010, TOSOH; Tokyo, Japan) equipped with a TSKgel IC-Anion HS column (TOSOH; Tokyo, Japan).

3.2.4 Isotope ratio analyses

NH_4^+ nitrogen isotope analyses were performed by using the ammonium diffusion method (Sigman *et al.*, 1997; Holmes *et al.*, 1998) and subsequently measured by a EA-IRMS (Flash EA1112, ConFlo IV interface, Delta plus Advantage; ThremoFinnigan). International and internal NH_4^+ isotopic standards, USGS25 ($\delta^{15}N$ = -30.4‰), USGS26 ($\delta^{15}N$ = 53.7‰), and IAEA-N-2 ($\delta^{15}N$ = 20.3‰) were used for the calibration. Replicate analyses yielded respective precision of 0.3‰ for $\delta^{15}N_{NH4+}$.

NO_2^- nitrogen and oxygen isotope ratios were measured by chemical conversion of NO_2^- to nitrous oxide (N_2O) with the azide method (McIlvin and Altabet, 2005). All samples and standards were exactly adjusted to same pH (pH=12) and salinity (0.5 M NaCl) as mentioned above. The N_2O was then analyzed in duplicate using a GC-IRMS (SerCon) with

in-house calibrated NO_2^- isotopic standards that were calibrated against N-23, N-7373 and N-10219 (Casciotti *et al.*, 2007); NO2-1 ($\delta^{15}N$ = -66.9 ‰, $\delta^{18}O$ = 27.0 ‰), NO2-2 ($\delta^{15}N$ = -64.8‰, $\delta^{18}O$ = 1.1‰), NO2-3 ($\delta^{15}N$ = -67.3‰, $\delta^{18}O$ = 20.3‰), NO2-4 ($\delta^{15}N$ = -68.4‰, $\delta^{18}O$ = 14.9‰), NO2-5 ($\delta^{15}N$ = 0.2‰, $\delta^{18}O$ = 20.2‰). Replicate analyses yielded respective precisions of 0.3‰ for $\delta^{15}N_{NO2-}$ and 0.5‰ for $\delta^{18}O_{NO2-}$, respectively.

NO_3^- nitrogen and oxygen isotope ratios were measured by microbial conversion of NO_3^- to N_2O with the denitrifier method (Sigman *et al.*, 2001; Casciotti *et al.*, 2002). N_2O was analyzed in triplicate using a GC-IRMS (SerCon) with international NO_3^- isotopic standards; IAEAN3 ($\delta^{15}N$ = 4.7‰, $\delta^{18}O$ = 25.6‰), USGS32 ($\delta^{15}N$ = 180‰, $\delta^{18}O$ = 25.7‰), USGS34 ($\delta^{15}N$ = -1.8‰, $\delta^{18}O$ = -27.9‰), and USGS35 ($\delta^{18}O$ = 57.5‰). Replicate analyses yielded respective precisions of 0.2‰ for $\delta^{15}N_{NO3-}$ and 1.0‰ for $\delta^{18}O_{NO3-}$, respectively.

3.2.5 Calculations of isotope effects

Anammox bacteria oxidize NH_4^+ directly to N_2 gas with NO_2^- as the terminal electron acceptor in the absence of oxygen, and NO_2^- is concomitantly oxidized to NO_3^- as shown in the following stoichiometric equation (Lotti *et al.*, 2014).

$$1NH_4^+ + 1.146NO_2^- + 0.071HCO_3^- + 0.057H^+ \rightarrow 0.986N_2 + 0.161NO_3^- + 0.071CH_{1.74}O_{0.31}N_{0.20} + 2.002H_2O$$

The continuous MBR system is considered as an open system with balanced input and two or three output fluxes (product(s) and residual substrate) (Fry, 2006). The N isotope effects were analyzed for the following redox reaction: (1) NH_4^+ oxidation to N_2, (2) NO_2^- reduction to N_2, and (3) NO_2^- oxidation to NO_3^-.

1) N isotope effect of NH_4^+ oxidation to N_2.

Ammonium (NH_4^+) was continuously fed into the MBR where NH_4^+ oxidation to N_2 ($NH_4^+ \rightarrow N_2$) occurs with fractionation ($^{15}\varepsilon_1$), and unused NH_4^+ exits without further fractionation (i.e., $^{15}\varepsilon_2 = 0$) (**Fig. 3.2.2. A**). The isotope compositions of product N_2 ($\delta_{product}$) and residual NH_4^+ (δ_{RS}) at steady state can be given simply by subtracting ε fractionations from the isotope composition of intermediate pool (δ_p) (Fry, 2006).

$$\delta_{product} = \delta_p - {}^{15}\varepsilon_1 \quad \cdots \text{eq. (1)}$$

$$\delta_{RS} = \delta_p - {}^{15}\varepsilon_2 = \delta_p \quad (\text{when } {}^{15}\varepsilon_2 = 0) \quad \cdots \text{eq. (2)}$$

The steady state isotope mass balance can be described as follow;

$$\delta_{IN} = f\,\delta_{product} + (1 - f)\,\delta_{RS}$$

$$\delta_{IN} = f\,(\delta_p - {}^{15}\varepsilon_1) + (1 - f)\,(\delta_p - {}^{15}\varepsilon_2)$$

$$\delta_p = \delta_{IN} + f\,{}^{15}\varepsilon_1 \quad \cdots \text{eq. (3)}$$

where f is the fraction of NH_4^+ consumed at steady state.

Therefore, from equations (2) and (3), the kinetic isotope effects associated with NH_4^+ oxidation to N_2 ($^{15}\varepsilon_1$) can be determined as follows, when δ_{IN}, δ_{RS}, and f are measured experimentally:

$$^{15}\varepsilon_1 = (\delta_{RS} - \delta_{IN}) / f \quad \cdots \text{eq. (4)}$$

$$f = (C_{in\text{-}NH4+} - C_{out\text{-}NH4+}) / C_{in\text{-}NH4+}$$

where $C_{in\text{-}NH4+}$ and $C_{out\text{-}NH4+}$ are the NH_4^+ concentrations of MBR influent and effluent, respectively.

2) N isotope effects of NO_2^- reduction and oxidation.

Nitrite (NO_2^-) is also continuously fed together with NH_4^+ into the MBR where NO_2^- reduction to N_2 and NO_2^- oxidation to NO_3^- concomitantly occur with fractionations (defined as $^{15}\varepsilon_3$ and $^{15}\varepsilon_5$, respectively), and unused residual NO_2^- exits the MBR without further fractionation (i.e., $^{15}\varepsilon_4 = 0$) (**Fig. 3.2.2. B**). The isotope compositions of product N_2 ($\delta_{product1}$), product NO_3^- ($\delta_{product2}$), and residual NO_2^- (δ_{RS}) at steady state can be given simply by subtracting ε fractionations from the isotope composition of intermediate pool (δ_p):

$$\delta_{product1} = \delta_p - {}^{15}\varepsilon_3 \quad \cdots \text{eq. (5)}$$

$$\delta_{RS} = \delta_p - {}^{15}\varepsilon_4 = \delta_p \quad ({}^{15}\varepsilon_4 = 0) \quad \cdots \text{eq. (6)}$$

$$\delta_{product2} = \delta_p - {}^{15}\varepsilon_5 \quad \cdots \text{eq. (7)}$$

Now it is assumed that input flux is 1 and output flux is divided into α, β and γ (**Fig. 3.2.2. B**)

$$1 = \alpha + \beta + \gamma \quad \cdots \text{eq. (8)}$$

where α is the fraction of NO_2^- converted to N_2. It is represented by NH_4^+ consumption, because NH_4^+ and NO_2^- react at 1 : 1 ratio to form N_2 (excluding NO_2^- oxidation to NO_3^- from the overall anammox reaction).

$$\alpha = (C_{in\text{-}NH4+} - C_{out\text{-}NH4+}) / C_{in\text{-}NO2-} \quad \cdots \text{eq. (9)}$$

β is the fraction of residual NO_2^- (unused) at steady state, which is experimentally determined.

$$\beta = C_{out\text{-}NO2\text{-}} / C_{in\text{-}NO2\text{-}} \quad \cdots \text{eq. (10)}$$

γ is the fraction of NO_2^- oxidized to NO_3^-. Although γ could be determined from the NO_3^- concentration in MBR effluent at steady state, the influence of heterotrophic denitrification and dissimilatory nitrate reduction to ammonium (DNRA) by anammox bacteria cannot be excluded. Therefore, γ was determined as follows:

$$\gamma = 1 - \alpha - \beta \quad \cdots \text{eq. (11)}$$

Applying equations (5), (6), and (7) yields the following steady state isotope mass balance:

$$\delta_{IN} = \alpha\, \delta_{product1} + \beta\, \delta_{RS} + \gamma\, \delta_{product2} \quad \cdots \text{eq. (12)}$$

$$\delta_{IN} = \alpha\, (\delta_p - {}^{15}\varepsilon_3) + \beta\, \delta_p + \gamma\, (\delta_p - {}^{15}\varepsilon_5)$$

$$= (\alpha + \beta + \gamma)\, \delta_p - \alpha\, {}^{15}\varepsilon_3 - \gamma\, {}^{15}\varepsilon_5 \quad \cdots \text{eq. (13)}$$

$$= \delta_p - \alpha\, {}^{15}\varepsilon_3 - \gamma\, {}^{15}\varepsilon_5 = \delta_{RS} - \alpha\, {}^{15}\varepsilon_3 - \gamma\, {}^{15}\varepsilon_5 \quad \cdots \text{eq. (14)}$$

Therefore, ${}^{15}\varepsilon_3$ and ${}^{15}\varepsilon_5$ can be calculated as follows, when δ_{IN}, δ_{RS}, and $\delta_{product2}$ are measured experimentally:

$${}^{15}\varepsilon_3 = (\delta_{RS} - \delta_{IN} - \gamma\, {}^{15}\varepsilon_5) / \alpha \quad \cdots \text{eq. (15)}$$

$${}^{15}\varepsilon_5 = \delta_{RS} - \delta_{product2} \quad \cdots \text{eq. (16)}$$

$\delta_{product2}$ in the equations (7) and (16) is not simply $\delta_{out\text{-}NO3\text{-}}$ because the influent media contained 0.84 ~ 1.21mmol-N/L of NO_3^-, which was originated from the university ground water **(Table 3.3)**. Thus, the background isotope ratio of NO_3^- should be considered.

Isotope mass balance

$$\delta_{out\text{-}NO3\text{-}} \times C_{out\text{-}NO3\text{-}} = \delta_{in\text{-}NO3\text{-}} \times C_{in\text{-}NO3\text{-}} + \delta_{produced\text{-}NO3\text{-}} \times C_{produced\text{-}NO3\text{-}} \quad \cdots \text{eq. (17)}$$

Mass balance

$$C_{out\text{-}NO3\text{-}} = C_{in\text{-}NO3\text{-}} + C_{produced\text{-}NO3\text{-}} \quad \cdots \text{eq. (18)}$$

Applying equations (17) and (18) yields the following equation for $\delta_{produced\text{-}NO3\text{-}}$:

$$\delta_{produced\text{-}NO3\text{-}} = \delta_{product2} = (\delta_{out\text{-}NO3\text{-}} \times C_{out\text{-}NO3\text{-}} - \delta_{in\text{-}NO3\text{-}} \times C_{in\text{-}NO3\text{-}}) / C_{produced\text{-}NO3\text{-}} \quad \cdots \text{eq. (19)}$$

3) **O isotope effect of nitrite oxidation.**

For calculation of oxygen isotope effect for nitrite oxidation ($NO_2^- \rightarrow NO_3^-$), the produced NO_3^- contains three oxygen atoms: two oxygen atoms come from NO_2^- and one oxygen atom comes from H_2O. The incorporation of an oxygen atom from water should be considered (${}^{18}\varepsilon_6$ in **Fig. 3.2.2. B**). Thus, for oxygen isotopes, equation (7) is rewritten as:

$$\delta_{product2} = 2/3(\delta_{RS} - {}^{18}\varepsilon_5) + 1/3(\delta_{H2O} - {}^{18}\varepsilon_6) \quad \cdots \text{eq. (20)}$$

$$\delta_{product2} = 2/3\delta_{RS} + 1/3\delta_{H2O} - (2/3{}^{18}\varepsilon_5 + 1/3{}^{18}\varepsilon_6) \quad \cdots \text{eq. (21)}$$

$^{18}\varepsilon_6$ is the isotope effect for water incorporation. Since there are two unknown values ($^{18}\varepsilon_5$ and $^{18}\varepsilon_6$) in the equation (21), $^{18}\varepsilon_5$ and $^{18}\varepsilon_6$ cannot be calculated independently. Thus, the term ($2/3\ {}^{18}\varepsilon_5 + 1/3\ {}^{18}\varepsilon_6$) in eq. (21) is denoted as a combined oxygen isotope effect $^{18}E_{NO2^-\rightarrow NO3^-}$.

$$^{18}E_{NO2^-\rightarrow NO3^-} = (2/3\ {}^{18}\varepsilon_5 + 1/3\ {}^{18}\varepsilon_6) = 2/3\delta_{RS} + 1/3\delta_{H2O} - \delta_{product2} \quad \cdots \text{eq. (22)}$$

This combined oxygen isotope effect can be calculated from the obtained data set in this study.

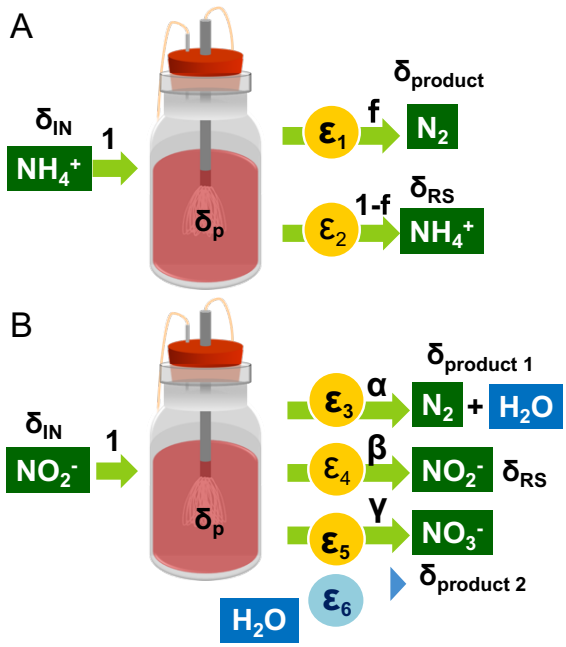

Figure 3.2.2 Diagram of a steady state box model. (**A**) a substrate (NH_4^+) entering to a MBR and a product (N_2) is formed and unused substrate (NH_4^+) exits without further fractionation. (**B**) a substrate (NO_2^-) entering to a MBR and two products (N_2 and NO_3^-) are formed and unused substrate (NO_2^-) exits without further fractionation. See SI text for more detailed description of this model.

3. 3. Results

3.3.1 Reactor performance

After the MBRs have reached a steady state, three or four sub-samples of MBR influent and effluent (permeate) were taken and analyzed for the concentrations and N and O isotope ratios of NH_4^+, NO_2^-, and NO_3^-, respectively. The steady state concentrations of NH_4^+, NO_2^- and NO_3^- in the MBR effluents were very stable during the entire experiments (**Table 3.3**). NO_2^- was almost completely consumed, whereas 1.3 - 3.1 mM NH_4^+ remained in all the MBR effluents and a small amount of NO_3^- was produced. The average stoichiometric ratios of consumed NO_2^- and consumed NH_4^+ ($\Delta NO_2^-/\Delta NH_4^+$, ranging from 1.11 ± 0.5 to1.28 ± 0.5) and produced NO_3^- and consumed NH_4^+ ($\Delta NO_3^-/\Delta NH_4^+$, ranging from 0.10 ± 0.01 to 0.2 ± 0.03) (**Table 3.3)** agreed with the previously observed stoichiometry of anammox process (*i.e.* 1.15 and 0.16 for $\Delta NO_2^-/\Delta NH_4^+$ and $\Delta NO_3^-/\Delta NH_4^+$, respectively) (Lotti *et al.*, 2014), suggesting that the anammox process being responsible for transformation of nitrogen compounds occurring in all three MBRs.

Although influent NH_4^+ and NO_2^- concentrations were different (approximately10 mM for "*Ca.* S. japonica", 10 mM for "*Ca.* J. caeni" and 16 mM for "*Ca.* B. sinica"), anammox activity in each MBR culture was consistent as demonstrated by similar volumetric NH_4^+ consumption, NO_2^- consumption, and NO_3^- production rates (**Table 3.3**). Furthermore, there were no significant difference in specific NH_4^+ consumption rates (ranging from 1.14 ± 0.06 to 1.27 ± 0.06 mg-N mg-protein^{-1} h^{-1}), NO_2^- consumption rates (ranging from 1.41 ± 0.05 to 1.48 ± 0.04 mg-N mg-protein^{-1} h^{-1}), and NO_3^- production rates (ranging from 0.11 ± 0.01 to 0.24 ± 0.03 mg-N mg-protein^{-1} h^{-1}) among three MBR cultures.

The ratio of anammox bacteria to the cell culture (degree of enrichment cultures) was determined by fluorescent *in situ* hybridization (FISH); 94.4 ± 6.5% for "*Ca.* S. japonica", 86.1 ± 4.9% for "*Ca.* J. caeni", and 96.9 ± 2.6% for "*Ca.* B. sinica", respectively.

3.3.2 Nitrogen isotope effects ($^{15}\varepsilon$)

The culture media with an equimolar amount of NH_4^+ ($\delta^{15}N_{IN}$ = -7.0 ± 0.3‰ to -2.4 ± 0.2‰) and NO_2^- ($\delta^{15}N_{IN}$ = -3.7 ± 0.1‰ to -2.6 ± 0.7‰ and $\delta^{18}O_{IN}$ = 6.0 ± 0.5‰ to 8.1 ± 0.7‰) were continuously fed to the individual MBR cultures (**Table 3.3**). N isotope effects of NH_4^+

oxidation to N_2 ($^{15}\varepsilon_{NH4\rightarrow N2}$), NO_2^- reduction to N_2 ($^{15}\varepsilon_{NO2\rightarrow N2}$), and NO_2^- oxidation to NO_3^- ($^{15}\varepsilon_{NO2\rightarrow NO3}$) were calculated for all three species using the equations described in Materials and Methods (**Fig. 3.2.2 and Table 3.3**). In the case of NH_4^+ oxidation to N_2, the values of $^{15}\varepsilon_{NH4\rightarrow N2}$ were consistent among three species (30.9 ± 0.2‰ - 32.7 ± 0.7‰). In contrast, there were significant differences in the $^{15}\varepsilon_{NO2\rightarrow N2}$ values (NO_2^- reduction to N_2). "*Ca.* J. caeni" showed the largest value (29.5 ± 3.9‰), whereas "*Ca.* B. sinica" yielded the smallest value (5.9 ± 4.5‰). The value of "*Ca.* S. japonica" was $^{15}\varepsilon_{NO2\rightarrow N2}$ = 19.9 ± 1.7‰, which was close to the previously reported value of "*Ca.* K. stuttgartiensis" (16.0 ± 4.5‰) (Brunner *et al.*, 2013). In the case of NO_2^- oxidation to NO_3^-, all three species showed strong inverse kinetic isotope effects ($^{15}\varepsilon_{NO2\rightarrow NO3} < 0$); -30.1 ± 3.0‰ for "*Ca.* S. japonica", - 45.3 ± 4.2‰ for "*Ca.* J. caeni", and -31.5 ± 4.0‰ for "*Ca.* B. sinica", respectively (**Fig. 3.3** and **Table 3.3**), which consists with the previously reported value of "*Ca.* K. stuttgartiensis" (-31.1 ± 3.9‰) (Brunner et al., 2013).

3.3.3 Oxygen isotope effect ($^{18}\varepsilon$)

$\delta^{18}O_{H2O}$ of ground water which was used for medium preparation was determined to be -11.12‰ ± 0.2‰ (n=3) and remained stable during an entire experimental period. Both $\delta^{18}O_{NO2-}$ and $\delta^{18}O_{NO3-}$ in MBR influents were consistent among three anammox cultures, respectively (**Table 3.3**). Under steady-state conditions, similar values of $\delta^{18}O_{NO2-}$ were determined in all three MBR effluents; 6.4 ± 0.2‰ for "*Ca.* S. japonica", 5.2 ± 0.3‰ for "*Ca.* J. caeni", and 4.9 ± 1.4 ‰ for "*Ca.* B. sinica", respectively (**Table 3.3**). In contrast, the "*Ca.* S. japonica" MBR yielded a higher $\delta^{18}O_{NO3-\ produced}$ value (12.7 ± 0.8‰) as compared with those of "*Ca.* J. caeni" (1.7 ± 0.8‰) and "*Ca.* B. sinica" (1.0 ± 0.4‰). Based on these $\delta^{18}O$ data, the combined O isotope effect during NO_2^- oxidation to NO_3^- was calculated for all three species using the equation (22) ($^{18}E_{NO2\rightarrow NO3} = (2/3\ ^{18}\varepsilon_5 + 1/3\ ^{18}\varepsilon_6) = 2/3\delta_{RS} + 1/3\delta_{H2O} - \delta_{product2}$) (**Table 3.3** and **Fig. 3.3**). All three species showed inverse kinetic isotope effects; -12.1 ± 0.8‰ for "*Ca.* S. japonica", -1.9 ± 0.8‰ for "*Ca.* J. caeni", and -1.5 ± 1.2‰ for "*Ca.* B. sinica", respectively.

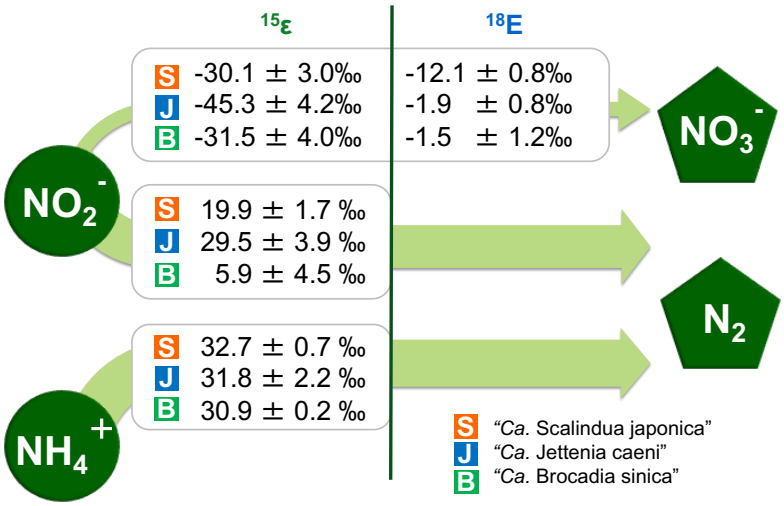

Figure 3.3 Summary of N and O isotope effects induced by different anammox species.

Table 3.3 Summary of MBR performance and N and O isotope analyses

		"*Ca.* Scalindua japonica"		"*Ca.* Jettenia caeni"		"*Ca.* Brocadia sinica"	
		In	Out	In	Out	In	Out
Concentration (mmol-N/L)	NH_4^+	10.5±0.5	1.5±0.2	9.3±0.6	1.6±0.2	16.1±0.6	2.6±0.4
	NO_2^-	10.0±0.4	0.01±0.00	9.9±0.3	0.03±0.01	16.5±0.6	0.21±0.16
	NO_3^-	0.85±0.01	1.72±0.08	0.96±0.02	1.74±0.09	0.93±0.01	3.55±0.33
	$NO_3^-{}_{produced}$	0.87±0.08		0.78±0.08		2.63±0.34	
Fraction reacted	f	0.86±0.01		0.83±0.02		0.84±0.02	
	α	0.90±0.04		0.78±0.03		0.82±0.02	
	β	0.00088±0.00032		0.0033±0.0011		0.012±0.009	
	γ	0.097±0.04		0.21±0.03		0.17±0.01	
$\delta^{15}N$ (‰)	NH_4^+	-2.8±0.1	25.4±0.3	-7.0±0.3	19.5±2.6	-2.4±0.2	23.4±0.7
	NO_2^-	-3.1±0.1	12.0±1.9	-2.6±0.7	10.6±0.7	-3.7±0.1	-4.3±4.6
	NO_3^-	12.4±0.3	27.3±0.2	13.3±0.2	32.2±0.8	15.3±0.1	24.1±0.9
	$NO_3^-{}_{produced}$	42.0±1.5		55.9±4.7		27.2±0.95	
$\delta^{18}O$ (‰)	NO_2^-	6.0±0.5	6.4±0.2	8.1±0.7	5.2±0.3	6.3±0.4	4.9±1.4
	NO_3^-	1.1±0.1	6.9±0.1	-1.7±0.4	-0.2±0.6	0.8±0.2	1.0±0.3
	$NO_3^-{}_{produced}$	12.7±0.8		1.7±0.8		1.0±0.4	
NH_4^+ removal rate (kg $m^{-3}d^{-1}$)		0.127±0.006		0.119±0.006		0.188±0.003	
NO_2^- removal rate (kg $m^{-3}d^{-1}$)		0.140±0.005		0.152±0.004		0.228±0.006	
NO_3^- production rate (kg $m^{-3}d^{-1}$)		0.012±0.001		0.012±0.001		0.037±0.005	
Specific NH_4^+ consumption rate (mg-N mg-protein^{-1} h^{-1})		1.27±0.06		1.14±0.06		1.22±0.02	
Specific NO_2^- consumption rate (mg-N mg-protein^{-1} h^{-1})		1.41±0.05		1.45±0.04		1.48±0.04	
Specific NH_4^+ production rate (mg-N mg-protein^{-1} h^{-1})		0.12±0.01		0.11±0.01		0.24±0.03	
$\Delta NO_2^- / \Delta NH_4^+$		1.11±0.05		1.28±0.05		1.21±0.02	
$\Delta NO_3^- / \Delta NH_4^+$		0.10±0.01		0.10±0.01		0.20±0.03	

3.4. Discussion

3.4.1 Continuous culture method

In this study, the N and O isotope effects induced by anammox bacteria were measured using continuous MBR anammox enrichment cultures. There are some advantages of use of the continuous culture system over batch system. A steady-state fractionation model is basically simpler than a batch model such as the Rayleigh model, in which the isotope effect (ε) values can be directly determined from the isotopic compositions of reactants in the influent and products in the effluent at steady state (**Fig. 3.2.2**). Two sampling campaigns (October 2015 (C-1) and May 2016 (C-2)) were conducted for "*Ca.* B. sinica" to analyze the N and O isotope effects (**Table 3.4.1**). In each campaign, samplings were conducted three or four times every other day, and three sub-samples were collected for each sampling day, pretreated and analyzed in the same manner. Nearly identical results of the N and O isotope effects were obtained from the different sampling campaigns for "*Ca.* B. sinica" (**Table 3.4.1**), which indicate the high reproducibility of continuous steady-state culturing systems for isotope effect analyses. The precision of $^{15}\varepsilon$ and $^{18}\varepsilon$ as measured in the steady-state continuous systems compares favorably with that of batch culture experiments (Nishizawa *et al.*, 2016). In batch experiments, the growth conditions (i.e., pH, concentrations of reactants and products, and so on) vary over time, which may also significantly affect the isotope fractionations. However, oxygen isotope exchange between NO_2^- and H_2O cannot be evaluated in the continuous culture experiment alone, and thus batch culture experiments must be conducted in parallel.

Table 3.4.1 Summary of two sampling campaign data for "*Ca*. Brocadia sinica"

	Campaign 1	Campaign 2	Average ±SD (between two campaign)
NRR (kg $m^{-3}day^{-1}$)	0.3	0.38	—
$^{15}\varepsilon_{NH4+\rightarrow N2}$	34.6±2.0	30.9±0.2	32.8±2.6
$^{15}\varepsilon_{NO2-\rightarrow N2}$	3.7±6.8	5.9±4.5	4.8±1.6
$^{15}\varepsilon_{NO2-\rightarrow NO3-}$	-36.5±3.8	-31.5±4.0	-34.0±3.5
$^{18}E_{NO2-\rightarrow NO3-}$	-3.6±1.5	-1.5±1.2	-2.6±1.5

Table 3.4.2 Summary of N and O isotope compositions of NH_4^+, NO_2^-, and NO_3^- in the influent and effluent (permeate) of MBRs.

"*Ca.* S. japonica"

Sampling day		1		2		3	
In/Out		In	Out	In	Out	In	Out
$\delta^{15}N$(‰)	NH_4^+(n=2)	-2.9±0.0	25.1±0.1	-2.8±0.1	25.5±0.0	-2.7±0.2	25.7±0.3
	NO_2^-(n=2)	-3.2±0.0	11.1±0.9	-3.0±0.0	10.7±0.1	-3.1±0.1	14.1±3.0
	NO_3^-(n=3)	12.7±0.1	27.6±0.1	12.4±0.2	27.2±0.0	12.2±0.0	27.2±0.0
$\delta^{18}O$(‰)	NO_2^-(n=2)	6.3±0.3	6.4±0.1	6.4±0.4	6.6±0.2	5.4±0.1	6.3±1.0
	NO_3^-(n=3)	1.0±0.8	7.0±0.2	1.2±0.6	6.8±0.2	1.1±0.7	6.9±0.5

"*Ca.* J. caeni"

Sampling day		1		2		3		4	
In/Out		In	Out	In	Out	In	Out	In	Out
$\delta^{15}N$(‰)	NH_4^+(n=1)	-6.7	23.3	-7.4	18.5	-7.0	18.4	-7.0	17.8
	NO_2^-(n=2)	-2.1±0.2	11.3±0.9	-2.1±0.1	10.9±0.9	-2.5±0.0	10.5±0.1	-3.6±0.0	9.7±1.1
	NO_3^-(n=1)	13.1	33.3	13.1	31.7	13.2	32.2	13.6	31.7
$\delta^{18}O$(‰)	NO_2^-(n=2)	8.3±0.1	5.6±0.0	7.8±0.1	5.1±0.4	7.3±0.0	5.1±2.7	9.0±0.0	5.0±0.4
	NO_3^-(n=1)	-1.4	0.0	-2.0	-0.7	-2.0	-0.6	-1.3	0.5

"*Ca.* B. sinica"

Sampling day		1		2		3	
In/Out		In	Out	In	Out	In	Out
$\delta^{15}N$(‰)	NH_4^+(n=2)	-2.6±0.1	23.2±0.0	-2.5±0.1	22.9±0.4	-2.1±0.2	24.2±2.4
	NO_2^-(n=2)	-3.5±0.2	-8.8±0.1	-3.8±0.2	-4.5±0.1	-3.8±0.2	0.4±0.1
	NO_3^-(n=3)	15.2±0.0	23.6±0.0※	15.3±0.1	23.6±0.1	15.4±0.0	25.1±0.1
$\delta^{18}O$(‰)	NO_2^-(n=2)	6.7±0.0	6.0±0.3	6.2±0.1	3.3±0.2	5.8±0.6	5.3±0.7
	NO_3^-(n=3)	1.0±0.5	0.7±0.2※	0.9±0.5	1.2±0.1	0.5±0.2	1.1±0.4

3.4.2 Species-level differences

Among five tentatively proposed candidatus genera of anammox bacteria, one putative marine strain ('*Ca.* Scalindua japonica') and two freshwater strains ('*Ca.* Brocadia sinica' and '*Ca.* Jettenia caeni') were examined for N and O isotope effects of anammox metabolism in this study. The results revealed species-dependent isotope effects of NO_2^- reduction to N_2. During anammox metabolism ($NO_2^- + NH_4^+ \rightarrow N_2$), the following three enzymatic reactions occur; (i) NO_2^- reduction to nitric oxide (NO) or hydroxylamine (NH_2OH) (Oshiki, Ali, *et al.*, 2016), (ii) hydrazine (N_2H_4) formation from NO or NH_2OH and NH_4^+, and (iii) N_2H_4 oxidation to N_2 (Kartal *et al.*, 2013). Hydrazine synthesis is considered to be the rate-limiting step in this reaction sequence due to three-electron reduction reaction (Kartal *et al.*, 2013).

For the conversion of NH_4^+ to N_2, the N isotope effects ($^{15}\varepsilon_{NH4 \rightarrow N2}$) of all three species are consistent (30.9‰ to 32.7‰), which also do not significantly differ from the range of $^{15}\varepsilon_{NH4 \rightarrow N2}$ reported previously for "*Ca.* K. stuttgartiensis" (23.5‰ to 29.1‰) (Brunner *et al.*, 2013). This is probably because this reaction is mediated through the same enzymes such as hydrazine synthase (hzs) and hydrazine dehydrogenase (hdh) in all anammox bacteria species (**Fig. 3.4.1**).

On the other hand, for the conversion of NO_2^- to N_2, significant variations of the N isotope effects ($^{15}\varepsilon_{NO2 \rightarrow N2}$) were found among the three species: $^{15}\varepsilon_{NO2 \rightarrow N2}$ = 19.9 ± 1.7‰ for "*Ca.* S. japonica", $^{15}\varepsilon_{NO2 \rightarrow N2}$ = 29.5 ± 3.9‰ for "*Ca.* J. caeni", and $^{15}\varepsilon_{NO2 \rightarrow N2}$ = 5.9 ± 4.5‰ for "*Ca.* B. sinica", respectively (**Fig. 3.3** and **Table 3.3**). The previously reported $^{15}\varepsilon_{NO2 \rightarrow N2}$ values of "*Ca.* K. stuttgartiensis" ranged between 11.9‰ and 18.9‰ (average = 16.0 ± 4.5‰) (Brunner *et al.*, 2013).

Different degree of N isotopic fractionation could be imparted by different nitrite reductase (**Fig. 3.4.1**). It has been reported that "*Ca.* S. japonica" and "*Ca.* K. stuttgartiensis" possess a cytochrome *cd*$_1$ (iron, Fe)-type NO-forming nitrite reductase (Fe-NIR) (Strous *et al.*, 2006; Oshiki *et al.*, 2017) whereas "*Ca.* J. caeni" has a copper (Cu)-containing NO-forming nitrite reductase (Cu-NIR) (Ali *et al.*, 2015). "*Ca.* B. sinica", however, does not possess canonical nitrite reductase genes (neither Fe-NIR nor Cu-NIR) and reduces NO_2^- to NH_2OH, instead of NO (Oshiki, Ali, *et al.*, 2016). Interestingly, both "*Ca.* S. japonica" and "*Ca.* K. stuttgartiensis" yielded similar $^{15}\varepsilon_{NO2 \rightarrow N2}$ values ($^{15}\varepsilon_{NO2 \rightarrow N2}$ = 19.9 ± 1.7‰ and 16.0 ± 4.5‰), while "*Ca.* J. caeni" yielded higher values ($^{15}\varepsilon_{NO2 \rightarrow N2}$ = 29.5 ± 3.9‰). Furthermore, "*Ca.* B. sinica" yielded distinctively lower $^{15}\varepsilon_{NO2 \rightarrow N2}$ values (5.9 ± 4.5‰) (**Fig. 3.4.1**). The different N and O isotope effects between Fe-NIR and Cu-NIR were also demonstrated for nitrite reduction by denitrifying bacteria (Martin and Casciotti, 2016). This difference was explained by the difference in NO_2^- and enzyme binding mechanism: the Cu-NIR binds to both O atoms of NO_2^- whereas the Fe-NIR binds to the N atom, resulting in a smaller N isotope effect for Fe-NIR (Martin and Casciotti, 2016).

However, the recent literatures have reported that Fe-NirS was not hardly expressed at the transcriptional level in both "*Ca*. K. stuttgartiensis" (Kartal and Keltjens, 2016) and Scalindua related single amplified genomes from ODZs (Maalcke *et al.*, 2016; Ganesh *et al.*, 2018). In addition, Cu-NirK expression was not identified in "*Ca.* J. caeni" (Ali *et al.*, 2015). It has been postulated recently that the reduction of NO_2^- to NO could be catalyzed by a HAO-like

octahaem oxidoreductase in the case of "*Ca*. K. stuttgartiensis" (Kartal and Keltjens, 2016). The highly similar protein was also identified in the ODZ SAGs (Ganesh *et al.*, 2018). "*Ca.* B. sinica" that has neither NirS nor NirK also possesses the identical HAO-like octahaem oxidoreductase (Oshiki, Ali, *et al.*, 2016). However, nitrite reductase that actually works in individual anammox species is not identified yet. To confirm this enzyme-level differences in $^{15}\varepsilon_{NO2\rightarrow N2,}$ true nitrite reductase must be identified.

Three anammox bacterial species were cultured at different pH and temperature in this study; pH 7.9 - 8.0 and 25°C for "*Ca*. S. japonica", pH 8.6 - 8.9 and 30°C for "*Ca.* J. caeni", and pH 7.3 - 7.4 and 37°C for "*Ca.* B. sinica", respectively. However, this probably does not cause variations in $^{15}\varepsilon_{NO2\rightarrow N2}$. To our best knowledge, there were no studies that show a dependence of the organism-level N isotope effect on either pH or temperature so far, although temperature and pH influence the O isotope effect of NO_2^- due to isotopic exchange with H_2O (Buchwald and Casciotti, 2013; Nishizawa *et al.*, 2016). Taken together, a difference in nitrite reductase would most likely cause the differences in NO_2^- reduction isotope effects ($^{15}\varepsilon_{NO2\rightarrow N2}$)

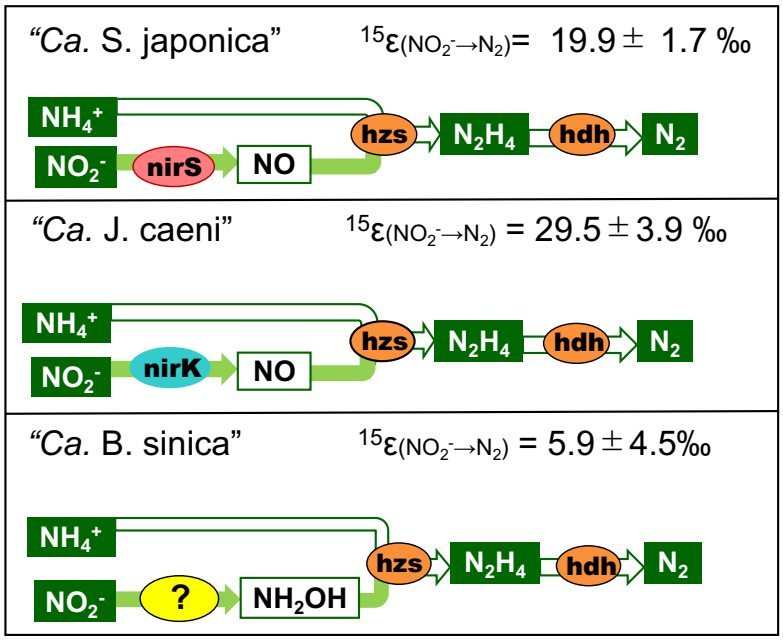

in this study.

Figure 3.4.1 Proposed species-level difference in N and O isotope effects of nitrite ($^{15}\varepsilon_{NO2\rightarrow N2}$ and $^{18}\varepsilon_{NO2\rightarrow N2}$) among anammox bacteria species.

For the oxidation of NO_2^- to NO_3^-, all three anammox species exhibited pronounced inverse N isotope effects (-45.3 ± 4.2‰ to -30.1 ± 3.0‰), which agreed with the previously reported value for "*Ca.* K. stuttgartiensis" (-31.1‰ ± 3.9‰) (Brunner *et al.*, 2013), but exceeded the values for nitrite-oxidizing bacteria (NOB) (-9.1‰ to -20.6‰)(Buchwald and Casciotti, 2010). Anammox bacteria can reverse this enzymatic reaction, namely they can reduce NO_3^- back to NO_2^- (Kartal *et al.*, 2007a; Oshiki *et al.*, 2013b). It is thus hypothesized that this reversible reaction would promote isotope exchange between NO_2^- and NO_3^- and lead to more pronounced isotope effects as observed in sulfur metabolism (Holler *et al.*, 2012). Intriguingly, it has been also speculated that environmental stresses cause a significant N isotope exchange between NO_2^- and NO_3^- (-60.5 ± 1.0‰) in a "*Ca.* K. stuttgartiensis" batch culture (Brunner *et al.*, 2013). However, since this phenomenon was not ubiquitously observed, it still remained unclear whether this was caused by cell lysis during cultivation and/or sample preparation. In the present study, all samples for isotope effect measurements were collected from steady-state continuous anammox enrichment cultures grown under physiological anoxic conditions. Thus, environmental stresses could be minimized, and active biomass dominated in all cultures (>98% were active cells as determined Live/Dead staining, data not shown). Since isotope exchange between NO_2^- and NO_3^- is indeed an interesting and important phenomenon for interpretation of the N and O isotope effects, it must be addressed in the future.

It should be also noted that N and O isotope effects are influenced even by subcellular localization and amino acid sequences of enzymes **(Fig. 3.4.2)**. For example, membrane-bound cytoplasmic and periplasmic Nxr of *Nitrobacter* and *Nitrospira* yielded significantly different $^{15}\varepsilon_{NO2^-\rightarrow NO3^-}$ and $^{18}\varepsilon_{NO2^-\rightarrow NO3^-}$ (Buchwald and Casciotti, 2010). In the case of anammox bacterial Nxr, "*Ca*. K. stuttgartiensis" *nxr*AB (corresponding to the kustd1700 and kustd1703 genes) have the TAT signal sequences involved in the twin-arginine translocation pathway, and the "*Ca*. K. stuttgartiensis" NxrAB are localized in the anammoxosome, an innermost compartment of anammox bacterial cells (de Almeida *et al.*, 2015). The "*Ca.* S. japonica" (the SCALIN_C03_117 and SCALIN_C03_113), "*Ca.* B. sinica" (the BROSI_A0941 and BROSI_A0944 genes), and "*Ca.* J. caeni" (the KSU1_B0257 and KSU1_B0260 genes) *nxr*AB also have the TAT signal, suggesting that these anammox bacterial NxrAB are also localized in the anammoxosome. Despite the same subcellular localization, species-level differences of

$^{15}\varepsilon_{NO2^-\rightarrow NO3^-}$ and $^{18}\varepsilon_{NO2^-\rightarrow NO3^-}$ were observed in the present study, especially from "*Ca*. S. japonica" **(Fig. 3.3)**. The differences possibly resulted from differences in amino acid sequences of the anammox bacterial NxrAB as previously discussed with ammonia monooxygenase subunit A (AmoA) (Casciotti *et al.*, 2003). Bacterial Nxr have the conserved amino acid residues to form a substrate pocket in NxrA and to bind iron-sulfur cluster in NxrB, respectively (Martinez-Espinosa *et al.*, 2007; Lucker *et al.*, 2010). Alignment of anammox bacterial NxrAB revealed that the "*Ca.* Scalindua" NxrAB has different features in those conserved regions (**Fig. 3.4.1**); i.e., the conserved Thr_{291} residue of NxrA is substituted with Ala_{291} and the conserved Cys_{45} residue of NxrB is substituted with His_{45} in the "*Ca*. S. japonica" NxrAB. Because the hydrophobicities of Thr and Ala and Cys and His are different, those substitution results in structural change of "*Ca*. S. japonica" Nxr, which might result in the large difference in $^{15}\varepsilon_{NO2^-\rightarrow NO3^-}$ and $^{18}\varepsilon_{NO2^-\rightarrow NO3^-}$, compared to "*Ca*. J. caeni" and "*Ca*. B. sinica". However, since the actual subcellular localization and amino acid sequences of enzymes in anammox bacteria are not fully understood currently, their influences need to be further investigated.

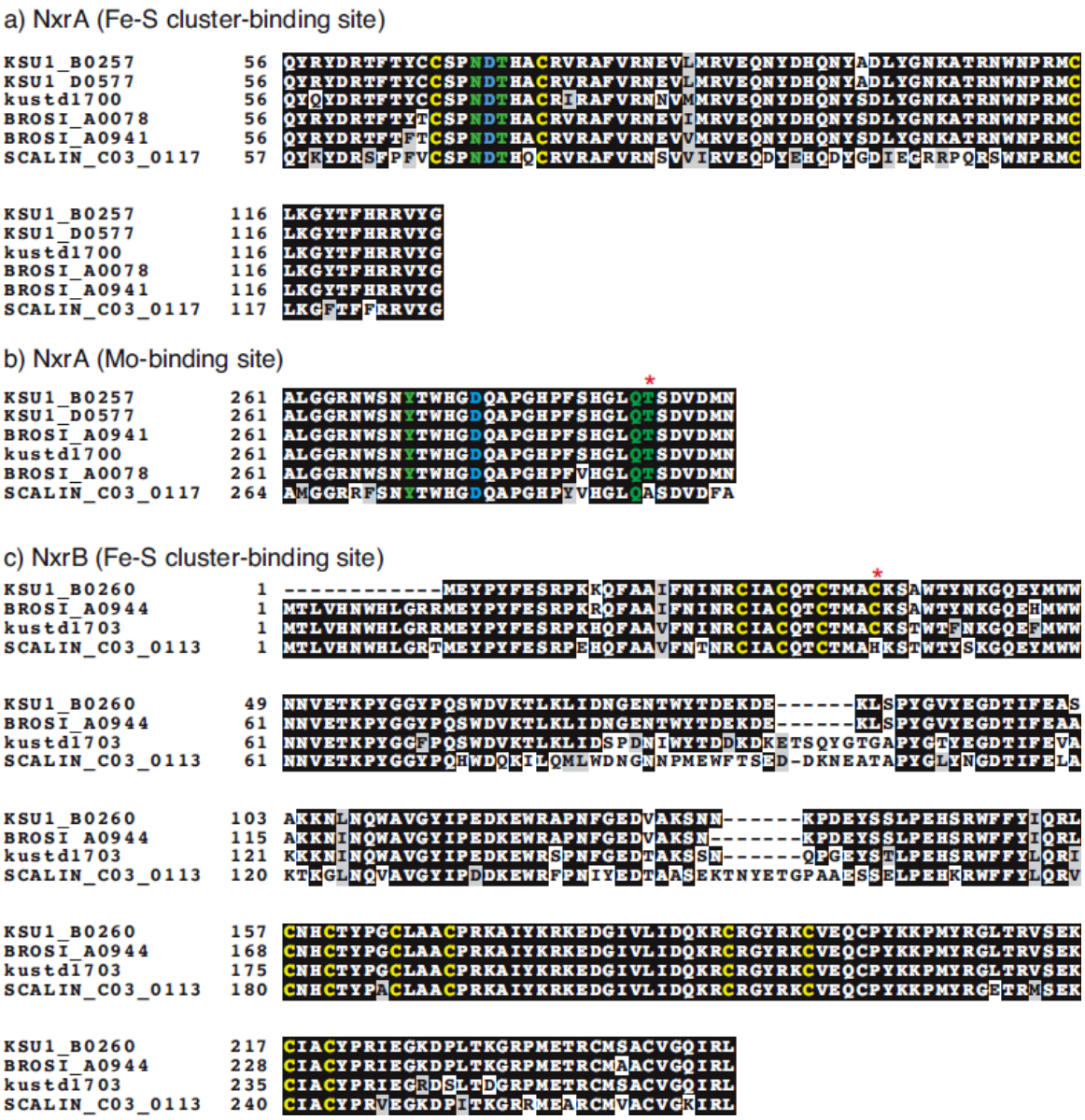

Figure 3. 4. 2 Alignment of anammox bacterial NxrAB.

The conserved regions corresponding to a [Fe-S] cluster-binding site and Mo-binding site in NxrA (panel **a** and **b**) and [Fe-S] cluster-binding site in NxrB (panel **c**) are shown. Anammox bacterial NxrAB were aligned using the clustalW program (version 1.83), and the locus tags registered in genome sequence data are indicated at the left of the NxrAB sequences. Signature residues and Mo-binding residue conserved in NxrA (Lücker et al., 2010 PNAS) are highlighted in green and blue, respectively (panel **b**). [Fe-S] binding residues in NxrB are highlighted in yellow (panel **c**). The conserved residues substituted in "*Ca*. Scalindua japonica" NxrAB are indicated by an asterisk.

3.4.3 O isotope effects of NO_2^- and NO_3^-

We could report only the combined O isotope effects for NO_2^- oxidation to NO_3^- ($^{18}E_{NO2\text{-}\rightarrow NO3\text{-}}$ = 2/3 $^{18}\varepsilon_{NO2\text{-}\rightarrow NO3\text{-}}$ +1/3 $^{18}\varepsilon_{H2O}$, eq. (22)) by anammox bacteria in this study. Since both NO_2^- reduction to N_2 and oxidation to NO_3^- are simultaneously occurring in anammox process (**Fig. 3. 4. 3.**), the $\delta^{18}O$ values of NO_2^- represents a superimposed signal of the two processes. In addition, the $\delta^{18}O_{NO2}$ value is affected by abiotic O isotope exchange between NO_2^- and H_2O ($^{18}\varepsilon_{eq}$ in **Fig. 3. 4. 3.**). A water-derived O atom is also incorporated into NO_3^- during NO_2^- oxidation to NO_3^- (Kumar *et al.*, 1983). Therefore, the $\delta^{18}O_{NO3}$ value of the MBR effluent is directly related to the culture medium (water) $\delta^{18}O_{H2O}$ through both O isotope equilibration of NO_2^- ($^{18}\varepsilon_{eq}$) and incorporation of a water-derived O atom ($^{18}\varepsilon_{H2O}$) (Granger and Wankel, 2016). Thus, O isotope effect for NO_2^- oxidation to NO_3^- ($^{18}\varepsilon_{NO2\text{-}\rightarrow NO3\text{-}}$) and O isotope effect for water incorporation ($^{18}\varepsilon_{H2O}$) cannot be determined separately in the continuous culture experiment alone in this study. These parameters could be species dependent and thus should be separately determined for individual anammox bacteria species for better understanding of N and O isotope systematics and nitrogen cycling in natural environments.

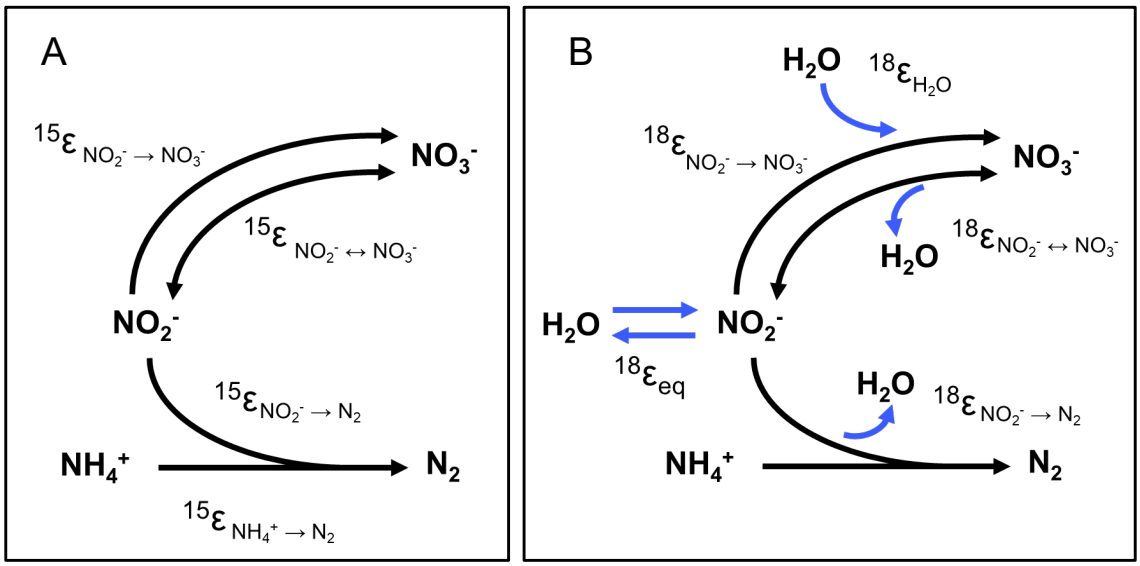

Figure 3. 4. 3 Isotope systematics during anammox process (A) Nitrogen isotope effect (B) Oxygen isotope effect

The combined O isotope effects for NO_2^- oxidation ($^{18}E_{NO2\text{-}\rightarrow NO3\text{-}}$) showed inverse kinetic isotope effects; $^{18}E_{NO2\rightarrow NO3}$: -12.1 ± 0.8 ‰ for "*Ca.* S. japonica", -1.9 ± 0.8‰ for "*Ca.* J. caeni"

and -1.5 ± 1.2‰ for "*Ca.* B. sinica", respectively (**Fig. 3.3** and **Table 3.3**). According to the equation (22) for the combined O isotope effect ($^{18}E_{NO2\text{-}\rightarrow NO3\text{-}} = 2/3\ ^{18}\varepsilon_{NO2\text{-}\rightarrow NO3\text{-}} + 1/3\ ^{18}\varepsilon_{H2O}$), $^{18}\varepsilon_{NO2\text{-}\rightarrow NO3\text{-}}$ by anammox bacteria can be estimated when O isotope effect for water incorporation ($^{18}\varepsilon_{H2O}$) was assumed to be 14 ‰ as assumed for NOB previously (Buchwald et al., 2015; Granger and Wankel, 2016): -25.2 ‰ for "*Ca.* S. japonica", -9.9 ‰ for "*Ca.* J. caeni", and -9.3 ‰ for "*Ca.* B. sinica", respectively. Aerobic nitrite oxidizing bacteria (NOB) also yielded inverse kinetic isotope effects of NO_2^- oxidation ($^{18}\varepsilon_{NO2\rightarrow NO3}$) ranging from -1.3 ± 0.4 ‰ to -8.2 ± 2.5 ‰ (Buchwald and Casciotti, 2010). It should be noted again that we report a combined O isotope effect (eq. 22) whereas Buchwald and Casciotti (2010) report the kinetic isotope effect on NO_2^- alone (equivalent to $^{18}\varepsilon_5$ in eq. 20).

The rate of abiotic O isotope exchange between NO_2^- and H_2O is rapid relative to the biological NO_2^- turnover rate and dependent on temperature and pH (Buchwald and Casciotti, 2013; Nishizawa *et al.*, 2016). The rate is faster at lower pH and higher temperature. Three anammox bacterial species were cultured at different pH and temperature in this study, which might cause variations in $\delta^{18}O_{NO2}$ and $\delta^{18}O_{NO3}$ values of MBR effluent and consequently the combined O isotope effects for NO_2^- oxidation ($^{18}E_{NO2\rightarrow NO3}$) (**Table 3.3**).

3.4.4 Application to ecological studies

Although natural abundance N and O isotope ratios of nitrate ($\delta^{15}N_{NO3}$ and $\delta^{18}O_{NO3}$) have been used as an invaluable tool to identify the source and to determine the biogeochemical transformation processes (Kendall *et al.*, 2007), the isotope balances of oceanic NO_3^- are still poorly constrained at present. This is partly because NO_3^- can be produced during anammox (**Fig. 3. 1**), which has been overlooked and led to divergent interpretation of $\delta^{15}N_{NO3}$ in freshwater and marine systems. Therefore, the contribution of anammox bacteria to NO_2^- reoxidation to NO_3^- (recycling N) in the environments is currently one of the most prominent research topics.

A numerical NO_3^- isotope dynamics model was developed to evaluate the relative contribution of anammox to NO_3^- production in the marine and freshwater systems (Granger and Wankel, 2016). In this model, since O isotope effect of NO_2^- oxidation to NO_3^- ($^{18}\varepsilon_{NO2\text{-}\rightarrow NO3\text{-}}$) by anammox bacteria was not available, the $^{18}\varepsilon_{NO2\text{-}\rightarrow NO3\text{-}}$ values of NOB (-7.0 to -3.0‰) were used instead. According to this model, the inverse N and O isotope effects

significantly influence the $\delta^{15}N$ and $\delta^{18}O$ of produced NO_3^- and consequently the corresponding $\Delta\delta^{18}O$: $\Delta\delta^{15}N$ trajectories. More negative (i.e., lower) $^{15}\varepsilon_{NO2-\rightarrow NO3-}$ value pushes up $\delta^{15}N_{NO3-}$ value, thereby lowering the $\Delta\delta^{18}O$: $\Delta\delta^{15}N$ trajectories. In contrast, more negative $^{18}\varepsilon_{NO2-\rightarrow NO3-}$ value pushes up $\delta^{18}N_{NO3-}$ value, thereby lifting up the $\Delta\delta^{18}O$: $\Delta\delta^{15}N$ trajectories. It should be noted that the lower $^{18}E_{NO2-\rightarrow NO3-}$ value (i.e., more negative) was yielded for a marine species "*Ca.* S. japonica" than other two freshwater species (**Fig. 3.3**), suggesting that the higher $\Delta\delta^{18}O$: $\Delta\delta^{15}N$ trajectories could be expected in marine systems than in freshwater systems. This can partly explain the widely observed $\Delta\delta^{18}O$: $\Delta\delta^{15}N$ trajectories in freshwater systems (< 1) and in marine systems (≥ 1).

Nitrite is an important branch compound between N loss by denitrification and anammox and N retention by NO_2^- reoxidation to NO_3^-. Natural abundance N and O isotopes of nitrite ($\delta^{15}N_{NO2}$ and $\delta^{18}O_{NO2}$) also provided an additional diagnostic to estimate the relative contribution of anammox to the NO_3^- pool (Granger and Wankel, 2016). Nitrite $\delta^{15}N$ and $\delta^{18}O$ measurements have been used to evaluate what oxidative and reductive NO_2^- transformation processes are occurring and to what extent in ODZs (Casciotti, 2016).

Anammox bacteria in ODZs do not affiliate with the genus *Scalindua*, but with distinct clusters that are clearly separated from the sediment species (Ganesh *et al.*, 2018). Thus, dual N and O isotope effects of NO_2^- reoxidation should be further explored for other marine water and sediment anammox species for better model simulations for the oceanic N budget.

References

Ali, M., Oshiki, M., Awata, T., Isobe, K., Kimura, Z., Yoshikawa, H., et al. (2015) Physiological characterization of anaerobic ammonium oxidizing bacterium "*Candidatus* Jettenia caeni." *Environ Microbiol* 17: 2172–2189.

APHA, AWWA, and WEF (2005) Standard Methods for the Examination of Water and Wastewater. Washington, D.C.

Awata, T., Oshiki, M., Kindaichi, T., Ozaki, N., Ohashi, A., and Okabe, S. (2013) Physiological characterization of an anaerobic ammonium-oxidizing bacterium belonging to the "*Candidatus* scalindua" group. *Appl Environ Microbiol* 79: 4145–4148.

Babbin, A.R., Peters, B.D., Mordy, C.W., Widner, B., Casciotti, K.L., and Ward, B.B. (2017) Multiple metabolisms constrain the anaerobic nitrite budget in the Eastern Tropical South Pacific. *Global Biogeochem Cycles* 31: 258–271.

Bourbonnais, A., Altabet, M.A., Charoenpong, C.N., Larkum, J., Hu, H., Bange, H.W., and Stramma, L. (2015) N-loss isotope effects in the Peru oxygen minimum zone studied using a mesoscale eddy as a natural tracer experiment. *Global Biogeochem Cycles* 29: 793–811.

Brandes, J.A. and Devol, A.H. (2002) A global marine-fixed nitrogen isotopic budget: Implications for Holocene nitrogen cycling. *Global Biogeochem Cycles* 16: 1120.

Brunner, B., Contreras, S., Lehmann, M.F., Matantseva, O., Rollog, M., Kalvelage, T., et al. (2013) Nitrogen isotope effects induced by anammox bacteria. *Proc Natl Acad Sci U S A* 110: 18994–18999.

Buchwald, C. and Casciotti, K.L. (2013) Isotopic ratios of nitrite as tracers of the sources and age of oceanic nitrite. *Nat Geosci* 6: 308–313.

Buchwald, C. and Casciotti, K.L. (2010) Oxygen isotopic fractionation and exchange during bacterial nitrite oxidation. *Limnol Oceanogr* 55: 1064–1074.

Buchwald, C., Santoro, A.E., McIlvin, M.R., and Casciotti, K.L. (2012) Oxygen isotopic composition of nitrate and nitrite produced by nitrifying cocultures and natural marine assemblages. *Limnol Oceanogr* 57: 1361–1375.

Buchwald, C., Santoro, A.E., Stanley, R.H.R., and Casciotti, K.L. (2015) Nitrogen cycling in the secondary nitrite maximum of the eastern tropical North Pacific off Costa Rica. *Global Biogeochem Cycles* 29: 2061–2081.

Casciotti, K.L. (2009) Inverse kinetic isotope fractionation during bacterial nitrite oxidation. *Geochim Cosmochim Acta* 73: 2061–2076.

Casciotti, K.L. (2016) Nitrite isotopes as tracers of marine N cycle processes. *Phil Trans R Soc A* 374: 20150295.

Casciotti, K.L., Bohlke, J.K., McIlvin, M.R., Mroczkowski, S.J., and Hannon, J.E. (2007) Oxygen isotopes in nitrite: Analysis, calibration, and equilibration. *Anal Chem* 79: 2427–2436.

Casciotti, K.L., Buchwald, C., and McIlvin, M. (2013) Implications of nitrate and nitrite isotopic measurements for the mechanisms of nitrogen cycling in the Peru oxygen deficient zone. *Deep Res Part I Oceanogr Res Pap* 80: 78–93.

Casciotti, K.L., McIlvin, M., and Buchwald, C. (2010) Oxygen isotopic exchange and fractionation during bacterial ammonia oxidation. *Limnol Oceanogr* 55: 753–762.

Casciotti, K.L. and McIlvin, M.R. (2007) Isotopic analyses of nitrate and nitrite from reference mixtures and application to Eastern Tropical North Pacific waters. *Mar Chem* 107: 184–201.

Casciotti, K.L., Sigman, D.M., Hastings, M.G., Bohlke, J.K., and Hilkert, A. (2002) Measurement of the oxygen isotopic composition of nitrate seawater and freshwater using the dentirifier method. *Anal Chem* 74: 4905-4912.

Casciotti, K.L., Sigman, D.M., and Ward, B.B. (2003) Linking Diversity and Stable Isotope Fractionation in Ammonia-Oxidizing Bacteria. *Geomicrobiol J* 20: 335–353.

Codispoti, L. a. (2007) An oceanic fixed nitrogen sink exceeding 400 Tg N a? vs the concept of homeostasis in the fixed-nitrogen inventory. *Biogeosciences Discuss* 3: 1203–1246.

Fry, B. (2006) Stable Isotope Ecology, Spribger Science + Business Media, LLC.

Ganesh, S., Bertagnolli, A.D., Bristow, L.A., Padilla, C.C., Blackwood, N., Aldunate, M., et al. (2018) Single cell genomic and transcriptomic evidence for the use of alternative nitrogen substrates by anammox bacteria. *ISME J* 12: 2706–2722.

Granger, J. and Sigman, D.M. (2008) Nitrogen and oxygen isotope fractionation during dissimilatory nitrate reduction by denitrifying bacteria. *Limnol Oceanogr* 53: 2533–2545.

Granger, J., Sigman, D.M., Rohde, M.M., Maldonado, M.T., and Tortell, P.D. (2010) N and O isotope effects during nitrate assimilation by unicellular prokaryotic and eukaryotic plankton cultures. *Geochim Cosmochim Acta* 74: 1030–1040.

Granger, J. and Wankel, Scott D (2016) Isotopic overprinting of nitrification on denitrification as a ubiquitous and unifying feature of environmental nitrogen cycling. *Proc Natl Acad Sci* 113(42): E6391-E6400.

Gruber, N. and Galloway, J.N. (2008) An Earth-system perspective of the global nitrogen cycle. *Nature* 451: 293–6.

Holmes, R.M., McClelland, J.W., Sigman, D.M., Fry, B., and Peterson, B.J. (1998) Measuring $^{15}N\text{-}NH_4$ in marine, estuarine, and freshwaters: An adaptation of the ammonia diffusion method for samples with low ammonium concentrations. *MarChem* 60: 235–243.

Hu, H., Bourbonnais, A., Larkum, J., Bange, H.W., and Altabet, M.A. (2016) Nitrogen cycling in shallow low-oxygen coastal waters off Peru from nitrite and nitrate nitrogen and oxygen isotopes. *Biogeosciences* 13: 1453–1468.

Kalvelage, T., Lavik, G., Lam, P., Contreras, S., Arteaga, L., Löscher, C.R., et al. (2013) Nitrogen cycling driven by organic matter export in the South Pacific oxygen minimum zone. *Nat Geosci* 6: 228–234.

Karsh, K.L., Granger, J., Kritee, K., and Sigman, D.M. (2012) Eukaryotic assimilatory nitrate reductase fractionates N and O isotopes with a ratio near unity. *Environ Sci Technol* 46: 5727–5735.

Kartal, B., De Almeida, N.M., Maalcke, W.J., Op den Camp, H.J.M., Jetten, M.S.M., and Keltjens, J.T. (2013) How to make a living from anaerobic ammonium oxidation. *FEMS Microbiol Rev* 37: 428–461.

Kartal, B. and Keltjens, J.T. (2016) Anammox Biochemistry: a Tale of Heme c Proteins. *Trends Biochem Sci* 41: 998–1011.

Kartal, B., Kuypers, M.M.M., Lavik, G., Schalk, J., Op Den Camp, H.J.M., Jetten, M.S.M., and Strous, M. (2007) Anammox bacteria disguised as denitrifiers: Nitrate reduction to dinitrogen gas via nitrite and ammonium. *Environ Microbiol* 9: 635–642.

Kartal, B., Rattray, J., van Niftrik, L.A., van de Vossenberg, J., Schmid, M.C., Webb, R.I., et al. (2007) Candidatus "Anammoxoglobus propionicus" a new propionate oxidizing species of anaerobic ammonium oxidizing bacteria. *Syst Appl Microbiol* 30: 39–49.

Kendall, C., Elliott, E.M., and Wankel, S.D. (2007) Tracing anthropogenic inputs of nitrogen to ecosystems. In *Stable Isotopes in Ecology and Environmental Science*. pp. 375–449.

Kritee, K., Sigman, D.M., Granger, J., Ward, B.B., Jayakumar, A., and Deutsch, C. (2012) Reduced isotope fractionation by denitrification under conditions relevant to the ocean. *Geochim Cosmochim Acta* 92: 243–259.

Kumar, S., Nicholas, D.J.D., and Williams, E.H. (1983) Definitive ^{15}N NMR evidence that water serves as a source of "O" during nitrite oxidation by Nitrobacter agilis. *FEBS Lett* 152: 71–74.

Kuypers, M.M.M., Lavik, G., Woebken, D., Schmid, M., Fuchs, B.M., Amann, R., et al. (2005) Massive nitrogen loss from the Benguela upwelling system through anaerobic ammonium oxidation. *Proc Natl Acad Sci* 102: 6478–6483.

Kuypers, M.M.M., Sliekers, A.O., Lavik, G., Schmid, M., Jorgensen, B.B., Kuenen, J.G., et al. (2003) Anaerobic Ammonium Oxidation by Anammox Bacteria in the Black Sea. *Nature* 422: 608–611.

Lotti, T., Kleerebezem, R., Lubello, C., and van Loosdrecht, M.C.M. (2014) Physiological and kinetic characterization of a suspended cell anammox culture. *Water Res* 60: 1–14.

Maalcke, W.J., Reimann, J., De Vries, S., Butt, J.N., Dietl, A., Kip, N., et al. (2016) Characterization of anammox hydrazine dehydrogenase, a Key -producing enzyme in the global nitrogen cycle. *J Biol Chem* 291: 17077–17092.

Martin, T.S. and Casciotti, K.L. (2016) Nitrogen and oxygen isotopic fractionation during microbial nitrite reduction. *Limnol Oceanogr* 61: 1134–1143.

McIlvin, M.R. and Altabet, M.A. (2005) Chemical conversion of nitrate and nitrite to nitrous oxide for nitrogen and oxygen isotopic analysis in freshwater and seawater. *Anal Chem* 77: 5589–5595.

Nishizawa, M., Sakai, S., Konno, U., Nakahara, N., Takaki, Y., Saito, Y., et al. (2016) Nitrogen and oxygen isotope effects of ammonia oxidation by thermophilic *Thaumarchaeota* from a geothermal water stream. *Appl Environ Microbiol* 82: AEM.00250-16.

Nunoura, T., Takaki, Y., Hirai, M., Shimamura, S., Makabe, A., Koide, O., et al. (2015) Hadal biosphere: Insight into the microbial ecosystem in the deepest ocean on Earth. *Proc Natl Acad Sci U S A* 112: E1230-1236.

Oshiki, M., Ali, M., Shinyako-Hata, K., Satoh, H., and Okabe, S. (2016) Hydroxylamine-dependent anaerobic ammonium oxidation (anammox) by "*Candidatus* Brocadia sinica." *Environ Microbiol* 18: 3133–3143.

Oshiki, Mamoru, Awata, T., Kindaichi, T., Satoh, H., and Okabe, S. (2013) Cultivation of planktonic anaerobic ammonium oxidation (anammox) bacteria using membrane bioreactor. *Microbes Environ* 28: 436–443.

Oshiki, M., Ishii, S., Yoshida, K., Fujii, N., Ishiguro, M., Satoh, H., and Okabe, S. (2013) Nitrate-dependent ferrous iron oxidation by anaerobic ammonium oxidation (anammox) bacteria. *Appl Environ Microbiol* 79: 4087–4093.

Oshiki, M., Mizuto, K., Kimura, Z.I., Kindaichi, T., Satoh, H., and Okabe, S. (2017) Genetic diversity of marine anaerobic ammonium-oxidizing bacteria as revealed by genomic and proteomic analyses of 'Candidatus Scalindua japonica.' *Environ Microbiol Rep* 9: 550–561.

Oshiki, M., Satoh, H., and Okabe, S. (2016) Ecology and Physiology of Anaerobic Ammonium Oxidizing (anammox) Bacteria. *Environ Microbiol* 18: 2784–2796.

Quan, Z.X., Rhee, S.K., Zuo, J.E., Yang, Y., Bae, J.W., Park, J.R., et al. (2008) Diversity of ammonium-oxidizing bacteria in a granular sludge anaerobic ammonium-oxidizing (anammox) reactor. *Environ Microbiol* 10: 3130–3139.

Santoro, A.E. and Casciotti, K.L. (2011) Enrichment and characterization of ammonia-oxidizing archaea from the open ocean: phylogeny, physiology and stable isotope fractionation. *Isme J* 5: 1796–1808.

Schmid, M., Twachtmann, U., Klein, M., Strous, M., Juretschko, S., Jetten, M., et al. (2000) Molecular Evidence for Genus Level Diversity of Bacteria Capable of Catalyzing Anaerobic Ammonium Oxidation. *Syst Appl Microbiol* 23: 93–106.

Schmid, M., Walsh, K., Webb, R., Rijpstra, W.I., van de Pas-Schoonen, K., Verbruggen, M.J., et al. (2003) *Candidatus* “Scalindua brodae”, sp. nov., *Candidatus* “Scalindua wagneri”, sp. nov., two new species of anaerobic ammonium oxidizing bacteria. *Syst Appl Microbiol* 26: 529–538.

Sigman, D.M., Altabet, M. a, Michener, R., McCorkle, D.C., Fry, B., and Holmes, R.M. (1997) Natural abundance-level measurements of the nitrogen isotopic composition of oceanic nitrate: an adaption of the ammonia diffusion method. *Mar Chem* 57: 227–242.

Sigman, D.M., Casciotti, K.L., Andreani, M., Barford, C., Galanter, M., and Bhlke, J.K. (2001) A bacterial method for the nitrogen isotopic snalysis of nitrate in seawater and freshwater. *Anal Chem* 73: 4145–4153.

Sigman, D.M., DiFiore, P.J., Hain, M.P., Deutsch, C., Wang, Y., Karl, D.M., et al. (2009) The dual isotopes of deep nitrate as a constraint on the cycle and budget of oceanic fixed nitrogen. *Deep Res Part I Oceanogr Res Pap* 56: 1419–1439.

Sigman, D.M., Granger, J., DiFiore, P.J., Lehmann, M.M., Ho, R., Cane, G., and van Geen, A. (2005) Coupled nitrogen and oxygen isotope measurements of nitrate along the eastern North Pacific margin. *Global Biogeochem Cycles* 19: 1–14.

Strous, M., Fuerst, J. a, Kramer, E.H., Logemann, S., Muyzer, G., van de Pas-Schoonen, K.T., et al. (1999) Missing lithotroph identified as new planctomycete. *Nature* 400: 446–449.

Strous, M., Pelletier, E., Mangenot, S., Rattei, T., Lehner, A., Taylor, M.W., et al. (2006) Deciphering the evolution and metabolism of an anammox bacterium from a community genome. *Nature* 440: 790–794.

Thamdrup, B., Jensen, M.M., Ulloa, O., Farı, L., and Escribano, R. (2006) Anaerobic ammonium oxidation in the oxygen-deficient waters off northern Chile. *Limnol Ocean* 51: 2145–2156.

Chapter 4

Influence of $\delta^{18}O$ of water on measurements of $\delta^{18}O$ of nitrite and nitrate

Abstract

Oxygen isotope ratio measurements of NO_2^- and NO_3^- by the azide method and denitrifier method are sensitive to the $\delta^{18}O$ of sample water. However, the influence of $\delta^{18}O_{H2O}$ on those measurements has not been quantitatively evaluated and documented so far. Therefore, we investigated the influence of $\delta^{18}O_{H2O}$ of sample on $\delta^{18}O$ analysis of NO_2^- and NO_3^-, respectively. We prepared NO_2^- and NO_3^- standards (with known $\delta^{18}O_{NO2-}$ and $\delta^{18}O_{NO3-}$) dissolved in waters having different $\delta^{18}O_{H2O}$ values ($\delta^{18}O_{H2O}$ = -12.6, 25.9, 56.7, and 110.1‰). Nitrite and nitrate was converted to N_2O using the azide method and the denitrifier method, respectively. The isotope ratios of the generated N_2O were analyzed with a Sercon PT-GC/IRMS system. The measured $\delta^{18}O$ of produced N_2O was plotted against known $\delta^{18}O_{NO2-}$ and $\delta^{18}O_{NO3-}$ values to evaluate the influence of exchange of oxygen atom with H_2O during the conversion of NO_2^- to N_2O and NO_3^- to N_2O, respectively. As a result, the degree of O isotope exchange was 10.8 ± 0.3 % in the azide method and 5.5 ± 1.0 % in the denitrifier method, indicating that the azide method is more susceptible to artifacts arising from differences in the $\delta^{18}O_{H2O}$ of water than the denitrifier method. Thus, the intercept of the standard calibration curve must be corrected to account for differences in $\delta^{18}O_{H2O}$. In short, oxygen isotope ratio measurements of NO_2^- by the azide method are highly sensitive to $\delta^{18}O_{H2O}$ resulting from significant oxygen isotope exchange between NO_2^- and H_2O. Therefore, the same $\delta^{18}O_{H2O}$ as that of the sample must be used to make the NO_2^- and NO_3^- standards for the most accurate measurements. Abiotic NO_2 - H_2O equilibrium isotope effect experiments yielded a rate constant of (1.13 ± 007) × 10^{-2} (h^{-1}) and an equilibrium isotope effect of 11.9 ± 0.1‰ under the condition of pH = 7.5, 30℃, and 2.5% salinity.

4.1 Introduction

Nitrate (NO_3^-) is the dominant form of bioavailable nitrogen (N) in the ocean, and nitrite (NO_2^-) is a central intermediate in the N cycle. The natural abundance stable N isotope ratios of NO_3^- and NO_2^- ($\delta^{15}N_{NO3-}$ and $\delta^{15}N_{NO2-}$, respectively) record the history of processes that have contributed to production and consumption of NO_3^- and NO_2^-. Thus, $\delta^{15}N$ has been used to constrain the marine fixed N budget (Brandes and Devol, 2002; Deutsch *et al.*, 2004). Since the development of the denitrifier method and the azide method for $\delta^{15}N$ and the oxygen (O) isotope ratio ($\delta^{18}O$) of NO_3^- ($\delta^{18}O_{NO3-}$) (Sigman *et al.*, 2001; Casciotti *et al.*, 2002) and NO_2^- ($\delta^{18}O_{NO3-}$) (McIlvin and Altabet, 2005; Casciotti *et al.*, 2007), respectively, many studies have begun focusing on the use of coupled $\delta^{15}N$ and $\delta^{18}O$ of NO_3^- and NO_2^- to constrain N cycling (Casciotti and McIlvin, 2007; Casciotti and Buchwald, 2012; Bourbonnais *et al.*, 2015; Buchwald *et al.*, 2015; Hu *et al.*, 2016; Peters *et al.*, 2016, 2018). In this way, dual N and O isotope analyses provide complementary signatures of co-occurring N transformation processes that cannot be revealed by $\delta^{15}N$ measurement alone. It can contribute to more accurate modeling and a better understanding of N cycling. For instance, coupled $\delta^{15}N$ and $\delta^{18}O$ of NO_2^- measurements have potential to distinguish NO_2^- sources: ammonia oxidation, nitrite oxidation and partial nitrate assimilation in primary nitrite maximum (PNM) (Casciotti, 2016).

To date, several modifications have been made to the denitrifier method including pretreatment to remove NO_2^-(Granger and Sigman, 2009), optimization of bacterial culture conditions(McIlvin and Casciotti, 2011), and updates to analytical instrumentation (McIlvin and Casciotti, 2011; Weigand *et al.*, 2016), which have improved analytical precision and sensitivity while also increasing sample throughput. Notably, the exchange of O atoms with water during the conversion of NO_3^- or NO_2^- to nitrous oxide (N_2O) for analysis was recognized early as an analytical issue requiring careful attention (Casciotti *et al.*, 2002). For correct $\delta^{18}O_{NO3-}$ analysis, according to "Identical treatment principle" (Werner and Brand, 2001), $\delta^{18}O_{H2O}$ of NO_3^- isotope standard solutions should be identical with the $\delta^{18}O_{H2O}$ of the samples (Berhanu *et al.*, 2015) due to the incorporation of O atoms from water to N_2O. However, information on the relative influence of the $\delta^{18}O$ value of water ($\delta^{18}O_{H2O}$) on the resulting NO_3^- oxygen isotope ratio ($\delta^{18}O_{NO3-}$) analysis has not been fully documented.

As for the azide method, protocols for sample storage pH (Casciotti *et al.*, 2007; Granger *et al.*, 2019) and temperature(Casciotti *et al.*, 2007) were optimized to minimize O

isotope exchange between NO_2^- and water during sample storage. Recently, the influence of sample salinity on measured $\delta^{15}N_{NO2-}$ and $\delta^{18}O_{NO2-}$ values was also revealed (Granger *et al.*, 2019). Minimizing O isotope exchange between NO_2^- and water during chemical conversion from NO_2^- to N_2O was also noted as being important (McIlvin and Altabet, 2005). However, information about O isotope exchange rate and the amount of O isotope exchange during reaction between NO_2^- and azide is limited. In addition, any dependence of the NO_2^- oxygen isotope ratio analysis on the $\delta^{18}O_{H2O}$ value has not been clearly documented yet, possibly because the application of the method is, so far, limited to the samples where $\delta^{18}O_{H2O}$ does not vary significantly such as seawater samples. Actually, $\delta^{18}O_{H2O}$ values in environment vary widely (i. e. Global surface seawater: -7.7 ‰ < $\delta^{18}O_{H2O}$ < 1.8 ‰ (LeGrande and Schmidt, 2006), Precipitation: -34 ‰ < $\delta^{18}O_{H2O}$ < 2 ‰(Bowen and Revenaugh, 2003)) because of isotope effects associated with evaporation and condensation (Bowen, 2010). Thus, it is essential to evaluate $\delta^{18}O_{H2O}$ dependance of $\delta^{18}O_{NO2-}$ and $\delta^{18}O_{NO3-}$ analysis in order to widely apply those analysis to environmental samples.

The rate of abiotic O isotope exchange between NO_2^- and water, as well as equilibrium isotope effects are important for understanding $\delta^{18}O_{NO2-}$ and $\delta^{18}O_{NO3-}$ in the environment (Casciotti *et al.*, 2007). The rate of abiotic O atom exchange between NO_2^- and H_2O has been used to estimate NO_2^- turnover time in a wide range of oceanic environments (e.g. the primary NO_2^- maximum and the secondary NO_2^- maximum which are prominent in highly productive and low-dissolved oxygen regions of the ocean or terrestrial ecosystems) (Buchwald and Casciotti, 2013). The $\delta^{18}O$ of newly produced NO_3^- is also known to be sensitive to $\delta^{18}O$ of ambient water and the equilibrium isotope effects between NO_2^- and H_2O (Granger and Wankel, 2016). However, the experimentally determined NO_2^- equilibration rates(Buchwald and Casciotti, 2013; Nishizawa *et al.*, 2016) and equilibrium isotope effects (Casciotti *et al.*, 2007; Buchwald and Casciotti, 2013; Nishizawa *et al.*, 2016) across relevant environmental conditions remain quite limited. In the abiotic equilibration experiments, ^{18}O-labeled water was commonly used (Casciotti *et al.*, 2007; Nishizawa *et al.*, 2016) because equilibrium $\delta^{18}O_{NO2}$ value depends on $\delta^{18}O_{H2O}$ and equilibrium isotope effect. Thus, it is important to understand the $\delta^{18}O_{H2O}$ dependence of the NO_2^- oxygen isotope ratio analysis to analyze accurate equilibrium isotope effect.

In this study, the influence of the value of $\delta^{18}O_{H2O}$ on $\delta^{18}O_{NO2-}$ and $\delta^{18}O_{NO3-}$ sample calibration was investigated. The $\delta^{18}O_{H2O}$ dependance of $\delta^{18}O_{NO2-}$ and $\delta^{18}O_{NO3-}$ analysis was experimentally quantified by preparing NO_2^- and NO_3^- isotope standards with a variety of water having different $\delta^{18}O$ ($\delta^{18}O_{H2O}$ = -12.6, 25.9, 56.7, and 110.1‰). We lay out a detailed protocol for NO_2^- isotopic analysis by the azide method to measure samples preserved at high pH (~12). Several modifications for the denitrifier method such as bacterial culture conditions and updates to aspects of the instrumentation are also described. In addition, we determined the rate of abiotic O isotope exchange between NO_2^- and H_2O and equilibrium isotope effects under a variety of $\delta^{18}O_{H2O}$ values conditions ($\delta^{18}O_{H2O}$ = -12.6, 25.9, 56.7, and 110.1‰) in a series of laboratory experiments.

4. 2 Material and method

4.2.1 Abiotic NO_2^--water equilibrium isotope effect experiments

The first experiment was performed using a buffered marine medium (Kindaichi *et al.*, 2011). The rate of abiotic O isotope exchange between NO_2^- and H_2O was determined at a temperature of 30°C, pH = 7.5, and salinity = 2.5% with different $\delta^{18}O_{H2O}$ values ($\delta^{18}O_{H2O}$ = -12.6 (unlabeled), 25.9, 56.7, and 110.1‰) by adding $H_2{}^{18}O$ (97% ^{18}O; Aldrich, prod. no. 329878). Buffer medium was prepared with ^{18}O labeled water, and pH was adjusted to 7.5 by adding HEPES (4- (2-hydroxyethyl)-1-piperazineethanesulfonic acid) buffer (final concentration: 2 mM) (DOJINDO Laboratories, Japan, prod. no. 348-01372) and 1 M NaOH prepared with NaOH for N analysis (Wako, Japan, prod. no. 191-08625). Other chemical components of buffer medium were as follows: KH_2PO_4 (the final concentration is 24.4 mg L^{-1}) (Wako, prod. no. 166-04255), $MgSO_4 \cdot 7H_2O$ (99 mg L^{-1}) (Wako, prod. no. 131-00405), $CaCl_2$ (86 mg L^{-1}) (Wako, prod. no. 038-24985), and 0.5 mL trace element solution I and II(Graaf *et al.*, 1996). An artificial sea salt SEALIFE (Marine Tech, Japan) was supplemented into the media to achieve 2.5% salinity. Medium was filtered using 0.2-μm cellulose acetate filter (Advantec, Japan, prod no. 13CP020AS). Fifty-mL polypropylene tubes (AS ONE, Japan, prod. no. VIO-50BN) were filled with 50 mL of buffer medium. For each $\delta^{18}O_{H2O}$ value, a series of three tubes was prepared. To begin an experiment, $NaNO_2$ (Wako, prod. no. 199-02565) solution (at a final concentration of 2.0 mM) was added to each bottle. In addition, $NH_4(SO_4)_2$ (Wako, prod. no. 019-03435) solution (at a final concentration of 2.5 mM) was also added because our research goal was to determine N and

O isotope effects of anaerobic ammonium oxidizing (anammox) bacteria (Kobayashi *et al.*, 2019), in which growth medium contains both NO_2^- and NH_4^+ as substrates. In the first experiment, buffered medium didn't contain NO_3^-. In order to also evaluate abiotic O atom exchange between NO_2^- and NO_3^-, we prepared another batch with buffered medium which contained both of NO_2^- (2.0 mM) and NO_3^- (0.23 mM) under $\delta^{18}O_{H2O}$ of -12.6‰.

4.2.2 Sampling and sample storage

A 2.0 mL sample of the incubated solution was periodically withdrawn over 60 days. Immediately afterwards, the pH was measured using 0.5 mL of the sample solution with pH meter (pH meter B-712, Horiba, Ltd., Kyoto, Japan), while the remaining sample was filtered through a 0.2-μm cellulose acetate filter (Advantec, prod no. 13CP020AS). Concentration analyses were conducted on a separate 0.5 mL aliquot. For NO_2^- isotope analysis, 0.5 mL of the filtrate was adjusted to pH 12 by adding 2 M low-N-blank NaOH (Wako, prod. no. 191-08625) solution (28 μL) to the sample immediately after filtration and stored at -20℃ until analysis to prevent O isotope exchange between NO_2^- and H_2O during sample storage (Casciotti *et al.*, 2007). This ratio of NaOH solution to the sample was determined empirically by testing various volumes of 2 M NaOH to buffer medium in advance. For NO_3^- isotope analysis, NO_2^- was removed immediately by addition of 15 μL of 20 mM sulfamic acid (Wako, prod. no. 196-04471) to the 0.5 mL sample to avoid interference of NO_2^- with NO_3^- isotopic analyses(Granger and Sigman, 2009). The volume of the sulfamic acid (15 μL) was determined by testing various volumes of sulfamic acid to the buffer medium in advance, which results in the reaction pH < 1.7. After 20 min, the concentration of NO_2^- was measured by Griess reaction(APHA *et al.*, 2005) to confirm the complete removal of NO_2^-. Sample solutions were then stored at -20°C until analysis.

4.2.3 Chemical analyses

On the day of sampling, concentrations were analyzed by using 0.5 mL sample filtrate. The NO_2^- concentration was measured by Griess reaction(APHA *et al.*, 2005). The NO_3^- concentration was measured using ion chromatography (IC-2010, TOSOH; Tokyo, Japan) equipped with a TSKgel IC-Anion HS column (TOSOH; Tokyo, Japan).

4.2.4 Isotopic analysis of NO_2^-

Sample preparation

$\delta^{15}N_{NO2-}$ and $\delta^{18}O_{NO2-}$ were measured by chemical conversion of NO_2^- to N_2O using the azide method (McIlvin and Altabet, 2005). All samples had been adjusted to exactly the same pH (pH=12) and salinity (2.5% NaCl) with different $\delta^{18}O_{H2O}$ depending on the experiments ($\delta^{18}O_{H2O}$ = -12.6 (unlabeled), 25.9, 56.7, and 110.1‰). For NO_2^- standards (JAM1 to 4; see below), solutions had the same pH, salinity and $\delta^{18}O_{H2O}$ as the batch of the samples to be analyzed, to account for any effects arising from pH-dependent incorporation of water O atoms into N_2O during the N_2O generation (i.e. for the samples with $\delta^{18}O_{H2O}$ = 110.1‰, NO_2^- standards must be prepared with the MillQ water with $\delta^{18}O_{H2O}$ = 110.1‰). In addition, we kept the volume of the solution constant for samples and standards (1.0 mL in this study) to minimize the variations in pH of the solution during the azide reaction, and to minimize the effect of solution volume for the purge-and-trap procedure to recover analyte N_2O. Furthermore, we maintained a constant amount of N (50 nmol) for the samples and standards to minimize any sample size dependency in $\delta^{15}N$ and $\delta^{18}O$ analyses **(Fig. 4.2.1)**. Thus, the sample solution containing 50 nmol N was pipetted to the 20 mL glass headspace vial (Chromacol, prod. no. 20-CV, ashed at 450°C for 2hrs)**,** then deionized (DI) water with the same pH (12), salinity (2.5%, 0.43 M NaCl) and $\delta^{18}O_{H2O}$ as sample was added to adjust the total solution volume to 1.0 mL. The same adjustments of the total solution volume with the same pH, $\delta^{18}O$ and salinity were carried out for the standards. To do so, four types of DI water having different $\delta^{18}O_{H2O}$ values ($\delta^{18}O_{H2O}$ = -12.6, 25.9, 56.7, and 110.1‰) were prepared, but having the same pH and salinity. The vials were crimp-sealed with gray butyl septa (Wheaton, prod. no. 20-0025) and aluminum crimp caps (GL-Sciences, prod. no. 1030-51780).

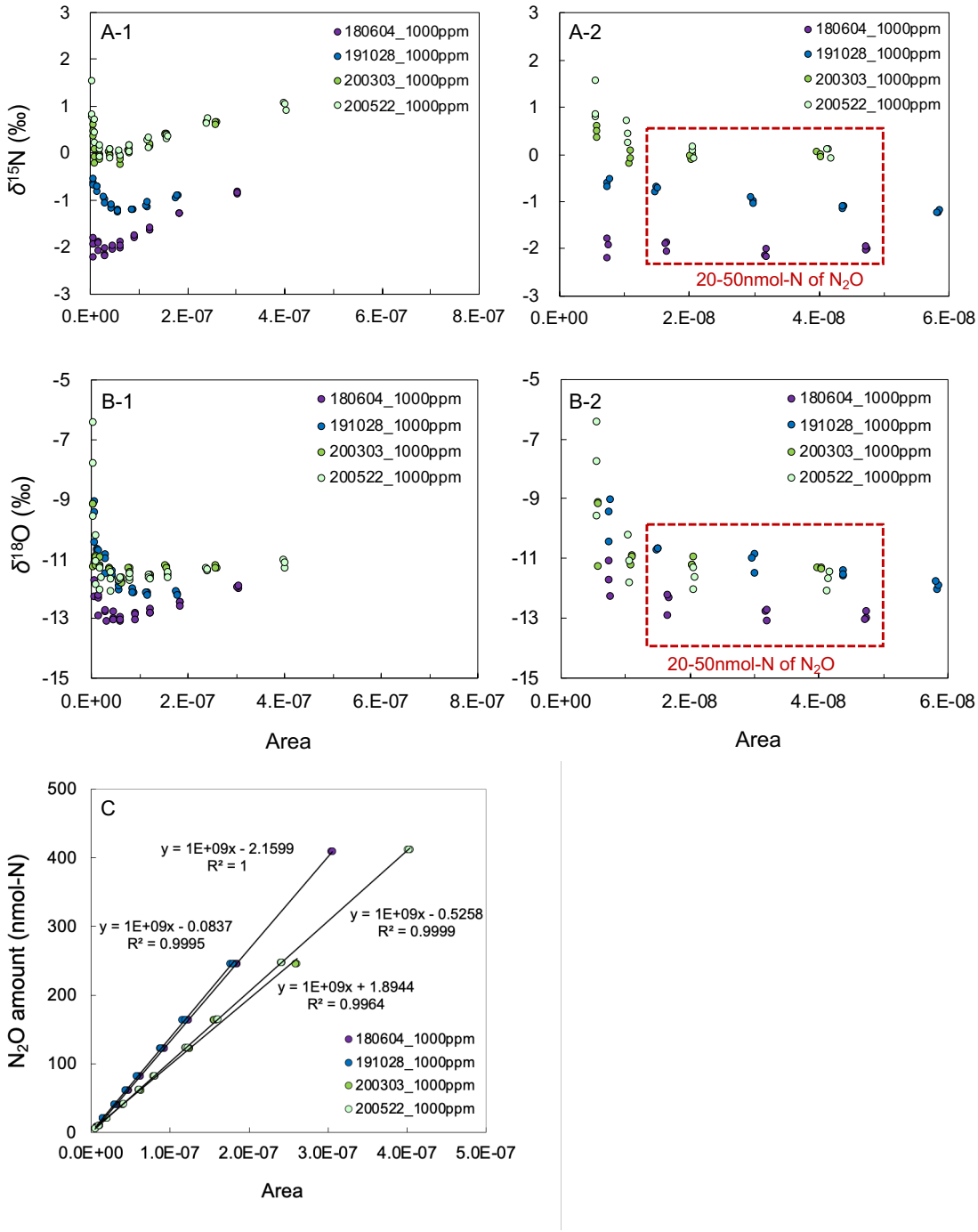

Figure 4.2.1 Relationship between detected peak areas (*m/z*=44) and δ^{15}N (A), δ^{18}O (B), and injected N_2O amounts (C). Figure A-2 and B-2 are magnified image of Figure A-1 and B1 to visualize the sample size range from 20 to 50nmol-N.

Azide buffer preparation

Preparation of azide buffer and conversion of NO_2^- to N_2O was performed in a fume hood due to the volatility and toxicity of HN_3 in the azide buffer. In addition, used labware (e.g., syringe, needle and vials) were rinsed with basic NaOH solution before the normal washing process of the labware to prevent HN_3 production. Because of the high pH (12) of the sample and standard solutions, the azide buffer was modified from the original protocol (1:1 by volume mixture of 10% acetic acid and 2 M sodium azide(McIlvin and Altabet, 2005)) by increasing the acetic acid concentration to 7.84 M(Happy *et al.*, 2016) and the sodium azide concentration to 4 M. Firstly, 90% acetic acid solution (Wako, prod. no. 012-00245) (10 mL) was pipetted to a 50 mL glass vial (Maruemu Corp., prod. no.7). Then, the vial was crimped-sealed with a gray butyl septum and Al crimp, and one short disposable needle (24-gauge, Terumo Corp., prod. no. NN-2432R) was pierced through the septa to vent gas to keep the inner pressure. Next, 10 mL of 4 M sodium azide (Wako, prod. no. 199-11095) was injected using a 20-mL disposable syringe with a 25-gauge needle (Terumo Corp., prod. no. SS-20LZ; Terumo Corp., prod. no. NN-2525R). After the removal of the syringe with the needle from the 50 mL vial, another long interchangeable needle (19-gauge, Luer Lock Type Common Needle; GL Sciences, prod. no. 3008-43010) was pierced through the septa reaching into the mixed solution, and a stream of high purity N_2 gas (99.999%, ultra-pure, Air Liquide Japan GK) was introduced to purge N_2O from the solution for 30 min. After purging, the short disposable needle and the long interchangeable needle were removed. For 100 vials (including samples and standards), 4.0 mL of the azide buffer is required in total, thus 2.0 mL each of 90% acetic acid solution and 4 M sodium azide solution were mixed for use in a single batch of analyses. It is highly recommended, however, to prepare extra amount of the azide buffer solution (e.g. 10 mL rather than 4.0 mL for 100 samples in this study) to prevent from the shortage of the buffer. In case of azide buffer shortage, newly prepared azide buffer could have different pH and HN_3 concentrations, resulting in different calibration lines.

Conversion of NO_2^- to N_2O

The injection volume of azide buffer must be adjusted to achieve reaction pH of 4.3 ~ 4.5(McIlvin and Altabet, 2005). To our 1.0 mL solution with pH 12, 40 μL of azide buffer was precisely injected to the vial by a gastight syringe (Hamilton 1750LT, prod. no. 81201) and

shaken vigorously for 1 min, bringing the pH down to 4.4. After 30 min, the sample pH was increased by addition of 2.0 mL of 1 M NaOH using a 20 mL disposable syringe with a 25-gauge needle (Terumo Corp., prod. no. SS-20LZ; Terumo Corp., prod. no. NN-2525R) and shaken vigorously to stop the reaction. We used 2.0 mL of the diluted NaOH solution in this study rather than 0.1 - 0.2 mL of 6 M or 10 M NaOH solution used in many studies (McIlvin and Casciotti, 2011) to bring the total volume of the solution in the vial to greater than 3 mL. This was necessary for the tip of the autosampler's purging needle to be submerged in the solution and ensure complete purging of N_2O from the solution. The vials were stored upside down to minimize leakage of N_2O through the septum until the PT-GC/IRMS analysis.

4.2.5 Isotopic analysis of NO_3^-

Bacterial culture condition

$\delta^{15}N_{NO3-}$ and $\delta^{18}O_{NO3-}$ were measured with the denitrifier method (microbial conversion of NO_3^- to N_2O) (Sigman *et al.*, 2001; Casciotti *et al.*, 2002) according to the protocol provided by (McIlvin and Casciotti, 2011) . We usually prepare 120 - 260 vials (including samples, blanks and standards) in a week. At first, 440 mL growth medium was prepared in a 500 mL medium bottle (Wheaton prod. no. 223952, combusted at 450°C for 4 hrs). The chemical compositions of growth medium were following: Tryptic Soy Broth (Hach, prod. no. 2253534) (30 g L^{-1}), 36 mM KH_2PO_4aq (Wako, prod. no. 169-04245), 10 mM KNO_3 (Wako, prod. no. 160-04035) and 1mM NH_4Cl (Wako, prod. no. 017-02995). Three bottles (total 1320 mL) are needed for analysis of 120 vials. These bottles were sealed with 30-mm gray butyl septa (Wheaton, prod. no. 224100-331) and 30-mm aluminum tear-out seals (Wheaton, prod. no. 224187-01), and then autoclaved at 121°C for 50 min. Note that the autoclave time is long (50 min) compared with the normal use (e.g. 15 or 30 min), and the color of the autoclaved media must be dark brown (**Fig. 4.2.2. A**) rather than light brown (**Fig. 4.2.2. B**) (McIlvin and Casciotti, 2011; Coplen *et al.*, 2012). Although we generally prepared this growth media 3-5 days prior to the inoculation, we experienced that the growth media prepared 3 weeks before the inoculation can be used (no data shown). Two mL of the 6 - 14 days old growth media inoculated with *Pseudomonas aureofaciens* (ATCC#13985) in the previous round were transferred to this new growth media. In general, we have found that liquid to liquid transfer causes no contamination problems, in comparison to the previously recommended inoculation

from an isolated colony of the denitrifier grown on agar plates(McIlvin and Casciotti, 2011; Weigand *et al.*, 2016). The inoculated growth media was incubated with gentle shaking at approximately 47 - 48 rpm with a shaker (EYELA MMS-3010, Tokyo Rikakikai Co. Ltd.) at 29℃ in the dark incubator (EYELA FMS-1000, Tokyo Rikakikai Co. Ltd.) for 6 - 14 days. It should be confirmed that NO_2^- is not detected in the 6 - 14 days old pre-incubated *P. aureofaciens* cultures because the existence of the residual NO_2^- in the media indicates the incomplete denitrification of NO_3^-, which will result in incomplete conversion of sample NO_3^- and consequently inaccurate determination of sample isotope ratios. We measured NO_2^- concentration with the nitrite test reagent (Hach0596 NitriVer3, TOA-DKK, prod. no. 2107169). We seldom detected NO_2^- left in the incubated growth media after 6 to 14 days incubation (roughly two bottles in 3 years, out of more than 1200 bottles), and when we had that (**Fig. 4.2.2. B**), we did not use that bottle with NO_2^- for the further processes.

A

B

Figure 4.2.2. TSB media before autoclaving (Left), after autoclaving (Middle), and 1-week incubated culture after denitrifier inoculation (A). Red-colored culture by a nitrite test in case of deactivation of denitrifiers (Left bottle) (B).

Sample preparation for NO_3^-

The day before sample preparation, the NO_3^--free glucose medium was prepared in 390 mL in a 500 mL autoclavable glass bottle with screw cap (PYREX ®, prod. no. 1395-500). The chemical composition of the glucose medium was as follows: 1.8 g L^{-1} glucose (Wako, prod. no. 04931165), 36 mM KH_2PO_4 (Wako, prod. no. 169-04245), and 14 mM K_2HPO_4

(Wako, prod. no. 164-04295). The medium was autoclaved at 121℃ for 20 min and allowed to cool.

For 120 vials, we sacrificed three 500 mL pre-inoculated bottles (with 440 mL of working culture). Three of the 400 mL working cultures were poured into three 500 mL polypropylene centrifuge bottle tubes with plug seal cap (Corning®, prod. no. 431123) and were centrifuged at 4000 rpm (3420 *g*) and 4℃ for 30 min with the centrifuge (KUBOTA corp., Model 5930). The supernatant in each bottle was discarded completely, and the harvested denitrifier cells in the three 500 mL centrifuge bottles were collected and resuspended into 130 ml of glucose medium in one centrifuge bottle finally, representing a 3.4-fold concentration of cells. One or two drops of Antifoam SI (Wako, prod. no. 016-17431) was added to the cell suspension and stirred loosely. This cell suspension was purged for at least 1 hr at approximately 100 - 200 mL min^{-1} with high purity N_2 gas (99.999%, ultra-pure, Air Liquide Japan GK) to ensure anaerobic conditions and incubated at 4℃ overnight to allow the denitrifiers to consume NO_3^- completely in their cells. In the case for 260 vials, we repeated these processes twice; preparation of the glucose media, centrifuging the inoculated growth media, and preparation of the cell suspension, which usually takes half a day.

On the next day, 3 mL of the cell suspension were pipetted into each of 20-mL headspace crimp top vials (Chromacol prod. no. 20-CV, ashed at 450℃ for 2 hrs), capped with gray butyl septa (Wheaton, prod. no. 20-0025) and 20-mm aluminum crimp seals (GL Sciences, prod. no. 1030-51780). The capped vials were inserted upside down onto the purging manifold (**Fig. 4.2.3** ; see (Coplen *et al.*, 2012) and purged for at least 2 hr at approximately 40 mL min^{-1} with high purity N_2 gas (99.999%, ultra-pure, Air Liquide Japan GK). Thereafter, each vial was labeled and measured for weight. A sample was then injected into each vial using 1 mL disposable syringe with a 25-gauge needle (Terumo Corp., prod. no. SS-01T; Terumo Corp., prod. no. NN-2525R). All samples had been adjusted to exactly the same pH and salinity (2.5% NaCl). NO_3^- standard solutions had been prepared as the same pH, salinity and $\delta^{18}O_{H2O}$ as the batch of the samples to be analyzed. The volume of sample and reference solutions were adjusted to achieve a final sample size of 50 nmol N. Then each vial was shaken well and weighed again to confirm sample injection volume. Those vials were stored upside down at 25℃ overnight in an incubator (OF-600SB, AS ONE Corp.) to allow for complete conversion of NO_3^- to N_2O. After the overnight incubation, 0.1 mL of 10 M NaOH was injected into each vial using a 1 mL

disposable syringe with a 26- gauge needle (Terumo Corp., prod. no. SS-01T; Terumo Corp., prod. no. NN-2613S) to stop the reaction and to dissolve denitrifier-derived gaseous CO_2. The vials were stored upside down to minimize leakage of N_2O through the septum until the PT-GC/IRMS analysis.

Figure 4.2.3 Connected N_2 gas purging lines with gas flow controller (Right side) and the state of purging 3-mL denitrifier-concentrated glucose media in 15 mL vials with N_2 gas (Left side). 24 vials are available in each line (6 vials × 4 blocks).

4.2.6 PT-GC/IRMS system

A purge-and-trap, gas-chromatography, isotope ratio mass spectrometry (PT-GC/IRMS) was used for isotopic analyses. In order to measure 112 vials in the single analytical run (a batch), we modified the original Sercon PT-GC/IRMS system (Sercon 20-22 IRMS with Liquid Handler (GX-271, Gilson), Cryoprep (Sercon), and GC (GC-4000, GL Science)) according to primarily the following recommendation given by (McIlvin and Casciotti, 2011). Briefly, we installed a -60℃ ethanol trap to trap water vapor and possibly volatile organic carbon (VOC) (**A3** in **Figure 4.2.4**). This trap is dropped into the ethanol chilled by the cooler (EK90, Thermo Fisher Scientific) at -60℃ at the beginning of the analytical program (for 400 s) to remove the water vapor and VOC from the vial while being purged with ultra-pure

Helium (ultra-pure, Air Liquide Japan GK.) (**Table 4.2.1, Fig. 4.2.5**). At 400 s in the acquisition sequence, this trap is lifted from the ethanol and heated up to 100℃ by a self-made sheathed heater with temperature controller for 270 s (A3, **Table 4.2.1**) to foreflush and remove any trapped water vapor and VOC. After the heating, the A3 trap is dropped and lifted up twice to mix the chilled ethanol and then dropped into the ethanol again. The next sample must be introduced into this trap when this trap is chilled enough to capture water vapor and VOC effectively. In our setting with the room temperature of ca. 25℃, the temperature of A3 trap is ca. -10℃ when the purging of the next sample is started. The analytical time for one sample was 1100 s **(Table 4.2.1)** which depends on the time required for ethanol trap (A3 in **Fig. 4.2.4**) to be cooled. We used two GC columns (GC1 w Restek RT-Q-Bond, 0.53 mm, 20 µm, 30 m and GC2 w Varian CP-Poraplot Q, 0.32 mm, 10 µm, 25m, in **Fig. 4.2.4**) and applied the backflush system for the GC1 column to keep the background signal of *m/z* 46(Röckmann *et al.*, 2003; McIlvin and Casciotti, 2011), low during the analysis. In addition, we incorporated a liquid N_2 autofill system (ALC Model-SXDII, Taiyo-Nissan) which had been originally tested by Kazama Laboratory in Yamanashi University, Japan (Nakamura *et al.*, 2007, 2011; Wijayanti *et al.*, 2012) to run this PT-GC/IRMS system continuously for up to 34 hr.

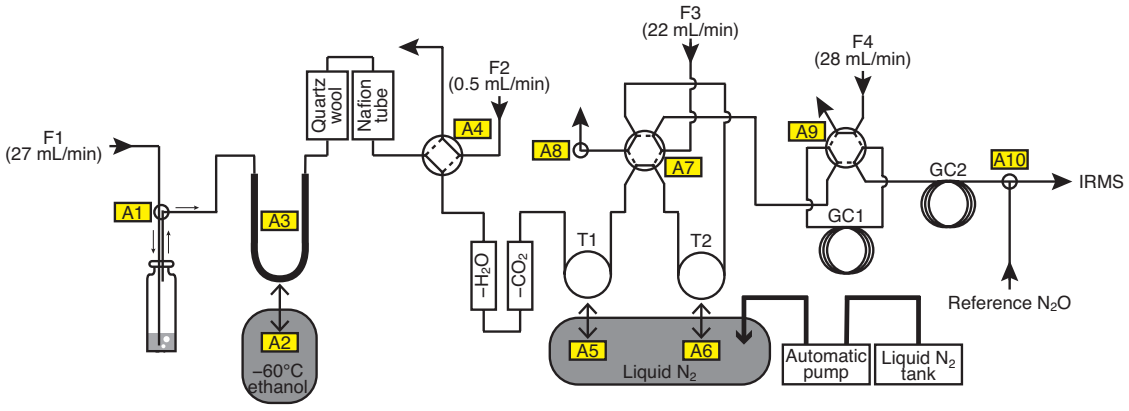

Figure 4.2.4 Schematic diagram of a modified Sercon PT-GC/IRMS system for N_2O isotope analysis. T represents cryotrap. A1-A10 are automation controlled by Sercon (corresponding with Table S1). GC represents gas chromatograph.

Figure 4.2.5 Ethanol trap in Sercon system.

	A1	A2	A3	A4	A5	A6	A7	A8	A9	A10		IRMS		
Time(s)	Sample sparging	Cold trap	Cold trap heater	4-port valve (Vent/Line)	Cryoloop1	Cryoloop2	6-port valve (Cryofocus)	Vent	6-port valve (GC column)	Reference N_2O gas	Autosampler needle	Reference N_2O gas	Sample CO_2 gas	Sample N_2O gas
1		down					disconnect							
4														
5	on				down						positioning			
20										inject				
23								close						
25										uninject	inject			
28								open						
310									backflush					
380						down	connect							
385	off										uninject			
387														
390					up									
400		up	on	to vent										
480									connect					
490	on						disconnect							
495						up								
610	off													
670			off											
840		down		to line										
845		up												
850		down												
855		up												
860		down												
1100														
1120												Integrate Start		
1210												Integrate End		
1435													Integrate Start	
1525													Integrate End	
1535														Integrate Start
1705														Integrate End
2200														

Table 4.2.1. Time sequence for Sercon N_2O acquisition

4.2.7 Isotopic analysis

Molecular (N_2O^+) ion measurements at *m/z* 44, 45 and 46 were made on each gas sample using a Sercon 20/22 IRMS. Analyses of $\delta^{15}N$ (= $(^{15}N/^{14}N)_{sample}$ / $(^{15}N/^{14}N)_{AIR}$ − 1) and $\delta^{18}O$ (= $(^{18}O/^{16}O)_{sample}$ / $(^{18}O/^{16}O)_{VSMOW}$ − 1) were provisionally referenced to atmospheric N_2 (AIR) and Vienna standard mean ocean water (VSMOW) scales, respectively, by normalizing the N_2O reference gas (Sumitomo Seika Chemicals Co., Ltd., Japan) peak injected at the beginning of the N_2O detection (at 20-25s, **Table 4.2.1**). Since our system exhibits some non-linearity for $\delta^{15}N$ and $\delta^{18}O$ of N_2O with respect to the amount of N_2O introduced to IRMS (**Fig. 4.2.1**), we controlled the sample size for each analysis batch (i.e. 50 nmol N for the samples and standards). Although our sample size was constant, we corrected the raw $\delta^{15}N$ and $\delta^{18}O$ values with the relationship between N_2O amount and $\delta^{15}N$ and $\delta^{18}O$ (**Fig. 4.2.1**) before the blank correction. This linearity test is carried out with 1000 ppm N_2O gas (balanced with He, Taiyo-Nissan Co. Ltd.) occasionally after the blackout and changing of the filament in the IRMS source. We also obtained the relationship between the amount of N_2O introduced to IRMS and N_2O peak area detected by IRMS (**Fig. 4.2.1. c**), which can be used for the calculation of N_2O amount recovered from the vial. The blank from the denitrifier media (3 mL of the cell suspension plus 0.1 - 0.2 mL of NaOH solution) was ca. 0.12 nmol N, and the blank from the azide (1 mL MillQ water with pH 12 and 2.5 % salinity, 40 µL azide buffer and 2.0 mL NaOH solution) was ca. 1.03 nmol N. This relatively high blank for NO_2^- might be attributable to the artificial sea salt we used in this study. We also checked yields of N_2O (N_2O detected by IRMS / N_2O expected from NO_2^- or NO_3^- concentration and the amount of injected solution) after the non-linearity and the blank corrections.

For NO_2^- and NO_3^- isotope measurements, the N_2O reference gas is not the absolute reference. The slope and intercept of the linear regression between the measured isotopic values of the standards (normalized to AIR and VSMOW using the N_2O reference gas tank) and known isotopic values of the standards (vs AIR and VSMOW) are used to calculate the isotopic values of NO_2^- and NO_3^- samples vs AIR and VSMOW from the corrected values(Casciotti *et al.*, 2002; McIlvin and Casciotti, 2011). The corrected $\delta^{15}N$ and $\delta^{18}O$ values of the sample N_2O converted from NO_2^- were calibrated against the values from in-house NO_2^- standards; JAM 1 ($\delta^{15}N$ = -2.5 ‰, $\delta^{18}O$ = 91.7 ‰), JAM 2 ($\delta^{15}N$ = 1.8 ‰, $\delta^{18}O$ = 9.9 ‰), JAM 3 ($\delta^{15}N$ = -26.4 ‰, $\delta^{18}O$ = 39.4 ‰), and JAM 4 ($\delta^{15}N$ = -1.5 ‰, $\delta^{18}O$ = -15.2 ‰). These in-house NO_2^- standards

were prepared with several nitrite reagents with the help of the rapid exchange of O-atoms between H_2O and NO_2^- at high temperature (e.g. 70℃) observed by (Nishizawa *et al.*, 2016), and calibrated against internal lab standards developed in the Wankel lab at WHOI (Wankel *et al.*, 2017) ; WILIS 10 ($\delta^{15}N$ = -1.7 ‰, $\delta^{18}O$ = 13.2 ‰), WILIS 11 ($\delta^{15}N$ = 57.1 ‰, $\delta^{18}O$ = 8.6 ‰) and WILIS 20 ($\delta^{15}N$ = -7.8 ‰, $\delta^{18}O$ = 46.6 ‰) with GC/IRMS system in JAMSTEC. Waters with different $\delta^{18}O$ values were prepared with 97% ^{18}O-H_2O (Cambridge Isotope Laboratories, Inc.) and MillQ water. The heaviest water for in-house standards (112‰-H_2O) was prepared with 50 μL of 99% ^{18}O-H_2O water (Cambridge Isotope Laboratories, Inc.) and 200 mL MillQ water. For JAM1, 30 g of KNO_2 (Wako, prod. no. 169-27325) was dissolved in 100 mL of 112‰-H_2O. For JAM2, 30 g of $NaNO_2$ (Junsei, prod. no. 10285-0301) was dissolved in the mixture of 40 mL of 112‰-H_2O and 60 mL of MillQ water. JAM 3 was prepared with 30 g of $NaNO_2$ (Sigma, prod. no. V800392-500G) dissolved in 100 mL of MillQ water, and JAM4 was prepared with 30 g of $NaNO_2$ (Wako, prod. no. 199-02565) dissolved in the mixture of 20 mL of ^{18}O-depleted water by the distillation of 80 mL of MillQ water. These NO_2^- solutions in the 250 mL bottle with the cap (Schott, prod. no. 017200-250A) were incubated more than 1 month at 85℃ in the oven. After the incubation, these solutions were dried up at 80℃ in the oven for 3 days with the caps open and occasional stirring. After homogenization with the agate mortar, the nitrite salts were dried at 105℃ for 5 hrs. Stock solutions of 10 mM of each NO_2^- standard were prepared with MillQ water with high pH (12) and frozen until the analysis. Each reference solution was analyzed three times, and replicate analyses yielded respective precisions of generally 0.04 ~ 0.16‰ for $\delta^{15}N_{NO2-}$ (maximum = 0.51%) and 0.09 ~ 0.28‰ (maximum = 0.48%) for $\delta^{18}O_{NO2-}$, respectively. For NO_3^-, we used IAEAN3 ($\delta^{15}N$ = 4.7‰, $\delta^{18}O$ = 25.6‰), USGS32 ($\delta^{15}N$ = 180‰, $\delta^{18}O$ = 25.7‰), USGS34 ($\delta^{15}N$ = -1.8‰, $\delta^{18}O$ = -27.9‰), and USGS35 ($\delta^{18}O$ = 57.5‰) for the calibration(Thuan *et al.*, 2018). Replicate analyses yielded respective precisions of generally 0.05 ~ 0.17‰ (maximum = 0.81%) for $\delta^{15}N_{NO3-}$ and 0.15 ~ 0.46% (maximum = 1.40%) for $\delta^{18}O_{NO3-}$, respectively.

The $\delta^{18}O_{H2O}$ was measured by equilibration with NO_2^- and subsequent conversion of NO_2^- to N_2O using a modified azide method(McIlvin and Casciotti, 2011) with 0.5 mL of the samples and standards. The $\delta^{18}O$ data was finally calibrated against GISP (-24.8 ‰) and the in-house water standards; Alaskan bottled mineral water (-19.0 ‰) and bottled de-salted seawater (0.2 ‰) (those $\delta^{18}O$ values were determined by SI Science. Co. ltd). The sample with

high $\delta^{18}O_{H2O}$ was mixed with MillQ water (-12.6 ‰) to yield measured $\delta^{18}O$ values falling into the range of the standards (i.e. between -24.8 to 0.2 ‰), calculated according to the mixing ratio. Replicate analyses yielded respective precisions of 0.20‰ for $\delta^{18}O_{H2O}$.

4.2.8 Inference of $^{18}\varepsilon_{eq}$ and k_{eq} by non-linear mixed model

The approach of $\delta^{18}O_{NO2}$ to isotope equilibrium ($\delta^{18}O_{NO2,eq}$) is modeled as an following exponential form:

$$\delta^{18}O_{NO2} = \delta^{18}O_{NO2,eq,ij} + (\delta^{18}O_{NO2,initial} - \delta^{18}O_{NO2,eq,ij}) \times \exp(-kt) + e_{ij} \quad \cdots(1)$$

k (h^{-1}) represents the rate constant for abiotic equilibration of O atoms, and t is reaction time (h). The $\delta^{18}O_{NO2,initial}$ is $\delta^{18}O_{NO2-}$ at the initial time(Buchwald and Casciotti, 2013). Subscripts i and j indicate experimental ID regarding replication in each experiment and each $\delta^{18}O_{H2O}$ value setting for random effects. e_{ij} is a normal error term, which is $e_{ij} \sim N(0, \sigma_{ij})$. Here, σ_{ij} is variance parameter for each i th and j th experiment. The equilibrium fractionation of oxygen isotopes between nitrite and water ($^{18}\varepsilon_{eq}$) was calculated as follows:

$$^{18}\varepsilon_{eq} = [(^{18}O/^{16}O)_{NO2-} / (^{18}O/^{16}O)_{H2O} - 1] \times 1000 \fallingdotseq \delta^{18}O_{NO2-} - \delta^{18}O_{H2O} \quad \cdots(2)$$

In order to calculate k and $^{18}\varepsilon_{eq}$, the exponential equation was fitted using the nlme (non-linear mixed effect) package in R (Pinheiro *et al.*, 2020). The data sets of the four different experiments having different $\delta^{18}O_{H2O}$ values ($\delta^{18}O_{H2O}$ = -12.6, 25.9, 56.7, and 110.1‰) were applied to the model. The exponential fits yielded values for both k and $^{18}\varepsilon_{eq}$.

4.3. Result and Discussion

4.3.1 Standard calibration with different $\delta^{18}O_{H2O}$ values in azide method

The $\delta^{18}O$ of N_2O produced from sample NO_2^- by azide reaction depends on 1) the $\delta^{18}O$ of sample NO_2^-, 2) O isotope exchange between NO_2^- and H_2O during the NO_2^- and azide reaction (conversion of NO_2^- to N_2O), 3) isotopic fractionation during loss of O atoms in the NO_2^- and azide reaction, and 4) $\delta^{18}O$ of H_2O. Thus, the calibration should be corrected by the slope and intercept of the standard curves that are made from NO_2^- standards with known $\delta^{18}O$ and actual measured values of $\delta^{18}O_{N2O}$ (McIlvin and Altabet, 2005).

$\delta^{18}O_{N2O} = m_{standards} \bullet \delta^{18}O_{NO2} + b$ ···(3)

where b is the y intercept, and $m_{standards}$ is the slope obtained by the relationship. A plot of $\delta^{18}O_{N2O}$ versus $\delta^{18}O_{NO2}$ should have the slope of 1 if no oxygen exchange occurs with H_2O. The slope would be zero if complete exchange with H_2O occurred (McIlvin and Altabet, 2005). The deviation from slope of 1 reflects the degree of O isotope exchange during the conversion of NO_2^- to N_2O. Ideally, NO_2^- should be converted to N_2O by azide with minimal O isotope exchange. In our experiments, the slopes of the standard curves were constant (0.888 ~ 0.895, r^2 = 0.999; **Fig. 4.3.1**), indicating the O isotope exchange of 10.8 ± 0.4% at pH 4.4 regardless of $\delta^{18}O_{H2O}$ value. The O isotope exchange of 19% (the slope of standard curve was 0.81) at pH 4.0 was previously reported (McIlvin and Altabet, 2005) , suggesting that lower pH can induce greater exchange of O atoms between H_2O and NO_2^-. It has been demonstrated that increasing pH inhibits the O isotope exchange but slows the reaction between NO_2^- and azide. For example, the NO_2^- and azide reaction rate was reduced by roughly 20% above pH 5(McIlvin and Altabet, 2005). In this study, the azide reaction was completed within 30 min with O isotope exchange ratio of 10 - 11 % at pH 4.4. Because of O isotope exchange between NO_2^- and H_2O, the y-intercept of the standard calibration curve also increased with increasing $\delta^{18}O_{H2O}$ (**Fig. 4.3.1**, $\delta^{18}O_{H2O}$ = -12.6‰: -9.735, $\delta^{18}O_{H2O}$ = 25.9‰: -4.203, $\delta^{18}O_{H2O}$ = 56.7‰: -0.765, and $\delta^{18}O_{H2O}$ = 110.1‰: 6.305). Even though O isotope exchange remained unchanged, there was a 16‰ difference in the y-intercept between $\delta^{18}O_{H2O}$ of -12.6‰ and 110.1‰ arising from the ~10% incorporation of O atom from ambient water into the product N_2O. The empirical relationship between $\delta^{18}O_{H2O}$ and y-intercept ($b_{expt.NO2}$) can be given as follows (**Fig. 4.3.2**, Eq. 4):

$b_{expt.NO2} = 0.129 \times \delta^{18}O_{H2O} - 7.926, \quad r^2 = 0.999$ ···(4)

A positive linear relationship between $\delta^{18}O_{H2O}$ and y-intercept ($b_{expt.NO2}$) was observed. The y-intercept of the standard calibration curve was affected by $\delta^{18}O_{H2O}$ used to make the NO_2^- standards. Thus, we emphasize here that the $\delta^{18}O_{H2O}$ used to make the NO_2^- standards should be as similar to the $\delta^{18}O_{H2O}$ of the sample water as possible.

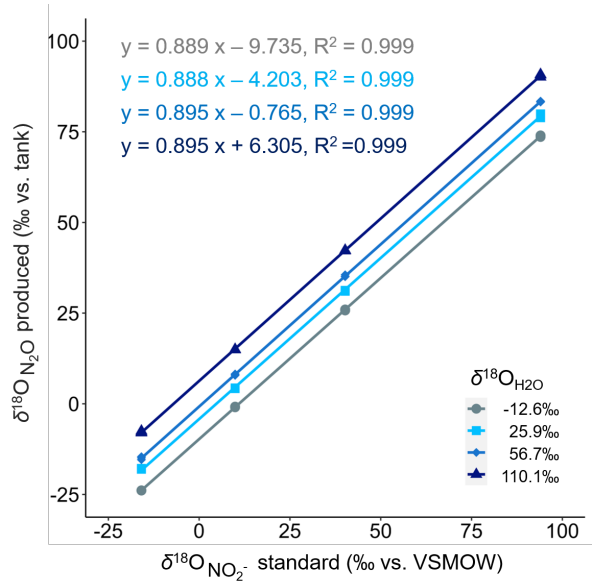

Figure 4.3.1 Oxygen isotopic composition of NO_2^- standards converted to N_2O using the azide method. Four in-house NO_2^- standards (JAM1 - 4) were prepared with water having different $\delta^{18}O_{H2O}$ ($\delta^{18}O_{H2O}$ = -12.6, 25.9, 56.7, and 110.1‰). The measured $\delta^{18}O$ values of N_2O produced from NO_2^- standards are plotted against assigned $\delta^{18}O$ values of the NO_2^- standards. Identical colors and plot symbols represent data obtained from NO_2^- standards prepared with water having the same $\delta^{18}O_{H2O}$.

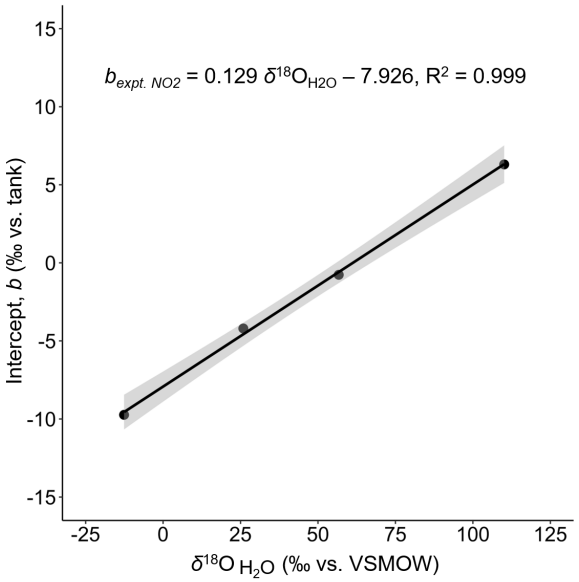

Figure 4.3.2 The relationship between $\delta^{18}O_{H2O}$ and experimentally determined intercept ($b_{expt.NO2}$) in the azide method. Filled circles are actual measured y-intercepts for respective $\delta^{18}O_{H2O}$ ($\delta^{18}O_{H2O}$ = -12.6‰: -9.735, $\delta^{18}O_{H2O}$ = 25.9‰: -4.203, $\delta^{18}O_{H2O}$ = 56.7‰: -0.765, and $\delta^{18}O_{H2O}$ = 110.1‰: 6.305 from **Fig. 4.3.1.**). The solid line is the regression line of actual measured y-intercept. The grey area shows the 95% confidence interval.

4.3.2 Standard calibration with different $\delta^{18}O_{H2O}$ values in denitrifier method

The $\delta^{18}O$ of N_2O produced by the denitrifier method depends on 1) isotopic fractionation associated with the loss of O atoms from NO_3^-, 2) the abiotic exchange of O atoms between NO_3^- and denitrification intermediates and H_2O during conversion of NO_3^- to N_2O by denitrifying bacteria(Casciotti *et al.*, 2002) , and 3) $\delta^{18}O$ of H_2O. The measured $\delta^{18}O_{N2O}$ values derived from known $\delta^{18}O$ NO_3^- standards were plotted against the $\delta^{18}O$ of NO_3^- standards prepared using waters with different $\delta^{18}O_{H2O}$ values (**Fig. 4.3.3.**). The slopes of the individual standard curves appeared to be constant (0.934~0.957, r^2=0.999), indicating an oxygen isotope exchange with water of 5.2 ± 1.0% **(Fig. 4.3.3.)**. The degree of O isotope exchange in the denitrifier method was smaller than that in the azide method (10.8 ± 0.3%). The previous study using ^{18}O-labeled water indicated that water exchange contributed between 2.4 and 8.7% of the O atoms in the N_2O produced by *Pseudomonas aureofaciens*(Casciotti *et al.*, 2002). The degree of O exchange with water varies greatly among bacterial strains, which may be related to the biochemistry of nitrite reduction(Casciotti *et al.*, 2002)(Ye *et al.*, 1991). Indeed, bacteria possessing the copper-type nitrite reductase (as *P. aureofaciens* does) exhibited less O isotope exchange than denitrifiers possessing the heme-type nitrite reductase (e.g., *Pseudomonas chlororaphis*)(Coplen *et al.*, 2012). Even though the degree of O atom exchange is small, the y-intercepts of standard calibration curves slightly increased with increasing $\delta^{18}O_{H2O}$ of water (**Fig. 4.3.3.**, $\delta^{18}O_{H2O}$ = -12.6‰: -2.453, $\delta^{18}O_{H2O}$ = 25.9‰: -2.201, $\delta^{18}O_{H2O}$ = 56.7‰: -2.024, and $\delta^{18}O_{H2O}$ = 110.1‰: -1.735). The difference in the intercept was smaller than that observed in the azide method (**Fig. 4.3.1.**, azide method, $\delta^{18}O_{H2O}$ = -12.6‰: -9.735, $\delta^{18}O_{H2O}$ = 25.9‰: -4.203, $\delta^{18}O_{H2O}$ = 56.7‰: - 0.765, and $\delta^{18}O_{H2O}$ = 110.1‰: 6.305). The relationship between measured $\delta^{18}O_{H2O}$ and intercept ($b_{expt.NO3}$) was described as follows: (**Fig. 4.3.4.**, Eq. (5))

$$b_{expt.NO3} = 0.00582 \times \delta^{18}O_{H2O} - 2.366,\ r^2 = 0.998 \quad \cdots (5)$$

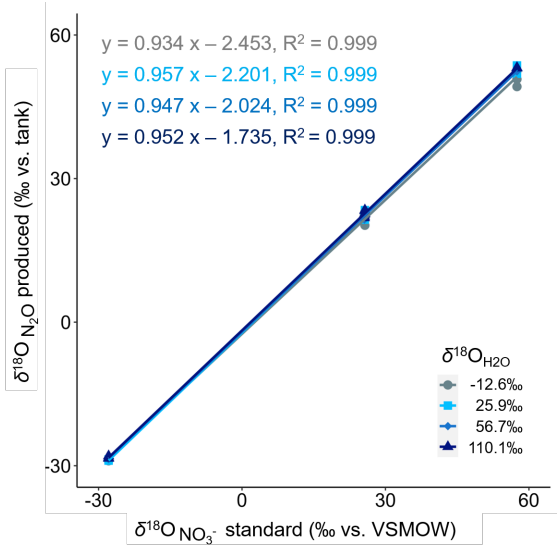

Figure 4.3.3 Oxygen isotopic composition of NO_3^- standards converted to N_2O using the denitrifier method. Four NO_3^- isotope standards (IAEAN3, USGS32, USGS34, and USGS35) were prepared with water having different $\delta^{18}O_{H2O}$ ($\delta^{18}O_{H2O}$ = -12.6, 25.9, 56.7, and 110.1‰). The measured $\delta^{18}O$ values of N_2O produced from NO_3^- standards are plotted against assigned $\delta^{18}O$ values of the NO_3^- standards. Assigned values of $\delta^{18}O_{NO3-}$ of IAEAN3 ($\delta^{18}O$ = 25.6‰) is close to that of USGS32 ($\delta^{18}O$ = 25.7‰). Thus, those plots are overlapped.

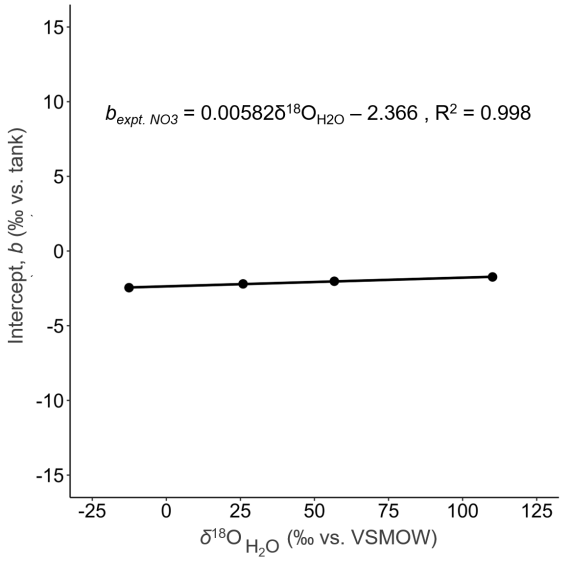

Figure 4.3.4 The relationship between $\delta^{18}O_{H2O}$ and experimentally determined intercept ($b_{expt.\ NO3}$) in the denitrifier method. Filled circles are actual measured y-intercepts for respective $\delta^{18}O_{H2O}$ ($\delta^{18}O_{H2O}$ = -12.6 ‰: -2.453, $\delta^{18}O_{H2O}$ = 25.9‰: -2.201, $\delta^{18}O_{H2O}$ = 56.7‰: -2.024, and $\delta^{18}O_{H2O}$ = 110.1‰: -1.735 from **Fig. 4.3.3.**) The solid line is the regression line of actual measured y-intercept. The gray area shows the 95% confidence interval, but it hides behind the solid line.

4.3.3 Abiotic equilibrium isotope effect between nitrite and water

The rate of abiotic O atom exchange was measured in laboratory experiments (**Fig. 4.3.5. A**)**.** Based on the isotope exchange defined in Eq (1) with the inferred parameters, the equilibrium arrival time, which is defined as the time when the isotope ratio change per minutes is less than 10^{-6} ‰, was found to be less than 650 h for the exchange of O atoms between nitrite and water (**Fig. 4.3.5. A**). The exponential fitting of the experimental results for $\delta^{18}O_{NO2}$ versus reaction time yielded a rate constant of $(1.13 \pm 0.007) \times 10^{-2}$ (h^{-1}), which is consistent with the calculated k_{eq} (1.14×10^{-2} h^{-1}; **Table 4.3.1**) with the equation provided in (Buchwald and Casciotti, 2013). The equilibrium oxygen isotope effect between nitrite and water ($^{18}\varepsilon_{eq}$) was determined to be 11.9 ± 0.1‰ based on $\delta^{18}O_{NO2}$ and $\delta^{18}O_{H2O}$ at equilibrium. The value of $^{18}\varepsilon_{eq}$ was also consistent with previous reports (**Table 4.3.1**). For this experiment, the $\delta^{18}O_{H2O}$ used to make the NO_2^- standards was same as $\delta^{18}O_{H2O}$ of the sample water (**Fig. 4.3.5. A**). In order to visualize the $\delta^{18}O_{H2O}$ dependence of the NO_2^- oxygen isotope ratio analysis, samples calibrated by standards made with same $\delta^{18}O_{H2O}$ water and different $\delta^{18}O_{H2O}$ water were compared (**Fig. 4.3.5. B**). Actual values of $\delta^{18}O_{N2O}$ under $\delta^{18}O_{H2O}$ of 25.9, 56.7, and 110.1‰ were calibrated against NO_2^- standards made with water ($\delta^{18}O_{H2O}$ = -12.6‰). Using NO_2^- standards made with different $\delta^{18}O_{H2O}$ water ($\delta^{18}O_{H2O}$ = -12.6‰) induced constant discrepancy of 6.3‰ ± 0.003‰, 10.3 ± 0.2‰, and 18.3 ± 0.4‰ for $\delta^{18}O_{H2O}$ of 25.9, 56.7, and 110.1‰, respectively (**Fig. 4.3.5. B**). The gap between $\delta^{18}O_{H2O}$ of sample and $\delta^{18}O_{H2O}$ of the NO_2^- standards leads to inaccurate measurement of $\delta^{18}O_{NO2-}$ and consequently results in $^{18}\varepsilon_{eq}$ determination in error.

In order to confirm that no abiotic O atom exchange between NO_3^- and NO_2^- occurs, we prepared another batch with NO_3^- (0.23 mM-N) under $\delta^{18}O_{H2O}$ of -12.6 ‰ (**Fig. 4.3.6).** The time course of $\delta^{18}O_{NO2}$ behavior with NO_3^- addition (**Fig. 4.3.6. B**) was exactly same as $\delta^{18}O_{NO2}$ without NO_3^- addition (**Fig. 4.3.6. A**). In addition, the values of the $\delta^{18}O_{NO3}$ were consistent during the abiotic NO_2^--water equilibrium isotope effect experiment (**Fig. 4.3.6. B**). As for the experiment with NO_3^- (**Fig. 4.3.6. B**), the exponential fitting by the non-linear mixed effect model of the experimental results for $\delta^{18}O_{NO2}$ versus reaction time yielded a rate constant of $(1.19 \pm 0.067) \times 10^{-2}$ (h^{-1}) and an oxygen equilibrium isotope effect of 11.9 ± 0.1‰, which are identical with those without NO_3^- addition. Thus, we confirmed no O atom exchanges between NO_2^- and NO_3^-, and NO_3^- and water during the incubation (1400 hrs) with the moderate pH and temperature.

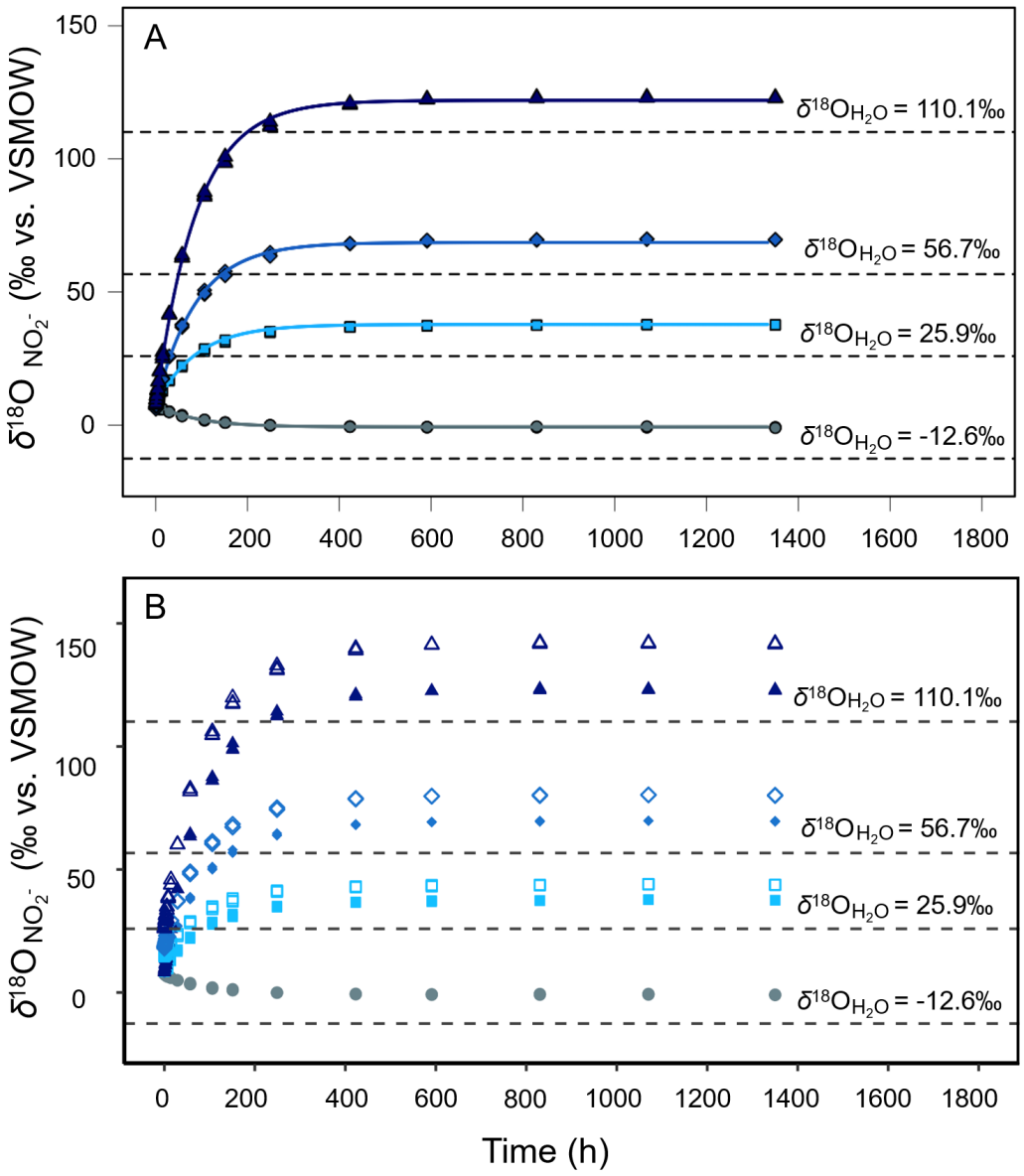

Figure 4.3.5 Time course of $\delta^{18}O_{NO2}$ behavior during the abiotic NO_2^--water equilibrium isotope effect experiments with four different $\delta^{18}O_{H2O}$ values. (A) Triplicate incubations at each $\delta^{18}O_{H2O}$ were conducted, and all data are plotted but some of the data points are overlapped due to small variations. Identical colors and plot symbols indicate data obtained from the same batches using the same water of $\delta^{18}O_{H2O}$. Dashed lines indicate $\delta^{18}O_{H2O}$. Solid line indicates result of fitting. (B) Comparison between samples calibrated by standards made by same $\delta^{18}O_{H2O}$ water and different $\delta^{18}O_{H2O}$ water. Filled symbols were calibrated by NO_2^- standards made by water, of which $\delta^{18}O_{H2O}$ was same as samples. Open symbols were calibrated by NO_2^- standards made by water, of which $\delta^{18}O_{H2O}$ was 12.6‰.

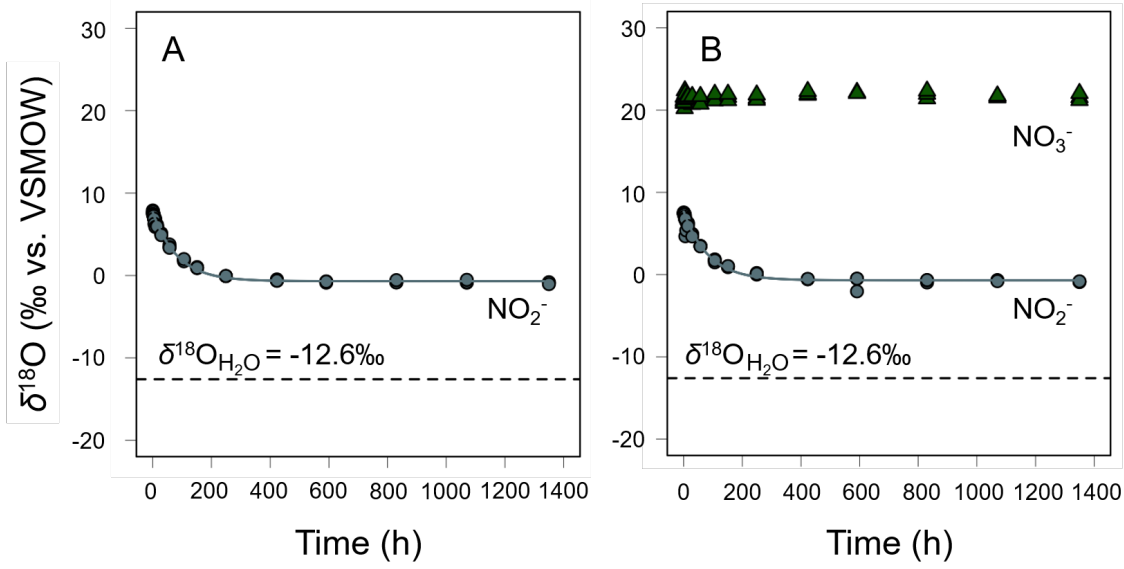

Figure 4.3.6 Time course of $\delta^{18}O_{NO2}$ and $\delta^{18}O_{NO3}$ behavior during the abiotic NO_2^--water equilibrium isotope effect experiment with (B) and without (A) nitrate under $\delta^{18}O_{H2O}$ of -12.6 ‰. Grey circles indicate $\delta^{18}O_{NO2-}$. Green triangles indicate $\delta^{18}O_{NO2-}$. Dashed lines indicate $\delta^{18}O_{H2O}$.

Table. 4.3.1. Comparison with reported equilibrium oxygen isotope effects and rate constants

Temp.(°C)	pH	k(h^{-1})	$^{18}\varepsilon_{eq}$(‰)	Reference
70	6.5	2.10×10^{-2}	10 ± 4	Nishizawa et al., 2016
70	8.0	0.96×10^{-2}	12 ± 2.9	Nishizawa et al., 2016
30	7.5	1.14×10^{-2}	12.4	Buchwald and Casciotti 2012
30	7.5	1.13×10^{-2}	11.9 ± 0.1	This study

4.4. Conclusions

In this study, the influence of the value of $\delta^{18}O_{H2O}$ on the measurement of NO_2^- and NO_3^- isotope ratio was quantitatively evaluated. Measurement of $\delta^{18}O_{NO2-}$ by the azide method was highly sensitive to $\delta^{18}O_{H2O}$ due to large O isotope exchange between NO_2^- and H_2O during azide reaction. Compared to the azide method, the $\delta^{18}O_{NO3-}$ measurement by the denitrifier method showed smaller O isotope exchange between NO_3^- and H_2O during conversion of NO_3^- to N_2O. Based on these experimental results, we therefore strongly recommend that water having the same $\delta^{18}O_{H2O}$ as that of the sample be used to make appropriate NO_2^- and NO_3^- standards. Abiotic NO_2^--H_2O equilibrium isotope exchange experiments yielded a rate constant of $(1.13 \pm 0.007) \times 10^{-2}$ (h^{-1}) and an equilibrium isotope effect of 11.9 ± 0.1‰ under the condition of pH=7.5, 30°C, and 2.5% salinity.

4.5 References

APHA, AWWA, and WEF (2005) Standard Methods for the Examination of Water and Wastewater. Washington, D.C.

Berhanu, T.A., Savarino, J., Erbland, J., Vicars, W.C., Preunkert, S., Martins, J.F., and Johnson, M.S. (2015) Isotopic effects of nitrate photochemistry in snow: A field study at Dome C, Antarctica. *Atmos Chem Phys* 15: 11243–11256.

Bourbonnais, A., Altabet, M.A., Charoenpong, C.N., Larkum, J., Hu, H., Bange, H.W., and Stramma, L. (2015) N-loss isotope effects in the Peru oxygen minimum zone studied using a mesoscale eddy as a natural tracer experiment. *Global Biogeochem Cycles* 793–811.

Bowen, G.J. (2010) Isoscapes: Spatial pattern in isotopic biogeochemistry. *Annu Rev Earth Planet Sci* 38: 161–187.

Bowen, G.J. and Revenaugh, J. (2003) Interpolating the isotopic composition of modern meteoric precipitation. *Water Resour Res* 39: 1–13.

Brandes, J.A. and Devol, A.H. (2002) A global marine-fixed nitrogen isotopic budget: Implications for Holocene nitrogen cycling. *Global Biogeochem Cycles* 16: 1120.

Buchwald, C. and Casciotti, K.L. (2013) Isotopic ratios of nitrite as tracers of the sources and age of oceanic nitrite. *Nat Geosci* 6: 308–313.

Buchwald, C., Santoro, A.E., Stanley, R.H.R., and Casciotti, K.L. (2015) Nitrogen cycling in the secondary nitrite maximum of the eastern tropical North Pacific off Costa Rica. *Global Biogeochem Cycles* 29: 2061–2081.

Casciotti, K.L. (2016) Nitrite isotopes as tracers of marine N cycle processes. *Phil Trans R Soc A* 374: 20150295.

Casciotti, K.L., Bohlke, J.K., McIlvin, M.R., Mroczkowski, S.J., and Hannon, J.E. (2007) Oxygen isotopes in nitrite: Analysis, calibration, and equilibration. *Anal Chem* 79: 2427–2436.

Casciotti, K.L. and Buchwald, C. (2012) Insights on the marine microbial nitrogen cycle from isotopic approaches to nitrification. *Front Microbiol* 3: 1–14.

Casciotti, K.L. and McIlvin, M.R. (2007) Isotopic analyses of nitrate and nitrite from reference mixtures and application to Eastern Tropical North Pacific waters. *Mar Chem* 107: 184–201.

Casciotti, K.L., Sigman, D.M., Hastings, M.G., Bohlke, J.K., and Hilkert, A. (2002) Measurement of the oxygen isotopic composition of nitrate seawater and freshwater using the dentirifier method. *Anal Chem* 74: 4905-4912.

Coplen, T.B., Qi, H., Revesz, K., Casciotti, K.L., and Hannon, J.E. (2012) Determination of the δ 15 N of Nitrate in Water ; RSIL Lab Code 2899. In *Book 10, Methods of the Reston Stable Isotope Laboratory*. U.S. Geological Survey Techniques and Methods.

Deutsch, C., Sigman, D.M., Thunell, R.C., Meckler, A.N., and Haug, G.H. (2004) Isotopic constraints on glacial/interglacial changes in the oceanic nitrogen budget. *Global Biogeochem*

Cycles 18: GB4012.

Graaf, A.A. Van De, Bruijn, P. De, Robertson, L.A., Jetten, M.S.M., and Kuenen, J.G. (1996) Autotrophic growth of anaerobic in a fluidized bed reactor. *Microbiology* 142: 2187–2196.

Granger, J., Boshers, D.S., Böhlke, J.K., Yu, D., Chen, N., and Tobias, C.R. (2019) The influence of sample matrix on the accuracy of nitrite N and O isotope ratio analyses with the azide method. *Rapid Commun Mass Spectrom* 34: e8569.

Granger, J. and Sigman, D.M. (2009) Removal of nitrite with sulfamic acid for nitrate N and O isotope analysis with the denitrifier method. *Rapid Commun Mass Spectrom* 23: 3753–3762.

Granger, J. and Wankel, S.D. (2016) Isotopic overprinting of nitrification on denitrification as a ubiquitous and unifying feature of environmental nitrogen cycling. *Proc Natl Acad Sci*.

Happy, H., Bourbonnais, A., Larkum, J., Bange, H.W., and Altabet, M.A. (2016) Nitrogen cycling in shallow low-oxygen coastal waters off Peru from nitrite and nitrate nitrogen and oxygen isotopes. *Biogeosciences* 13: 1453–1468.

Hu, H., Bourbonnais, A., Larkum, J., Bange, H.W., and Altabet, M.A. (2016) Nitrogen cycling in shallow low-oxygen coastal waters off Peru from nitrite and nitrate nitrogen and oxygen isotopes. *Biogeosciences* 13: 1453–1468.

Kindaichi, T., Awata, T., Suzuki, Y., Tanabe, K., Hatamoto, M., Ozaki, N., and Ohashi, A. (2011) Enrichment using an up-flow column reactor and community structure of marine anammox bacteria from coastal sediment. *Microbes Environ* 26: 67–73.

Kobayashi, K., Makabe, A., Yano, M., Oshiki, M., Kindaichi, T., Casciotti, K.L., and Okabe, S. (2019) Dual nitrogen and oxygen isotope fractionation during anaerobic ammonium oxidation by anammox bacteria. *ISME J* 13:.

LeGrande, A.N. and Schmidt, G.A. (2006) Global gridded data set of the oxygen isotopic composition in seawater. *Geophys Res Lett* 33: 1–5.

McIlvin, M.R. and Altabet, M.A. (2005) Chemical conversion of nitrate and nitrite to nitrous oxide for nitrogen and oxygen isotopic analysis in freshwater and seawater. *Anal Chem* 77: 5589–5595.

McIlvin, M.R. and Casciotti, K.L. (2011) Technical Updates to the Bacterial Method for Nitrate Isotopic Analyses. *Anal Chem* 83: 1850–1856.

Nakamura, T., Osaka, K., Hiraga, Y., and Kazama, F. (2011) Nitrogen and Oxygen Isotope Composition of Nitrate in Stream Water of Fuji River Basin. *J Japanese Assoc Hydrol Sci* 41: 79–89.

Nakamura, T., Shrestha, S., Satake, H., and Kazama, F. (2007) Effects of groundwater recharge on nitrate-nitrogen loadings. *J Water Environ Technol* 5: 87–93.

Nishizawa, M., Sakai, S., Konno, U., Nakahara, N., Takaki, Y., Saito, Y., et al. (2016) Nitrogen and oxygen isotope effects of ammonia oxidation by thermophilic *Thaumarchaeota* from a

geothermal water stream. *Appl Environ Microbiol* 82: AEM.00250-16.

Peters, B., Horak, R., Devol, A., Fuchsman, C., Forbes, M., Mordy, C.W., and Casciotti, K.L. (2018) Estimating fixed nitrogen loss and associated isotope effects using concentration and isotope measurements of NO3–, NO2–, and N2 from the Eastern Tropical South Pacific oxygen deficient zone. *Deep Sea Res Part II Top Stud Oceanogr* 156: 121–136.

Peters, B.D., Babbin, A.R., Lettmann, K.A., Mordy, C.W., Ulloa, O., Ward, B.B., and Casciotti, K.L. (2016) Vertical modeling of the nitrogen cycle in the eastern tropical South Pacific oxygen deficient zone using high-resolution concentration and isotope measurements. *Global Biogeochem Cycles* 30: 1661–1681.

Pinheiro, J., Bates, D., DebRoy, S., and Sarkar, D. (2020) nlme: Linear and Nonlinear Mixed Effects Models.

Röckmann, T., Kaiser, J., Brenninkmeijer, C.A.M., and Brand, W.A. (2003) Gas chromatography/isotope-ratio mass spectrometry method for high-precision position-dependent 15N and 18O measurements of atmospheric nitrous oxide. *Rapid Commun Mass Spectrom* 17: 1897–1908.

Sigman, D.M., Casciotti, K.L., Andreani, M., Barford, C., Galanter, M., and Bhlke, J.K. (2001) A Bacterial Method for the Nitrogen Isotopic Analysis of Nitrate in Seawater and Freshwater. *Anal Chem* 73: 4145–4153.

Thuan, N.C., Koba, K., Yano, M., Makabe, A., Kinh, C.T., Terada, A., et al. (2018) N2O production by denitrification in an urban river: evidence from isotopes, functional genes, and dissolved organic matter. *Limnology* 19: 115–126.

Wankel, S.D., Ziebis, W., Buchwald, C., Charoenpong, C., De Beer, Di., Dentinger, J., et al. (2017) Evidence for fungal and chemodenitrification based N2O flux from nitrogen impacted coastal sediments. *Nat Commun* 8: 1–11.

Weigand, M.A., Foriel, J., Barnett, B., Oleynik, S., and Sigman, D.M. (2016) Updates to instrumentation and protocols for isotopic analysis of nitrate by the denitrifier method. *Rapid Commun Mass Spectrom* 30: 1365–1383.

Werner, R.A. and Brand, W.A. (2001) Referencing strategies and techniques in stable isotope ratio analysis. *Rapid Commun Mass Spectrom* 15: 501–519.

Wijayanti, Y., Nakamura, T., Nishida, K., Haramoto, E., and Sakamoto, Y. (2012) Identification of groundwater recharge and nitrate pollution in the Kanegawa alluvial fan of the Kofu Basin, Japan, using stable isotopes and ions. *J Japan Soc Civ Eng Ser B1 (Hydraulic Eng* 68: I_199-I_204.

Ye, R.W., Toro-Suarez, I., Tiedje, J.M., and Averill, B.A. (1991) H218O Isotope Exchange Studies on the Mechanism of Reduction of Nitric Oxide and Nitrite to Nitrous Oxide by Denitrifying Bacteria. *J Biol Cgemistry* 266: 12848–12851.

Chapter 5

Nitrogen and oxygen isotope effects of marine anaerobic ammonium oxidation (anammox)

5.1. Introduction

Anaerobic ammonium oxidation (anammox) and denitrification are the two major sinks of fixed N in marine ecosystems. Anammox bacteria oxidize NH_4^+ directly to N_2 gas with NO_2^- as the terminal electron acceptor. It also re-oxidize NO_2^- to NO_3^- for CO_2 fixation into biomass (Kartal *et al.*, 2013). The occurrence of anammox in the environment was mainly observed in oxygen deficient water columns and sediments. In those ecosystems, natural abundance of stable nitrogen (N) and oxygen (O) isotope are invaluable biogeochemical tracers for assessing N transformations. Nitrate (NO_3^-) is the primary form of fixed nitrogen in the sea. To quantitatively assess the impacts of microbial processes on their pools, the degree of isotope fractionation is quantified by the kinetic isotope effect, ε (‰) = [k_L / k_H) – 1] ×1000, where k_L / k_H is the ratio of the reaction rate constants between the light (k_L) and heavy (k_H) isotopically substituted substrates. The kinetic N and O isotope effects ($^{15}\varepsilon$ and $^{18}\varepsilon$) for key microbial processes provide the basis for interpretation of natural abundance N isotopic distributions in the ocean. The N isotope effects ($^{15}\varepsilon$) associated with anammox metabolism have been determined for four anammox species, '*Ca.* Kuenenia stuttgartiensis' (Brunner *et al.*, 2013), '*Ca.* Scalindua japonica', '*Ca.* Jettenia caeni', and '*Ca.* Brocadia sinica'(Kobayashi *et al.*, 2019). On the other hand, the O isotope effect ($^{18}\varepsilon$) of each anammox reaction pathway has never been determined, independently. Only a combined oxygen isotope effect ($^{18}E_{NO2^-\rightarrow NO3^-} = 2/3\,^{18}\varepsilon_{NO2^-\rightarrow NO3^-} + 1/3\,^{18}\varepsilon_{H2O}$) was reported in the previous work by using continuous culture (Kobayashi *et al.*, 2019). However, the value of $^{18}E_{NO2^-\rightarrow NO3^-}$ depends on $^{18}\varepsilon_{NO2^-\rightarrow NO3^-}$ and $^{18}\varepsilon_{H2O}$, which could be species dependent and thus should be determined separately (Kobayashi *et al.*, 2019). Furthermore, the O isotope effect of nitrite (NO_2^-) reduction ($^{18}\varepsilon_{NO2^-\rightarrow N2}$) has not been determined yet. The determination of O isotope effects associated with anammox metabolism is essential to estimate its contribution to both of $\delta^{18}O_{NO2^-}$ and $\delta^{18}O_{NO3^-}$ in the natural environments.

To determine O isotope effects of anammox bacteria, four reactions should be considered (**Fig. 5.1**). Anammox bacteria oxidize NH_4^+ directly to N_2 gas with NO_2^- as the terminal electron acceptor (1) in the absence of oxygen, and NO_2^- is concomitantly oxidized to NO_3^- (2) as shown in

the following stoichiometric equation (Lotti *et al.*, 2014).

$1NH_4^+ + 1.146NO_2^- + 0.071HCO_3^- + 0.057H^+$

$\rightarrow 0.986N_2 + 0.161NO_3^- + 0.071CH_{1.74}O_{0.31}N_{0.20} + 2.002H_2O$

During oxidation of NO_2^- to NO_3^-, one oxygen atom in H_2O is incorporated (3). In addition, the abiotic equilibrium isotope exchange between NO_2^- and H_2O might affect the $\delta^{18}O$ of NO_2^- and NO_3^- (4).

Here I analyzed the oxygen kinetic isotope effects and oxygen atom exchange associated with anammox metabolism by a marine anammox species '*Ca.* Scalindua sp.'. In order to determine this complex oxygen isotope effects, batch incubation experiments were conducted with different $\delta^{18}O_{H2O}$ medium experiments.

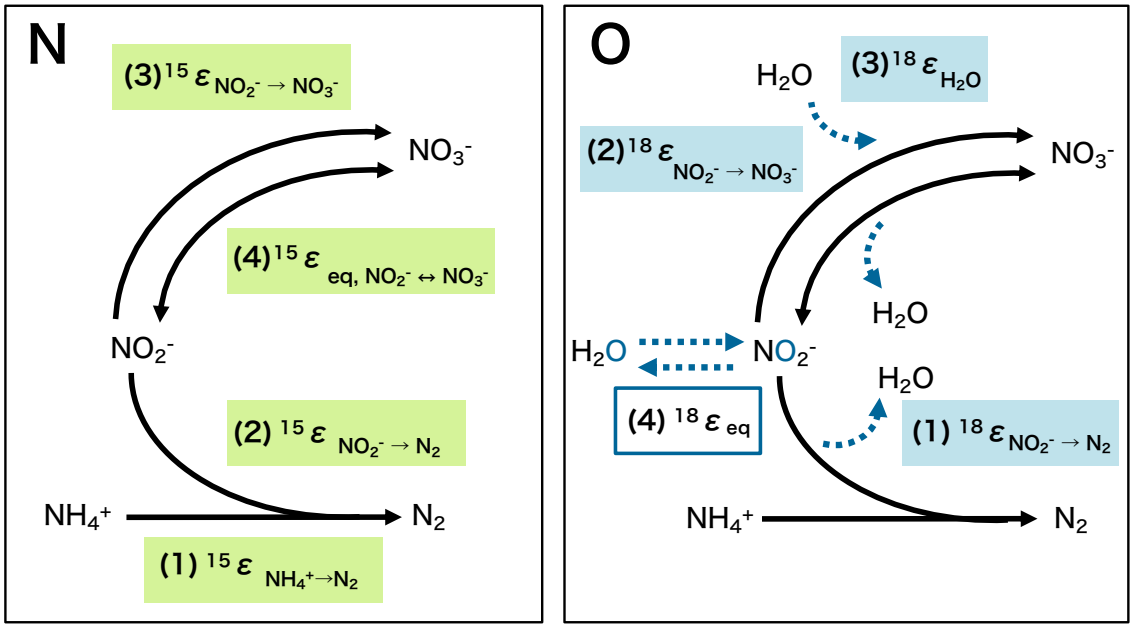

Figure 5.1 Nitrogen and oxygen isotope systematics of anaerobic ammonium oxidation

5.2. Materials and Methods

5.2.1 Enrichment culture

Free-living planktonic enrichment cultures of a marine anammox bacteria species '*Ca.* Scalindua sp.' was cultivated in 3 L membrane bioreactor (MBR) equipped with a hollow fiber membrane module (pore size 0.1 μm, polyethylene) as previously described (Awata *et al.*, 2013; Oshiki *et al.*, 2013; Ali *et al.*, 2015). Inorganic nutrient medium continuously fed into the MBR contained following: KH_2PO_4 (24.4 mg L^{-1}), $MgSO_4 \cdot 7H_2O$ (99 mg L^{-1}), $CaCl_2$ (86 mg L^{-1}), and 0.5 ml trace element solution I and II (Graaf *et al.*, 1996). Equimolar amounts of $NH_4(SO_4)_2$ and $NaNO_2$ were added to achieve 10 mmol-N L^{-1}. An artificial sea salt SEALIFE (Marine Tech, Tokyo, Japan) was supplemented into the media to achieve 2.5% salinity. The culture fluid in the MBR was continuously mixed with a magnetic stirrer at 200 rpm and sparged with 95% Ar-5% CO_2 at a flow rate of 10 mL min^{-1}. The pH was not controlled but was always between 7.3-7.8. The temperature was controlled at 30°C.

5.2.2 Experiments on nitrogen and oxygen isotope effects during anammox

After the MBRs have reached a steady state, the anammox cells were collected and then further enriched by percoll density gradient centrifugation (Strous *et al.*, 1999). The ratio of anammox bacteria to total cells (degree of enrichment cultures) was determined by fluorescent in situ hybridization (FISH). Enriched biomass (99% pure) was washed with mineral medium without NH_4^+ and NO_2^- and resuspended in 0.9 L medium (ca. ~10^9 cells mL^{-1}). The biomass was incubated in 1 L storage glass bottles (Shibata Scientific Technology, Ltd., Saitama, Japan) overnight to consume the residual NH_4^+ and NO_2^- (**Fig. 5.2.1**). The media for incubation experiments were prepared as described above, with following modification. The $\delta^{18}O$ of the H_2O in the medium was adjusted to four different values ($\delta^{18}O_{H2O}$ = -12.6 (unlabeled), 25.9, 56.7 and 110.1‰) by adding $H_2{}^{18}O$ (97% ^{18}O; Aldrich, prod. no. 329878). For each medium $\delta^{18}O_{H2O}$ value, batch experiment was conducted in triplicate. The temperature was controlled at 30°C. The batch cultures were flushed with an Ar: CO_2 gas mixture and stirred continuously. The pH was not controlled but was always between 7.2-7.9 (Average 7.5). The experiments were initiated by adding $NaNO_2$ (at a final concentration of 2.0mmol-N L^{-1}) and $(NH_4)_2SO_4$ (at a final concentration of 2.5 mmol L^{-1}). After adding substrates, a total of 25 - 40 mL of the incubated solution was periodically sampled. Time course experiments lasted until the nitrite had been completely consumed, which took approximately

5-7 hours. All samples were filtered using 0.2-μm cellulose acetate filter (Advantec) immediately. The pH was measured using 0.5 mL of the solution sample with a pH meter (pH meter B-712, Horiba, Ltd., Kyoto, Japan).

After filtration, immediately samples were adjusted to pH 2 by adding 1 M H_2SO_4 solution and then stored at -20°C until analysis for N isotope of NH_4^+ to prevent NH_4^+ from volatilizing. To analyze N and O isotope of NO_2^-, after filtration, immediately sample solution was adjusted to pH 12 by adding 2 M low-N-blank NaOH solution and stored at -20°C until analysis to prevent O isotope exchange between NO_2^- and H_2O during sample storage (Casciotti *et al.*, 2007). To analyze N and O isotope of NO_3^-, after filtration, if NO_2^- remained in sample, immediately NO_2^- in the sample solution was removed by adding sulfamic acid (H_3NSO_3), because NO_2^- interferes with NO_3^- isotope analysis (Granger and Sigman, 2009). The concentration of NO_2^- was measured with naphthylethylenediamine method (APHA *et al.*, 2005) to confirm NO_2^- was completely removed. Then, sample solution was stored at -20°C until analysis.

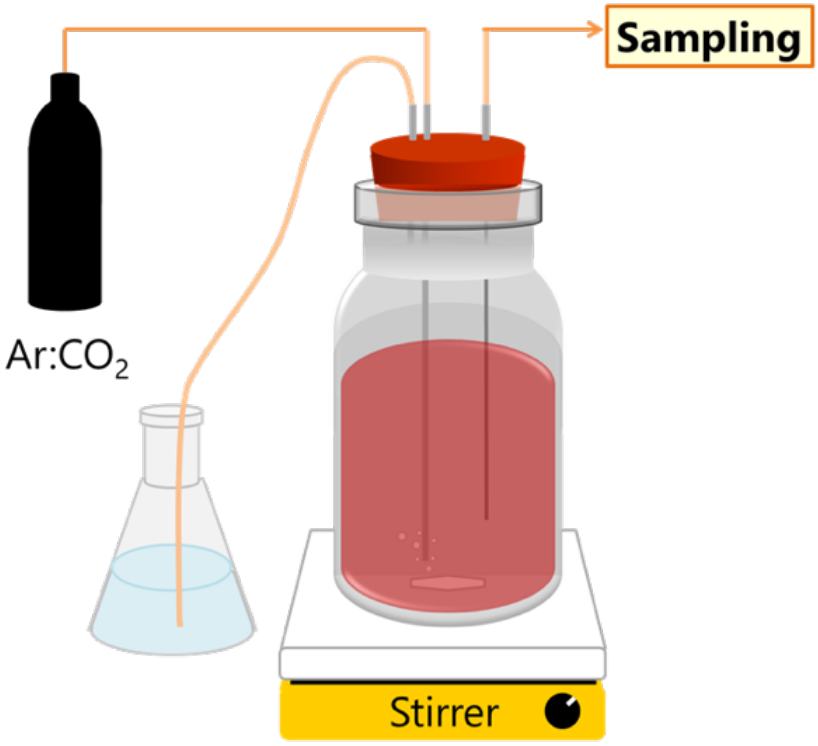

Figure 5.2.1 Schematic drawing of batch culture experiment. The culture medium was continuously mixed using a magnetic stirrer working at 200 rpm. To maintain anoxic condition, a mixed gas (Ar: CO_2 = 95:5) was purged into the culture medium at a flow rate of 10 ml min^{-1}.

5.2.3 Experiments to examine N isotope exchange between NO_2^- and NO_3^-

Anammox bacteria can reverse this enzymatic reaction, namely they can reduce NO_3^- back to NO_2^- (Kartal *et al.*, 2007; Oshiki *et al.*, 2013). The previous research on nitrogen isotope effect of anammox has reported rapid and large nitrogen isotope exchange between NO_2^- and NO_3^- ($^{15}\varepsilon_{NO2-\leftrightarrow NO3-}$ = -60.5‰) (Brunner *et al.*, 2013). However, since this phenomenon was not ubiquitously observed in our previous work (Kobayashi *et al.*, 2019), it still remained unclear whether this was caused by cell lysis during cultivation and/or sample preparation. Thus, another batch to examine nitrogen isotope exchange between NO_2^- and NO_3^- was prepared. In order to analyze the nitrogen isotope exchange between NO_2^- and NO_3^-, another batch experiments were conducted by adding NO_2^- with low $\delta^{15}N$ value ($\delta^{15}N_{NO2-}$ = -35.5 ‰), NO_3^- with high $\delta^{15}N$ value ($\delta^{15}N_{NO3-}$ = 121.0 ‰), and NH_4^+, in which the initial $\delta^{15}N$ gap between nitrite and nitrate was induced. In this experiment $\delta^{18}O$ of the H_2O in the medium was -12.6‰. Other experimental procedure was same as above.

5.2.4 Chemical analyses

On the day of sampling, concentration was analyzed by using 1.0 mL sample filtrate. The concentration of NH_4^+ was measured by the indophenol blue method (APHA *et al.*, 2005) with a multi-label plate reader (ARVO MX 1420-01J; PerkinElmer; Waltham, MA, USA). The NO_2^- concentration was measured by the naphthylethylenediamine method (APHA *et al.*, 2005). The concentration of NO_3^- was measured using ion chromatographs (IC-2010, TOSOH; Tokyo, Japan) equipped with a TSKgel IC-Anion HS column (TOSOH; Tokyo, Japan).

5.2.5 Isotopic analyses

NH_4^+ nitrogen isotope analyses were performed by using the ammonium diffusion method (Sigman *et al.*, 1997; Holmes *et al.*, 1998) and subsequently measured by a EA-IRMS (Flash EA1112, ConFlo IV interface, Delta plus Advantage; ThremoFinnigan). International and internal NH_4^+ isotopic standards, USGS25 ($\delta^{15}N$ = -30.41‰), USGS26 ($\delta^{15}N$ = 53.75‰), and IAEA-N-2 ($\delta^{15}N$ = 20.3‰) were used for the calibration. The one-sigma standard deviations of $\delta^{15}N$-NH_4^+ measurements of standards were 0.04 ~0.26 ‰ (maximum = 0.85‰).

NO_2^- nitrogen and oxygen isotope ratios were measured by chemical conversion of NO_2^- to nitrous oxide (N_2O) with the azide method (McIlvin and Altabet, 2005). All samples and standards

had been adjusted to exactly the same pH (pH=12) and salinity (2.5% NaCl). Because of high sample pH (pH=12), azide buffer was modified by increasing the acetic acid concentration to 7.84 M (Hu *et al.*, 2016) and the sodium azide concentration to 4 M (Kobayashi *et al.*, 2020). The sample solution was buffered at pH 4.4 during the reaction. The N_2O was then analyzed in duplicate using a purge-and-trap, gas-chromatography, isotope ratio mass spectrometry (PT-GC-IRMS). The corrected $\delta^{15}N$ and $\delta^{18}O$ values of the sample N_2O converted from NO_2^- were calibrated against the values from in-house NO_2^- standards; JAM 1 ($\delta^{15}N$ = -2.5 ‰, $\delta^{18}O$ = 91.7 ‰), JAM 2 ($\delta^{15}N$ = 1.8 ‰, $\delta^{18}O$ = 9.9 ‰), JAM 3 ($\delta^{15}N$ = -26.4 ‰, $\delta^{18}O$ = 39.4 ‰), JAM 4 ($\delta^{15}N$ = -1.5 ‰, $\delta^{18}O$ = -15.2 ‰) (Kobayashi *et al.*, 2020). Each reference solution was analyzed three times, and triplicate analyses yielded the respective precisions of generally 0.04 ~ 0.16‰ for $\delta^{15}N_{NO2-}$ (maximum = 0.51‰) and 0.09 ~ 0.28‰ (maximum = 0.48‰) for $\delta^{18}O_{NO2-}$, respectively.

NO_3^- nitrogen and oxygen isotope ratios were measured by microbial conversion of NO_3^- to N_2O with the denitrifier method (Sigman *et al.*, 2001; Casciotti *et al.*, 2002). N_2O was analyzed in triplicate using a PT-GC-IRMS The corrected $\delta^{15}N$ and $\delta^{18}O$ values of the sample N_2O converted from NO_2^- were calibrated against the values from international NO_3^- isotopic standards; IAEAN3 ($\delta^{15}N$ = 4.7‰, $\delta^{18}O$ = 25.6‰), USGS32 ($\delta^{15}N$ = 180‰, $\delta^{18}O$ = 25.7‰), USGS34 ($\delta^{15}N$ = -1.8‰, $\delta^{18}O$ = -27.9‰), and USGS35 ($\delta^{18}O$ = 57.5‰) for the calibration (Thuan *et al.*, 2018). Triplicate analyses yielded the respective precisions of generally 0.05 ~ 0.17‰ (maximum = 0.81‰) for $\delta^{15}N_{NO3-}$ and 0.15 ~ 0.46% (maximum = 1.40%) for $\delta^{18}O_{NO3-}$, respectively.

The $\delta^{18}O_{H2O}$ was measured by equilibration with NO_2^- and subsequent conversion of NO_2^- to N_2O using a modified azide method (McIlvin and Casciotti, 2006) with 0.5 mL of the samples and standards. The $\delta^{18}O$ data was finally calibrated against GISP (-24.8 ‰) and the in-house water standards; Alaskan bottled mineral water (-19.0 ‰) and bottled de-salted seawater (0.2 ‰) (those $\delta^{18}O$ values were determined by SI Science. Co. ltd). The sample with high $\delta^{18}O_{H2O}$ was mixed with MillQ water (-12.6 ‰) to yield the measured $\delta^{18}O$ values falling into the range of the standards (i.e. between -24.8 to 0.2 ‰), calculated according to the mixing ratio. Triplicate analyses yielded the respective precisions of 0.20‰ for $\delta^{18}O_{H2O}$.

5.2.6 Calculation of isotope effects

Anammox bacteria oxidize NH_4^+ directly to N_2 gas with NO_2^- as the terminal electron acceptor in the absence of oxygen, and NO_2^- is concomitantly oxidized to NO_3^- as shown in the following stoichiometric equation (Lotti *et al.*, 2014).

$$1NH_4^+ + 1.146NO_2^- + 0.071HCO_3^- + 0.057H^+$$
$$\rightarrow 0.986N_2 + 0.161NO_3^- + 0.071CH_{1.74}O_{0.31}N_{0.20} + 2.002H_2O$$

Nitrogen isotope effect of ammonium oxidation $^{15}\varepsilon$ ($NH_4^+ \rightarrow N_2$) could be calculated by using closed-system Rayleigh isotope fractionation systematics (Brunner *et al.*, 2013). $^{15}\varepsilon$ ($NH_4^+ \rightarrow N_2$) could be determined from $R^{15}N(NH_4^+)$ vs. ln (f NH_4^+) plot according to,

$$-\ln\left(R^{15}N_{NH4+}\right) = {}^{15}\varepsilon\ (NH_4^+ \rightarrow N_2) \cdot \ln(f_{NH4+}) \cdots (1)$$

Where

$$\ln\left(R^{15}N_{NH4+}\right) = \ln\left(\frac{\delta^{15}N_{NH4+}(t)+1000‰}{\delta^{15}N_{NH4+}(t_0)+1000‰}\right) \cdots (2)$$

and

$$\ln(f_{NH4+}) = ln\left(\frac{NH_4^+(t)}{NH_4^+(t_0)}\right) \cdots (3)$$

t_0 was initial time. The nitrogen isotope effect of ammonium oxidation $^{15}\varepsilon$ ($NH_4^+ \rightarrow N_2$) is slope of equation (1), therefore it is determined by plotting -ln($R^{15}NNH_4^+$) vs. ln (f NH_4^+).

Except the reaction pathway of NH_4^+ oxidation, a numerical model need to be constructed in order to determine both of N and O isotope effect of anammox bacteria, because of complicated anammox reactions (**Fig. 5.1**). The basic policy of this numerical model is taking mass balance of isotope pools (^{14}N, ^{15}N, ^{16}O, and ^{18}O) of NH_4^+, NO_2^-, and NO_3^-. The amount of change of each pool is expressed in differential equations.

5.2.7 Nitrogen isotope effects model

Determine the ^{14}N flux by the change of concentration

The amount of ^{14}N (99.6337%) is much larger than that of ^{15}N (0.36630%). Thus, the ^{14}N flux was represented by the change of concentration in this model. In brief, the simulated NH_4^+ pool is influenced by NH_4^+ oxidation (AMO). The NO_2^- pool reflects the balance of consumption by NO_2^- reduction (NIR), as well as NO_2^- oxidation (NXR). The NO_3^- pool is influenced by NXR (**Fig. 5.2.2**)

14NAMO ([N]/ time) = ^{14}N flux of NH_4^+ oxidation to N_2

14NNIR ([N]/ time) = ^{14}N flux of NO_2^- reduction to N_2

14NNXR ([N]/ time) = ^{14}N flux of NO_2^- oxidation to NO_3^-

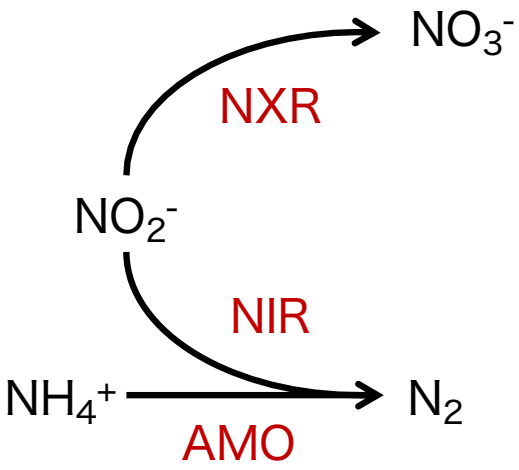

Figure 5.2.2 N isotope model description

In anammox reaction, the rate of NH_4^+ oxidation to N_2 is equal to the rate of NO_2^- reduction to N_2.

14NAMO = 14NNIR … (4)

The parameter X is designated to the ratio of N flux from NO_2^- to NO_3^- to N flux from NO_2^- to N_2.

X = 14NNXR/(14NNIR+14NNXR) … (5)

14NNXR=(X/(1-X))×14NNIR … (6)

From the equation (1) 14NNIR = 14NAMO

14NNXR= (X/(1-X))×14NAMO … (7)

14NNXR is now described with two parameters X and 14NAMO. The X and 14NAMO can be determined by taking mass balance and fitted to the actual measured time course changes in NH_4^+, NO_2^-, and NO_3^- concentrations.

$d/dt[^{14}N_{NH4+}] = -14NAMO$ … (8)

$d/dt[^{14}N_{NO2-}] = -14NNIR - 14NNXR = -14NAMO - (X/(1-X))\times14NAMO$ … (9)

$d/dt[^{14}N_{NO3-}] = +14NNXR = (X/(1-X))\times14NAMO$ … (10)

Calculation of ^{15}N flux based on nitrogen isotope composition

The definition of nitrogen isotope composition is as follows:

$\delta^{15}N = (^{15}R_{sample} / {}^{15}R_{air} - 1) \times 1000‰$

$^{15}R_{sample} = (\delta^{15}N/1000 + 1) \times {}^{15}R_{air}$

^{15}R is a ratio of heavy isotope and light isotope ($^{15}R = {}^{15}N / {}^{14}N$)

$^{15}R_{std}$ is a ^{15}R value of international N reference standards ($^{15}R_{std} = 0.0036765$).

^{15}R of each nitrogen compound is defined as follows:

R_AmmoniumN = Ammonium15N / Ammoniumu14N … (11)

R_NitriteN = Nitrite15N / Nitrite14N … (12)

R_NitrateN = Nitrate15N / Nitrate15N … (13)

The definition of isotope effect (ε) is as follows:

$\varepsilon = (\alpha - 1) \times 1000$ (‰)

α is an isotope fractionation factor explained by following equation.

$^{15}\alpha = (^{14}N \text{ flux} / [^{14}N]) / (^{15}N \text{ flux} / [^{15}N])$

$^{15}N \text{ flux} = ([^{15}N] / [^{14}N]) \times (^{14}N \text{ flux} / {}^{15}\alpha)$

$[^{15}N] / [^{14}N] = {}^{15}R$

$^{15}N \text{ flux} = {}^{15}R \times (^{14}N \text{ flux} / {}^{15}\alpha)$

As a result, the ^{15}N flux is explained by ^{15}R, ^{14}N flux and isotope fractionation factor ($^{15}\alpha$). ^{15}N flux by each anammox reaction is defined as following.

15NAMO = R_AmmoniumuN*14NAMO/$^{15}\alpha_{AMO}$ … (14)

15NNIR = R_NitriteN*14NNIR/$^{15}\alpha_{NIR}$ … (15)

15NNXR = R_Nitrite N*14NNXR/$^{15}\alpha_{NXR}$ … (16)

Those three parameters ($^{15}\alpha_{AMO}$, $^{15}\alpha_{NIR}$, and $^{15}\alpha_{NXR}$) were determined by taking mass balance of ^{15}N of N compounds and modeled to fit to the actual measured time course change in ^{15}N of NH_4^+, NO_2^-, and NO_3^-.

$d/dt[^{15}N_{NH4+}] = -15NAMO$ … (17)

$d/dt[^{15}N_{NO2-}] = -15NNIR - 15NNXR$ … (18)

$d/dt[^{15}N_{NO3-}] = +15NNXR$ … (19)

In order to calculate $^{15}\alpha_{AMO}$, $^{15}\alpha_{NIR}$, and $^{15}\alpha_{NXR}$, the differential equations were fitted using the FME (Soetaert and Petzoldt, 2010) package in R. The R package FME is a modeling package designed to confront a mathematical model with data. It includes algorithms for sensitivity and Monte Carlo analysis, parameter identifiability, and model fitting and provides a Markov-chain based method to estimate parameter confidence intervals. In my model, modMCMC function was used to run a Markov chain Monte Carlo (MCMC) to estimate all parameters.

5.2.8 Oxygen isotope effect model

Determination of ^{16}O flux based on the change of concentration

The amount of ^{16}O (99.76206%) of nitrogen compounds is much larger than that of ^{18}O (0.0020004%). Thus, the ^{16}O flux was represented by the change of concentration in this model. In brief, the NO_2^- pool reflects the balance of consumption by NO_2^- reduction (NIR), as well as NO_2^- oxidation (NXR). The NO_3^- pool is influenced by NXR. During NO_2^- oxidation, one oxygen atom is incorporated from H_2O (**Fig. 5.2.3.**). The oxygen incorporation flux is defined as 16ONXRadjust (**Fig. 5.2.2.**).

16ONIR ([O]/ time) = ^{16}O flux of NO_2^- reduction to N_2

16ONNXR ([O]/ time) = ^{16}O flux of NO_2^- oxidation to NO_3^-

16ONNXRadjust ([O]/ time) = ^{16}O flux of oxygen incorporation from H_2O during NO_2^- oxidation to NO_3^-

^{16}O flux could be defined based on ^{14}N flux.

NIR: $NO_2^- \rightarrow N_2$

When one NO_2^- reduced to N_2, two oxygen molecules are lost from NO_2^- pool.

16ONIR = 14NNIR × 2 = 14NAMO × 2 … (20)

NXR: $NO_2^- \rightarrow NO_3^-$

When one NO_2^- is oxidized to NO_3^-, two oxygen molecules are lost from NO_2^- pool.

16ONXR = 14NNXR × 2 = (X/(1-X)) × 14NAMO × 2 … (21)

When one NO_2^- is oxidized to NO_3^-, one oxygen molecule is incorporated from H_2O.

16ONXRadjust = 16ONXR/2 = (X/(1-X)) × 14NAMO … (22)

^{16}O mass balance was taken by following equations.

$d/dt[^{16}O_{NO2-}] = -16ONIR - 16ONXR$ … (23)

$d/dt[^{16}O_{NO3-}] = 16ONXR + 16ONXRadjust$ … (24)

Calculation of ^{18}O flux by anammox based on oxygen isotope composition

The definition of oxygen isotope composition is as follows:

$\delta^{18}O = (^{18}R_{sample} / {}^{18}R_{VSMOW} - 1) \times 1000‰$

$^{18}R_{sample} = (\delta^{18}O/1000 + 1) \times {}^{18}R_{VSMOW}$

Where $^{18}R = {}^{18}O/{}^{16}O$ and VSMOW refers to standard Vienna Standard Mean Ocean Water

$^{18}R_{VSMOW} = 0.00200517$

^{18}R of each nitrogen compounds are defined as follows:

R_NitriteO = Nitrite18O / Nitrite16O … (25)

R_NitrateO = Nitrate18O/Nitrate16O … (26)

R_waterO = $((\delta^{18}O\text{water} / 1000) + 1) * {}^{18}R_{vsmow}$ … (27)

The ^{18}O flux is explained by ^{18}R, ^{16}O flux and isotope fractionation factor ($^{18}\alpha$). ^{18}O flux by each anammox reaction is defined as following as same as ^{15}N flux.

18ONIR = R_NitriteO*16ONIR/$^{18}\alpha_{NIR}$ … (28)

18ONXR = R_NitriteO*16ONXR/$^{18}\alpha_{NXR}$ … (29)

The ^{18}O flux due to oxygen incorporation from water during NO_2^- oxidation to NO_3^- (18ONXRincorp) could be described as follows (Granger and Wankel, 2016).

18ONXRincorp = {R_waterO*(16ONXR/2)}/$^{18}\alpha_{incorp}$ … (30)

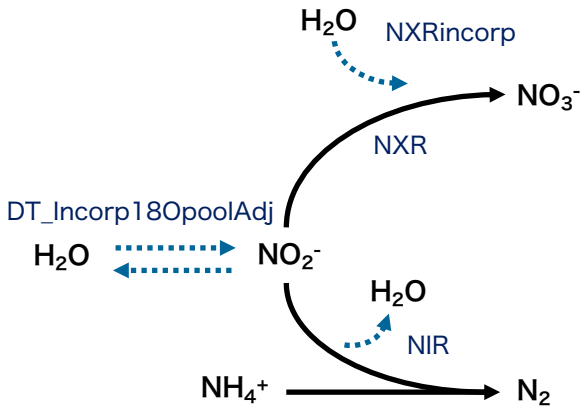

Figure 5.2.3. Description of O isotope model

5.2.9 Abiotic oxygen isotope exchange between nitrite and water

The oxygen atom of NO_2^- is abiotically exchanged with H_2O (Casciotti *et al.*, 2007). The $\delta^{18}O$ of newly produced NO_3^- is also known to be sensitive to $\delta^{18}O$ of ambient water and the equilibrium isotope effects between NO_2^- and H_2O (Granger and Wankel, 2016). However, the experimentally determined NO_2^- equilibration rates (Buchwald and Casciotti, 2013; Nishizawa *et al.*, 2016) and equilibrium isotope effects (Casciotti *et al.*, 2007; Buchwald and Casciotti, 2013; Nishizawa *et al.*, 2016) under relevant environmental conditions remain quite limited. In our previous work, we determined the rate of abiotic O isotope exchange between NO_2^- and H_2O (k_{eq}) and equilibrium isotope effects ($^{18}\varepsilon_{eq}$) under growth condition of "*Ca.* Scalindua sp." at variety of $\delta^{18}O_{H2O}$ values conditions ($\delta^{18}O_{H2O}$ = -12.6, 25.9, 56.7, and 110.1‰) in a series of laboratory experiments (Kobayashi *et al.*, 2020). The abiotic oxygen isotope exchange between NO_2^- and H_2O was explained by using previously determined k_{eq} and $^{18}\varepsilon_{eq}$.

The approach of $\delta^{18}O_{NO2}$ to isotope equilibrium ($\delta^{18}O_{NO2,eq}$) is modeled as an following exponential form (Buchwald and Casciotti, 2013), where $\delta^{18}O_{NO2,initial}$ and $\delta^{18}O_{NO2,eq}$ are value of $\delta^{18}O_{NO2}$ at initial and equilibrium state, respectively:

$$\delta^{18}O_{NO2}(t) = \delta^{18}O_{NO2,eq} + (\delta^{18}O_{NO2,initial} - \delta^{18}O_{NO2,eq}) \times \exp(-kt) \quad \ldots (31)$$

According to equation (31), the value of $\delta^{18}O_{NO2}$ (t) is determined by time, $\delta^{18}O_{NO2,initial}$ and $\delta^{18}O_{NO2,eq}$. During anammox reaction, however, not only abiotic oxygen isotope exchange but also reaction of NO_2^- oxidation and reduction affect $\delta^{18}O_{NO2}$. As a result, the behavior of $\delta^{18}O_{NO2}$ is different from abiotic oxygen isotope exchange between NO_2^- and H_2O happens (**Fig. 5.2.4**).

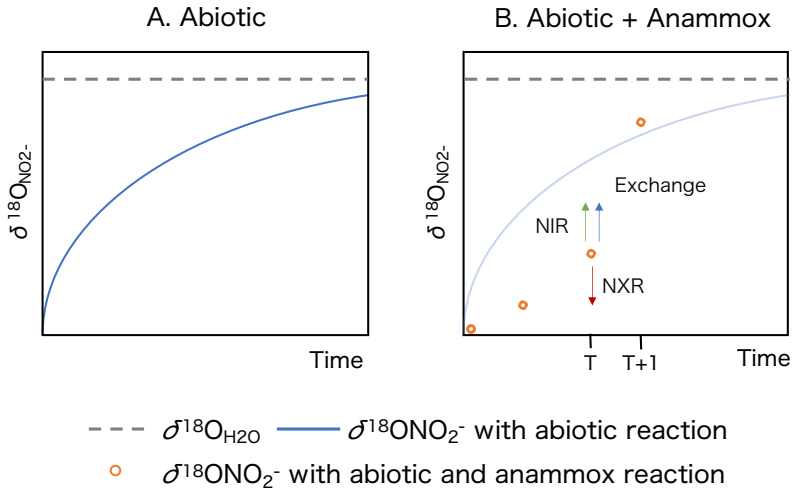

Figure 5.2.4 $\delta^{18}O_{NO2-}$ behavior during only abiotic oxygen isotope exchange between nitrite and water (A) and simultaneous abiotic oxygen exchange and anammox reaction (B).

In order to determine the change of $\delta^{18}ONO_2^-$ per unit time, equation (31) was differentiated by time.

$d/dt\ (\delta^{18}O_{NO2}) = -k \times (\delta^{18}O_{NO2,initial} - \delta^{18}O_{NO2,eq}) \times \exp(-kt)$ … (32)

According to equation (32), the change of $\delta^{18}ONO_2^-$ is determined by difference between $\delta^{18}O_{NO2,initial}$ and $\delta^{18}O_{NO2,eq}$. We defined δ^{18}ONitriteT is the value of $\delta^{18}ONO_2^-$ at time t in the batch incubation.

δ^{18}ONitriteT = ((Nitrite18O/Nitrite16O) / $^{18}R_{VSMOW}$ – 1) ×1000 … (33)

The change of $\delta^{18}ONO_2^-$ per unit time (DT_δ^{18}ONitrite_18Oincorp) at time t could be given by the following equation, where the δ^{18}ONitriteEQ is the value of $\delta^{18}ONO_2^-$ at equilibrium state.

DT_δ^{18}ONitrite_18Oincorp = $-k \times (\delta^{18}$ONitriteT - δ^{18}ONitriteEQ) × exp(-k×DT) … (34)

Time = 1 min = 1DT

In our numerical model, ^{18}O mass balance ($d/dt[^{18}O_{NO2-}]$) were taken. Therefore, equation (35) was rearranged to the change of ^{18}O pool of NO_2^-.

Example

$\delta^{18}O = (^{18}R_{sample} / {}^{18}R_{VSMOW} - 1) \times 1000‰$

$^{18}R_{sample} = (\delta^{18}O/1000 + 1) \times {}^{18}R_{VSMOW}$

$^{18}R = {}^{18}O / {}^{16}O$ (mole ratio)

$^{18}O_{sample} = (\delta^{18}O / 1000 + 1) \times {}^{18}R_{VSMOW} \times {}^{16}O_{sample}$

As same as example, the change of ^{18}O pool of NO_2^- (DT_Incorp18OpoolAdj) could be presented by following equation.

DT_Incorp18OpoolAdj = (DT_δ^{18}ONitrite_18Oincorp / 1000 +1) * R_{VSMOW} * Nitrite16O… (36)

When $\delta^{18}ONO_2^-$ achieves the equilibrium state, the value of DT_Incorp18OpoolAdj should be zero. At equilibrium state, DT_δ^{18}ONitrite_18Oincorp is zero. Therefore, this equation (36) was compensated as follows.

DT_Incorp18OpoolAdj = (DT_δ^{18}ONitrite_18Oincorp / 1000 +1) * R_{VSMOW} * Nitrite16O – (0/1000 + 1) * R_{VSMOW} * Nitrite16O… (37)

Finally, ^{18}O pool of NO_2^- and NO_3^- could be presented.

$d/dt[^{18}O_{NO2-}]$ = - 18ONIR – 18ONXR + 1*DT_Incorp18OpoolAdj… (38)

$d/dt[^{18}O_{NO3-}]$ = NXR18Oincorp + NXR18O… (39)

In order to calculate $^{18}\alpha_{NIR}$, $^{18}\alpha_{NXR}$, and $^{18}\alpha_{incorp}$, the differential equations were fitted using the FME (Soetaert and Petzoldt, 2010) package in R which can perform model fitting and provide a Markov-chain based method to estimate parameter confidence intervals. In this model, modMCMC function was used to run a Markov chain Monte Carlo (MCMC) to estimate parameters.

5.3. Results and discussions

Anammox batch incubation experiments

5.3.1 Anammox stoichiometry

The $\delta^{18}O_{H2O}$ in the medium was adjusted to four different values ($\delta^{18}O_{H2O}$ = -12.6 (unlabeled), 25.9, 56.7, and 110.1‰). Batch incubation experiments were conducted with addition of 2.5 mM-N of $(NH_4)_2SO_4$ and 2.0 mM-N of $NaNO_2$ in triplicate for respective $\delta^{18}O_{H2O}$ values. There was about one-hour lag before the anammox reaction was initiated in several experiments (**Fig. 5.3.1. A, E, F, I, J**). Both NH_4^+ and NO_2^- decreased linearly, and NO_3^- was produced concomitantly (**Fig. 5.3.1**). From those observation, the anammox reaction in the numerical modelling was assumed to be the zero order reaction (the reaction rate is independent of the concentrations of reactants). Therefore, data sets during about one-hour lag phase (data point at 0 min of **Fig. 5.3.1 A, E, F, I, J**) was excluded from the model estimation. The average stoichiometric ratios of consumed NO_2^- and consumed NH_4^+ ($\Delta NO_2^-/\Delta NH_4^+$) were 1.36 ± 0.08 and produced nitrate and consumed ammonium ($\Delta NO_3^-/\Delta NH_4^+$) were 0.32 ± 0.09, which agreed with the previously observed stoichiometry of anammox process (i.e. 1.15 and 0.16 for $NO_2^-/\Delta NH_4^+$ and $\Delta NO_3^-/\Delta NH_4^+$, respectively) (Lotti *et al.*, 2014). Nitrite was completely consumed within 295 min - 450 min, while substantial amounts of NH_4^+ remained in all batch cultures, indicating that NO_2^- was a limiting substrate (**Fig. 5.3.1**). Three independent batch incubations revealed similar experimental results of NH_4^+ oxidation, which highlighted the high reproducibility of this study.

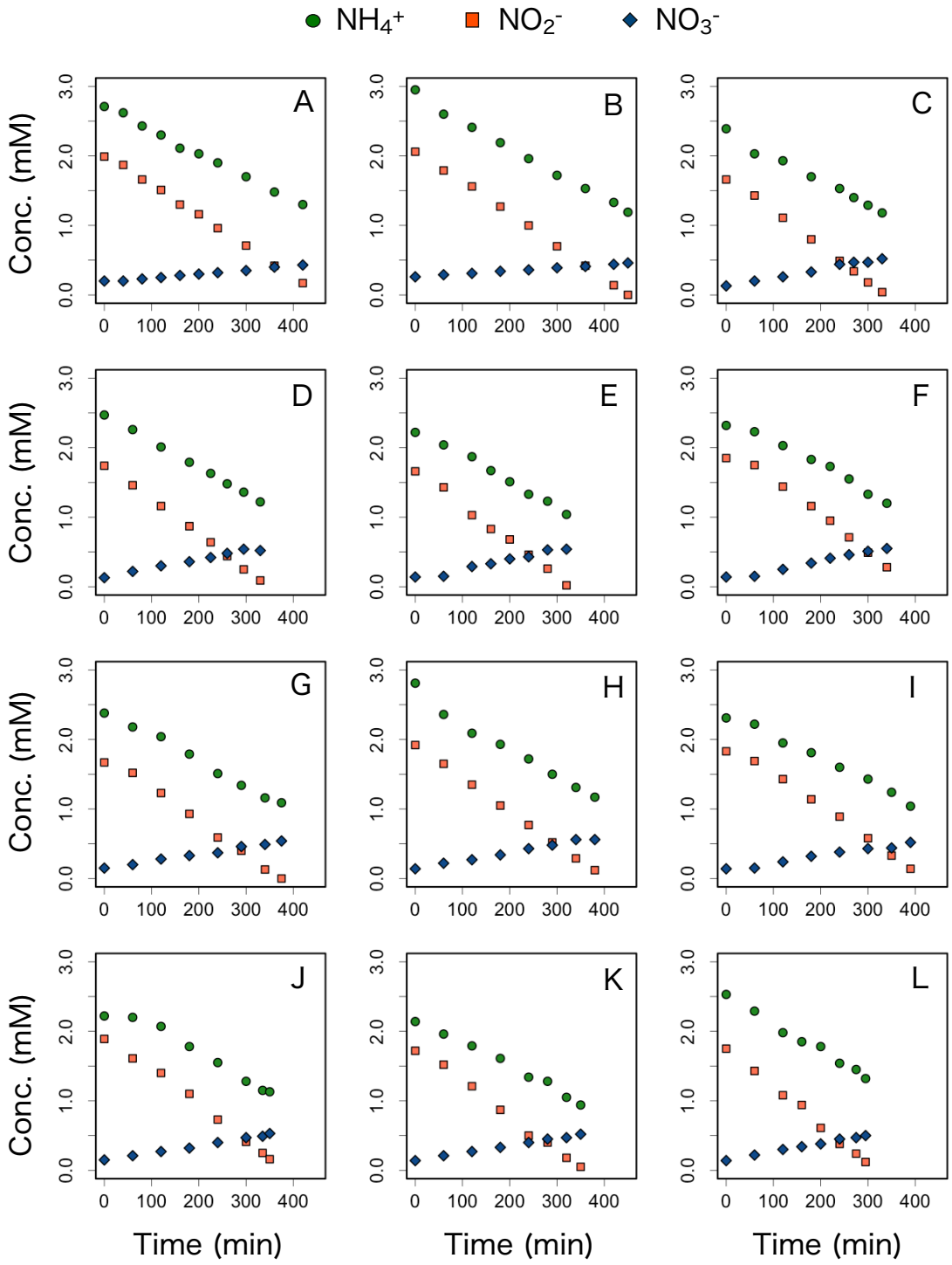

Figure 5.3.1. Time course of concentrations of nitrogen compounds during anammox batch culture experiments. Triplicate experimental data obtained under $\delta^{18}O_{H2O}$ = -12.6‰ (A-C), $\delta^{18}O_{H2O}$ = 25.9‰ (D-F), $\delta^{18}O_{H2O}$ = 56.7‰ (G-I), and $\delta^{18}O_{H2O}$ = 110.1‰ (J-L) were shown.

5.3.2 Changes in nitrogen isotope compounds

$\delta^{15}N_{NH4+}$ and $\delta^{15}N_{NO2-}$ increased during the anammox reaction, whereas $\delta^{15}N_{NO3-}$ values remained unchanged in all experiments (**Fig. 5.3.2**). $\delta^{15}N_{NO2-}$ was affected by both of NO_2^- reduction and oxidation. The produced $\delta^{15}N_{NO3-}$ was much higher than $\delta^{15}N_{NO2-}$, indicating that anammox exhibits inverse kinetic N isotope effect associated with the NO_2^- oxidation to NO_3^-.

A batch incubation experiment with ^{15}N-poor NO_2^- (ACROSS; $\delta^{15}N_{NO2-}$ = -35.5‰) and ^{15}N-rich NO_3^- standard (USGS32; $\delta^{15}N_{NO3-}$ = 121.0‰) was conducted to examine nitrogen isotope exchange between NO_2^- and NO_3^-. In this experiment, since the initial δ^{15}N difference between NO_2^- and NO_3^- was large (-156.5%), it is relatively easy to identify equivalent changes in $\delta^{15}N_{NO2-}$ and $\delta^{15}N_{NO3-}$ if nitrogen isotope exchange occurs (**Fig. 5.3.3**). Concomitant consumption of NH_4^+ and NO_2^- and production of NO_3^- were observed, whose conversion ratios agreed with anammox stoichiometric rations (**Fig. 5.3.3. A**). Approximately 0.44 mM of NO_3^- was newly produced from ^{15}N-poor NO_2^- (ACROSS; $\delta^{15}N_{NO2-}$ = -35.5‰). The N isotope composition analysis revealed that $\delta^{15}N_{NO3-}$ rapidly decreased, while $\delta^{15}N_{NO2-}$ gradually increased like the results of natural isotope fractionation experiments (**Fig. 5.3.2**). This rapid decrease in $\delta^{15}N_{NO3-}$ was attributed to NO_3^- production from NO_2^- with low δ^{15}N value ($\delta^{15}N_{NO2-}$ = -35.5‰). Based on the simple N isotope mass balance, the final $\delta^{15}N_{NO3}$- at the end of incubation could be estimated to be 13.4‰ (0.2/0.64 × 121.0 ‰ ＋ 0.44/0.64 × -35.5 ‰ ＝ 13.4 ‰) without taking into account the N isotope effect. This $\delta^{15}N_{NO3}$- value is close to an actual measured $\delta^{15}N_{NO3}$- (2.18‰). It is concluded that nitrogen isotope exchange between NO_2^- and NO_3^- was not observed in this experiment and natural abundance N isotope experiments (**Fig. 5.3.2**). Therefore, the nitrogen isotope exchange between NO_2^- and NO_3^- was not included in the following numerical model to calculate N and O isotope effects.

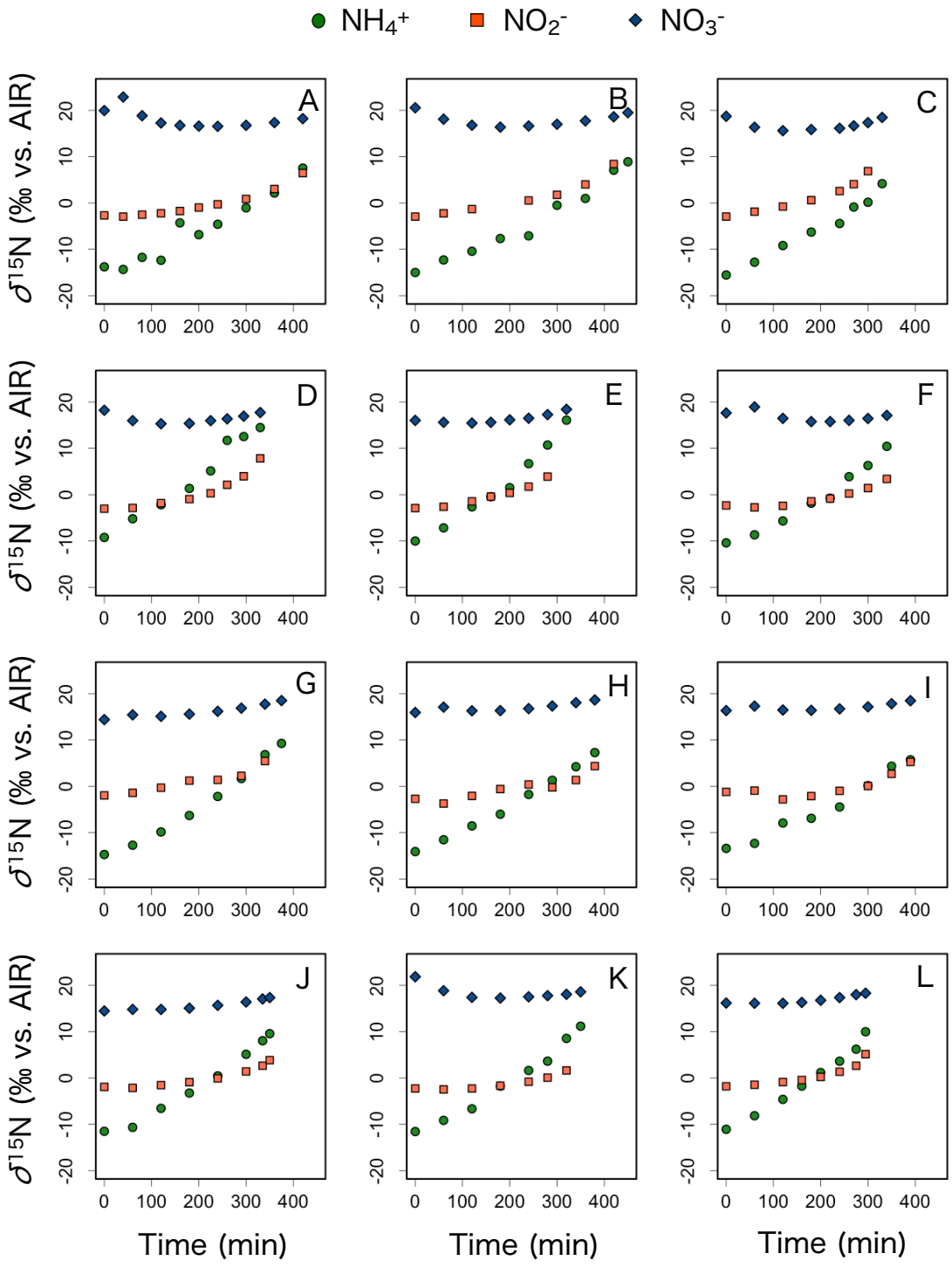

Figure 5.3.2 Changes in $\delta^{15}N$ of nitrogen compounds during anammox batch culture experiments. Triplicate experimental data obtained under $\delta^{18}O_{H2O}$ = -12.6‰ (A-C), $\delta^{18}O_{H2O}$ = 25.9‰ (D-F), $\delta^{18}O_{H2O}$ = 56.7‰(G-I), and $\delta^{18}O_{H2O}$ = 110.1‰(J-L) were shown.

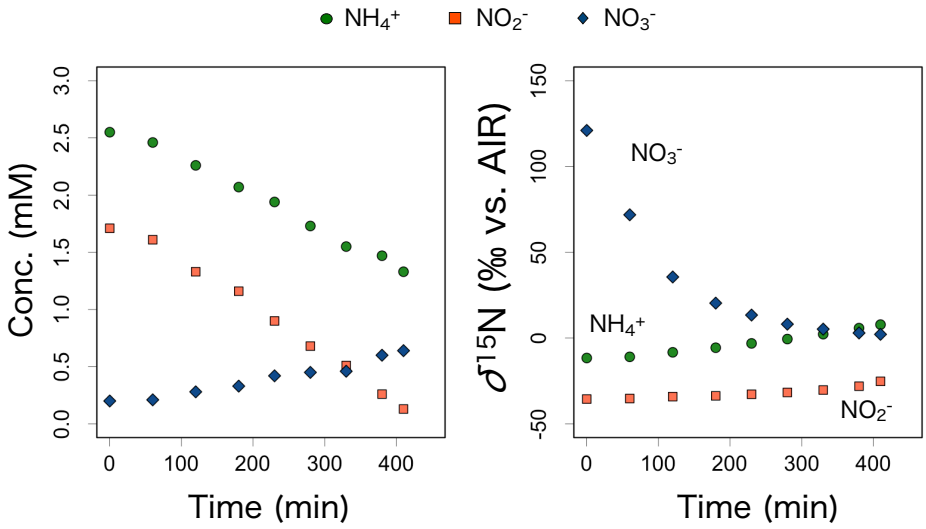

Figure 5.3.3 Changes in concentrations and $\delta^{15}N$ of nitrogen compounds during anammox batch culture experiments with ^{15}N-poor nitrite (ACROSS; $\delta^{15}N_{NO2-}$ = -35.5‰) and ^{15}N-rich nitrate (USGS32; $\delta^{15}N_{NO3-}$ = 121.0‰) to examine nitrogen isotope exchange between nitrite and nitrate.

5.3.3 Nitrogen isotope effect

The nitrogen isotope effect ($^{15}\varepsilon$) for respective reaction pathway was estimated by the Markov Chain Monte Carlo (MCMC) method (**Table 5.3.1**). Since anammox reaction was assumed to be the zero-order reaction in this model simulation, data points during lag-phase (data point at 0 min of **Fig. 5.3.2 A, E, F, I, J**) were excluded for parameter estimations. The estimation range of each parameter was set as follows ($0 < {}^{15}\varepsilon$ ($NH_4^+ \rightarrow N_2$) < 60, $0 < {}^{15}\varepsilon$ ($NO_2^- \rightarrow N_2$) < 60, and $-60 < {}^{18}\varepsilon$ ($NO_2^- \rightarrow NO_3^-$) < 0), which were based on the observed data sets and the reported $^{15}\varepsilon$ values of anammox bacteria (Brunner *et al.*, 2013; Kobayashi *et al.*, 2019). The sampling number was 100,000 to converge the parameters. The estimation results were shown in **Fig. 5.3.7~10, B, E, H**. The value of $^{15}\varepsilon$ ($NH_4^+ \rightarrow N_2$) was determined to be 30.7 ± 2.9 ‰, which is consistent with the previously reported value of '*Ca.* Scalindua' derived from continuous culture experiments ($^{15}\varepsilon$ ($NH_4^+ \rightarrow N_2$) =32.7 ± 0.7 ‰) (Kobayashi *et al.*, 2019). The values of $^{15}\varepsilon$ ($NO_2^- \rightarrow N_2$) and $^{15}\varepsilon$ ($NO_2^- \rightarrow NO_3^-$) were also determined to be 10.2 ± 1.8 ‰ and -16.9 ± 1.6 ‰, respectively. Those values are smaller than the reported values of '*Ca.* Scalindua' ($^{15}\varepsilon$ ($NO_2^- \rightarrow N_2$) = 19.9 ± 1.7 ‰ and $^{15}\varepsilon$ ($NO_2^- \rightarrow NO_3^-$) = -30.1 ± 3.0 ‰ (Kobayashi *et al.*, 2019). This difference might be caused by different growth conditions (mainly batch culture vs. continuous culture) and anammox activity. In the beginning of batch

experiment, anammox activity was unstable and there were about one-hour lag before the anammox reaction in several experiments. On the other hand, stable anammox activity was maintained in continuous culture MBR systems.

The kinetic N isotope effects of NH_4^+ oxidation by anammox bacteria were also determined using a Rayleigh isotope fractionation systematics (Brunner *et al.*, 2013). Obtained $^{15}\varepsilon$ ($NH_4^+ \rightarrow N_2$) by Rayleigh isotope fractionation systematics was summarized in **Table 5.3.2**. The results (Average 29.1 ± 3.2‰) were similar to those of the model fitting, implying that the developed model was robust.

Table 5.3.1 Summary of nitrogen isotope effects of anammox determined in batch incubation experiments

$\delta^{18}O_{H2O}$ of medium	Replication	$^{15}\varepsilon$ ($NH_4^+ \rightarrow N_2$)	$^{15}\varepsilon$ ($NO_2^- \rightarrow N_2$)	$^{15}\varepsilon$ ($NO_2^- \rightarrow NO_3^-$)
−12.6‰	1	33.7 ± 1.4	9.5 ± 0.6	− 12.9 ± 1.0
	2	27.5 ± 1.5	10.3 ± 0.6	− 16.6 ± 1.4
	3	29.7 ± 1.6	13.7 ± 0.7	− 15.9 ± 0.9
25.9‰	1	36.9 ± 1.3	10.2 ± 0.5	− 16.3 ± 0.8
	2	33.4 ± 1.9	11.7 ± 0.9	− 17.6 ± 1.2
	3	30.9 ± 1.5	11.7 ± 0.8	− 15.9 ± 0.9
56.7‰	1	28.9 ± 1.3	8.5 ± 0.5	− 18.0 ± 1.0
	2	28.5 ± 1.2	6.5 ± 0.4	− 19.6 ± 1.0
	3	27.8 ± 1.4	9.7 ± 0.6	− 17.0 ± 0.9
110.1‰	1	29.1 ± 1.2	9.0 ± 0.6	− 18.0 ± 1.1
	2	29.1 ± 1.4	10.9 ± 0.7	− 17.1 ± 0.8
	3	33.2 ± 1.3	10.7 ± 0.5	− 17.8 ± 0.8
Average		**30.7 ± 2.9**	**10.2 ± 1.8**	**− 16.9 ± 1.6**

Table 5.3.2 Summary of $^{15}\varepsilon$ ($NH_4^+ \rightarrow N_2$) determined by Rayleigh isotope fractionation systematics

$\delta^{18}O_{H2O}$ of medium	Replication	$^{15}\varepsilon$ ($NH_4^+ \rightarrow N_2$)
−12.6‰	1	25.3
	2	27.3
	3	27.7
25.9‰	1	35.2
	2	33.1
	3	31.1
56.7‰	1	30.3
	2	25.7
	3	25.4
110.1‰	1	28.7
	2	27.8
	3	32
Average		29.1 ± 3.2

5.3.4 Change in oxygen isotope compounds

During the anammox reaction, $\delta^{18}O$ of produced NO_3^- appeared to depend on the $\delta^{18}O_{H2O}$ of medium (**Fig. 5.3.4**). When the value of $\delta^{18}O_{H2O}$ was -12.6‰, the $\delta^{18}O_{NO3-}$ decreased from 20‰ to -0.3‰. Likewise, the $\delta^{18}O$ values of the produced NO_3^- approached to the values of $\delta^{18}O_{NO3-}$. Final $\delta^{18}O_{NO3-}$ were about 22‰, 42‰, and 64‰ at $\delta^{18}O_{H2O}$ of 25.9‰, 56.7‰ and 110.1‰, respectively. This observation suggested that water is an oxygen source of produced nitrate. $\delta^{18}O_{NO2-}$ increased during the anammox reaction (**Fig. 5.3.4**). More rapid increase in $\delta^{18}O_{NO2-}$ was observed in higher medium $\delta^{18}O_{H2O}$ compared to abiotic exchange. The $\delta^{18}O_{NO2}$ values almost reached the values of $\delta^{18}O_{H2O}$ within six to eight hours of incubation in high $\delta^{18}O_{H2O}$ of medium. It was much faster than abiotic oxygen isotope exchange (**Fig. 5.3.5**). Abiotically, the $\delta^{18}O_{NO2}$ achieved equilibrium around 650 h in this incubation condition (Kobayashi *et al.*, 2020). Anammox bacteria accelerated oxygen isotope exchange between NO_2^- and H_2O. The reaction rate of oxygen isotope exchange catalyzed by anammox bacteria was 17.8 to 45.7 times faster than the abiotic exchange rates (**Fig. 5.3.5**). Microbially catalyzed oxygen isotope exchanges between NO_2^- and H_2O were also reported with ammonia-oxidizing bacteria/archaea and nitrite-oxidizing bacteria (Buchwald and Casciotti, 2010; Casciotti *et al.*,

2010; Buchwald *et al.*, 2012; Nishizawa *et al.*, 2016; Boshers *et al.*, 2019). From those observations, we revised parameter setting for the numerical model (**Fig. 5.3.6**). Based on those observations, the influence of anammox catalyzed oxygen isotope exchange between NO_2^- and water was represented as a_{amx}. Therefore, combined abiotic and anammox catalyzed oxygen isotope exchange reaction constant was proposed as $k_{eq} \times a_{amx}$ (**Fig. 5.3.6**). As a result, the equation (34) was revised as following.

$$DT\_\delta^{18}ONitrite\_18Oincorp = -(a_{amx} \times k_{eq}) \times (\delta^{18}ONitriteT - \delta^{18}ONitriteEQ) \times \exp(-a_{amx} \times k_{eq}) \times DT) \quad \ldots(40)$$

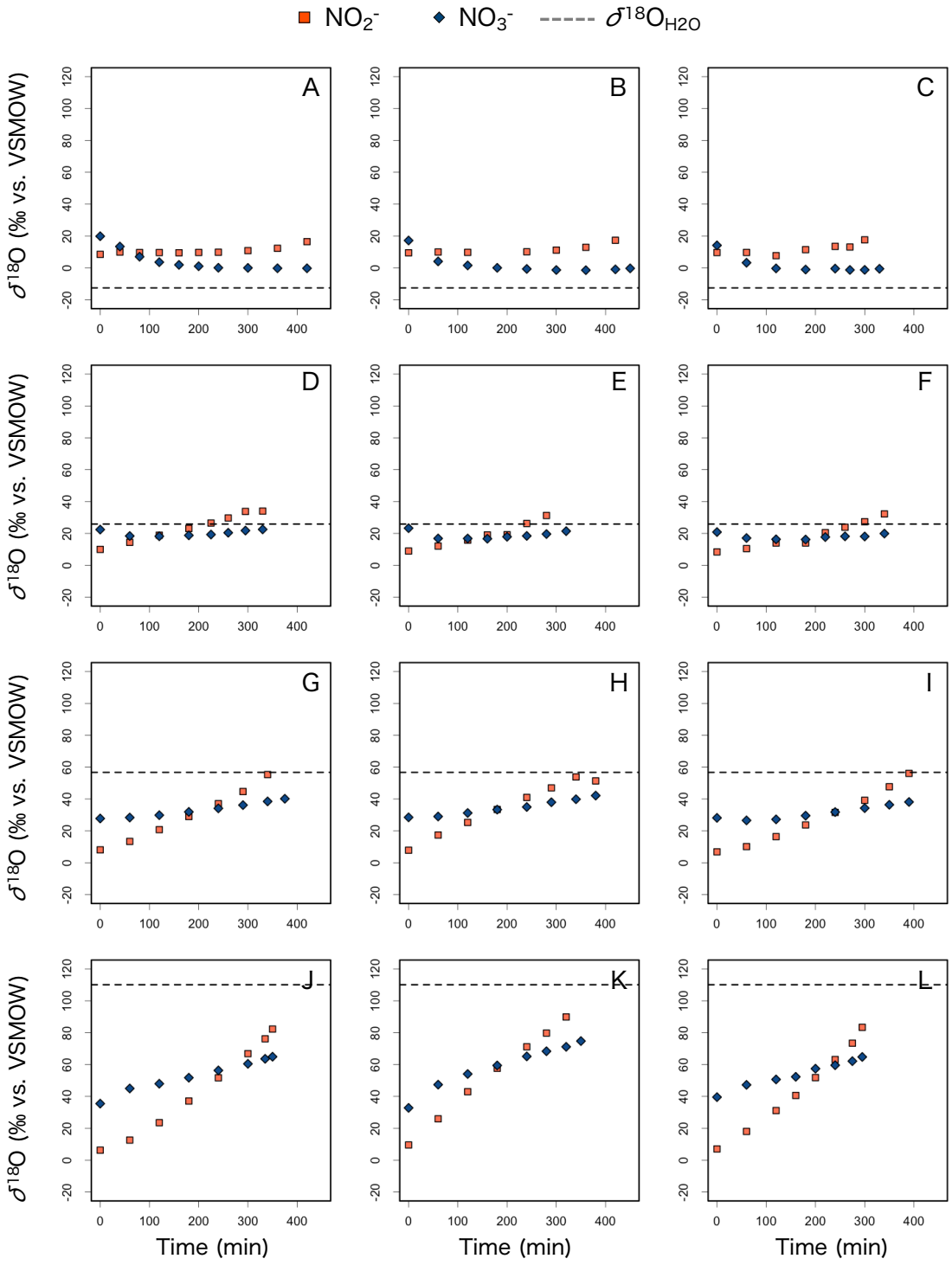

Figure 5.3.4 Changes in $\delta^{18}O$ of nitrogen compounds during anammox batch culture experiments. Triplicate experimental data obtained under $\delta^{18}O_{H2O}$ = -12.6‰ (A-C), $\delta^{18}O_{H2O}$ = 25.9‰ (D-F), $\delta^{18}O_{H2O}$ = 56.7‰(G-I), $\delta^{18}O_{H2O}$ = 110.1‰(J-L) were shown.

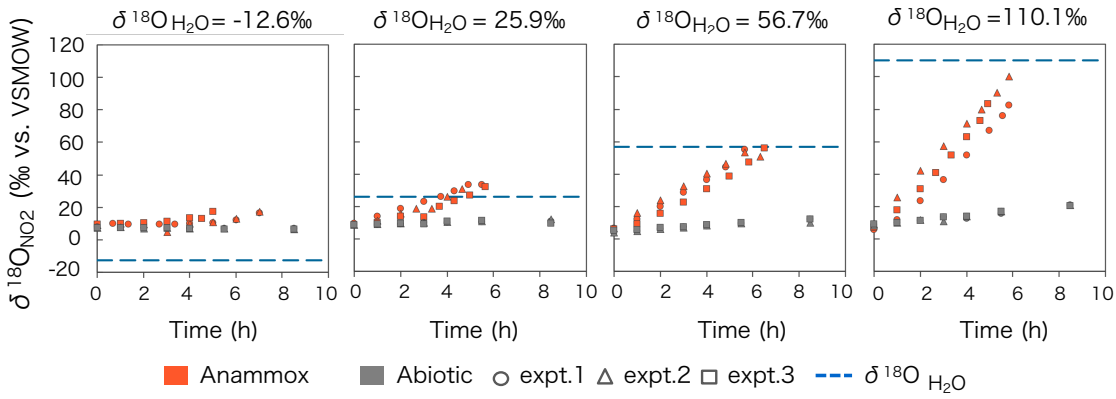

Figure 5.3.5 Comparison of change in $\delta^{18}O_{NO2-}$ values with and without anammox reaction. Triplicate experimental data obtained under $\delta^{18}O_{H2O}$ = -12.6‰, $\delta^{18}O_{H2O}$ = 25.9‰, $\delta^{18}O_{H2O}$ = 56.7‰ and $\delta^{18}O_{H2O}$ = 110.1‰ were plotted in respective figures.

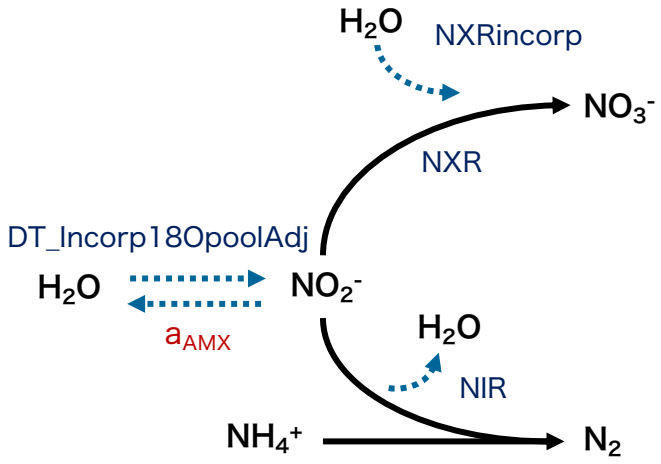

Figure 5.3.6 Revised O isotope model description

5.3.5 Oxygen isotope effects

The oxygen isotope effect ($^{18}\varepsilon$) for each reaction pathway was estimated with the Markov Chain Monte Carlo (MCMC) method using a numerical model (**Table 5.3.3**). Since anammox reaction was assumed to be the zero-order reaction in this model simulation, data points during lag-phase (data points at 0 min of **Fig. 5.3.4 A, E, F, I, J**) were excluded for parameter estimations. The estimation ranges of each parameter were set as follows ($0 < {}^{18}\varepsilon$ ($NO_2^- \rightarrow N_2$) < 30, $-30 < {}^{18}\varepsilon$ ($NO_2^- \rightarrow NO_3^-$) < 0, $0 < {}^{18}\varepsilon_{H2O} < 30$, and $10 < a_{amx} < 100$, which were based on the observed data sets and the reported value of $^{18}\varepsilon$ catalyzed by same enzyme. The sampling number was 10,0000 to converge the parameters. The estimation results were shown in **Fig. 5.3.7~10, C, F, I**. Constant

oxygen isotope exchange between NO_2^- and water was observed regardless of the value of $\delta^{18}O_{H2O}$ (**Table 5.3.3**). From the estimation of parameter a_{amx}, the reaction constants of anammox mediated oxygen isotope exchange were 10.1 to 17.7 times larger than that of abiotic reaction. This indicates that anammox bacteria substantially contributed to oxygen isotope exchange between NO_2^- and water. The oxygen isotope effect associated with NO_2^- reduction to N_2, $^{18}\varepsilon$ ($NO_2^-\rightarrow N_2$), was determined to be from 9.6 to 21.1‰ (**Table 5.3.3**). As for NO_2^- oxidation to NO_3^-, $^{18}\varepsilon$ ($NO_2^-\rightarrow NO_3^-$) was determined to be from -19.6 to -0.4‰. The oxygen isotope effect associated with the oxygen incorporation from water, $^{18}\varepsilon_{H2O}$, was in a range from 5.3 to 29.2‰. All these oxygen isotope effects seem to be dependent on the value of $\delta^{18}O_{H2O}$ (**Fig. 5.3.11**). There were linear relationships between the oxygen isotope effects and the value of $\delta^{18}O_{H2O}$. The$^{18}\varepsilon$ ($NO_2^-\rightarrow N_2$) increased with increasing $\delta^{18}O_{H2O}$ of medium. On the other hand, both of $^{18}\varepsilon$ ($NO_2^-\rightarrow NO_3^-$) and $^{18}\varepsilon_{H2O}$ decreased with increasing $\delta^{18}O_{H2O}$. The $\delta^{18}O_{H2O}$ dependency of oxygen isotope effects might be attributed to different oxygen isotope equilibrium among NO_2^-, NO_3^- and H_2O due to large ^{18}O concentration differences. The oxygen isotope equilibrium among NO_2^-, NO_3^- and H_2O might be achieved more quickly in higher $\delta^{18}O_{H2O}$ medium. More light oxygen isotope NO_2^- was consumed and light oxygen isotope H_2O was consequently produced in NO_2^- reduction when $\delta^{18}O_{H2O}$ increased (**Fig 5.3.11** and **Fig. 5.3.12**). In contrast, more heavy oxygen isotope H_2O was consumed when $\delta^{18}O_{H2O}$ increased in NO_2^- oxidation (**Fig 5.3.11** and **Fig. 5.3.12).** However, since this is the first time to report the oxygen isotope effects associated with anammox metabolism the information on the effect of different $\delta^{18}O_{H2O}$ on the oxygen isotope effects was very limited (Buchwald and Casciotti, 2010; Casciotti *et al.*, 2010). Thus, further study is required to validate the $\delta^{18}O_{H2O}$ dependency of oxygen isotope effects.

When these obtained oxygen isotope effects are applied to natural environmental studies, it is not realistic to set the $\delta^{18}O_{H2O}$ extensively high values like $\delta^{18}O_{H2O}$ = 56.7‰ and 110.1‰ applied in this study. The $\delta^{18}O_{H2O}$ of global surface ocean was generally reported to be the range from -7.7‰ to 1.8‰ (LeGrande and Schmidt, 2006). Therefore, the range of oxygen isotope effects that would be expressed in natural oceanic environments should be estimated. The oxygen isotope effects at the value of $\delta^{18}O_{H2O}$ from -7.7‰ to 1.8‰ could be estimated based on the linear relationship between oxygen isotope effects and $\delta^{18}O_{H2O}$ (**Fig 5.3.11**) as followings $^{18}\varepsilon$ ($NO_2^-\rightarrow N_2$) = 9.8 ~ 10.5‰, $^{18}\varepsilon$ ($NO_2^-\rightarrow NO_3^-$) = -3.3 ~ -1.9 ‰, and $^{18}\varepsilon_{H2O}$ = 24.1 ~ 25.6 ‰. The parameter a_{amx} was not dependent on $\delta^{18}O_{H2O}$ and thus remained 10.1 to 17.7.

Table 5.3.3. Summary of oxygen isotope effect of anammox

$\delta^{18}O_{H2O}$ of medium	Replication	$^{18}\varepsilon$ ($NO_2^- \rightarrow N_2$) ‰	$^{18}\varepsilon$ ($NO_2^- \rightarrow NO_3^-$) ‰	$^{18}\varepsilon_{H2O}$ ‰	a_{amx}
− 12.6‰	1	12.0 ± 2.3	− 0.4 ± 0.4	29.2 ± 0.8	16.9 ± 1.3
	2	9.6 ± 1.6	− 1.4 ± 1.1	26.8 ± 2.5	13.6 ± 1.3
	3	13.1 ± 3.0	− 0.9 ± 0.7	28.2 ± 1.5	17.7 ± 1.4
	Average	11.6 ± 1.8	− 0.9 ± 0.5	28.1 ± 1.2	16.0± 1.1
26.9‰	1	9.9 ± 2.4	− 5.9 ± 3.2	20.0 ± 6.5	12.9 ± 1.2
	2	9.7 ± 2.1	− 5.7 ± 3.8	16.1 ± 7.8	11.7 ± 1.1
	3	10.5 ± 1.9	− 5.8 ± 3.4	17.1 ± 7.2	10.9 ± 1.1
	Average	10.0 ± 0.4	− 5.8 ± 0.1	17.8 ± 2.0	11.8 ± 1.1
56.7‰	1	12.9 ± 1.1	− 15.6 ± 3.0	20.6 ± 6.3	10.4 ± 1.0
	2	12.1 ± 2.0	− 15.4 ± 3.5	15.4 ± 7.4	12.8 ± 1.1
	3	14.4 ± 1.7	− 8.4 ± 3.5	11.8 ± 6.6	10.5 ± 1.0
	Average	13.1 ± 1.2	− 13.2 ± 4.1	15.9 ± 4.4	11.2 ± 1.1
110.1‰	1	18.5 ± 1.4	− 17.7 ± 3.5	10.0 ± 7.3	10.3 ± 1.0
	2	21.1 ± 2.2	− 19.6 ± 1.8	5.3 ± 3.5	14.3 ± 1.0
	3	20.8 ± 1.3	− 15.4 ± 2.7	9.3 ± 5.8	10.1 ± 1.0
	Average	20.1 ± 1.4	− 17.6 ± 2.1	8.2 ± 2.6	11.4 ± 1.2

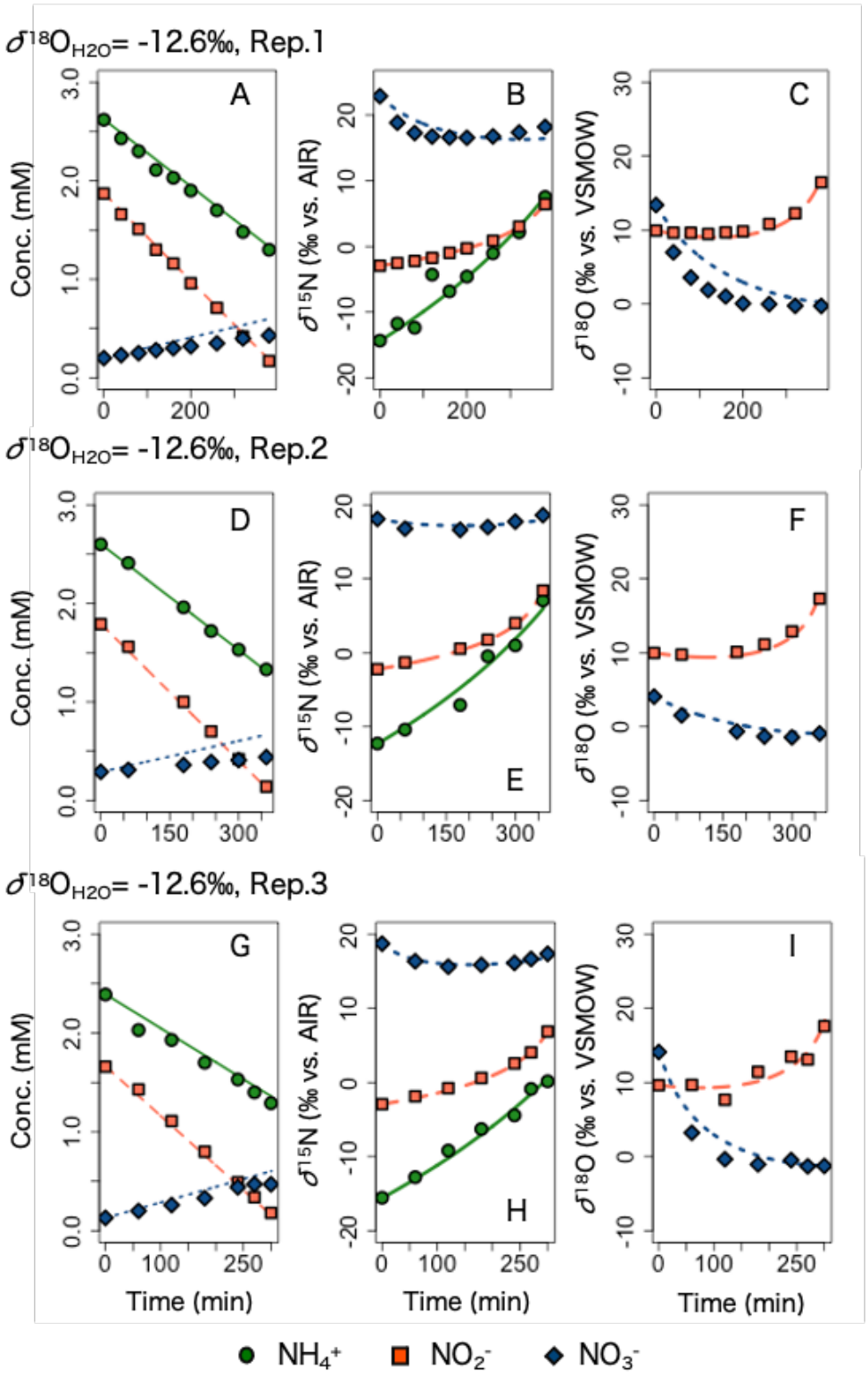

Figure. 5.3.7 Concentrations and isotopic signatures of N compounds in batch experiments with $\delta^{18}O_{H2O}$= -12.6‰. Lines represent change in the concentration and isotope signature estimated by MCMC.

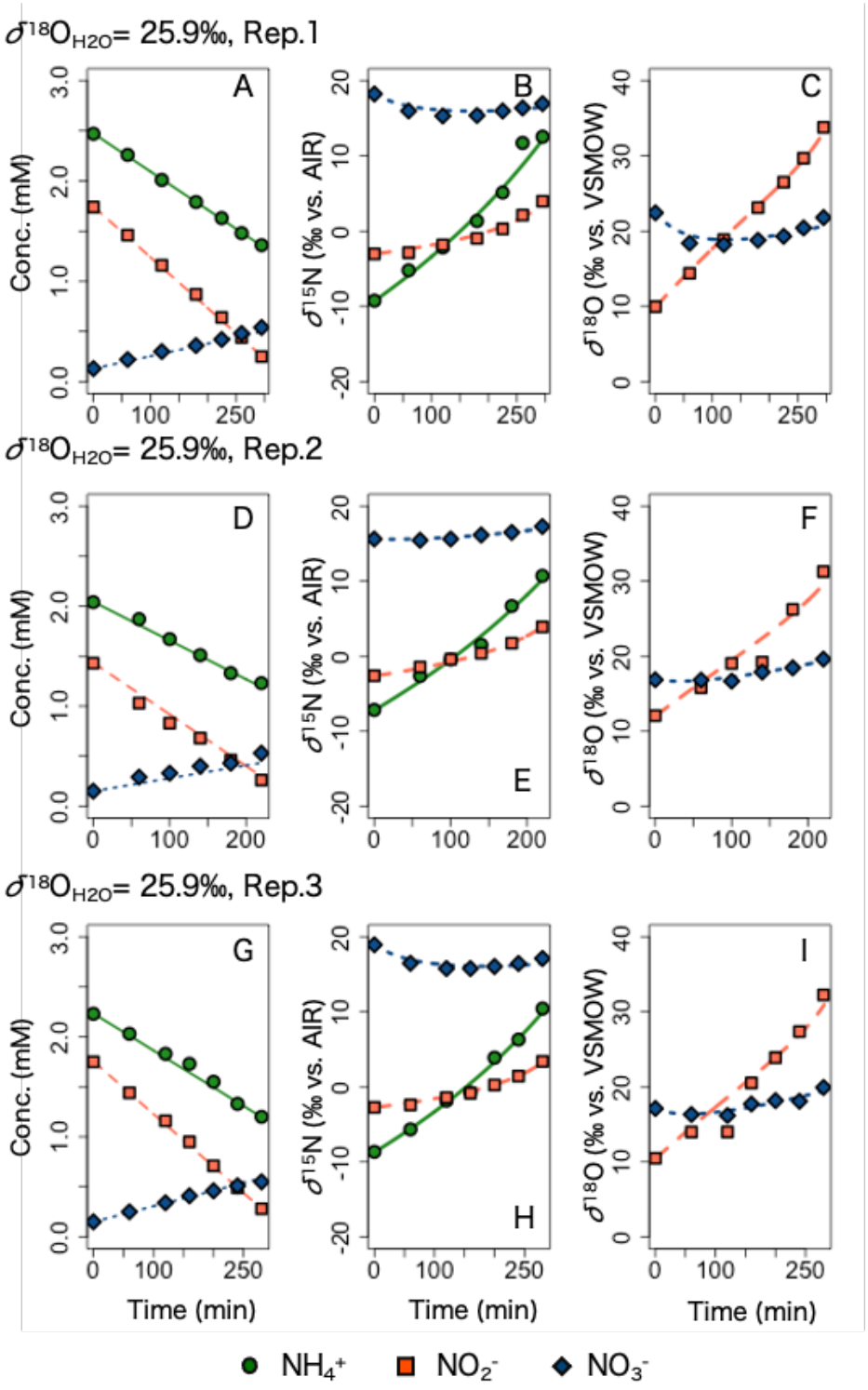

Figure. 5.3.8 Concentrations and isotopic signatures of N compounds in batch experiments with $\delta^{18}O_{H2O}$= 25.9‰. Lines represent change in the concentration and isotope signature estimated by MCMC.

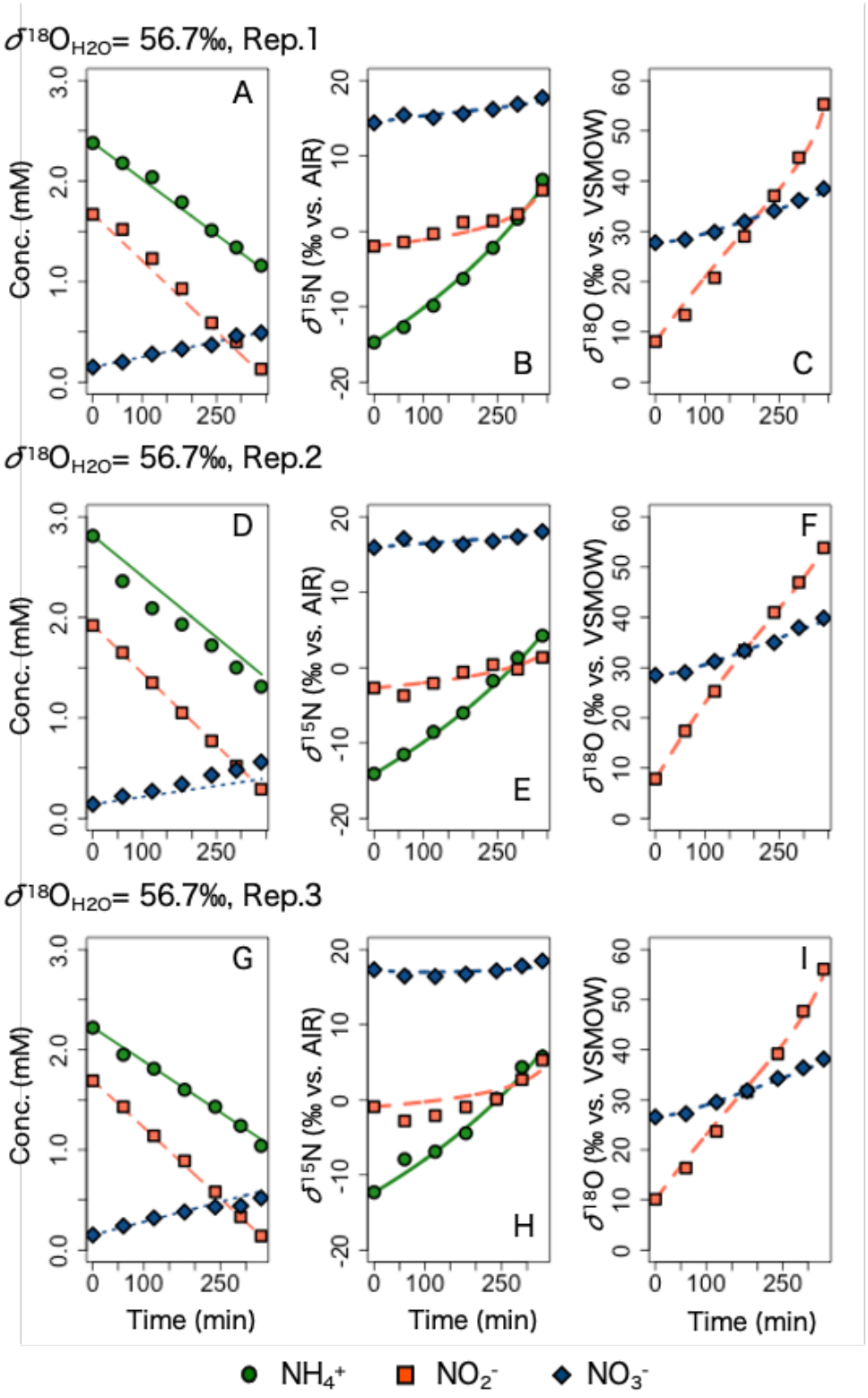

Figure. 5.3.9 Concentrations and isotopic signatures of N compounds in batch experiments with $\delta^{18}O_{H2O}$= 56.7‰. Lines represent change in the concentration and isotope signature estimated by MCMC.

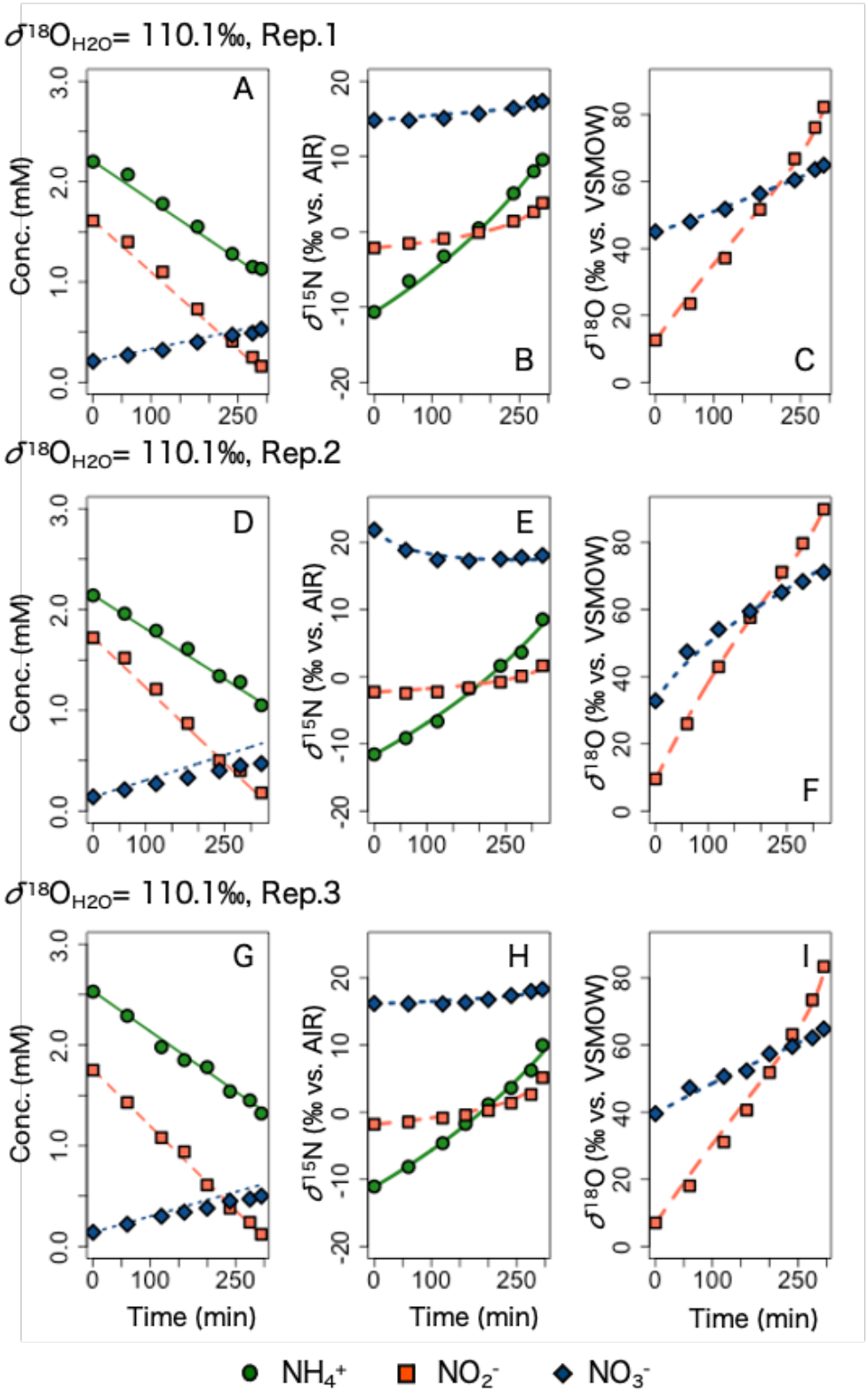

Figure. 5.3.10 Concentrations and isotopic signatures of N compounds in batch experiments with $\delta^{18}O_{H2O}$= 110.1‰. Lines represent change in the concentration and isotope signature estimated by MCMC.

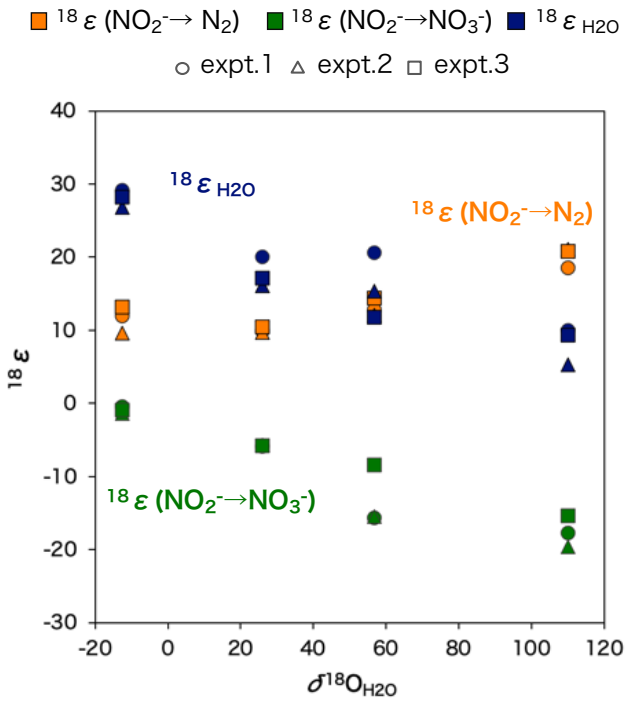

Figure 5.3.11 Summary of $^{18}\varepsilon$ dependency on $\delta^{18}O_{H2O}$. The circle is first replication, triangle is second replication, square is third replication.

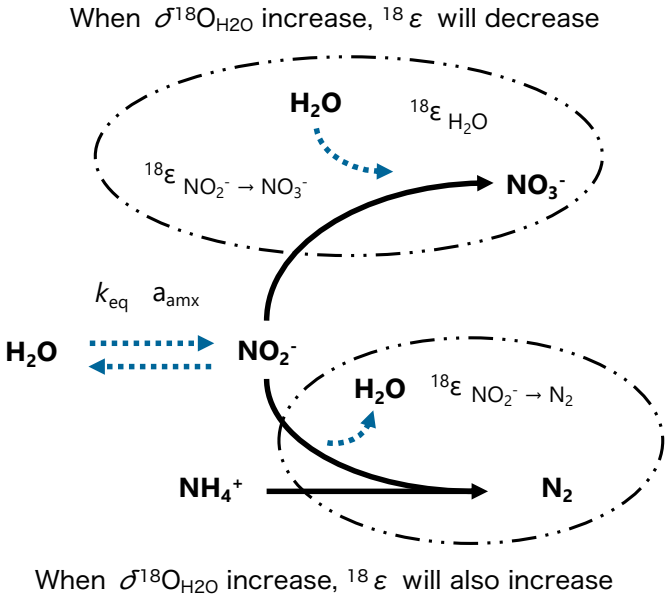

Figure 5.3.12 The relationship between increase of $\delta^{18}O_{H2O}$ and estimated $^{18}\varepsilon$ values in this study

5.3.6 Implication for a fixed nitrogen budget

NO_3^- is the dominant form of bioavailable nitrogen in the ocean. Natural abundance N and O stable isotope ratio of NO_3^- is known as an invaluable tool to differentiate source and determine the biogeochemical transformations. In the oceanic N budget, NO_3^- isotopes is affected by mainly three processes: denitrification, nitrification and anammox. NO_3^- is consumed by denitrification which is step wise reduction of NO_3^- to NO_2^-, nitric oxide, nitrous oxide, and finally N_2. Nitrification refers to the sequential oxidation of NH_3 to NO_2^- and then NO_3^-. Anammox also oxidize NO_2^- to NO_3^-. To evaluate the impact of each process, the interpretation of those N and O isotope effects are essential. Denitrification is known to yield nearly identical N and O isotope effects of NO_3^- ($^{18}\varepsilon : {}^{15}\varepsilon = 1$)(Sigman *et al.*, 2005; Granger *et al.*, 2008). However, anammox bacteria yielded larger inverse kinetic isotope effects on nitrogen compared to oxygen during NO_2^- oxidation to NO_3^- ($^{15}\varepsilon$ ($NO_2^- \rightarrow NO_3^-$) = -16.9 ± 1.6‰ and $^{18}\varepsilon$ ($NO_2^- \rightarrow NO_3^-$) = -3.3 ~ 1.9‰, thus $^{18}\varepsilon : {}^{15}\varepsilon$ = 0.1 ~ 0.2) in the present study. Although produced NO_3^- by anammox is affected by ambient water due to O incorporation from water ($^{18}\varepsilon_{H2O}$), there is possibility that NO_3^- isotope interpretation could differentiate reaction of denitrification and anammox. Both of anammox and nitrite-oxidizing bacteria show inverse kinetic isotope effects for NO_2^- oxidation. The values of N and O isotope effects of nitrite-oxidizing bacteria were varied among species ($^{15}\varepsilon$ ($NO_2^- \rightarrow NO_3^-$) = -9.1 ~ 20.6‰ and $^{18}\varepsilon$ ($NO_2^- \rightarrow NO_3^-$) = -8.2 ~ - 1.3‰) (Buchwald and Casciotti, 2010). The key enzyme for NO_2^- oxidation by anammox and nitrite-oxidizing bacteria is nitrite oxidoreductase (Nxr). Similar expressed isotope effects of anammox and nitrite-oxidizing bacteria might be attributed to similar reaction pathway. Even though, anammox and nitrite-oxidizing bacteria show similar isotope effect, impact of each process might be separated by isotope effects on NO_2^- by NO_2^- reduction by anammox and background information about the environment (e. g. O_2 concentration).

NO_2^- is a central intermediate in the nitrogen cycle. The rate of abiotic O atom exchange between NO_2^- and H_2O has been used to estimate NO_2^- turnover time in a wide range of oceanic environments (Buchwald and Casciotti, 2013). In this experiment, anammox bacteria contributed to accelerate oxygen isotope exchange between NO_2^- and water. Microbially catalyzed oxygen isotope exchange between NO_2^- and H_2O were also reported for ammonia-oxidizing bacteria and archaea and nitrite-oxidizing bacteria (Buchwald and Casciotti, 2010; Casciotti *et al.*, 2010; Buchwald *et al.*, 2012; Nishizawa *et al.*, 2016; Boshers *et al.*, 2019). Thus, it is better to imply microbial catalyzed oxygen isotope exchange to interpret NO_2^- isotopes.

5.4 Conclusions

In this study, the coupled nitrogen and oxygen isotope effects of anammox reaction by '*Ca*. Scalindua sp.', which is a putative marine species, were successfully determined at the first time by conducting batch culture experiments with different $\delta^{18}O_{H2O}$ values of medium ($\delta^{18}O_{H2O}$ = -12.6 ~ 110.1‰). A numerical model was developed with the Markov Chain Monte Carlo (MCMC) method for estimation of respective $^{15}\varepsilon$ and $^{18}\varepsilon$ of anammox reaction. The obtained values of $^{15}\varepsilon$ were $^{15}\varepsilon$ ($NH_4^+ \rightarrow N_2$) = 30.7 ± 2.9 ‰, $^{15}\varepsilon$ ($NO_2^- \rightarrow N_2$) = 10.2 ± 1.8 ‰ and $^{15}\varepsilon$ ($NO_2^- \rightarrow NO_3^-$) = -16.9 ± 1.6 ‰. Respective $^{18}\varepsilon$ of anammox reaction were determined to be $^{18}\varepsilon$ ($NO_2^- \rightarrow N_2$) = 9.6 ~ 21.1‰ and $^{18}\varepsilon$ ($NO_2^- \rightarrow NO_3^-$) = -19.6 ~ -0.4‰ and $^{18}\varepsilon_{H2O}$ = 5.3 to 29.2‰, respectively. The $^{18}\varepsilon$ values were dependent on $\delta^{18}O_{H2O}$ of the medium, and there were linear relationships between them. Furthermore, anammox bacteria accelerated oxygen isotope exchange between NO_2^- and water. The rate of oxygen isotope exchange catalyzed by anammox bacterium was 10.1 to 17.7 times larger than that of abiotic oxygen isotope exchange. To apply these obtained oxygen isotope effects to natural marine environment (which exhibit $\delta^{18}O_{H2O}$ = 7.7 ~1.8‰), the range of oxygen isotope effects were estimated to be $^{18}\varepsilon_{NO2\rightarrow N2}$ = 9.8 ~ 10.5‰, $^{18}\varepsilon_{NO2\rightarrow NO3}$ = -3.3 ~ -1.9 ‰, and $^{18}\varepsilon_{H2O}$= 24.1 ~ 25.6 ‰, respectively.

5.5 References

Ali, M., Oshiki, M., Awata, T., Isobe, K., Kimura, Z., Yoshikawa, H., et al. (2015) Physiological characterization of anaerobic ammonium oxidizing bacterium "*Candidatus* Jettenia caeni." *Environ Microbiol* 17: 2172–2189.

APHA, AWWA, and WEF (2005) Standard Methods for the Examination of Water and Wastewater. Washington, D.C.

Awata, T., Oshiki, M., Kindaichi, T., Ozaki, N., Ohashi, A., and Okabe, S. (2013) Physiological characterization of an anaerobic ammonium-oxidizing bacterium belonging to the "*Candidatus* scalindua" group. *Appl Environ Microbiol* 79: 4145–4148.

Boshers, D.S., Granger, J., Tobias, C.R., Böhlke, J.K., and Smith, R.L. (2019) Constraining the oxygen isotopic composition of nitrate produced by nitrification. *Environ Sci Technol* 53: 1206–1216.

Brunner, B., Contreras, S., Lehmann, M.F., Matantseva, O., Rollog, M., Kalvelage, T., et al. (2013) Nitrogen isotope effects induced by anammox bacteria. *Proc Natl Acad Sci* 110: 18994–18999.

Buchwald, C. and Casciotti, K. (2013) Isotopic ratios of nitrite as tracers of the sources and age of oceanic nitrite. *Nat Publ Gr* 6: 1–6.

Buchwald, C. and Casciotti, K.L. (2013) Isotopic ratios of nitrite as tracers of the sources and age of oceanic nitrite. *Nat Geosci* 6: 308–313.

Buchwald, C. and Casciotti, K.L. (2010) Oxygen isotopic fractionation and exchange during bacterial nitrite oxidation. *Limnol Oceanogr* 55: 1064–1074.

Buchwald, C., Santoro, A.E., McIlvin, M.R., and Casciotti, K.L. (2012) Oxygen isotopic composition of nitrate and nitrite produced by nitrifying cocultures and natural marine assemblages. *Limnol Oceanogr* 57: 1361–1375.

Casciotti, K.L., Bohlke, J.K., McIlvin, M.R., Mroczkowski, S.J., and Hannon, J.E. (2007) Oxygen isotopes in nitrite: Analysis, calibration, and equilibration. *Anal Chem* 79: 2427–2436.

Casciotti, K.L., McIlvin, M., and Buchwald, C. (2010) Oxygen isotopic exchange and fractionation during bacterial ammonia oxidation. *Limnol Oceanogr* 55: 753–762.

Casciotti, K.L., Sigman, D.M., Hastings, M.G., Bohlke, J.K., and Hilkert, A. (2002) Measurement of the oxygen isotopic composition of nitrate seawater and freshwater using the dentirifier method. *Anal Chem* 74: 4905-4912.

Graaf, A.A. Van De, Bruijn, P. De, Robertson, L.A., Jetten, M.S.M., and Kuenen, J.G. (1996) Autotrophic growth of anaerobic in a fluidized bed reactor. *Microbiology* 142: 2187–2196.

Granger, J. and Sigman, D.M. (2009) Removal of nitrite with sulfamic acid for nitrate N and O isotope analysis with the denitrifier method. *Rapid Commun Mass Spectrom* 23: 3753–3762.

Granger, J., Sigman, D.M., Lehmann, M.F., and Tortell, P.D. (2008) Nitrogen and oxygen isotope fractionation during dissimilatory nitrate reduction by denitrifying bacteria. 53: 2533–2545.

Granger, J. and Wankel, S.D. (2016) Isotopic overprinting of nitrification on denitrification as a ubiquitous and unifying feature of environmental nitrogen cycling. *Proc Natl Acad Sci* 113 (42): E6391-E6400.

Holmes, R.M., McClelland, J.W., Sigman, D.M., Fry, B., and Peterson, B.J. (1998) Measuring $^{15}N\text{-}NH_4$ in marine, estuarine, and freshwaters: An adaptation of the ammonia diffusion method for samples with low ammonium concentrations. *MarChem* 60: 235–243.

Hu, H., Bourbonnais, A., Larkum, J., Bange, H.W., and Altabet, M.A. (2016) Nitrogen cycling in shallow low-oxygen coastal waters off Peru from nitrite and nitrate nitrogen and oxygen isotopes. *Biogeosciences* 13: 1453–1468.

Kartal, B., De Almeida, N.M., Maalcke, W.J., Op den Camp, H.J.M., Jetten, M.S.M., and Keltjens, J.T. (2013) How to make a living from anaerobic ammonium oxidation. *FEMS Microbiol Rev* 37: 428–461.

Kartal, B., Kuypers, M.M.M., Lavik, G., Schalk, J., Op Den Camp, H.J.M., Jetten, M.S.M., and Strous, M. (2007) Anammox bacteria disguised as denitrifiers: Nitrate reduction to dinitrogen gas via nitrite and ammonium. *Environ Microbiol* 9: 635–642.

Kobayashi, K., Fukushima, K., Onishi, Y., Nishina, K., Makabe, A., Yano, M., et al. (2020) Influence of $\delta^{18}O$ of water on measurements of $\delta^{18}O$ of nitrite and nitrate . *Rapid Commun Mass Spectrom* 35 (2): e8979.

Kobayashi, K., Makabe, A., Yano, M., Oshiki, M., Kindaichi, T., Casciotti, K.L., and Okabe, S. (2019) Dual nitrogen and oxygen isotope fractionation during anaerobic ammonium oxidation by anammox bacteria. *ISME J* 13: 2426–2436.

LeGrande, A.N. and Schmidt, G.A. (2006) Global gridded data set of the oxygen isotopic composition in seawater. *Geophys Res Lett* 33: 1–5.

Lotti, T., Kleerebezem, R., Lubello, C., and van Loosdrecht, M.C.M. (2014) Physiological and kinetic characterization of a suspended cell anammox culture. *Water Res* 60: 1–14.

McIlvin, M.R. and Altabet, M.A. (2005) Chemical conversion of nitrate and nitrite to nitrous oxide for nitrogen and oxygen isotopic analysis in freshwater and seawater. *Anal Chem* 77: 5589–5595.

McIlvin, M.R. and Casciotti, K.L. (2006) Method for the analysis of delta ^{18}O in water. *Anal Chem* 78: 2377–2381.

Nishizawa, M., Sakai, S., Konno, U., Nakahara, N., Takaki, Y., Saito, Y., et al. (2016) Nitrogen and oxygen isotope effects of ammonia oxidation by thermophilic *Thaumarchaeota* from a geothermal water stream. *Appl Environ Microbiol* 82: AEM.00250-16.

Oshiki, Mamoru, Awata, T., Kindaichi, T., Satoh, H., and Okabe, S. (2013) Cultivation of planktonic anaerobic ammonium oxidation (anammox) bacteria using membrane Bioreactor. *Microbes Environ* 28: 436–443.

Oshiki, M., Ishii, S., Yoshida, K., Fujii, N., Ishiguro, M., Satoh, H., and Okabe, S. (2013) Nitrate-dependent ferrous iron oxidation by anaerobic ammonium oxidation (anammox) bacteria. *Appl Environ Microbiol* 79: 4087–4093.

Sigman, D.M., Altabet, M. a, Michener, R., McCorkle, D.C., Fry, B., and Holmes, R.M. (1997) Natural abundance-level measurements of the nitrogen isotopic composition of oceanic nitrate: an adaption of the ammonia diffusion method. *Mar Chem* 57: 227–242.

Sigman, D.M., Casciotti, K.L., Andreani, M., Barford, C., Galanter, M., and Bhlke, J.K. (2001) A Bacterial Method for the Nitrogen Isotopic Analysis of Nitrate in Seawater and Freshwater. *Anal Chem* 73: 4145–4153.

Sigman, D.M., Granger, J., DiFiore, P.J., Lehmann, M.M., Ho, R., Cane, G., and van Geen, A. (2005) Coupled nitrogen and oxygen isotope measurements of nitrate along the eastern North Pacific margin. *Global Biogeochem Cycles* 19: 1–14.

Soetaert, K. and Petzoldt, T. (2010) Inverse modelling, sensitivity and monte carlo analysis in R using package FME. *J Stat Softw* 33: 1–28.

Strous, M., Fuerst, J. A, Kramer, E.H., Logemann, S., Muyzer, G., van de Pas-Schoonen, K.T., et al. (1999) Missing lithotroph identified as new planctomycete. *Nature* 400: 446–449.

Thuan, N.C., Koba, K., Yano, M., Makabe, A., Kinh, C.T., Terada, A., et al. (2018) N2O production by denitrification in an urban river: evidence from isotopes, functional genes, and dissolved organic matter. *Limnology* 19: 115–126.

Chapter 6

Enzyme level nitrogen and oxygen isotope effects of nitrite oxidoreductase (Nxr) by anaerobic ammonium-oxidizing bacteria

6.1. Introduction

Analysis of natural abundance nitrogen (N) and oxygen (O) isotopes (δ^{15}N and δ^{18}O) of N compounds (NO_2^-, NO_3^-, N_2O, and NH_4^+) is an important tool for evaluating sources and transformations of natural and contaminant N compounds in the environment (Casciotti *et al.*, 2013; Peters *et al.*, 2016). To fully exploit these δ^{15}N and δ^{18}O signatures, both the N and O isotope effects ($^{15}\varepsilon$ and $^{18}\varepsilon$) associated with the respective N transformation processes must be known. Denitrification and anammox are two major N sinks in the oceanic oxygen minimum zones (OMZs). Anammox bacteria also contribute to re-oxidation of nitrite (NO_2^-) to nitrate (NO_3^-) (i.e., recycling N), which has been overlooked so far, in addition to aerobic NO_2^- oxidation by nitrite-oxidizing bacteria (NOB). NO_3^- could be reduced to NO_2^- by denitrifying bacteria. Although these overlapped NO_2^- oxidation and NO_3^- reduction reactions significantly influences the N and O isotope ratio of NO_2^- and NO_3^-, it is difficult to evaluate the respective contributions to the N and O isotope ratio of NO_2^- and NO_3^- and consequent total N budget. Therefore, understanding influence of each microbial reaction on the N and O isotope ratio of NO_2^- and NO_3^- is significantly important. It has been known that the re-oxidation of NO_2^- to NO_3^- by NOB shows inverse nitrogen and oxygen isotope effect (Casciotti, 2009; Buchwald and Casciotti, 2010). Anammox bacteria also showed nitrogen inverse kinetic isotope effect (Brunner *et al.*, 2013; Kobayashi *et al.*, 2019). The inverse kinetic isotope effect implies that the reaction constant of heavy isotope is larger than that of light isotope, which is rarely occurring in natural microbial processes. This unique isotope effect has a potential to distinguish from other reactions. However, the reaction mechanism of inverse kinetic isotope by NO_2^- oxidation was not fully understood. The key enzyme for NO_2^- oxidation by anammox and NOB is nitrite oxidoreductase (Nxr). However, limited mechanistic information of NO_2^- oxidation by Nxr is available, because of slow growth of NOB and anammox bacteria, the nature of Nxr as a membrane protein, and the lack of a crystal structure (Lancaster *et al.*, 2018). It has been reported that *Nitrobacter* Nxr consists of two (α_2 and β_2) (Meincke *et al.*, 1992) or three (α_2, β_2, and γ_1) subunits (Sundermeyer-Klinger *et al.*, 1984). Nitrite oxidoreductase purified from

Nitrobacter can either oxidize NO_2^- to NO_3^- or reduces NO_3^- to NO_2^-, depending on its redox state and experimental condition of pH (Sundermeyer-Klinger *et al.*, 1984; Meincke *et al.*, 1992). Anammox bacteria also can reverse this enzymatic reaction, namely they can reduce NO_3^- back to NO_2^-, in addition to NO_2^- oxidation to NO_3^- (Kartal *et al.*, 2007; Oshiki *et al.*, 2013). It is thus hypothesized that this reversible reaction would promote isotope exchange between NO_2^- and NO_3^- and lead to more pronounced isotope effects as observed in sulfur metabolism (Holler *et al.*, 2012). Intriguingly, it has been also speculated that environmental stresses cause a significant N isotope exchange between NO_2^- and NO_3^- (-60.5 ± 1.0‰) observed in a "*Ca.* K. stuttgartiensis" batch culture study (Brunner *et al.*, 2013). However, since this phenomenon was not ubiquitously observed, it remained unclear whether this exchange was caused by cell lysis during cultivation and/or sample preparation. Here, the N and O isotope effects during NO_2^- oxidation and NO_3^- reduction by anammox bacterial Nxr were determined to evaluate how the reversibility of anammox bacterial Nxr affects the N and O isotope effects of NO_2^- oxidation. For the purpose, anammox bacterial Nxr was partially purified from "*Ca*. Brocadia sinica", and the N and O isotope effects of NO_2^- oxidation and NO_3^- reduction were determined independently using an appropriate artificial electron acceptor and electron donor (**Fig. 6.1.1**).

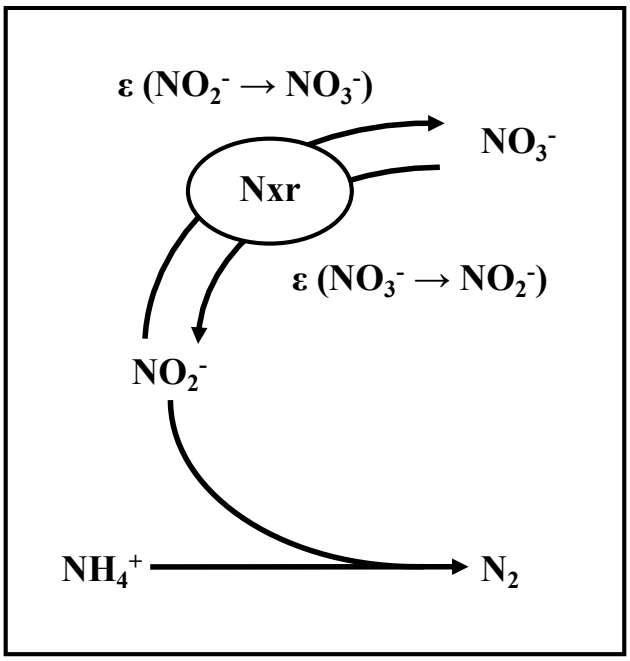

Figure 6.1.1 Anammox reaction systematics and the role of nitrite oxidoreductase (Nxr) in anammox reaction.

6.2. Material and method

6.2.1 Anammox cells and incubation condition

A fresh water anammox species "*Ca.* Brocadia sinica" was cultivated in an up-flow column reactor (1.15 L, φ=70 mm, height = 300 mm, AZONE). The column reactor has been operated over five years at 37°C, and "*Ca.* Brocadia sinica" proliferated in the form of granular biomass. Inorganic synthetic medium was continuously supplied into the column reactor at a hydraulic retention time (HRT) of 2 h, and the medium composition is as following; $FeSO_4 \cdot 7H_2O$ (9.0 mgL^{-1}), EDTA·2Na (5.0 mgL^{-1}), NaCl (1.0 mgL^{-1}), KCl (1.4 mgL^{-1}), $CaCl_2 \cdot 2H_2O$ (1.4 mgL^{-1}), $MgSO_4 \cdot 7H_2O$ (1.0 mgL^{-1}), $NaHCO_3$ (84 mgL^{-1}), KH_2PO_4 (54 mgL^{-1}), 0.5 ml trace element solution II (Graaf *et al.*, 1996). Equimolar amounts of $NH_4(SO_4)_2$ and $NaNO_2$ were supplemented into the media at the final concentrations of 10 mM.

Purification of anammox bacterial nitrite oxidoreductase (Nxr)

6.2.2 Preparation of soluble protein from granular 'Ca. Brocadia sinica' biomass

The granular biomass of "*Ca.* B. sinica" was homogenized by using Potter-Elehjem Tissue Grinder homogenizer (φ = 6 × 200 mm, 50 mL, AZONE). The homogenized biomass was centrifuged at 10000 rpm and 4℃ for 10 min. The harvested cells (ca. 50 g-wet) were suspended in 103mL of 50 mM phosphate buffer (pH 7). Then the cell membranes and walls were further gently disrupted by using a FRENCH press (at 40psi, Emulsi Flex B15, AVESTIN). The resulted suspension (Crude cell extracts; CE) was centrifuged at 45,000 rpm and 4℃ for 60 min, and the supernatant was collected as soluble protein (Sol.).

6.2.3 Purification of anammox bacterial Nxr

The soluble protein was purified by anion-exchange chromatography using Q sepharose XL media (GE health- care, Little Chalfont, UK) equilibrated with 20 mM Tris-HCl buffer (pH 7.5). Binding proteins were eluted by increasing NaCl concentration of the Tris-HCl buffer step wisely 1 M NaCl. The eluted fractions containing B. sinica Nxr were pooled, concentrated, and buffer exchange was performed by ultrafiltration using a Vivaspin 20 column (100 kDa MWCO; GE healthcare, Little Chalfont, UK). The buffer exchange was performed using 20 mM phosphate buffer (pH 6.0), and subjected to hydroxyapatite chromatography using CHT Ceramic Hydroxyapatite type I (bio-rad). Binding proteins were eluted by increasing

phosphate concentration step wisely in the 500 mM phosphate buffer (pH 6.0). The fractions containing NxrA or NxrB were collected and concentrated by ultrafiltration by using a Vivaspin 500 column (100 kDa MWCO; GE healthcare, Little Chalfont, UK).

Protein concentrations were measured using the DC-protein assay kit (Bio-Rad, Hercules, CA, USA) using bovine serum albumin as a protein standard. Homogeneity of the enzyme was analyzed by SDS-PAGE analysis. Proteins were separated on a 10% SDS-containing polyacryl-amide gel, and stained with Simply Blue Safe Stain (Invitrogen, USA) following the instruction manual supplied by manufactures. Protein bands corresponding to NxrA and NxrB (116 and 44.3 kDa, respectively) were excised from the gel, and subjected to protein identification using MALDI-TOF/MS. Briefly, the gel bands were destained, reduced, alkylated, and then in-gel trypsine digestion was performed. The digested peptides were recovered and subjected to a matrix-assisted laser desorption ionization-time of flight mass spectrometry (MALDI-TOF MS). The data set was analyzed by MASCOT Server (matrixscience).

6.2.4 Enzyme assay test

NO_2^- oxidation was determined with ferricyanide as an artificial electron acceptor as previously described by (Sundermeyer-Klinger *et al.*, 1984) with slight modification. The test system contained 30 mM Tris-HCl (pH 8.0), 10 mM $MgCl_2$, 13 mM $K_3[Fe(CN)_6]$, 1 mM NO_2^- in 3.5 mL total volume in a small glass vials (**Table 6.2.1**). NO_3^- reduction was determined with methyl viologen dichloride hydrate (MV) as an artificial donor (Kobayashi *et al.*, 2018). The test system contained 20 mM anoxic phosphate buffer (pH 6.5), 0.74 mM methyl viologen dichloride hydrate, 5 mM sodium dithionite, 1 mM NO_3^- in 2 ml total volume in a 3 ml vials sealed by rubber cap and stirred continuously **(Table 6.2.1)**. The reaction was started by the addition of enzyme. The final protein concentration was fixed at 250 µg-BSA/mL. The assay mixture was incubated for 120~180 min at 37℃. In control experiment, distilled water was added instead of the enzyme. Samples were mixed vigorously on a vortex mixer for 30 s immediately upon collection to halt the reaction through oxidation of MV. In order to ensure complete cessation of enzyme activity, samples were placed in an 80℃ water bath for 5 min, then filtrated by using 0.2-µm cellulose acetate filter (Advantec) for concentration and isotopic measurements of NO_2^- and NO_3^-. To analyze N and O isotope of NO_2^-, sample solution was

adjusted to pH 12 by adding 2M low-N-blank NaOH solution immediately after filtration and stored at -20°C until analysis to prevent O isotope exchange between NO_2^- and H_2O during sample storage (Casciotti et al., 2007). To analyze N and O isotope of NO_3^-, if NO_2^- remained in sample, NO_2^- in the sample solution was removed by adding sulfamic acid (H_3NSO_3) immediately after filtration, because NO_2^- interferes with NO_3^- isotope analysis (Granger and Sigman, 2009). The concentration of NO_2^- was measured with naphthylethylenediamine method (APHA et al., 2005) to confirm NO_2^- was completely removed. Thereafter, sample solution was stored at -20°C until analysis.

Table 6.2.1 Optimized experimental conditions for NO_2^- oxidation and NO_3^- reduction assay of anammox bacterial Nxr.

	NO_2^- oxidation	NO_3^- reduction
Buffer	30mM Tris-HCl buffer	Anoxic 20mM PO_4 buffer
Buffer pH	8.0	6.5
Electron accepter/donor	13mM $K_3[Fe(CN)_6]$	0.74mM Methyl viologen dichloride hydrate
reducing agent		5mM dithionite
Substrate	1mM $NaNO_2$	1mM $NaNO_3$
Others	10mM $MgCl_2$	
Incubation temp. (°C)	37	37
Protein conc.(μg-BSA/ml)	250	250

6.2.5 Chemical analyses

On the day of sampling, NO_2^- and NO_3^- concentrations were analyzed. The NO_2^- concentration was measured by the naphthylethylenediamine method (APHA *et al.*, 2005). The concentration of NO_3^- was measured using ion chromatographs (IC-2010, TOSOH; Tokyo, Japan) equipped with a TSKgel IC-Anion HS column (TOSOH; Tokyo, Japan).

6.2.6 Isotopic analyses

NO_2^- nitrogen and oxygen isotope ratios were measured by chemical conversion of NO_2^- to nitrous oxide (N_2O) with the azide method (McIlvin and Altabet, 2005). All samples and standards had been adjusted to exactly the same pH (pH=12) and salinity (2.5% NaCl). Because of high sample pH (pH=12), azide buffer was modified by increasing the acetic acid concentration to 7.84M (Hu *et al.*, 2016) and the sodium azide concentration to 4M (Kobayashi

et al., 2020). The sample solution was buffered at pH 4.4 during the reaction. The N_2O was then analyzed using a purge-and-trap, gas-chromatography, isotope ratio mass spectrometry (PT-GC-IRMS). The corrected $\delta^{15}N$ and $\delta^{18}O$ values of the sample N_2O converted from NO_2^- were calibrated against the values from in-house NO_2^- standards; JAM 1 ($\delta^{15}N$ = -2.5 ‰, $\delta^{18}O$ = 91.7 ‰), JAM 2 ($\delta^{15}N$ = 1.8 ‰, $\delta^{18}O$ = 9.9 ‰), JAM 3 ($\delta^{15}N$ = -26.4 ‰, $\delta^{18}O$ = 39.4 ‰), JAM 4 ($\delta^{15}N$ = -1.5 ‰, $\delta^{18}O$ = -15.2 ‰) (Kobayashi *et al.*, 2020). Each reference solution was analyzed three times, and replicate analyses yielded respective precisions of generally 0.04 ~ 0.16‰ for $\delta^{15}N_{NO2-}$ (maximum = 0.51‰) and 0.09 ~ 0.28‰ (maximum = 0.48‰) for $\delta^{18}O_{NO2-}$, respectively.

NO_3^- nitrogen and oxygen isotope ratios were measured by microbial conversion of NO_3^- to N_2O with the denitrifier method (Sigman *et al.*, 2001; Casciotti *et al.*, 2002). N_2O was analyzed in triplicate using a PT-GC-IRMS. The corrected $\delta^{15}N$ and $\delta^{18}O$ values of the sample N_2O converted from NO_2^- were calibrated against the values from international NO_3^- isotopic standards; IAEAN3 ($\delta^{15}N$ = 4.7‰, $\delta^{18}O$ = 25.6‰), USGS32 ($\delta^{15}N$ = 180‰, $\delta^{18}O$ = 25.7‰), USGS34 ($\delta^{15}N$ = -1.8‰, $\delta^{18}O$ = -27.9‰), and USGS35 ($\delta^{18}O$ = 57.5‰) for the calibration (Thuan *et al.*, 2018). Replicate analyses yielded respective precisions of generally 0.05 ~ 0.17‰ (maximum = 0.81‰) for $\delta^{15}N_{NO3-}$ and 0.15 ~ 0.46% (maximum = 1.40%) for $\delta^{18}O_{NO3-}$, respectively.

The $\delta^{18}O_{H2O}$ was measured by equilibration with NO_2^- and subsequent conversion of NO_2^- to N_2O using a modified azide method (McIlvin and Casciotti, 2006) with 0.5 mL of the samples and standards. The $\delta^{18}O$ data was finally calibrated against GISP (-24.8 ‰) and the in-house water standards; Alaskan bottled mineral water (-19.0 ‰) and bottled de-salted seawater (0.2 ‰) (those $\delta^{18}O$ values were determined by SI Science. Co. ltd). Replicate analyses yielded respective precisions of 0.20‰ for $\delta^{18}O_{H2O}$.

6.2.7 Calculation of nitrogen and oxygen isotope effect

The kinetic nitrogen and oxygen isotope effect of NO_2^- oxidation and NO_3^- reduction were calculated by using a closed-system Rayleigh distillation model (Mariotti *et al.*, 1981). The nitrogen isotope effect of NO_2^- oxidation ($^{15}\varepsilon_{NO2- \rightarrow NO3-}$) could be determined from a following plot. The slope of regression was equal to ε.

$$-10^3 \ln\left(\frac{10^{-3}\delta^{15}N_{NO_2^-}+1}{10^{-3}\delta^{15}N_{NO_2^-,0}+1}\right) = {}^{15}\varepsilon_{NO_2^-\rightarrow NO_3^-} \cdot \ln\left(f_{NO_2^-}\right) \cdots (1)$$

Where $\delta^{15}N_{NO2-,\,0}$ was the value of $\delta^{15}NNO_2^-$ at time zero, and f_{NO2-} was the fraction of NO_2^- remaining ($f_{NO2-} = [NO_2^-]/[NO_2^-]_{initial}$). The oxygen isotope effect of NO_2^- oxidation (${}^{18}\varepsilon_{NO2-\rightarrow NO3-}$) was determined by same way. During NO_2^- oxidation, abiotic oxygen isotope exchange between NO_2^- and H_2O (${}^{18}\varepsilon_{eq}$) affects the value of $\delta^{18}ONO_2^-$. However, this experiment was conducted in short time (three hours), and it produced only slightly change of $\delta^{18}ONO_2^-$ (0.4 ‰ for three hours at $\delta^{18}O_{H2O}$ = -12.6‰)(Kobayashi *et al.*, 2020). Thus, effect of ${}^{18}\varepsilon_{eq}$ was excluded from the calculation.

$$-10^3 \ln\left(\frac{10^{-3}\delta^{18}O_{NO_2^-}+1}{10^{-3}\delta^{18}O_{NO_2^-,0}+1}\right) = {}^{18}\varepsilon_{NO_2^-\rightarrow NO_3^-} \cdot \ln\left(f_{NO_2^-}\right) \cdots (2)$$

The nitrogen and oxygen isotope effect of NO_3^- reduction was also determined following plot.

$$-10^3 \ln\left(\frac{10^{-3}\delta^{15}N_{NO_3^-}+1}{10^{-3}\delta^{15}N_{NO_3^-,0}+1}\right) = {}^{15}\varepsilon_{NO_3^-\rightarrow NO_2^-} \cdot \ln\left(f_{NO_3^-}\right) \cdots (3)$$

$$-10^3 \ln\left(\frac{10^{-3}\delta^{18}O_{NO_3^-}+1}{10^{-3}\delta^{18}O_{NO_3^-,0}+1}\right) = {}^{18}\varepsilon_{NO_3^-\rightarrow NO_2^-} \cdot \ln\left(f_{NO_3^-}\right) \cdots (4)$$

Where f_{NO3-} was the fraction of NO_3^- remaining ($f_{NO3-} = [NO_3^-]/[NO_3^-]_{initial}$)

6.3 Result and discussion

6.3.1 First purification step: Anion-exchange chromatography

After centrifugation, the obtained soluble protein was firstly purified by anion-exchange chromatography using Q sepharose XL media (GE health care, Little Chalfont, UK). Three protein peaks were observed **(Fig. 6.3.1 A)**. The first peak corresponds to flow-through fraction. The second and third peaks were the fractions that were adsorbed in the Q sepharose XL column and eluted during a gradient elution. The fractions of second and third peaks (fraction number 24 to 46) were collected and examined by SDS-PAGE **(Fig. 6.3.1. B)**. According to preliminary experiment with "*Ca.* Kuenenia stuttgartiensis" (data were not shown), the molecular weight of NxrA and NxrB was found to be around 116 kDa and over 44.3 kDa, respectively. Other than the NxrAB, B. sinica HzsABC (85, 45 and 36 kDa, respectively)(Oshiki *et al.*, 2016) also appeared on the gel, indicating the purified fraction contains both NxrAB and HzsABC (**Fig. 6.3.1. B**). To reduce the contamination of HzsABC, the fraction 30 to 40 were pooled and subjected to hydroxyapatite chromatography.

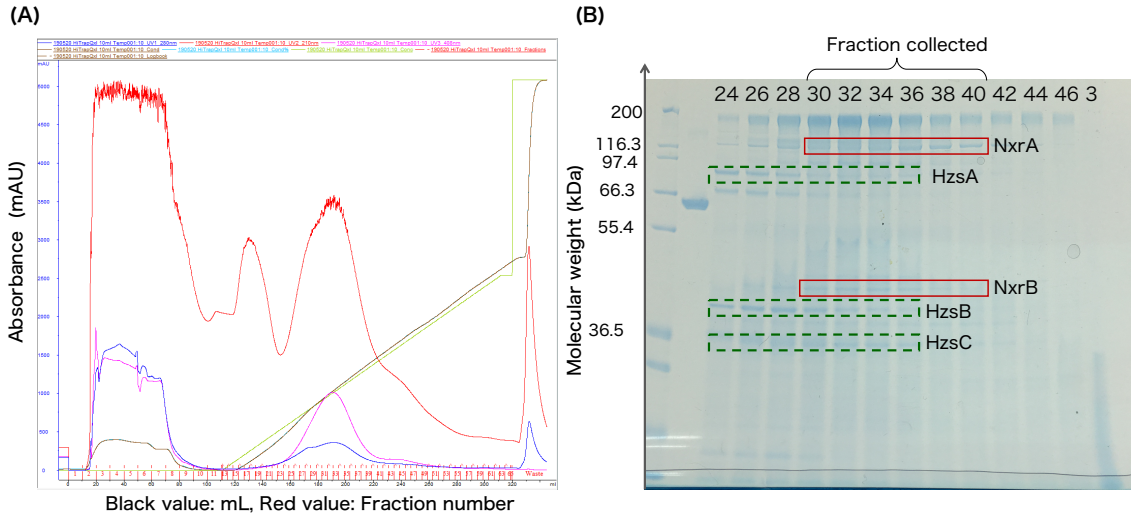

Figure 6.3.1 Elution profiles of soluble proteins after first purification by ion-exchange chromatography (A), which were examined by SDS-PAGE (B). The elution condition was as following. Column: HiTrap QXL 10 mL, buffer A: 20 mM Tris-HCl (pH=7.5), buffer B: Tris-HCl (pH=7.5) 1 M NaCl, Gradient: 50%B/ Gradient length 20 CV.

6.3.2 Second purification step: Hydroxyapatite chromatography

Chromatogram of the hydroxyapatite chromatography and a protein elution pattern were examined by SDS-PAGE (**Fig. 6.3.2**). Fraction 9-12 containing NxrAB were subjected to the following isotope study. After the hydroxyapatite chromatography, only 0.67 % of the crude extract (CE) proteins was recovered as the NxrAB in the present study (**Table 6.3.1**).

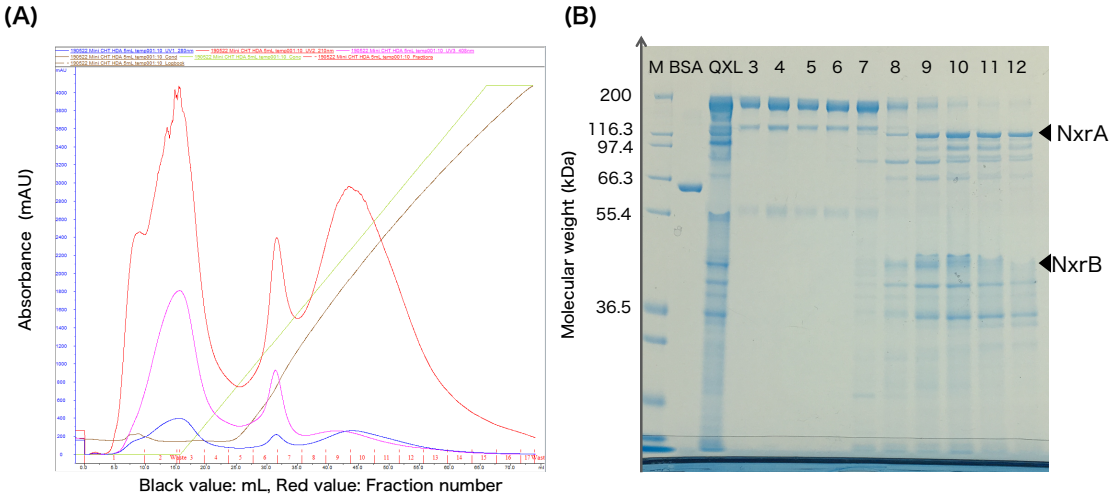

Figure 6.3.2 Elution profiles of soluble proteins after second purification by hydroxyapatite chromatography (A), which were separated by SDS-PAGE (B). The elution condition was as following. Column: Mini CHT HDA 5 mL, buffer A: 20 mM PO_4 Buffer pH=6, buffer B: 500 mMPO_4 buffer pH=6, Gradient: 100%B/ Gradient length 10 CV.

Table 6.3.1 Summary of three-step purification of nitrite oxidoreductase from "*Ca.* B. sinica" enrichment culture

Biomass 50g-wet

	mg-BSA/mL	mL	mg-BSA	% vs initial
CE	11.7	141	1650	100
Sol	5.53	120	664	40.2
UF QXL	2.15	19.0	40.8	2.47
UF HDA	7.61	1.45	11.0	0.67

Biomass (50 g-wet) was subjected to the protein purification

6.3.3 Identification of partially purified proteins

Two protein bands appeared around 116kDa and 44.3kDa were excised from the gel and subjected to a matrix-assisted laser desorption ionization-time of flight mass spectrometry (MALDI-TOF MS) analysis after in-gel tryptic digestion for protein identification, respectively (The more detailed data are described in the Appendix text, **Fig. S 6.9**). The MALDI-TOF MS analysis confirmed that those protein bands corresponded to "*Ca*. Brocadia sinica" NxrA (116 kDa) and NxrB (44.3 kDa), respectively (**Table S 6.2**). The major non-targeting proteins appeared around 85 kDa, 40 kDa, and 30 kDa were also identified as hydrazine synthase, HzsA (85kDa), HzsB (45kDa) and HzsC (36kDa) respectively. Since the substrate of "*Ca.* B. sinica" Hzs for N_2H_4 synthesis is NH_2OH (Oshiki *et al.*, 2016), the contaminated Hzs does not directly interfere the oxidation-reduction reaction of NO_2^- and NO_3^- by Nxr. Therefore, the partially purified Nxr by hydroxyapatite chromatography was used for subsequent enzymatic assays.

6.3.4 Determination of N and O isotope effects of Nxr

The purified B. sinica NxrAB oxidized NO_2^- using ferricyanide as an electron acceptor and produced NO_3^- stoichiometrically (**Fig. 6.3.3 B** and **C**). No NO_2^- oxidation and NO_3^- production was found in abiotic control experiment, indicating the observed NO_2^- oxidation to NO_3^- was catalyzed by the purified NxrAB. NO_2^- oxidation by the NxrAB resulted in the decrease of both of $\delta^{15}N$ and $\delta^{18}O$ of NO_2^- and NO_3^-. In addition, $\delta^{15}N$ and $\delta^{18}O$ of produced NO_3^- was higher than that of NO_2^- (**Fig. 6.3.3 B and C**). This indicates that NO_2^- oxidation reaction shows inverse kinetic isotope effect (meaning that heavy isotope NO_2^- is consumed faster than light isotope NO_2^-). On the other hand, the NO_3^- reduction activity was low, but could be confirmed in NO_3^- reduction assay. However, NO_2^- production was not observed (**Fig. 6.3.4 B and C**). NO_2^- might be further reduced to NO and/or NH_3 (dissimilatory nitrate reduction to ammonium, DNRA) (Kartal *et al.*, 2007) during the assay because the used electron donor (i.e., MV) has a very low redox potential (-440 mV) (Nagashima, 2009) and the formed NO_2^- can be easily further reduced to NO and/or NH_3 as previously described. NO_3^- reduction resulted in the increase of the $\delta^{15}N$ and $\delta^{18}O$ of NO_3^-, indicating that NO_3^- reduction shows normal kinetic isotope effect. The specific activity of NO_2^- oxidation by NxrAB was an order of magnitude higher than that of NO_3^- reduction (**Table 6.3.2**), suggesting B. sinica NxrAB preferentially catalyze NO_2^- oxidation. This result corresponds well to the result derived from the whole cells

that shows a strong inversed kinetic isotope effect (Kobayashi *et al.*, 2019).

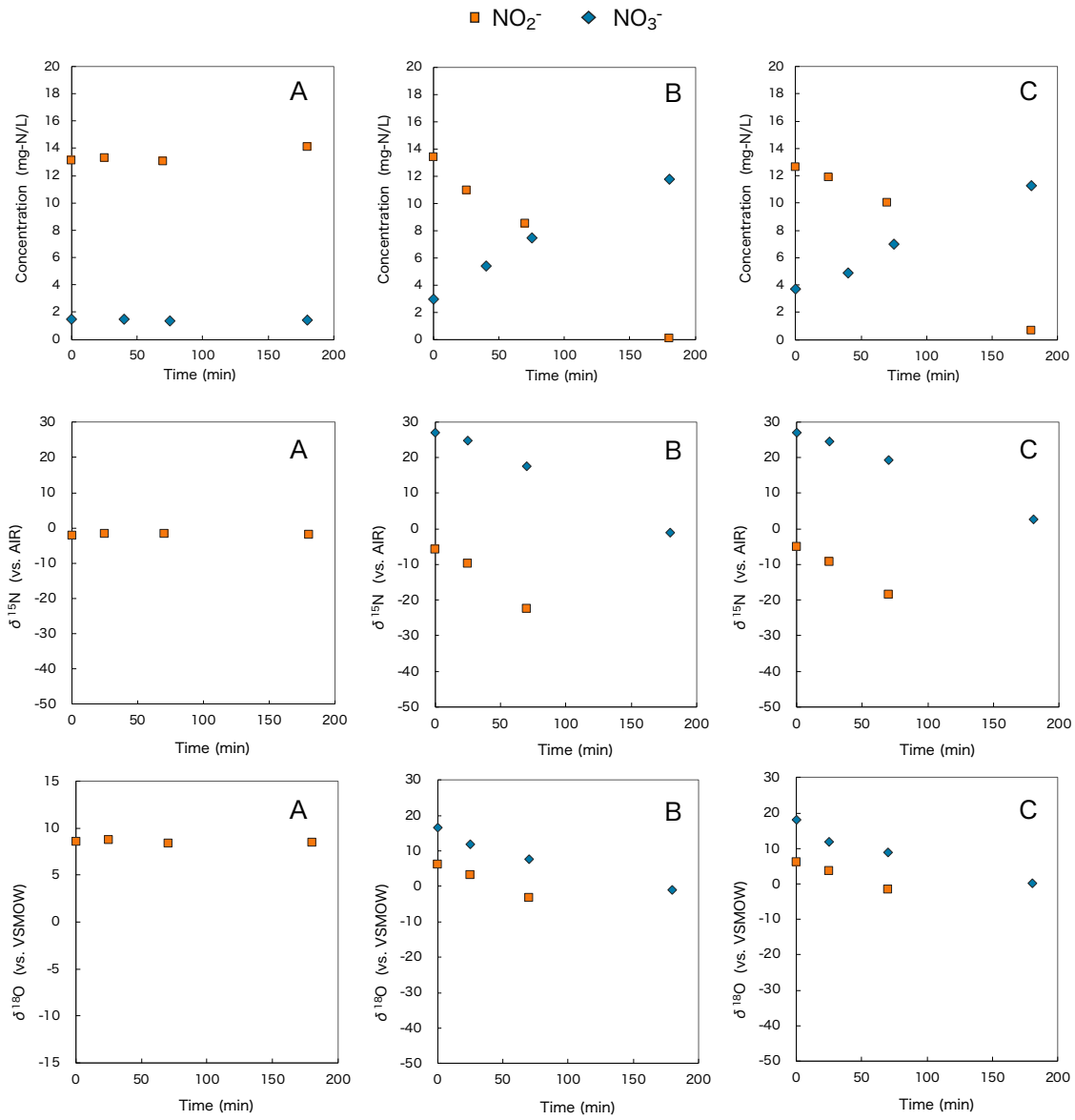

Figure 6.3.3 The time course changes in concentrations, δ^{15}N and δ^{18}O of NO_2^- and NO_3^- during NO_2^- oxidation by anammox bacterial Nxr. Assay without addition of partially purified Nxr (abiotic control) (**A**) and with addition of partially purified Nxr after hydroxyapatite chromatography in duplicate (**B**) and (**C**). The final data points of δ^{15}N and δ^{18}O of NO_2^- in Fig. (B) and (C) were missing because NO_2^- concentrations were too low to measure the isotope compositions.

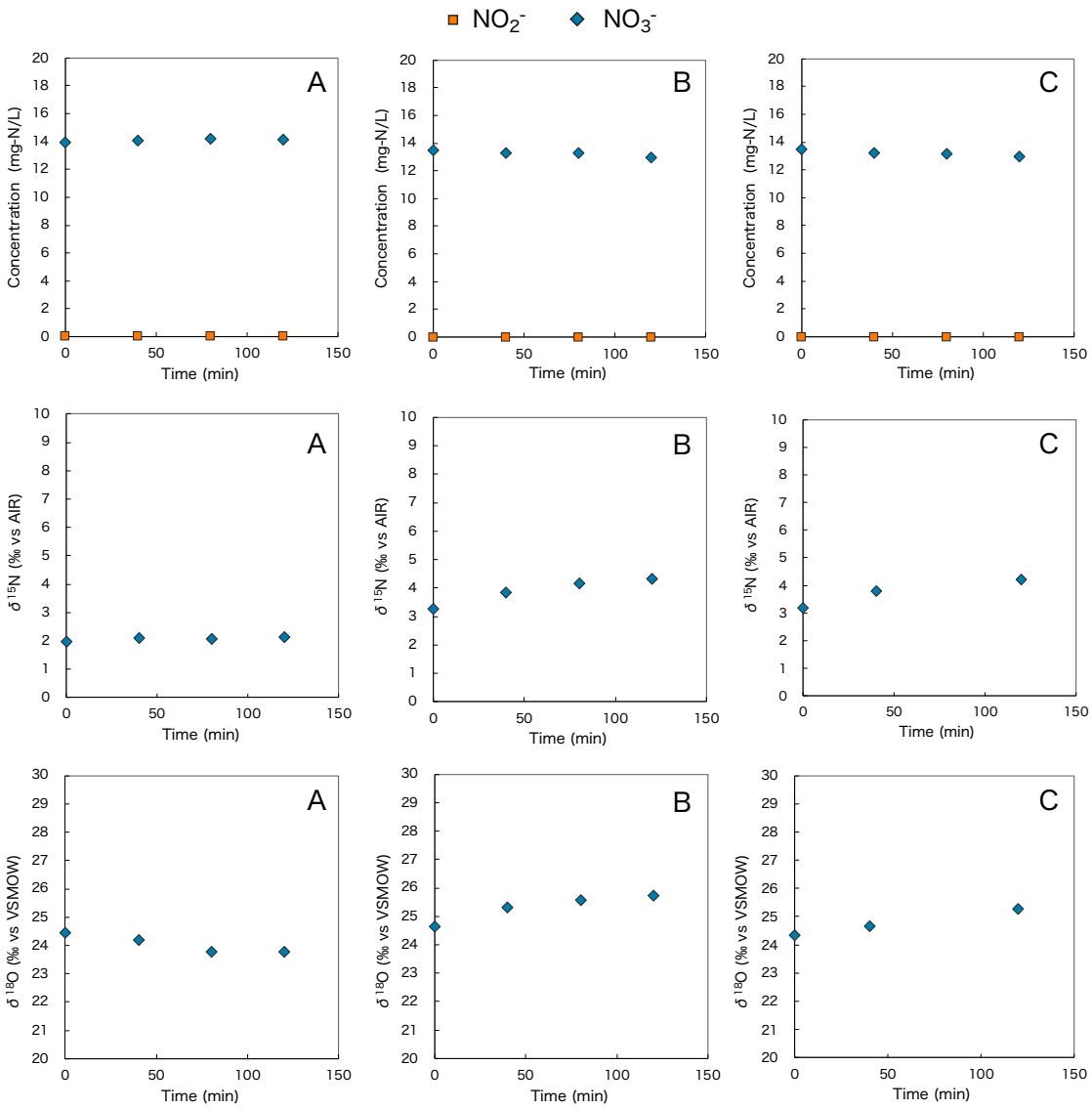

Figure 6.3.4 The time course change in concentrations, δ^{15}N and δ^{18}O of NO_2^- and NO_3^- during NO_3^- reduction by Nxr. Assay without addition of partially purified Nxr (abiotic control) (A) and with addition of partially purified Nxr after hydroxyapatite chromatography in duplicate (B) and (C). The δ^{15}N and δ^{18}O of NO_2^- could not be measured because of no NO_2^- production. The value δ^{15}N and δ^{18}O of NO_3^- at 80 min in Fig. (C) was excluded due to low measurement recovery ratio.

Table 6.3.2 Comparison of specific activity of NO_2^- oxidation and NO_3^- reduction by nitrite oxidoreductase (Nxr) of "*Ca.* B. sinica"

NO_2^- oxidation assay

Specific activity (nmol $mgBSA^{-1}$ min^{-1})

Condition	Expt.1	Expt.2	Average
Sol	-	-	-
QXL	27.83	-	27.83
HDA 1 and 2	48.46	43.62	46.04

NO_3^- reduction assay

Specific activity (nmol $mgBSA^{-1}$ min^{-1})

Condition	Expt.1	Expt.2	Average
Sol	0.29	0.36	0.33
QXL	1.52	-	1.52
HDA 1 and 2	1.95	1.98	1.96

6.3.5 Nitrogen and oxygen isotope effect of anammox bacterial Nxr

Nitrogen and oxygen isotope effect ($^{15}\varepsilon$ and $^{18}\varepsilon$) of NO_2^- oxidation and NO_3^- reduction were determined in duplicate by the Rayleigh model (**Fig. 6.3.5 and 6.3.6**). As for NO_2^- oxidation, nitrogen and oxygen isotope effects ($^{15}\varepsilon_{NO2\rightarrow NO3}$ and $^{18}\varepsilon_{NO2\rightarrow NO3}$) were -34.7‰ ~ -59.9‰ and -19.3‰ ~ -33.6‰, respectively (**Table 6.3.3**). Both of nitrogen and oxygen isotope effect were inverse. Relatively large N and O isotope effects were derived from the second NO_2^- oxidation assay (**Table 6.3.3**), which might be attributed to difference of specific activity between first and second experiment (**Table 6.3.2**). Enzyme level nitrogen isotope effects of NO_2^- oxidation by "*Ca.* B. sinica" determined in the present study were slightly larger than whole cell level isotope effect (-31.5 ± 4.0‰) in previous study (Kobayashi *et al.*, 2019). In both experiments, nitrogen isotope effect was larger than oxygen isotope effect. This tendency was similar as nitrogen and oxygen isotope effect of nitrite-oxidizing bacteria ($^{15}\varepsilon_{NO2\rightarrow NO3}$ = -20.6 ~ -9.1‰, $^{18}\varepsilon_{NO2\rightarrow NO3}$ =-8.2 ~ -1.3‰) (Buchwald and Casciotti, 2010). As for NO_3^- reduction, the nitrogen isotope effect ($^{15}\varepsilon_{NO3\rightarrow NO2}$) and oxygen isotope effect ($^{18}\varepsilon_{NO3\rightarrow NO2}$) were determined to be 31.2‰ ~ 31.7‰ and 26.0‰ ~ 22.0‰, respectively. Close values were obtained from duplicate experiments probably because specific activity was similar. Both of nitrogen and oxygen isotope effect of NO_3^- reduction was normal kinetic isotope effect, which cannot be determined with the whole cells.

6.3.6 Inverse kinetic isotope effect by anammox bacterial Nxr

Possible explanation for the inverse kinetic isotope effect by nitrite-oxidizing bacteria were discussed vigorously in previous report about nitrite-oxidizing bacteria (Casciotti, 2009). Two of the common causes for inverse kinetic isotope effects (1) pre-equilibrium between

HNO_2 and NO_2^- and (2) enzyme level reversibility were evaluated. However, those mechanisms could not explain the inverse kinetic isotope effect. They performed theoretical evaluation of isotope effect using transition state theory and provided an independent confirmation of the inverse enzyme-level inverse isotope effect for nitrite oxidoreductase (Casciotti, 2009). However, those evaluation have not been confirmed experimentally. In this study, we firstly reported isotope effect of partially purified anammox bacterial Nxr and examine the mechanism of the unique inverse kinetic isotope effect of NO_2^- oxidation by anammox. In this study, the enzyme level reversibility defined as the ratio of specific activity of NO_2^- oxidation (NXR) and NO_3^- reduction (NAR) was calculated to be 4% (x = NAR/NXR = 0.04). This low reversibility suggests that NO_2^- oxidation by anammox bacterial Nxr is the dominant reaction in isotope fractionation during anammox reaction mediated by whole cells.

The anammox cell is composed of three compartments (periplasm, cytoplasm, and anammoxosome), which are surrounded by outer cell membrane (Lindsay *et al.*, 2001). Since a series of anammox reactions takes place in the anammoxosome, substrates must be transported across the outer membrane, cytoplasmic membrane, anammoxosome membrane (Strous *et al.*, 2006; Kartal *et al.*, 2013). It has been reported that NO_2^- transport proteins were localized on anammoxome membrane and cytoplasmic membrane. Immunoelectron microscopy revealed that Nxr of the anammox bacterium *Kuenenia stuttgartiensis* was found on conspicuous tubule-like structures that was widely-stretched out in the anammoxsome (de Almeida *et al.*, 2015). To clarify how enzymatic level isotope effect affects isotope effect of NO_2^- oxidation catalyzed by whole cells, the following six steps of NO_2^- oxidation were considered (**Fig. 6.3.7**): (1) diffusion to the cell surface, (2) transport across the outer membrane, (3) transport across the cytoplasmic membrane, (4) transport of across the anammoxosome membrane, (5) enzymatic oxidation of NO_2^- by anammox bacterial Nxr (forward reaction), and (6) enzymatic reduction of NO_3^- by anammox bacterial Nxr (reverse reaction). Isotope effect associated with NO_2^- diffusion and NO_2^- transport have not been reported for anammox yet. Diffusion rates of heavy isotope-bearing NO_2^- ($^{15}NO_2^-$ and $N^{18}O_2^-$) could be slower than the lighter ones. However, this difference might be too small to cause significant impact on the isotope fractionation (Mariotti *et al.*, 1982, 1988). Although some chemical interactions could be expected in transport of NO_2^- across the outer membrane, cytoplasmic membrane, and anammoxosome membrane, which, however, had limited impact on isotope fractionation due to a lack of bond breakages of NO_2^-. Therefore, it is assumed that NO_2^- diffusion and transport could not account for substantial part of observed whole anammox cell level isotope effect of NO_2^- oxidation in this time. The enzyme assay with partially purified anammox bacterial Nxr revealed that NO_2^- oxidation by Nxr indicated an inverse N isotope effect ($^{15}\varepsilon_{NO2\rightarrow NO3}$ = -34.7‰ ~ -59.9‰), while NO_2^- reduction by Nxr showed normal N isotope effect ($^{15}\varepsilon_{NO3\rightarrow NO2}$ = 31.2‰ ~ 31.7‰). Nxr

reversibility defined as the ratio of specific activity of NO_2^- oxidation (NXR) and NO_3^- reduction (NAR) was about 4%, implying that isotope effect of NO_2^- reduction has limited impact on overall isotope effect by whole cells. The value of whole cell level isotope effect ($^{15}\varepsilon_{NO2\rightarrow NO3}$. = -31.5 ± 4.0‰) (Kobayashi *et al.*, 2019). was consistent with the enzyme level isotope effect of NO_2^- oxidation ($^{15}\varepsilon_{NO2\rightarrow NO3}$ = -34.7‰ ~ -59.9‰) with taking into account the reversible NO_2^- reduction ($^{15}\varepsilon_{NO3\rightarrow NO2}$ = 31.2‰ ~ 31.7‰). This result is important to expand our understanding on the origin of the inverse kinetic isotope effect associated with NO_2^- oxidation to NO_3^- by anammox bacteria.

6.3.7 Implications for coupling signature of $\delta^{15}N$ and $\delta^{18}O$ in the environment

Both nitrate assimilation and marine denitrification yielded nearly identical isotope effects on the N and O isotopes of NO_3^- ($^{18}\varepsilon$:$^{15}\varepsilon$ = 1)(Granger *et al.*, 2004; Sigman *et al.*, 2005; Granger and Sigman, 2008). The signature $\Delta\delta^{18}O/\Delta\delta^{15}N$ of NO_3^- ~1 was proposed as a unique signal of denitrification and nitrate assimilation. The deviations from $\Delta\delta^{18}O/\Delta\delta^{15}N$ = 1 in environmental samples indicate the presence of other N cycle transformations (nitrifications and anammox)(Granger and Wankel, 2016). In addition to the signals generated in NO_3^-, NO_2^- reduction and oxidation have characteristic effects on NO_2^- dual isotope signals (Casciotti, 2016). NO_2^- reduction increased $\delta^{15}N_{NO2}$ and $\delta^{18}O_{NO2,}$ but the trend of $^{18}\varepsilon$:$^{15}\varepsilon$ varied with the nitrite reductase enzymology (Martin and Casciotti, 2016). Since the inverse isotope effect for ^{15}N is much larger than that for ^{18}O, NO_2^- oxidation by nitrite-oxidizing bacteria causes a significant decrease in $\delta^{15}N_{NO2}$ and a relatively small decrease in $\delta^{18}O_{NO2}$ (Buchwald and Casciotti, 2010; Casciotti, 2016). However, uncertainties remain about O isotope effects associated with NO_2^- reduction and NO_3^- production by anammox. In order to evaluate the effect of NO_3^- production and reduction by anammox bacterial Nxr on $\Delta\delta^{18}O/\Delta\delta^{15}N$ of NO_3^- and NO_2^-, change of $\delta^{18}O$ against $\delta^{15}N$ was examined (**Fig. 6.3.8, A, B**). NO_2^- oxidation decreases both of $\delta^{15}N$ and $\delta^{18}O$ of NO_2^- and NO_3^- (**Fig. 6.3.8. A**). N isotope effect of NO_2^- oxidation was larger than O isotope effect (**Table 6.3.3**). Therefore, the slope of regression line ($\Delta\delta^{18}O/\Delta\delta^{15}N$) was deviated from~1, and were 0.54 ± 0.02 and 0.61 ± 0.07 for NO_2^- and NO_3^-, respectively. As for $\Delta\delta^{18}O/\Delta\delta^{15}N$ of NO_2^-, the trend was similar but slightly larger than nitrite-oxidizing bacteria ($\Delta\delta^{18}O/\Delta\delta^{15}N$ of NO_2^-= 0.2~0.4) (Buchwald and Casciotti, 2010). As for $\Delta\delta^{18}O/\Delta\delta^{15}N$ of NO_3^-, the $\delta^{18}O$ of produced NO_3^- is directly related to the water $\delta^{18}O_{H2O}$ due to the incorporation of an O atom from water during NO_2^- oxidation. In this study, $^{18}\varepsilon_{H2O}$ could not be calculated, but $\delta^{18}O_{H2O}$ was -12.6‰. Although more information on oxygen isotope effect by amammox

bacterial Nxr is required to interpret $\Delta\delta^{18}O/\Delta\delta^{15}N$ of NO_3^-, we revealed the deviations from an O to N ratio of~1 by NO_2^- oxidation by anammox bacterial Nxr ($\Delta\delta^{18}O/\Delta\delta^{15}N$ = 0.61). This signature might be variable to distinguish contribution of denitrification and anammox NO_3^- oxidation.

During NO_3^- reduction by anammox bacterial Nxr, both of $\delta^{18}O$ and $\delta^{15}N$ of NO_3^- increased. The slope of regression line ($\Delta\delta^{18}O/\Delta\delta^{15}N$) was 1.0 (**Fig. 6.3.8. B**). The trend of $\Delta\delta^{18}O/\Delta\delta^{15}N$ was similar to denitrification and nitrate assimilation ($^{18}\varepsilon:^{15}\varepsilon$ = 1)(Granger *et al.*, 2004; Sigman *et al.*, 2005; Granger and Sigman, 2008). However, NO_2^- oxidation by anammox bacterial Nxr is the dominant step in isotope fractionation during anammox reaction. Therefore, this trend of NO_3^- reduction might not be appeared during NO_2^- oxidation by anammox.

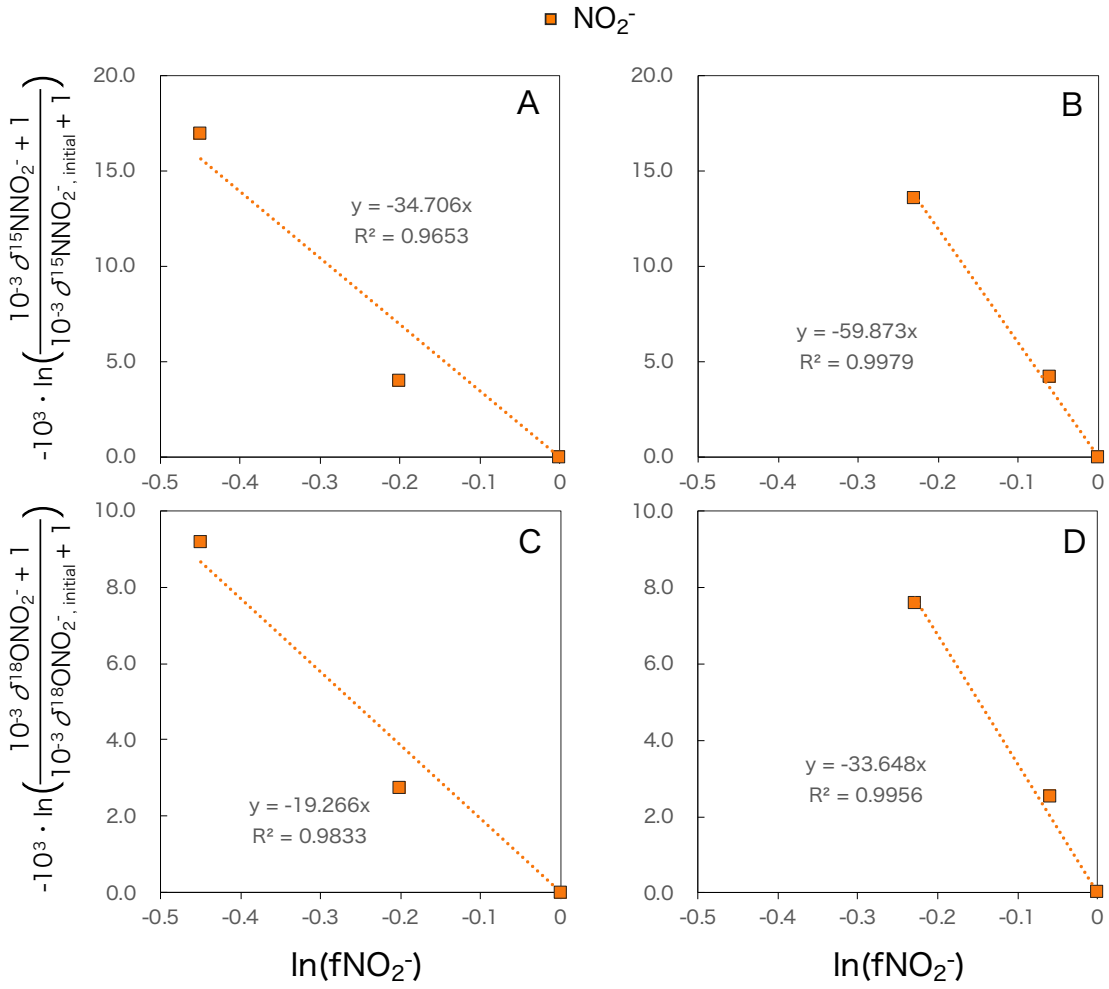

Figure 6.3.5 Rayleigh plots of NO_2^- from duplicated NO_2^- oxidation assays. (A), (B) graphs for determination of N isotope effect. (C), (D) graphs for determination of O isotope effect. The

slope of regression line was isotope effect. The result of experiment 1 was (A) and (C). The result of experiment 2 was (B) and (D)

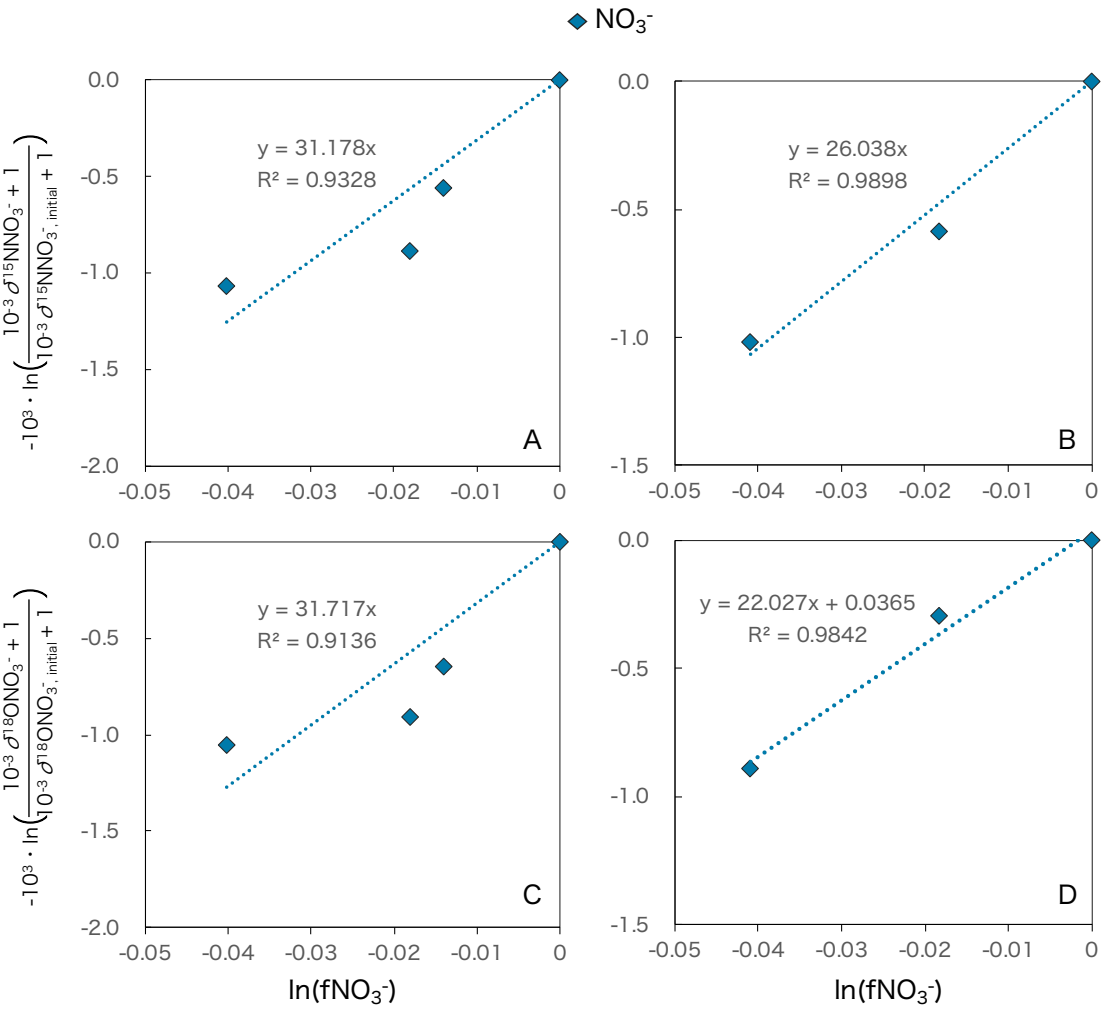

Figure 6.3.6 Rayleigh plots of NO_3^- from duplicated NO_3^- reduction assays. (A), (B) graphs for determination of N isotope effect. (C), (D) graphs for determination of O isotope effect. The slope of regression line was isotope effect. The result of experiment 1 was (A) and (C). The result of experiment 2 was (B) and (D). The value $\delta^{15}N$ and $\delta^{18}O$ of NO_3^- at 80 min in Fig. (B) and (D) was excluded due to low measurement recovery ratio.

Table 6.3.3 Summary of nitrogen and oxygen isotope effect of Nxr

Reaction	Replication	$^{15}\varepsilon$ (‰)	$^{18}\varepsilon$ (‰)
NO_2^- oxidation	1	-34.7	-19.3
	2	-59.8	-33.6
NO_3^- reduction	1	31.2	26.0
	2	31.7	22.0

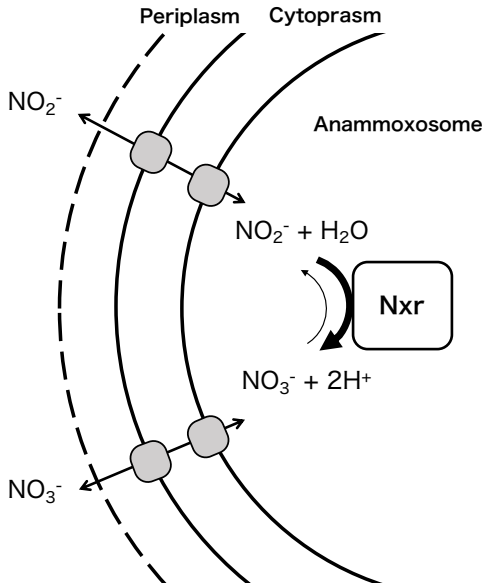

Figure 6.3.7 Schematic of isotope effect associated with NO_2^- oxidation and NO_3^- reduction by anammox.

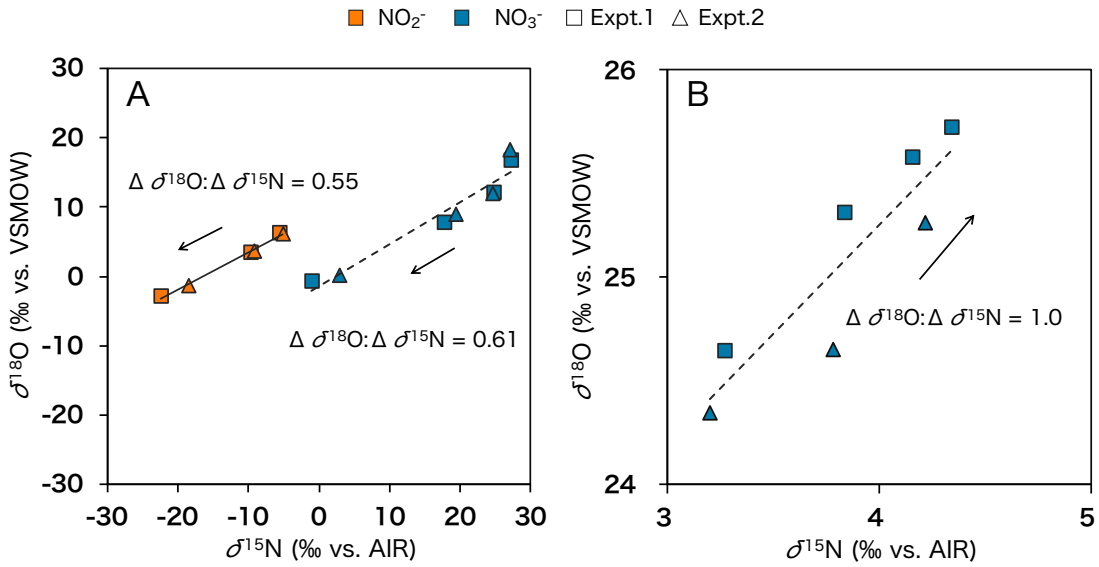

Figure 6.3.8 $\delta^{18}O$ plotted against the corresponding $\delta^{15}N$ for (A) NO_2^- oxidation test and (B) NO_3^- reduction test by anammox bacterial Nxr

6. 4. Conclusions

The nitrite oxidoreductase (Nxr) of a fresh water anammox species "*Ca.* Brocadia sinica" was partially purified from membrane protein fraction by using anion-exchange chromatography followed by hydroxyapatite chromatography. The nitrogen and oxygen isotope effects of NO_2^- oxidation and NO_3^- reduction were individually determined with the partially purified anammox bacterial Nxr. The N and O isotope effect of NO_2^- oxidation was determined to be $^{15}\varepsilon$ ($NO_2^- \rightarrow NO_3^-$) = -34.7 ~ -59.8‰ and $^{18}\varepsilon$ ($NO_2^- \rightarrow NO_3^-$) = -19.3 ~ -33.6‰, respectively, showing inverse kinetic isotope effects for both. The N and O isotope effect for NO_3^- reduction was $^{15}\varepsilon$ ($NO_3^- \rightarrow NO_2^-$) = 31.2 ~ 31.7‰ and $^{18}\varepsilon$ ($NO_3^- \rightarrow NO_2^-$) = 26.0 ~ 22.0‰, respectively. Since nitrite oxidoreductase is known as a reversible enzyme,$^{15}\varepsilon$ ($NO_2^- \rightarrow NO_3^-$) and $^{18}\varepsilon$ ($NO_2^- \rightarrow NO_3^-$) obtained from whole cells were combined N and O isotope effects of NO_2^- oxidation and NO_3^- reduction. The specific activity of NO_3^- reduction by anammox bacterial Nxr was 23 times lower than that of NO_2^- oxidation and thus the contribution of NO_3^- reduction to overall N and O isotope effects was trivial. Therefore, the $^{15}\varepsilon$ and $^{18}\varepsilon$ values associated with conversion of NO_2- to NO_3^- by the whole cells were governed by NO_2^- oxidation, which exhibited the inverse N and O isotope effects.

6.5 References

de Almeida, N.M., Neumann, S., Mesman, R.J., Ferousi, C., Keltjens, J.T., Jetten, M.S.M., et al. (2015) Immunogold localization of key metabolic enzymes in the anammoxosome and on the tubule-like structures of Kuenenia stuttgartiensis. *J Bacteriol* 197: 2432–2441.

APHA, AWWA, and WEF (2005) Standard Methods for the Examination of Water and Wastewater. Washington, D.C.

Brunner, B., Contreras, S., Lehmann, M.F., Matantseva, O., Rollog, M., Kalvelage, T., et al. (2013) Nitrogen isotope effects induced by anammox bacteria. *Proc Natl Acad Sci* 110: 18994–18999.

Buchwald, C. and Casciotti, K.L. (2010) Oxygen isotopic fractionation and exchange during bacterial nitrite oxidation. *Limnol Oceanogr* 55: 1064–1074.

Casciotti, K.L. (2009) Inverse kinetic isotope fractionation during bacterial nitrite oxidation. *Geochim Cosmochim Acta* 73: 2061–2076.

Casciotti, K.L. (2016) Nitrite isotopes as tracers of marine N cycle processes. *Phil Trans R Soc A* 374: 20150295.

Casciotti, K.L., Bohlke, J.K., McIlvin, M.R., Mroczkowski, S.J., and Hannon, J.E. (2007) Oxygen isotopes in nitrite: Analysis, calibration, and equilibration. *Anal Chem* 79: 2427–2436.

Casciotti, K.L., Buchwald, C., and McIlvin, M. (2013) Implications of nitrate and nitrite isotopic measurements for the mechanisms of nitrogen cycling in the Peru oxygen deficient zone. *Deep Res Part I Oceanogr Res Pap* 80: 78–93.

Casciotti, K.L., Sigman, D.M., Hastings, M.G., Bohlke, J.K., and Hilkert, A. (2002) Measurement of the oxygen isotopic composition of nitrate seawater and freshwater using the dentirifier method. *Anal Chem* 74: 4905-4912.

Graaf, A.A. Van De, Bruijn, P. De, Robertson, L.A., Jetten, M.S.M., and Kuenen, J.G. (1996) Autotrophic growth of anaerobic in a fluidized bed reactor. *Microbiology* 142: 2187–2196.

Granger, J. and Sigman, D.M. (2008) Nitrogen and oxygen isotope fractionation during dissimilatory nitrate reduction by denitrifying bacteria. *Limnol Oceanogr* 53: 2533–2545.

Granger, J. and Sigman, D.M. (2009) Removal of nitrite with sulfamic acid for nitrate N and O isotope analysis with the denitrifier method. *Rapid Commun Mass Spectrom* 23: 3753–3762.

Granger, J., Sigman, D.M., Lehmann, M.F., and Tortell, P.D. (2008) Nitrogen and oxygen isotope fractionation during dissimilatory nitrate reduction by denitrifying bacteria. 53: 2533–2545.

Granger, J., Sigman, D.M., Needoba, J.A., and Harrison, P.J. (2004) Coupled nitrogen and oxygen isotope fractionation of nitrate during assimilation by cultures of marine phytoplankton. *Limnol Oceanogr* 49: 1763–1773.

Granger, J. and Wankel, S.D. (2016) Isotopic overprinting of nitrification on denitrification as a ubiquitous and unifying feature of environmental nitrogen cycling. *Proc Natl Acad Sci*. 113 (42): E6391-6400.

Holler, T., Wegener, G., Niemann, H., Ferdelman, T.G., Boetius, A., Kristiansen, T.Z., et al. (2012) Carbon and sulfur back flux during anaerobic microbial oxidation of methane and coupled sulfate reduction. *Proc Natl Acad Sci* 109: 21170–21170.

Hu, H., Bourbonnais, A., Larkum, J., Bange, H.W., and Altabet, M.A. (2016) Nitrogen cycling in shallow low-oxygen coastal waters off Peru from nitrite and nitrate nitrogen and oxygen isotopes. *Biogeosciences* 13: 1453–1468.

Kartal, B., De Almeida, N.M., Maalcke, W.J., Op den Camp, H.J.M., Jetten, M.S.M., and Keltjens, J.T. (2013) How to make a living from anaerobic ammonium oxidation. *FEMS Microbiol Rev* 37: 428–461.

Kartal, B., Kuypers, M.M.M., Lavik, G., Schalk, J., Op Den Camp, H.J.M., Jetten, M.S.M., and Strous, M. (2007) Anammox bacteria disguised as denitrifiers: Nitrate reduction to dinitrogen gas via nitrite and ammonium. *Environ Microbiol* 9: 635–642.

Kobayashi, K., Fukushima, K., Onishi, Y., Nishina, K., Makabe, A., Yano, M., et al. (2020) Influence of δ^{18}O of water on measurements of δ^{18}O of nitrite and nitrate . *Rapid Commun Mass Spectrom* 35 (2): e8979.

Kobayashi, Kanae, Makabe, A., Yano, M., Oshiki, M., Kindaichi, T., Casciotti, K.L., and Okabe, S. (2019) Dual nitrogen and oxygen isotope fractionation during anaerobic ammonium oxidation by anammox bacteria. *ISME J* 13: 2426–2436.

Kobayashi, S., Hira, D., Yoshida, K., Toyofuku, M., Shida, Y., Ogasawara, W., et al. (2018) Nitric oxide production from nitrite reduction and hydroxylamine oxidation by copper-containing dissimilatory nitrite reductase (Nirk) from the aerobic ammonia-oxidizing archaeon, *Nitrososphaera viennensis*. *Microbes Environ* 33: 428–434.

Lancaster, K.M., Caranto, J.D., Majer, S.H., and Smith, M.A. (2018) Alternative bioenergy: Updates to and challenges in nitrification metalloenzymology. *Joule* 2: 421–441.

Lindsay, M.R., Webb, R.I., Strous, M., Jetten, M.S.M., Butler, M.K., Forde, R.J., and Fuerst, J.A. (2001) Cell compartmentalisation in planctomycetes: Novel types of structural organisation for the bacterial cell. *Arch Microbiol* 175: 413–429.

Mariotti, A., J. C. Germon, P. Hubert, Kaiser, P., Letolle, R., Tardieux, A., and Tardieux, P. (1981) Experimental determination of nitrogen kinetic isotope fractionation: Some principles; illustration for the denitrification and nitrification processes. *Plant Soil* 430: 413–430.

Mariotti, A., Landreau, A., and Simon, B. (1988) 15N isotope biogeochemistry and natural denitrification process in groundwater: Application to the chalk aquifer of northern France. *Geochim Cosmochim Acta* 52: 1869–1878.

Mariotti, A., Mariotti, F., Champigny, M.-L., Amarger, N., and Moyse, A. (1982) Nitrogen isotope fractionation associated with nitrate reductase activity and uptake of NO_3^- by Pearl Millet . *Plant Physiol* 69: 880–884.

Martin, T.S. and Casciotti, K.L. (2016) Nitrogen and oxygen isotopic fractionation during microbial nitrite reduction. *Limnol Oceanogr* 61: 1134–1143.

McIlvin, M.R. and Altabet, M.A. (2005) Chemical conversion of nitrate and nitrite to nitrous oxide for nitrogen and oxygen isotopic analysis in freshwater and seawater. *Anal Chem* 77: 5589–5595.

McIlvin, M.R. and Casciotti, K.L. (2006) Method for the analysis of delta ^{18}O in water. *Anal Chem* 78: 2377–2381.

Meincke, M., Bock, E., Kastrau, D., and Kroneck, P.M.H. (1992) Nitrite oxidoreductase from *Nitrobacter hamburgensis*: Redox centers and their catalytic role. *Arch Microbiol* 158: 127–131.

Nagashima, K. (2009) Redox titration for electron transfer proteins. *Low Temp Sci* 67: 545-550 (in Japanese).

Oshiki, M., Ali, M., Shinyako-Hata, K., Satoh, H., and Okabe, S. (2016) Hydroxylamine-dependent anaerobic ammonium oxidation (anammox) by "*Candidatus* Brocadia sinica." *Environ Microbiol* 18: 3133–3143.

Oshiki, M., Ishii, S., Yoshida, K., Fujii, N., Ishiguro, M., Satoh, H., and Okabe, S. (2013) Nitrate-dependent ferrous iron oxidation by anaerobic ammonium oxidation (anammox) bacteria. *Appl Environ Microbiol* 79: 4087–4093.

Peters, B.D., Babbin, A.R., Lettmann, K.A., Mordy, C.W., Ulloa, O., Ward, B.B., and Casciotti, K.L. (2016) Vertical modeling of the nitrogen cycle in the eastern tropical South Pacific oxygen deficient zone using high-resolution concentration and isotope measurements. *Global Biogeochem Cycles* 30: 1661–1681.

Sigman, D.M., Casciotti, K.L., Andreani, M., Barford, C., Galanter, M., and Bhlke, J.K. (2001) A bacterial method for the nitrogen isotopic analysis of nitrate in seawater and freshwater. *Anal Chem* 73: 4145–4153.

Sigman, D.M., Granger, J., DiFiore, P.J., Lehmann, M.M., Ho, R., Cane, G., and van Geen, A. (2005) Coupled nitrogen and oxygen isotope measurements of nitrate along the eastern North Pacific margin. *Global Biogeochem Cycles* 19: 1–14.

Strous, M., Pelletier, E., Mangenot, S., Rattei, T., Lehner, A., Taylor, M.W., et al. (2006) Deciphering the evolution and metabolism of an anammox bacterium from a community genome. *Nature* 440: 790–794.

Sundermeyer-Klinger, H., Meyer, W., Warninghoff, B., and Bock, E. (1984) Membrane-bound nitrite oxidoreductase of Nitrobacter: evidence for a nitrate reductase system. *Arch Microbiol* 140: 153–158.

Thuan, N.C., Koba, K., Yano, M., Makabe, A., Kinh, C.T., Terada, A., et al. (2018) N_2O production by denitrification in an urban river: evidence from isotopes, functional genes, and dissolved

organic matter. *Limnology* 19: 115–126.

6.6 Appendix

The nitrite oxidoreductase (Nxr) of a fresh water anammox species "*Ca.* Brocadia sinica" was tried to be purified by five strategies: ion chromatography, hydroxyapatite chromatography, gel chromatography, hydrophobic interaction chromatography and affinity chromatography in this study. After first and second step of purification (ion chromatography and hydroxyapatite chromatography) non-targeting protein were roughly excluded. However, the purified protein still contained non-targeting protein Hydrazine synthase (Hzs). In order to separate Nxr and Hzs, further purification procedures were tested. According to column screening, hydrophobic interaction chromatography was powerful tools to separate protein sample after hydroxyapatite chromatography. Especially with hydrophobic interaction chromatography carrier types of Octyl and Butyl, they could separate Hzs and Nxr, but Nxr could not be purified completely in this study. The reason why Nxr and Hzs could not be easily separated by gel chromatography might be that each Nxr and Hzs makes a similar molecular weight complex based on the result of BN-PAGE.

6.6.1 Appendix Materials and methods

Optimum column screening

After hydroxyapatite chromatography, the purified protein still contained non-targeting protein: Hydrazine synthase (Hzs). In order to separate Nxr and Hzs, further purification procedures were tested.

Gel filtration chromatography

Gel filtration chromatography separates protein by molecular weight. Gel filtration chromatography was performed by using HiLoad 16/600, Superdexs 200pg (GE healthcare, Little Chalfont, UK) equilibrated a 50 mM Tris buffer (pH7.5) containing 0.15 M NaCl.

Ion-exchange chromatography with different types of carrier: DEAE (diethylaminoethyl) and ANX (diethylaminopropyl)

Ion-exchange chromatography was performed by using HiTrap DEAE Sepharose Fast Flow 1 mL, and HiTrap ANX Sepharose 4 Fast Flow 1ml (GE healthcare, Little Chalfont, UK) equilibrated a 20 mM Tris buffer (pH7.5). Binding proteins were eluted by increasing NaCl

concentration step wisely in the Tris buffer with 1 M NaCl.

Hydrophobic interaction chromatography (HIC)

Hydrophobic interaction chromatography separate proteins by hydrophobicity. Hydrophobic interaction chromatography (HIC) was performed by using Phenyl Sepharose 6 Fast Flow 1mL, Butyl Sepharose 4 Fast Flow 1mL, and Octyl Sepharose 4 Fast Flow 1mL (GE healthcare, Little Chalfont, UK) equilibrated a 50 mM sodium phosphate (pH7.0) containing 1.5M $(NH_4)_2SO_4$.

Affinity chromatography (AC)

To reduce purification step, we tried to make affinity chromatography (AC) column having antibody of NxrA as ligand. Affinity chromatography separates proteins on the basis of a reversible interaction between the target protein and a specific ligand attached to a chromatography base matrix. It has potential to be used for single-step purifications, because of its high selectivity. The polyclonal antibody of NxrA and NxrB was supplied by GL Biochem (Shanghai) Ltd. The proposed antigen sequences were Cys-TGYTTGNENDFMTK, and GRRMEYPYFESRPKRQ-Cys for GAN32427.1 nitrate reductase subunit alpha [*Candidatu*s Brocadia sinica JPN1] and GAN32430.1 nitrate reductase subunit beta [*Candidatus* Brocadia sinica JPN1], respectively. In this time, we used only antibody for NxrA, because after Hydroxyapatite chromatography, NxrA and NxrB make complex. We considered if NxrA attached to ligand, NxrB might also attached to ligand.

The supplied antibody was lyophilized product. Distilled water was added to reconstitute the lyophilized antibody and mixed gently by inverting 5-6 times at room temperature. After reconstituting, if insoluble matter was observed, remove precipitation by centrifugation at 3000 rpm for 10 to 15 min, transfer supernatant to fresh tube. For this product, 0.02 % of sodium azide was added for preservation. However, sodium azide interacts with column bed (NHS-activated Sepharose) and decreases coupling efficiency. Before coupling, sodium azide should be removed and buffer should be exchanged to coupling buffer 0.2 M$NaHCO_3$, 0.5 MNaCl, pH = 8.3 by using PD-10 desalting column (GE health- care, Little Chalfont, UK). After desalting, the antibody of NxrA concentration was 0.716 mg/ml, which achieved the optimum ligand concentration from 0.5 to 10 mg/ml for HiTrap NHS- activated HP (GE health- care, Little Chalfont, UK).

HiTrap NHS-activated High Performance 1 mL (GE health- care, Little Chalfont, UK) was designed for the covalent coupling of ligands containing primary amino groups. Coupling method was as follows. 5 ml of ice cold 1 mM HCl was applied to column to wash out isopropanol. The medium could be irreversible compressed. Then, immediately 1 mL of ligand (antibody of NxrA) was injected at 0.2 mL/min. Seal the column and let it stand for 30 min at room temperature. After coupling, the coupling solution was washed out from the column with 3 column volume (CV) of coupling buffer 0.2 M$NaHCO_3$, 0.5 MNaCl, pH = 8.3. This washed-out coupling buffer was used to determine coupling efficiency explained later. To deactivate any excess active groups that have not couples to the ligand and wash out the non-specifically bound ligands, 6 mL blocking buffer; 0.5 M ethanolamine, 0.5 MNaCl, pH=8.3 and 6mL washing buffer; 0.1M sodium acetate, 0.5MNaCl, pH=4.0 were applied alternately for 3times. Finally, 2mL of binding buffer; 10mM Na_2HPO_4, pH7, 0.15MNaCl was applied.

Purification procedure with affinity column was as follows. The column was equilibrated with 10CV of binding buffer, and then sample (5mL enzyme solution (1.0mg-BSA/ml) after Hydroxyapatite chromatography) was applied at 0.5mL/min. Column was washed with 5CV of binding buffer to remove unbound sample, and then eluted with 3CV of elution buffer; 0.1M Glycine-HCl, pH=3.0. During elution, the sample might get damage by low pH. Thus, eluted fraction should be neutralized immediately by adding 1.0M Tris-HCl, pH=9.0.

Identification of proteins

Proteins were characterized by SDS-PAGE. Proteins were separated on a 10% SDS-containing polyacryl-amide gel, and stained with Simply Blue Safe Stain (Invitrogen, USA) following the instruction manual supplied by manufactures. The protein band was excised and performed in-gel tryptic digestion. Identification of NxrA and NxrB was conducted by Matrix-assisted laser desorption ionization-time of flight mass spectrometry MALDI-TOF/MS. The data set was analyzed by MASCOT Server (matrixscience).

To understand how many complex were contained in fraction, Blue Native Polyacrylamide Gel Electrophoresis (BN PAGE) was also performed. In BN PAGE, the Coomassie G-250 binds to proteins and confers a net negative charge while maintaining the

proteins in their native state without any protein denaturation. Proteins were separated on Native Page 4-16% Bis-Tris Gel (Invitrogen, USA), following the instruction manual supplied by manufactures.

6.6.2 Appendix Result

Gel filtration chromatography

The gel filtration chromatography separates proteins by molecular weight. Firstly, molecular weight standards: catalase (232 kDa), BSA (67 kDa), lysozyme (14.3 kDa) were eluted (**Fig. S 6.1 A**). Higher molecular weight standards eluted faster than lighter molecular weight standards. After defining peak retention, HDA sample were injected (**Fig. S 6.1 B**). One big peak (peak retention 63.78mL) and two small peaks (peak retention 53.45 mL and 72.82 mL) were observed, and those peaks were arranged into five fractions (**Fig. S 6.1 B**). Those five fractions were analyzed by SDS PAGE **(Fig. S 6.2)**. NxrA should be observed near 116k Da and NxrB should be observed near 44.3kDa, however, there are no fraction which containing only NxrA and B. In F3, NxrA band was the thickest. Compared with molecular standard **(Fig. S 6.1 A)**, molecular weight of F3 was estimated to be 165.1 kDa. If NxrA and NxrB make a complex, the molecular weight is about 180 kDa. Other enzymes didn't appear as other molecular weight peaks. Therefore, we estimated that there were Nxr complex and another similar molecular weight complex in HDA sample.

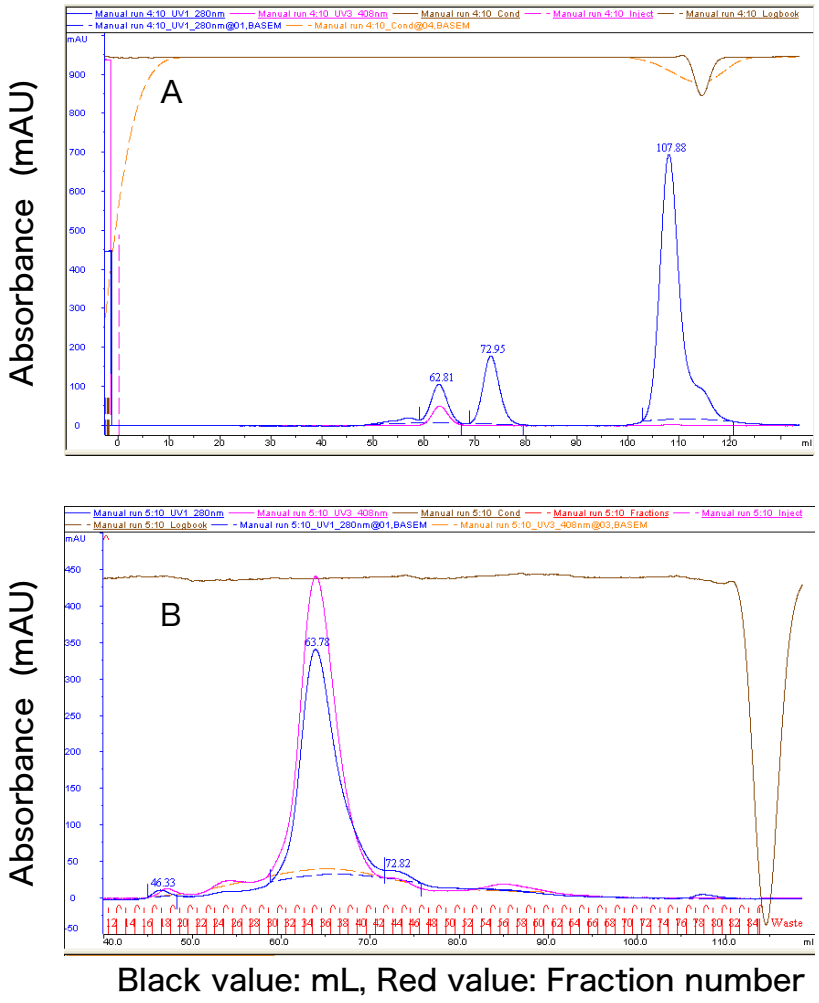

Figure S 6.1 Elution profiles during gel filtration chromatography. (A) Elution profiles of molecular weight standards 2 mg/ml catalase (232 kDa), 5 mg/ml BSA (67 kDa), 5 mg/lysozyme (14.3 kDa). Retention: catalase 62.81 ml, BSA 72.95 ml, lysozyme 107.88 ml, CV 114.35 ml. (B) Elution profiles of HDA sample (HiLoad 16/600, Superdexs 200pg) Fraction was rearranged to 5 fractions as follows. Fraction 1: F22-28, Fraction 2:F29-32, Fraction 3: F33-37, Fraction 4:F38-41, Fraction 5: F42-46. The elution condition was follows. Column: HiLoad 16/600, Superdexs 200pg, buffer 50 mM Tris pH7.5, 0,15M NaCl (flow rate, 1 ml/min)

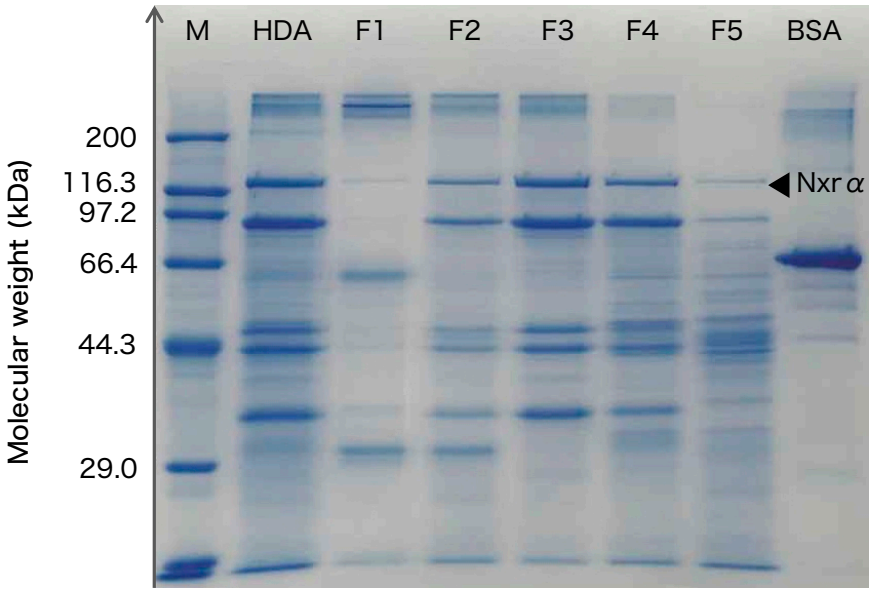

Figure S 6.2 Result of SDS-PAGE of gel filtration chromatography (10% PAGE gel, 50V 20 min, 200V 40 min)

Ion-exchange chromatography with different types of carrier: DEAE (diethylaminoethyl) and ANX (diethylaminopropyl)

As for DEAE, there were two big peaks and two small peaks. The first big peak appeared from fraction 5 to 6. The second big peak appeared in fraction 7 to 8 **(Fig. S 6.3).** However, when we look at result of SDS PAGE, there was no fraction which contained only NxrA and NxrB **(Fig. S 6.4).** As for HiTrap ANX FF, there was a peak from fraction 6 to13. Similarly, ANX didn't have fraction which contained only NxrA and B **(Fig.S 6.5)**. Thus, those Ion-exchange chromatography columns are not effective way to purify Nxr.

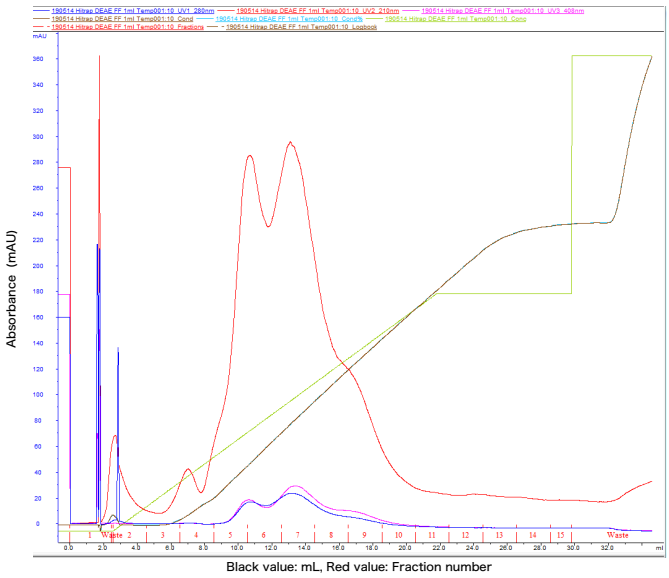

Figure S 6.3 Elution profiles during ion exchange chromatography with DEAE. Elution condition was as following. Column: HiTrap ANX FF 1ml, buffer A: 20 mM Tris-HCl (pH=7.5), buffer B: 20 mM Tris-HCl (pH=7.5) 1 M NaCl , 50%B/ Gradient length 20CV, injection: 100 µl

Figure S 6.4 Elution profiles during ion exchange chromatography with ANX. Elution condition was as following. Column: HiTrap DEAE FF 1ml, buffer A: 20mM Tris-HCl (pH=7.5), buffer B: 20 mM Tris-HCl (pH=7.5) 1MNaCl , 50 % B/ Gradient length 20CV ,injection: 100 µl

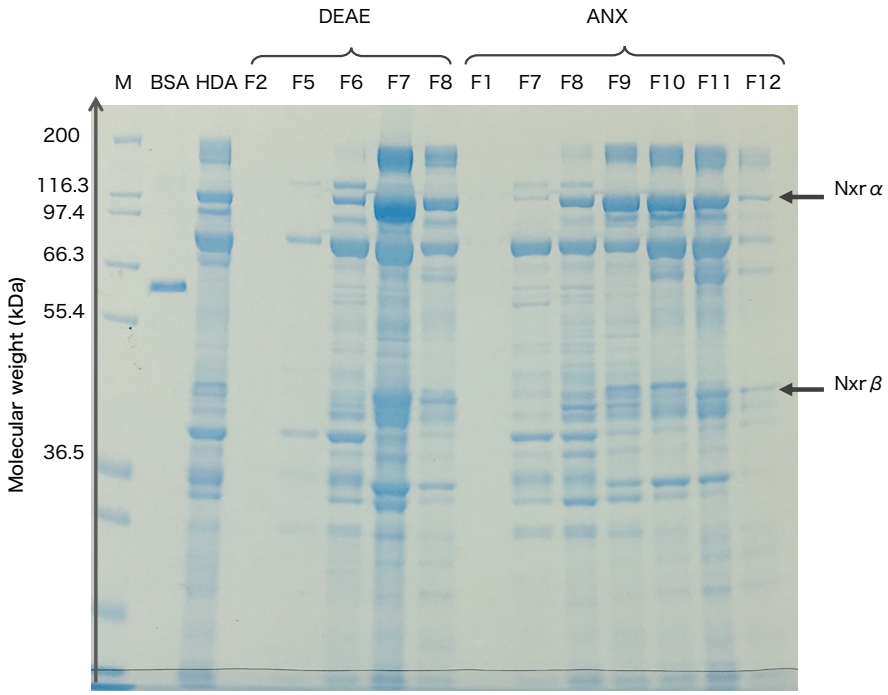

Figure S 6.5 Result of SDS-PAGE of Ion-exchange chromatography DEAE and ANX (Bis Tris 10%, 200V 50min)

Hydrophobic interaction chromatography (HIC)

Three types of carriers: Phenyl, Butyl, Octyl were used in this time. Among those three carriers, Phenyl has the strongest adsorption power, and Octyl has the weakest adsorption power. Therefore, the absorbance peak appeared from F8 to 11 in Octyl, from 9 to 13 in Butyl, and from 12 to 15 in Phenyl, respectively **(Fig.S 6.6 - S 6.8).** In Octyl and Phenyl, only one big peak was observed. In the result of Butyl, two peaks were observed at F10-11 and F12-13. The result of SDS PAGE **(Fig. S 6.9)** revealed that those HIC columns were powerful tools to separate enzyme in HDA sample, because they could reduce the number of bands from 11 to 6. Especially in Octyl and Butyl, second non-targeting thick band (2) appeared in the middle stage of peak, and NxrA (1) appeared latter half of peak. They have potential to separate band (1) and (2). However, the recovery of protein was very small because of many purification steps. After hydrophobic interaction chromatography (Butyl), the recovery protein was 0.01% (**Table S 6.1**). Unfortunately, it was not enough for performing enzyme assay test to measure isotope effect.

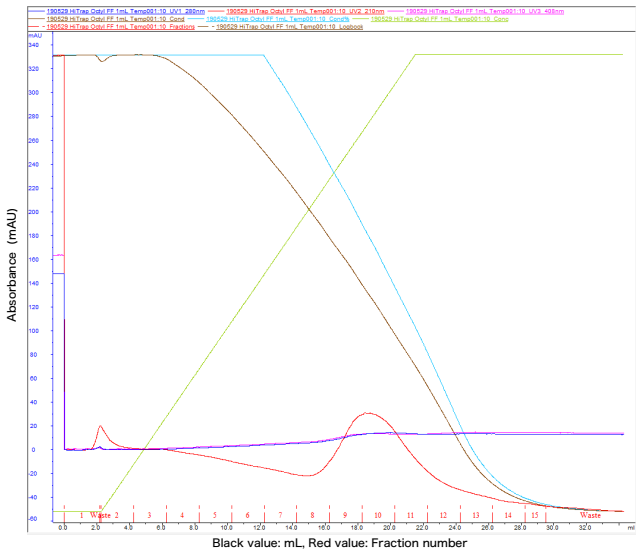

Figure S 6.6 Elution profiles of HDA sample (HiTrap Octyl FF). Elution condition was as following.Column: HiTrap Octyl FF 1mL, buffer A: 50mM sodium phosphate (pH=7.0) 1.5M $(NH_4)_2SO_4$, buffer B: 50mM sodium phosphate (pH=7.0), Gradient: 100%B/ Gradient length 20CV

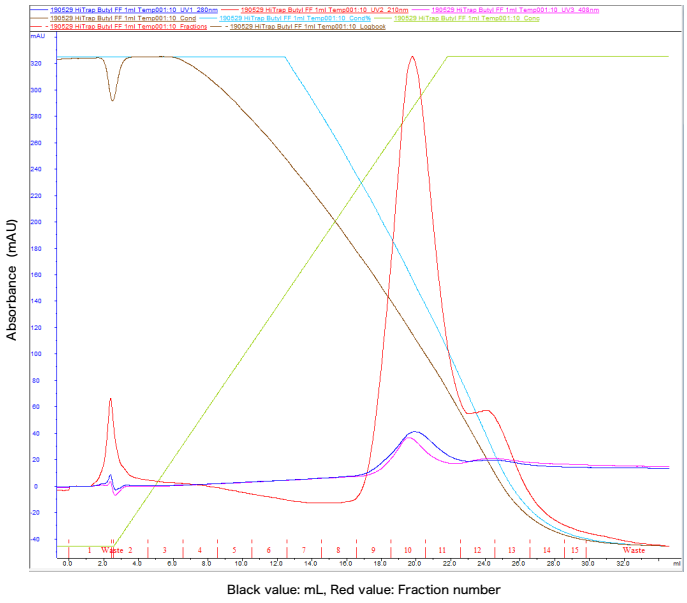

Figure S 6.7 Elution profiles of HDA sample (HiTrap Butyl FF). Elution condition was as following. Column: HiTrap Butyl FF 1mL buffer A: 50mM sodium phosphate (pH=7.0) 1.5M $(NH_4)_2SO_4$, buffer B: 50mM sodium phosphate (pH=7.0), Gradient: 100%B/ Gradient length 20CV

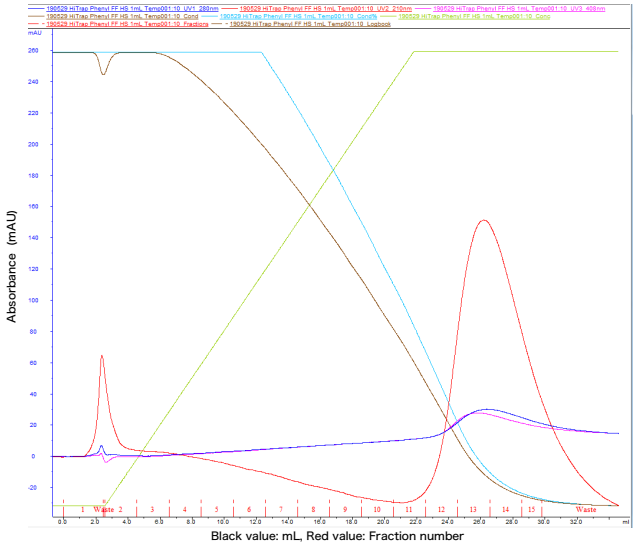

Figure S 6.8 Elution profiles of HDA sample (HiTrap Phenyl FF). Elution condition was as following. Column: HiTrap Phenyl FF 1mL, buffer A: 50mM sodium phosphate (pH=7.0) 1.5M $(NH_4)_2SO_4$, buffer B: 50mM sodium phosphate (pH=7.0), Gradient: 100%B/ Gradient length 20CV

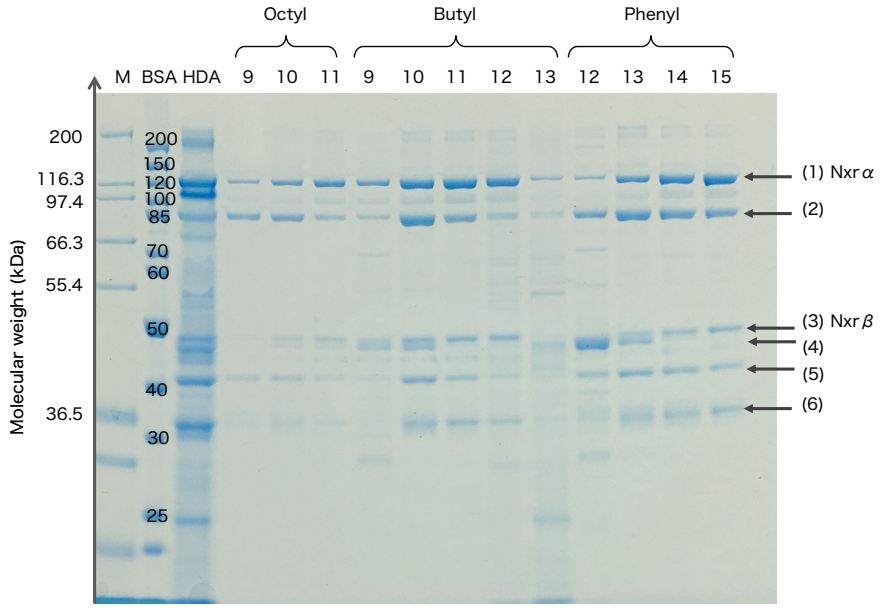

Figure S 6.9 Result of SDS-PAGE of Hydrophobic interaction chromatography (HIC) (Bis Tris 10%, 200V 50min)

Table S 6.1 Purification data of nitrite oxidoreductase from IEX(QXL) to HIC (Butyl)

Biomass 22.7g-wet

	mg-BSA/mL	mL	mg-BSA	% vs initial
CE	6.38	60	382.8	100
Sol	2.52	45	113.4	29.62
UF QXL	2.75	2.5	6.8675	1.79
UF HDA	0.03	3.2	0.08	0.02
UF Butyl	0.18	0.25	0.044	0.0115

Identification of enzyme by MALDI-TOF/MS

The six protein bands of Butyl **(Fig. S 6.9)** were excised and performed in-gel tryptic digestion. Identification of enzyme was conducted by Matrix-assisted laser desorption ionization-time of flight mass spectrometry MALDI-TOF/MS. The data set was analyzed by MASCOT Server. According to the result, band (1) and band (3) were NxrA and Nxr B, respectively. The band (2), (4), (5) were Hydrazine synthase (Hzs) A, B, C. The band (4) might be contaminant enzyme from other bacteria (**Table S 6.2**). From this result, there might be Nxr complex and Hzs complex and one contaminant enzyme exist in Butyl fraction. This result was consistent with the result of gel filtration chromatography. '*Ca.* B. sinica' Hzs could utilize NH_2OH as a substrate for N_2H_4 synthesis (Oshiki *et al.*, 2016). Hzs does not directly relate to oxidation-reduction reaction of nitrite and nitrate. However, it is ideal that separate Nxr complex and Hzs complex. Looking back at SDS PAGE result of first purification (QXL) **(Fig. 6.3.1.)**, Hzs complex appeared faster than Nxr complex. Hzs appeared from F24 to F36, and Nxr appeared from F30 to F40. I took F30 to 40 in this time. However, If we narrow fraction range to F38 - F40, Hzs can be separated. In addition, looking back at SDS PAGE result of Butyl **(Fig. S 6.9)**, Hzs appeared in middle of peak. On the other hand, Nxr appeared in the beginning and latter of peaks. Therefore, narrowing fraction range of fist ion exchange chromatography (QXL) and Butyl could have potential to get purified Nxr.

Table S 6.2 The result of MASCOT Peptide Mass Fingerprint

Sample	Locus-tag	Product	MW（Da)	Socre	Statistically significant
Butyl (1)	BROSI_A0941	nitrate_reductase_subunit_alpha (*Ca.* B. sinica JPN1)	131795	89	○
Butyl (2)	BROSI_A2676	hydrazine_synthase_alpha_subunit (*Ca.* B. sinica JPN1)	90964	165	○
Butyl (3)	BROSI_A0944	nitrate_reductase_subunit_beta (*Ca.* B. sinica JPN1)	48110	114	○
Butyl (4)	KMM16275.1	hypothetical protein SYNGFB01_12185 [Synechococcus sp. GFB01]	7899	63	×
Butyl (5)	BROSI_A2674	hydrazine_synthase_beta_subunit (*Ca.* B. sinica JPN1)	41136	79	×
Butyl (6)	BROSI_A2675	hydrazine_synthase_gamma_subunit (*Ca.* B. sinica JPN1)	37571	73	×

Blue Native Polyacrylamide Gel Electrophoresis (BN PAGE)

To confirm how many complexes existing in the fraction, Blue Native PAGE was performed. Samples after 1st QXL, after 2nd HDA, and Butyl F9-13 **(Fig. S 6.9)** were analyzed. As for Butyl F10, I forgot to inject sample. Two thin bands ((1) and (2) in **Fig. S 6. 10**) and two thick bands ((3) and (4) in **Fig. S 6. 10**) were observed in B9, B11, B12, B13. Calculating by ladder marker, band (1), (2), (3), (4) was about 480kDa, 425kDa, 335kDa, 220kDa, respectively. If Nxr make a complex, molecular weight is about 180kDa. The reported Hzs molecular weight is 329kDa. Therefore, thick band (3) might be Hzs, and (4) might be Nxr.

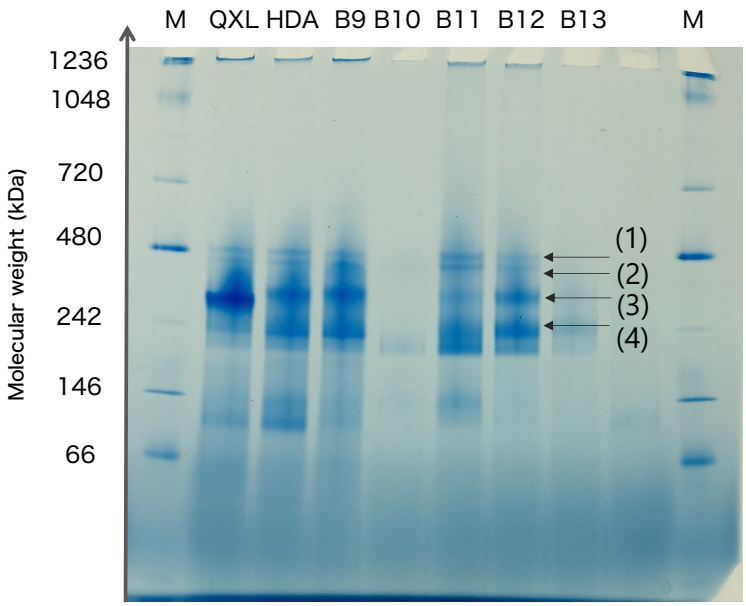

Figure S 6.10 Result of BN PAGE (4-16% Bis-Tris Gel, 150V 120minutes)

Affinity chromatography (AC)

Coupling efficiency

To calculate coupling efficiency; the ratio of how much ligand attached to column, the protein concentration of ligand solution and coupling buffer was measured. The protein concentration of ligand solution was 0.716mg-BSA/ml, and that of coupling buffer was 0mg-BSA/ml. Therefore, the coupling efficiency was (0.716-0)/0.716×100= 100%. All ligand (antibody of NxrA) was attached to column bed.

Purification with affinity column

During applying sample (Fraction 1 to 2), there was big one peak which passed through column **(Fig. S 6.11).** After applying elution buffer (from fraction 5 in **Fig. S 6.11**), there was no protein peaks. The UV2 210nm increased gradually, but this is because elution buffer; Glycine-HCl, pH=3.0 has 210nm absorption. There were several possible reasons why target enzyme was not appeared in elution step. 1. Sample injection rate was fast, and target enzyme couldn't attach to the column, 2. Binding power was strong and target protein didn't elute yet, 3. The amount of ligand was not enough, 4. Ligand did not bind to native target enzyme. As for 1st reason; Sample injection rate was fast, and target enzyme couldn't attach to the column, the optimum sample flow rate was from 0.2ml/min to 1.0ml/min according to the manual. Thus, the flow rate was reduced to 0.2ml/min in second trial (**Fig. S 6.11 (B)**). The sample concentration also affected binding. Therefore, the sample concentration was reduced to 0.5mg-BSA/ml. However, those amendments didn't improve binding efficiency. As for 2nd reason; Binding power was strong and target protein didn't elute yet, SDS-PAGE was performed to confirm whether Nxr was contained in flow through fraction (Fraction 1 to 2) or not **(Fig. S 6.12).** The Sample UF HDA was injected as sample, NxrA was observed around 116.3kDa, and NxrB was observed between 40 and 50kDa. In 1st and 2nd purification, both protein bands of NxrA and Nxr B were clearly observed in F1 and F2. Therefore, target enzyme NxrA and NxrB didn't bind to ligand and pass through the column. In order to confirm remained possible reasons; 3. The amount of ligand was not enough, 4. Ligand does not bind to native target enzyme, the binding efficiency between native NxrA and NxrB and supplied antibody was analyzed by performing Western Blotting (WB). However, the specificity of the antibody could not be examined. Therefore, using affinity chromatography was terminated.

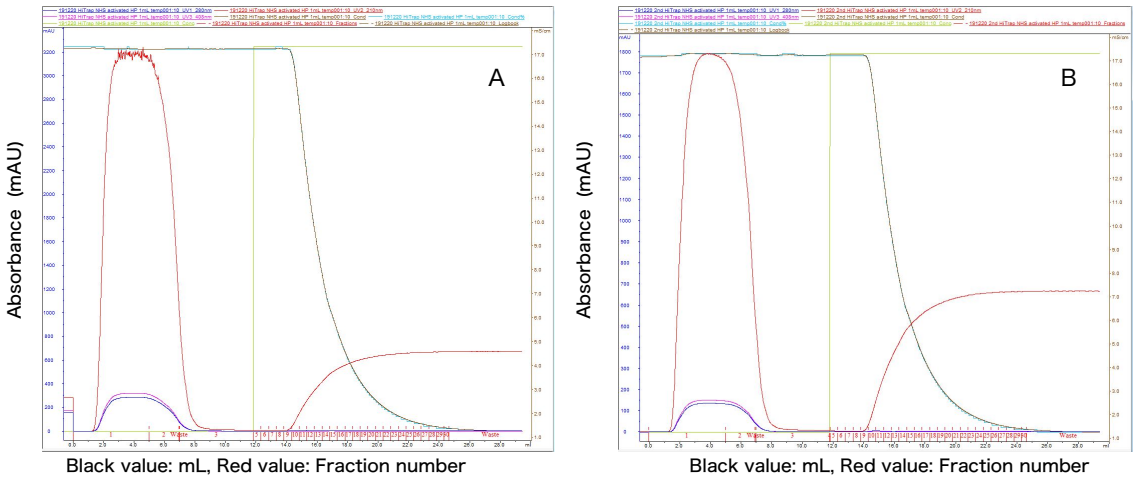

Figure S 6.11 Elution profiles during Affinity chromatography. (A) sample injection rate was 0.5 ml/min, (B) sample injection rate was 0.2ml/min. Elution condition was as following. (A) Column: HiTrap NHS-activated HP 1mL, Binding buffer:10mM Na_2HPO_4, pH7, 0.15MNaCl, Elution buffer: 0.1M Glycine-HCl, pH=3.0, injection volume: 5mL HDA sample (1mg-BSA/ml in (A), 0.5mg-BSA/ml in (B)), injection flow rate: 0.5ml/min in (A), 0.2ml/min in (B).

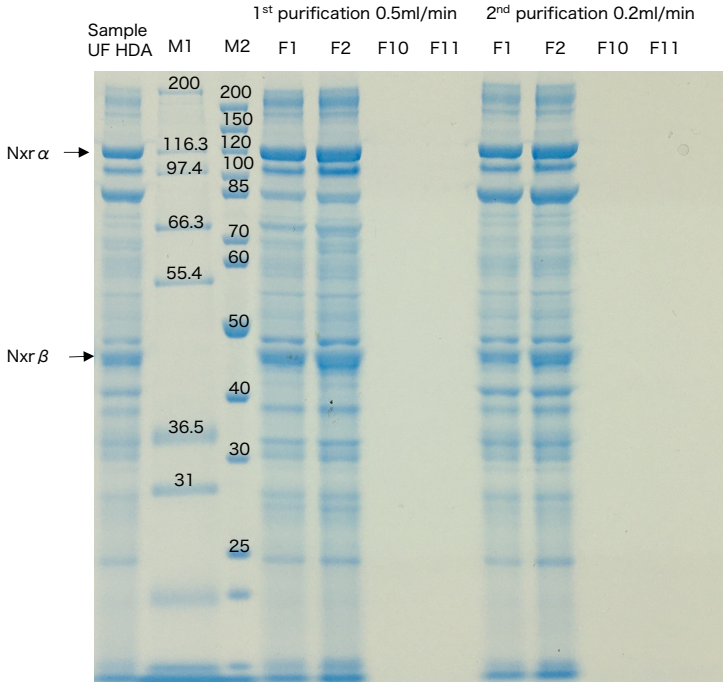

Figure S 6.12 Result of SDS-PAGE during affinity chromatography (Bis Tris 10%, 200V 50min)

Optimization of enzyme assay test

Enzyme assay test after first purification step: Ion-exchange chromatography

Nitrite oxidation activity and nitrate reduction activity was measured about purified protein after first purification: ion-exchange chromatography. In order to determine optimum protein concentration, the amount of protein concentration in assay vials were varied. There were three vials with enzyme concentration of 70μg-BSA/ml, 140μg-BSA/ml, 280 μg-BSA/ml. As for nitrite oxidation assay, with 70 μg-BSA/ml enzyme concentration, nitrite consumption was not observed (**Fig. S 6.13**). With 140μg-BSA/ml enzyme concentration, nitrite concentration decreased from 14.1mg-N/L to 7.6mg-N/L. Finally, with 280μg-BSA/ml nitrite was completely consumed after 75minutes. From those result, optimum enzyme concentration is over 140μg-BSA/ml to track decreasing nitrite concentration and nitrate production. The mass balance between nitrite and nitrate (the ratio of Nitrate production/ Nitrite consumption) was 1.06 for 140μg-BSA/ml, and 0.81 for 280μg-BSA/ml. The nitrogen and oxygen isotope compounds of nitrite and nitrate were measured except experiment with 70μg-BSA/ml, because there was no nitrite oxidation activity with 70μg-BSA/ml (**Fig. S 6.14**). In the experiment of abiotic reaction (A), there was no nitrite consumption and both of $\delta^{15}N$ and $\delta^{18}O$ were constant value. As for experiment with 140μg-BSA/ml, 280 μg-BSA/ml, both of $\delta^{15}N$ and $\delta^{18}O$ of nitrite decreased. In addition, $\delta^{15}N$ and $\delta^{18}O$ of produced nitrate was higher than that of nitrite. Those changes of $\delta^{15}N$ and $\delta^{18}O$ indicated that nitrite oxidation reaction itself show inverse kinetic isotope effect which means heavy isotope nitrite consumed faster than light isotope nitrite. In this experimental condition only nitrite reduction reactions happens because only artificial electron accepter was added.

As for nitrate reduction assay test, three vials with enzyme concentration of 140μg-BSA/ml, 210μg-BSA/ml, 280 μg-BSA/ml were prepared. The reason why the protein concentration was higher than nitrite oxidation assay was that there was no activity with the concentration of 70 μg-BSA/ml in nitrite oxidation experiment. However, there was no nitrate consumption in all experimental systems (**Fig. S 6.13 (F), (G), (H)**). Even though enzyme concentration was increased to 280 μg-BSA/ml, nitrate reduction reaction didn't happen. Optimization of experimental condition for nitrate reduction assay is essential.

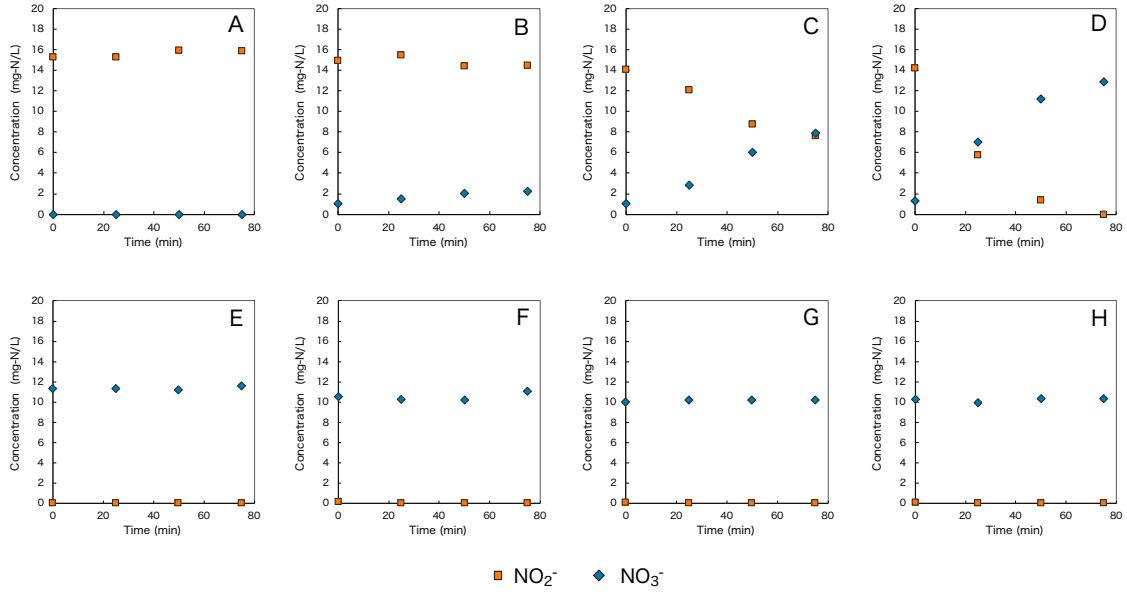

Figure S 6.13 Time course change of concentration during nitrite oxidation and nitrate reduction assay. Nitrite oxidation assay was from (A) to (D). Nitrate reduction assay was from (E) to (H). (A), (E) Abiotic reaction measurement, no addition of purified protein, (B), (F) 70μg-BSA/ml , (C), (G) 140μg-BSA/ml, (D), (H) 280 μg-BSA/ml protein was added.

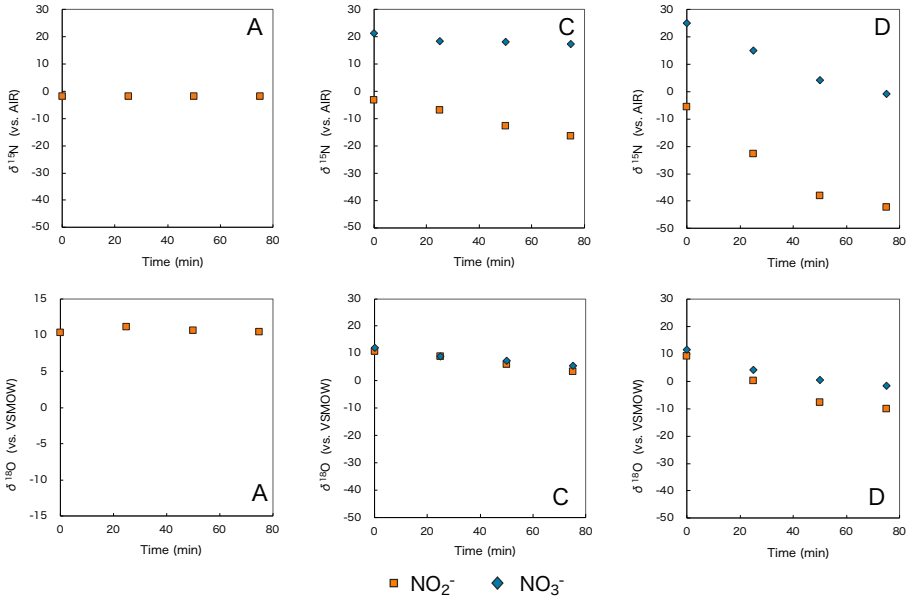

Figure S 6.14 Time course change of δ^{15}N and δ^{18}O during nitrite oxidation assay. Upper figures show change in δ^{15}N of nitrite and nitrate. Lower figures show change in δ^{18}O of nitrite and nitrate. (A) Abiotic reaction measurement, no addition of purified protein, (C) 140μg-BSA/ml, (D) 280 μg-BSA/ml protein was added.

Optimization of experimental condition for nitrate reduction assay

Generally, enzyme activity decreases during purification steps. Therefore, nitrate reduction assay test with soluble protein without purification process was conducted in the same way of previous assay test. The final protein concentration in assay vial was set as 85 µg-BSA/ml. Duplicate assay were performed (**Fig. S 6.15**). In both batches, nitrate reduction was observed((A):14.9mg-N/L→11.8mg-N/L, (B):14.5mg-N/L→13.2mg-N/L), but nitrite production was not observed so far. The specific nitrate reduction rate was 1.1nmol $mgBSA^{-1}$ min^{-1}, 0.452nmol $mgBSA^{-1}$ min^{-1} for (A) and (B) respectively. Nitrate reduction was confirmed with soluble protein. To optimize experimental condition, literature review of experimental condition with nitrite oxidoreductase purified by nitrite oxidizing bacteria was conducted (**Table S 6. 3**). In our experiment, Metylviologen was used as electron donor. Benzylvilogen and NADH also work as electron donor with Nxr (Sundermeyer-Klinger *et al.*, 1984). The optimum condition for nitrite oxidation and nitrate reduction was different for nitrite oxidoreductase. Nitrite oxidation occurs at pH from 7.5 to 8.0 and optimum pH is 8.0. Nitrate reduction occurs at pH 6.0 to 7.0 and optimum pH was 7.0 (Sundermeyer-Klinger *et al.*, 1984). Two literature used $MgCl_2$ as an activating factor (Yamanaka and Fukumori, 1988; Meincke *et al.*, 1992).

In initial experimental condition was pH set at 6.5. Therefore, two additional experimental condition was performed. One was pH set at 6.0, another was pH set at 6.5 but $MgCl_2$ was added. The final protein concentration was increased to 276.5µg-BSA/ml. In the experiment of abiotic reaction (A), there was no nitrite consumption (**Fig. S 6.16 A**). On the other hand, nitrate consumption was observed in all three experiments with soluble protein. However, nitrite production was not found (**Fig. S6.16, B,C,D**). According to specific activity calculation, the condition with pH=6.5 has higher activity. The addition of $MgCl_2$ didn't change the activity (**Table S 6.4**). Nitrite was not detected. It might be attributed to exitance of electron donor (Methyl viologen). Nitrite might be further reduced, and not detected.

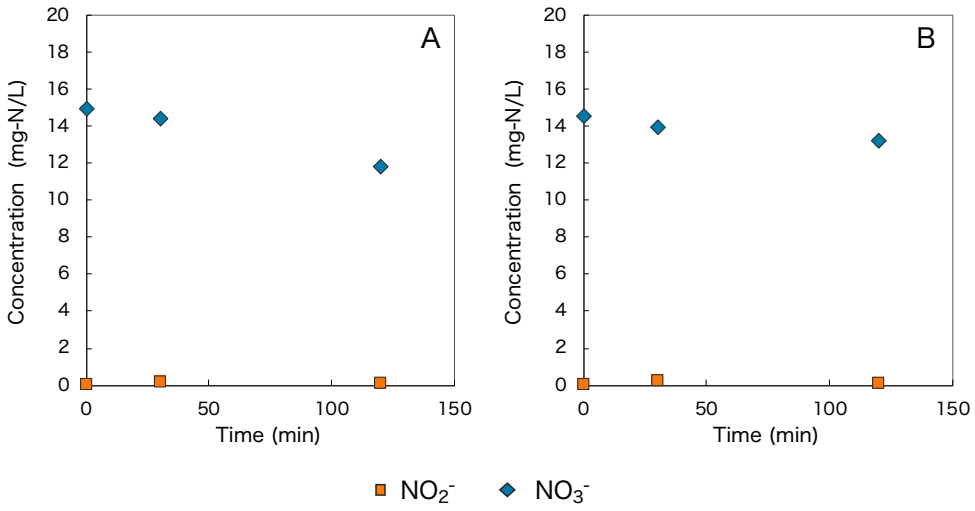

Figure S 6.15 Nitrate reduction assay with soluble protein. (A) and (B) were duplicate assay test in same experimental condition with protein concentration of 85 μg-BSA/ml.

Table S 6.3 Summary of experimental condition of nitrate reduction assay with nitrite oxidoreductase purified from nitrite oxidizing bacteria

species	Nitrobacter hamburgensis	Nitrobacter hamburgensis	Nitrobacter winogradskyi
NO_3^- concentration	0.9-2.9mM	5.4mM	50mM
Buffer	30mM Tris-HCl	50mM NaOu buffer	appropreate buffer
pH	7	6.5	6
Electron donor	0.2mM Metylviologen 0.2mM Benzylviologen 1.4mM NADH	20μM Metylviologen	ferrocytochrome c
Reducing agent	4.5mM sodium dithionite	4.5mM sodium dithionite	-
Others	0.1mM flavinmononucleotide 10 mM $MgC1_2$		4.6ｍM $MgCl_2$
enzyme	100μL		-
Total volume	2.3ｍL		1mL
Reaction time	30min		
Temperature	30˚C	30˚C	
Km value for nitrate	0.9ｍM Metylviologen 0.9ｍM Benzylviologen 1.4mM NADH		-
Specific nitrate reductase activity	1147nmol NO_3^- reduced/mg protein ×min	1740 nmol NO_3^- consumed /min	
experimental system	1cm light path cuvettes		
Reference	Sundermeyer-Klinge et al., 1984	Meincke et al., 1992	Yamanaka and Fukumori 1988

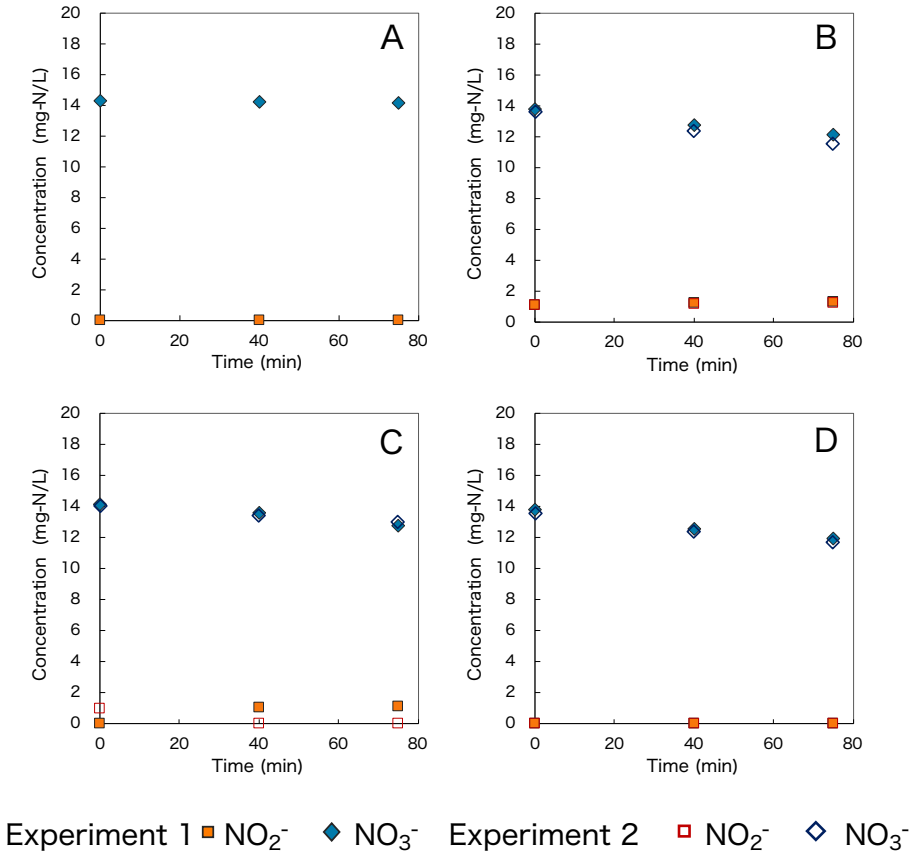

Figure S 6.16 Nitrate reduction assay with soluble protein (A) Abiotic reaction no protein, (B) pH = 6.5, (C) pH = 6.0, (D) pH = 6.5, $MgCl_2$ was added.

Table S 6.4 Summary of specific activity at different experimental conditions

Specific activity (nmol $mgBSA^{-1}$ min^{-1})

Condition	Expt.1	Expt.2	Average
pH=6.5	0.29	0.36	0.33
pH=6.0	0.23	0.18	0.20
pH=6.5 $MgCl_2$	0.32	0.31	0.31

6.6.3 Appendix References

Meincke, M., Bock, E., Kastrau, D., and Kroneck, P.M.H. (1992) Nitrite oxidoreductase from *Nitrobacter hamburgensis*: Redox centers and their catalytic role. *Arch Microbiol* **158**: 127–131.

Oshiki, M., Ali, M., Shinyako-Hata, K., Satoh, H., and Okabe, S. (2016) Hydroxylamine-dependent anaerobic ammonium oxidation (anammox) by "*Candidatus* Brocadia sinica." *Environ Microbiol* **18**: 3133–3143.

Sundermeyer-Klinger, H., Meyer, W., Warninghoff, B., and Bock, E. (1984) Membrane-bound nitrite oxidoreductase of *Nitrobacter*: evidence for a nitrate reductase system. *Arch Microbiol* **140**: 153–158.

Yamanaka, T. and Fukumori, Y. (1988) The nitrite oxidizing system of *Nitrobacter winogradskyi*. *FEMS Microbiol Lett* **54**: 259–270.

Chapter 7
Conclusions

Natural abundance of stable nitrogen (N) and oxygen (O) isotopes (δ^{15}N and δ^{18}O) are invaluable biogeochemical tracers for assessing the N transformations in the environment. To fully exploit these tracers, the N and O isotope effects ($^{15}\varepsilon$ and $^{18}\varepsilon$) associated with the respective N transformation processes must be known. Anaerobic ammonium oxidation (anammox) and denitrification are the two major sinks of fixed N. In addition, anammox bacteria contribute to re-oxidation of nitrite (NO_2^-) to nitrate (NO_3^-), because they fix CO_2 into biomass with reducing equivalents generated from oxidation of NO_2^- to NO_3^-. NO_3^- production by anammox bacteria influences the NO_2^- and NO_3^- N and O isotope effects in freshwater and marine systems. Despite the significant importance of anammox bacteria in the global N cycle, $^{15}\varepsilon$ and $^{18}\varepsilon$ of anammox are not well known. Actually, $^{18}\varepsilon$ of anammox have not been determined yet. Therefore, $^{15}\varepsilon$ and $^{18}\varepsilon$ associated with anammox were investigated in this study.

In Chapter 2, recent progress in our understanding of N and O isotope effects of N related microorganisms and factors (pH, substrate concentration, temperature, species difference, and oxygen partial pressure) affecting the expressed isotope effects were reviewed to interpret natural abundance N and O isotopic distributions in the environment and make experimental strategy to analyze isotope effects.

In Chapter 3, the $^{15}\varepsilon$ were determined for highly enriched '*Ca.* Scalindua sp.', '*Ca.* Jettenia caeni', and '*Ca.* Brocadia sinica' growing in continuous membrane bioreactors (MBRs). Each $^{15}\varepsilon$ was calculated by the steady-state fractionation model. For the conversion of NH_4^+ to N_2, the N isotope effects ($^{15}\varepsilon_{NH4\rightarrow N2}$) of all three species are consistent (30.9‰ to 32.7‰). This is probably because this reaction is mediated through the same enzymes such as hydrazine synthase (hzs) and hydrazine dehydrogenase (hdh) in all anammox bacteria species. On the other hand, for the conversion of NO_2^- to N_2, significant variations of the N isotope effects ($^{15}\varepsilon_{NO2\rightarrow N2}$) were found among the three species: $^{15}\varepsilon_{NO2\rightarrow N2}$ = 19.9 ± 1.7‰ for '*Ca.* Scalindua sp.', $^{15}\varepsilon_{NO2\rightarrow N2}$ = 29.5 ± 3.9‰ for '*Ca.* Jettenia caeni', and $^{15}\varepsilon_{NO2\rightarrow N2}$ = 5.9 ± 4.5‰ for '*Ca.* Brocadia sinica', respectively. This is probably because individual anammox bacteria species possess different types of nitrite reductase. '*Ca.* Scalindua sp.' possesses a cytochrome *cd*$_1$ (iron, Fe)-type NO-forming nitrite reductase (Fe-NIR), whereas '*Ca.* Jettenia caeni' possesses a

copper (Cu)-containing NO-forming nitrite reductase (Cu-NIR). '*Ca.* Brocadia sinica', however, does not possess canonical nitrite reductase genes (neither Fe-NIR nor Cu-NIR). For the oxidation of NO_2^- to NO_3^-, all three anammox species exhibited pronounced inverse N isotope effects (-45.3 ‰ to -30.1 ‰), which agreed with the previously reported value for '*Ca.* K. stuttgartiensis' but exceeded the values for nitrite-oxidizing bacteria (NOB).

In Chapter 4, the influence of $\delta^{18}O_{H2O}$ of sample on $\delta^{18}O$ analysis of NO_2^- and NO_3^- were quantitatively evaluated. Although it has been recognized that oxygen isotope ratio measurements of NO_2^- and NO_3^- by the azide method and denitrifier method are sensitive to the $\delta^{18}O$ of sample water, the influence of $\delta^{18}O_{H2O}$ on those measurements has not been quantitatively evaluated and documented so far. To evaluate the influence of $\delta^{18}O_{H2O}$ of sample on $\delta^{18}O$ analysis of NO_2^- and NO_3^-, NO_2^- and NO_3^- standards (with known $\delta^{18}O_{NO2-}$ and $\delta^{18}O_{NO3-}$) were prepared with waters having different $\delta^{18}O_{H2O}$ values ($\delta^{18}O_{H2O}$ = -12.6, 25.9, 56.7, and 110.1‰). The measured $\delta^{18}O$ of produced N_2O was plotted against known $\delta^{18}O_{NO2-}$ and $\delta^{18}O_{NO3-}$ values to evaluate the influence of exchange of oxygen atom with H_2O during the conversion of NO_2^- to N_2O and NO_3^- to N_2O, respectively. As a result, the degree of O isotope exchange was 10.8 ± 0.3% in the azide method and 5.5 ± 1.0 % in the denitrifier method, indicating that the azide method is more susceptible to artifacts arising from differences in the $\delta^{18}O_{H2O}$ of water than the denitrifier method. Thus, the intercept of the standard calibration curve must be corrected to account for differences in $\delta^{18}O_{H2O}$. In short, oxygen isotope ratio measurements of NO_2^- by the azide method are highly sensitive to $\delta^{18}O_{H2O}$ resulting from significant oxygen isotope exchange between NO_2^- and H_2O. Therefore, the same $\delta^{18}O_{H2O}$ as that of the sample must be used to make the NO_2^- and NO_3^- standards for the most accurate measurements. Then, the rate of abiotic O isotope exchange between NO_2^- and H_2O: $k_{eq} = 1.13 \times 10^{-2}$ (h^{-1}), as well as equilibrium isotope effects: $^{18}\varepsilon_{eq}$ = 11.9‰ were experimentally determined by conducting abiotic batch experiment with different $\delta^{18}O_{H2O}$ values of medium ($\delta^{18}O_{H2O}$ = -12.6 ~ 110.1‰).

In Chapter 5, the $^{18}\varepsilon$ were determined for '*Ca*. Scalindua sp.', which is a putative marine species. Determination of $^{18}\varepsilon$ of anammox is more challenging because the $\delta^{18}O_{NO2}$ value is affected by abiotic O isotope exchange between NO_2^- and H_2O (k_{eq}, $^{18}\varepsilon_{eq}$). In addition, the $\delta^{18}O_{NO3}$ value is affected by incorporation of a water-derived O atom into NO_3^- during NO_2^- oxidation to NO_3^- ($^{18}\varepsilon_{H2O}$). Abiotic k_{eq}, $^{18}\varepsilon_{eq}$ was determined by abiotic batch experiments with different $\delta^{18}O_{H2O}$ values of medium in Chapter 4. To determine $^{18}\varepsilon$ of NO_2^- reduction ($^{18}\varepsilon$ (NO_2^-

→ N_2)), NO_2^- oxidation ($^{18}\varepsilon(NO_2^- \rightarrow NO_3^-)$) and O atom incorporation ($^{18}\varepsilon_{H2O}$), batch culture experiments with different $\delta^{18}O_{H2O}$ values of medium ($\delta^{18}O_{H2O}$ = -12.6 ~ 110.1‰) were conducted for '*Ca.* Scalindua sp.'. During the anammox reaction, $\delta^{18}O$ of produced NO_3^- appeared to depend on the $\delta^{18}O_{H2O}$ of medium. This observation suggested that water is oxygen source of NO_3^- production by anammox. Rapid increase in $\delta^{18}O$ of NO_2^- overtime in higher $\delta^{18}O_{H2O}$ medium was observed compared to abiotic exchange. This might be attributed to microbially catalyzed oxygen isotopic exchange. A numerical model was developed with the Markov Chain Monte Carlo (MCMC) method for estimation of respective $^{15}\varepsilon$ and $^{18}\varepsilon$ of anammox reaction. The obtained values of $^{15}\varepsilon$ were $^{15}\varepsilon$ ($NH_4^+ \rightarrow N_2$) = 30.7 ± 2.9 ‰, $^{15}\varepsilon$ ($NO_2^- \rightarrow N_2$) = 10.2 ± 1.8 ‰ and $^{15}\varepsilon$ ($NO_2^- \rightarrow NO_3^-$) = -16.9 ± 1.6 ‰. Respective $^{18}\varepsilon$ of anammox reaction were determined to be $^{18}\varepsilon$ ($NO_2^- \rightarrow N_2$) = 9.6 ~ 21.1‰ and $^{18}\varepsilon$ ($NO_2^- \rightarrow NO_3^-$) = -19.6 ~ -0.4‰ and $^{18}\varepsilon_{H2O}$ = 5.3 to 29.2‰, respectively. The $^{18}\varepsilon$ values were dependent on $\delta^{18}O_{H2O}$ of the medium, and there were linear relationships between them. Furthermore, anammox bacteria accelerated oxygen isotope exchange between NO_2^- and water. The rate of oxygen isotope exchange catalyzed by anammox bacterium was 10.1 to 17.7 times larger than that of abiotic oxygen isotope exchange. To apply these obtained oxygen isotope effects to natural marine environment (which exhibit $\delta^{18}O_{H2O}$ = 7.7 ~1.8‰), the range of oxygen isotope effects were estimated to be $^{18}\varepsilon_{NO2\rightarrow N2}$ = 9.8 ~ 10.5‰, $^{18}\varepsilon_{NO2\rightarrow NO3}$ = -3.3 ~ -1.9 ‰, and $^{18}\varepsilon_{H2O}$= 24.1 ~ 25.6 ‰, respectively.

In Chapter 6, the enzyme level $^{15}\varepsilon$ and $^{18}\varepsilon$ of NO_2^- oxidation and NO_3^- reduction was determined by using partially purified nitrite oxidoreductase (Nxr) from '*Ca.* Brocadia sinica'. Depending on its redox state and pH Nxr either oxidizes NO_2^- to NO_3^- or reduces NO_3^- to NO_2^-. However, how reversibility of anammox bacterial Nxr affects isotope effect of NO_2^- oxidation is not clarified yet. After several purification processes (anion-exchange chromatography followed by hydroxyapatite chromatography), NxrA and NxrB were partially purified. The N and O isotope effects of NO_2^- oxidation and NO_3^- reduction were individually determined with the partially purified anammox bacterial Nxr. The N and O isotope effect of NO_2^- oxidation was determined to be $^{15}\varepsilon$ ($NO_2^- \rightarrow NO_3^-$) = -34.7 ~ -59.8 ‰ and $^{18}\varepsilon$ ($NO_2^- \rightarrow NO_3^-$) = -19.3 ~ -33.6 ‰, respectively, showing inverse kinetic isotope effects for both. The N and O isotope effect for NO_3^- reduction was $^{15}\varepsilon$ ($NO_3^- \rightarrow NO_2^-$) = 31.2 ~ 31.7 ‰ and $^{18}\varepsilon$ ($NO_3^- \rightarrow NO_2^-$) = 26.0 ~ 22.0 ‰, respectively. Since nitrite oxidoreductase is known as a reversible enzyme, $^{15}\varepsilon$ ($NO_2^- \rightarrow NO_3^-$) and

$^{18}\varepsilon$ ($NO_2^- \rightarrow NO_3^-$) obtained from whole cells were combined N and O isotope effects of NO_2^- oxidation and NO_3^- reduction. The specific activity of NO_3^- reduction by anammox bacterial Nxr was 23 times lower than that of NO_2^- oxidation and thus the contribution of NO_3^- reduction to overall N and O isotope effects was trivial. Therefore, the $^{15}\varepsilon$ and $^{18}\varepsilon$ values associated with conversion of NO_2^- to NO_3^- by the whole cells were governed by NO_2^- oxidation, which exhibited the inverse N and O isotope effects.

In this work, $^{15}\varepsilon$ of three different anammox species were determined. The numerical model to calculate $^{18}\varepsilon$ of anammox was developed and determined $^{18}\varepsilon$ of a marine anammox species '*Ca*. Scalindua sp.'. Furthermore, the effect of reversibility of anammox bacterial Nxr on the N and O isotope effect of NO_2^- oxidation was clarified by using partially purified anammox bacterial Nxr. These obtained coupled N and O isotope effects of anammox bacteria could provide significant insights into the contribution of anammox bacteria to the fixed N loss and NO_2^- reoxidation in (recycling N) in various natural environments. However, the effects of physiological factors (*i.e.* pH, substrate concentration, temperature, and species difference) on N and O isotope effects ($^{15}\varepsilon$ and $^{18}\varepsilon$) of anammox should be further investigated to more accurately assess the nitrogen budgets in the environment.